Chronostratigraphy, vertical axis rotations and AMS in the Boltaña anticline (Southern Pyrenees): kinematic implications

TANIA MOCHALES LÓPEZ

TESIS DOCTORAL

Instituto Geológico y Minero de España
Unidad de Zaragoza
-
Departamento de Ciencias de la Tierra
Facultad de ciencias. Universidad de Zaragoza

Zaragoza a 25 de abril de 2011

Emilio L. Pueyo Morer, Investigador Titular del Instituto Geológico y Minero de España en la Unidad de Zaragoza y en su calidad de codirector de la Tesis Doctoral de Tania Mochales López, certifica que la Memoria de dicha Tesis se ajusta a los objetivos propuestos en el proyecto I+D del IGME titulado "Cronoestratigrafía de las unidades sintectónicas de la cuenca Surpirenaica centro-occidental (ChronoPyr)" y de los propuestos en el Proyecto de Tesis Doctoral aprobado por el Departamento de Ciencias de la Tierra de la Universidad de Zaragoza.

Fdo. Emilio L. Pueyo Morer

Instituto Geológico y Minero de España-Unidad de Zaragoza.
c/ Manuel Lasala 44, 9º, 50006 Zaragoza
+34 976 55 51 53, unaim@igme.es,
http://www.igme.es/internet/zaragoza/

Departamento de Ciencias de la Tierra
Universidad de Zaragoza

Antonio Casas Sainz, profesor Titular del Área de Geodinámica Interna del Departamento de Ciencias de la Tierra, y codirector de la tesis doctoral de Tania Mochales López, hago constar mi consentimiento para la presentación de dicha tesis, que se ajusta al proyecto presentado en su día.

Zaragoza, 26 de Abril de 2011

Fdo: Antonio M. Casas Sainz

This work was sponsored by a PhD fellowship from the Geological Survey of Spain (IGME). Research financial support comes from the projects Pmag3Drest (CGL-2006-2289-BTE MEC, CGL2009-14214 and CGL2008-00809/BTE) and CGL 2006-05817 from MICINN, ChronoPyr (IGME-346), 3DR3 (PI165/09 Gob. Aragón) and GeoKin3DPyr project INTERREGIIIa (CTP).

La actitud esencialmente es: tomar conciencia de la realidad.

No aceptar sin crítica propia, no aceptar sin discusión interior todo lo que nos dicen.

José Luis Sampedro

Se conoce que todo esto antes era mar

y los fósiles son las raspas de los pescaos.

Petra Sabio

Alberto Aragón. *Jorge y las sirenas.*

Agradecimientos

Este trabajo es el fruto de la colaboración de numeras personas e instituciones, cuyas aportaciones han contribuido tanto desde el punto de vista científico como desde el personal. En primer lugar quisiera agradecer a Emilio Pueyo y Antonio Casas, el conocimiento, cariño y comprensión prestados a lo largo de estos años. Por las facilidades con las que he contado para el desarrollo de este trabajo y por haberme animado a colaborar con otros centros. También quisiera agradecer el constante apoyo científico y anímico de Antonio Barnolas, cuyo profundo conocimiento del Pirineo ha quedado parcialmente aquí plasmado. Ellos son mis chamanes espirituales, excelentes geólogos pero mejores personas.

A los investigadores que han participado en los proyectos conjuntos y especialmente a los que han colaborado en la elaboración de las publicaciones relacionadas con la tesis, Josep Serra-Kiel, Javier Ramajo, Chema Samsó, Josep Sanjuán y Carles Marín-Closas por enseñarme otros puntos de vista y por los datos cedidos. También quiero agradecer las cuidadosas revisiones hechas por Josep Poblet, Richard Lisle, Dave Anastasio, Jaume Dinarès, Rob Van der Voo, Antoni Teixell y otros revisores anónimos que han ayudado a mejorar significativamente los artículos y el cuerpo de la tesis. Con especial cariño agradezco a Juanjo Villalaín y Borja Antolín la paciencia de iniciarme en el paleomagnetismo de laboratorio, a cualquier hora y distancia. En mi paso por los diversos laboratorios he tenido la suerte de contar con la ayuda de Ángel Carrancho (U. Burgos), Erwin Appel (U. Tübingen), Ken Kodama, Dario Bilardello y Dave Anastasio (Lehigh, USA), Fabio Speranza, Marco Maffione y Leonardo Sagnotti (INGV, Roma), y con las mediciones y consejos de Bet Beamud y Elisenda Costa (CSIC Barcelona, donde aún tengo que ir). Gracias a Antonio Barnolas y Alejandro Robador por la base cartográfica. Los momentos más felices pertenecen a las intensas campañas de muestreo en las cuales me ayudaron cantidad de mujeres de acero como Victoria Lafuente, Adriana Rodríguez, Cristina Pérez, Carlota Oliván, Ruth Soto e Inma Gil y hombres de nube como mi padre Pedro Mochales, Sergio Segura, Galo San Miguel y los tres chamanes. También quiero agradecer la ayuda de Nieves López, tristemente fallecida el años pasado, y de Geosfera (María Presumido y Juan A. Cárdaba) durante el muestreo biostratigráfico. A Sylvia Gracia y Belén Oliva, quienes se pegaron una currada midiendo muestras para ASM. A Ana Arauzo que me ayudó con las medidas magnéticas. Con especial cariño recuerdo las semanas de campo con Cai Puigdefàbregas de quien aprendí mucho. Quiero agradecer la bondad y comprensión de Antonio Azcón, mi jefe durante estos años, a las chicas del IGME su alegría y buñuelismo cotidianos, en especial a Lupe Piñón (creadora de la portada) y Ruth Soto por el continuo apoyo logístico. También quiero agradecer el cariño de todos los compañeros del IGME Zaragoza y del Dep. Geodinámica Interna (UZ). Gloria de la copistería Bruno Solano que siempre me facilitó las tareas de reprografía. Pedro del Río compañero, Manuela Harto de tercer ciclo, Nieves Iso y Enrique Arranz del Dep. Ciencias de la Tierra me informaron y asesoraron con la burocracia. Carlos Liesa y Andrés Pocoví con la literatura y Julen Urdangarín con el mundo informático. Gracias al IGME por la beca pre-doctoral que financió esta tesis y al Programa Europa (CAI-DGA) que financió las estancias de Alemania y Roma.

Con gran amor recuerdo mis estancias en Casa Piquero (Sieste) a lo largo de toda la tesis, donde Teresa y Alegría me trataron como en casa. Zumo de vida en Riofrío del Llano (Guadalajara) y Rodenas (Teruel). Gracias a mi panda de teatro "las cabezas pensantes", la de veterinari@s, geólo@as del foro y el löka, por tantos años de risas juntos. Agradezco el abrazo de los amigos que hice durante las estancias, en especial los Tübingueros. A mi familia Pedro, Lola, Pedrito y Marián por su apoyo incondicional a lo largo de tantos años, por escucharme y alentarme cada día. Al cariño y entusiasmo que me proporciona el resto de familia en cada encuentro. A los soles que iluminan mi cielo: Silvia, Rebeca, Alberto (artista de la primera página), Luchi, Victoria, Raquela, Olmo, Borja, Joana, Irene, Leo, Jorge, Elena, Elías, Analía, Paloma, Cris, Carlota, Félix…por hacerme este mundo más amable y en especial a Sergio por su inagotable apoyo, amor y fuerza. A quienes me he olvidado en estas líneas, que seguro que tengo mucho que agradecerles.

Por siempre en mi corazón.

INDEX

RESUMEN **1**

OBJECTIVES

1. Objectives **5**

1.1. Definition of this research 5

1.2. Goals of this project 6

FIRST PART: GEOLOGICAL SETTING

2. The Pyrenean Orogen **11**

2.1. Introduction 11

2.2. Structural partitioning of the Pyrenean range 15

2.3. Crustal-scale structure of the Pyrenees 18

2.4. Evolution of the Pyrenees 20

2.4.1. Paleogeography 20

2.4.2. Structural evolution 21

2.5. The South Pyrenean Central Unit (SPCU) 23

2.6. The Ainsa Basin 25

2.7. Oblique structures of the SPCU 29

3. Study area **31**

3.1. Stratigraphy 31

3.2. Structure 41

3.2.1. Foreland Basin development 41

3.2.2. The Sobrarbe synclinorium 41

3.2.2.1. The Boltaña anticline 42

3.2.2.2. The Mediano anticline 43

3.2.2.3. The Buil syncline 43

3.2.3. Cross-sections 44

3.2.3.1. Perpendicular cross-sections 45

3.2.3.2. Along-strike cross-sections 49

3.3. Previous paleomagnetic and AMS data 49

3.3.1. Magnetostratigraphic studies 50

3.3.2. Vertical Axis Rotations (VAR) studies 56

3.3.3. AMS studies 62

SECOND PART: METHODS AND RESULTS

4. Methods applied to the study area **69**

4.1. Introduction 69

4.2. Demagnetization 70

4.3. Stability tests 73

4.4. Applications to paleomagnetism 75

4.4.1. Magnetoestratigraphic dating 75

4.4.1.1. Laboratory and processing procedures 76

4.4.2. Structural Geology and Tectonics 76

4.4.2.1. Laboratory and processing procedures 78

4.5. Rock magnetism 79

4.5.1. Laboratory and processing procedures 80

4.6. Anisotropy of the Magnetic Susceptibility (AMS) 82

4.6.1. Laboratory procedures 83
4.7. Instruments 84
5. Magnetostratigraphy of the Boltaña anticline and the Ainsa Basin* 89
5.1. Chonostratigraphic frame and need of this work 89
5.2. Paleomagnetic methods. 90
5.2.1. Sampling 90
5.2.1.1. Ara River and Bal Ferrera sections 93
5.2.1.2. Coscollar secion 96
5.2.1.3. Mondot section 100
5.2.1.4. Eripol section from Bentham (1992) 102
5.2.2. Laboratory procedures 102
5.3. Biostratigraphic methods. 104
5.3.1. Sampling 104
5.3.2. Laboratory procedures 108
5.4. Results 108
5.4.1. Paleomagnetic directions 108
5.4.1.1. Ara River and Bal Ferrera sections 108
5.4.1.2. Coscollar secion 111
5.4.1.3. Mondot section 112
5.4.1.4. Reprocessing of the Eripol section 113
5.4.2. Rock magnetic properties 113
5.4.3. Origin of magnetic noise 116
5.4.4. Paleomagnetic stability 117
5.4.5. Biostratigraphic data 118
5.4.5.1. Ara River section 118
5.4.5.2. Coscollar section 119
5.4.5.3. Mondot and Eripol sections 121
5.5. Interpretation 122
5.5.1. Correlation with the GPTS 122
5.5.2. Sedimentary implications 126

* Mochales, T., Barnolas A., Pueyo E.L., Serra-Kiel J., Casas A.M., Samsó J.M., Ramajo J.; Sanjuán J., 2011a. Chronostratigraphy of the Boltaña anticline and the Ainsa Basin (Southern Pyrenees). Geological Society of America Bulletin (*accepted*)

6. Rotational kinematics of oblique structures: the Boltaña anticline 129**
6.1. Introduction 129
6.2. Paleomagnetic methods 130
6.2.1. Sampling 130
6.2.2. Laboratory procedures 137
6.3. Results 137
6.3.1. NRM components 137
6.3.2. Paleomagnetic stability 141
6.3.3. Reliability of data 142
6.4. Interpretations 142
6.4.1. Rotation magnitudes 142
6.4.2. Rotation dating 145
6.4.3. Paleomagnetic sequential restoration of the western flank of the Boltaña anticline (San Felizes area) 145

6.4.4. Paleocurrents and fold axis restoration 153

** Mochales, T.; Casas, A.M.; Pueyo, E.L.; Barnolas, A., 2011b. Non-steady rotational kinematics of oblique structures; a case study in the Boltaña anticline (Southern Pyrenees). Journal of Structural Geology (*accepted*).

** Mochales, T.; Pueyo, E.L.; Casas, A.M.; Barnolas, A., 2011c. Restoring paleomagnetic data in complex superposed folding settings: the Boltaña anticline (Southern Pyrenees). Geologica Acta (*in review*).

7. Anisotropy of magnetic susceptibility record of the kinematics of the Boltaña anticline* 157**

7.1. AMS as kinematics indicator. 157
7.2. AMS methods 158
7.2.1. Sampling 158
7.2.2. Laboratory procedures 162
7.3. Results 163
7.3.1. Magnetic mineralogy and scalar parameters 163
7.3.2. Directional and tensional data 165
7.3.3. Significance of directional data 171
7.4. Interpretation 174
7.4.1. Magnetic mineralogy and scalar parameters 174
7.4.2. Interpretation of scalar parameters 176

*** Mochales, T., Pueyo, E.L., Casas, A.M., Barnolas, A. and Oliva-Urcia, B., 2010, Anisotropic magnetic susceptibility record of the kinematics of the Boltaña Anticline (Southern Pyrenees): Geological Journal, v. 45, p. 562-581, doi: 10.1002/gj.1207.

*** Mochales, T., Pueyo, E.L., Casas, A.M., and Barnolas, A., 2010, Kinematic approach by means of AMS study in the Boltaña anticline (southern Pyrenees). Trabajos de Geología, Vol. 30, 95-87.

THIRD PART: DISCUSSION

8. Discussion and integration of results within the South Pyrenean Tectonosedimentary evolution. 179

8.1. Summary of acquired data. 179
8.2. Kinematic model 183
8.3. Basin-scale implications 190
8.3.1. Accumulation rates 190
8.3.2. Sedimentary implications 192
8.3.3. Thrust kinematics at regional scale 192
8.3.4. Dating the end of the Boltaña folding 194
8.3.5. Rotational kinematics in the South-Central Pyrenees 195
8.3.6. Map-view restoration 197
8.3.7. Relations between accumulation and rotational velocity rates 198

9. Conclusiones 203
10. References 207

Resumen

El interés científico que tradicionalmente ha suscitado la cuenca de Aínsa reside en la configuración oblicua de sus estructuras, implicadas en un contexto sintectónico caracterizado por el registro continuo de la secuencia estratigráfica Eocena. Por otra parte, el mundo de la investigación petrolera también ha centrado sus estudios en esta zona debido a que la secuencia turbidítica de la cuenca de Aínsa constituye un modelo análogo de reservorio excepcionalmente conservado. Dentro de este contexto, el anticlinal de Boltaña es de especial relevancia puesto que supone el límite estructural entre la cuenca siliclástica de Graus-Tremp y la cuenca turbidítica y molásica de Jaca y a su vez, constituye el límite occidental de la Unidad Surpirenaica Central, confiriendo un interés adicional a la compleja evolución de esta estructura oblicua.

En este sentido, en la primera parte de este trabajo se plantean los objetivos (capítulo 1) que proponen descifrar los pormenores cronológicos y cinemáticos de la cuenca de Aínsa y en particular del anticlinal de Boltaña. A continuación se trata el contexto geológico de la zona de estudio (capítulos 2 y 3) basado en el conocimiento previo. En el caso del capítulo 2 se explica la geología del orógeno pirenaico desde la escala de placa a la de cabalgamiento. En este capítulo se expone la evolución de la cuenca de Aínsa (sección 2.6) y de las estructuras oblicuas a la dirección predominantemente pirenaica (sección 2.7). En el capítulo 3, sección 3.1., una cartografía inédita (Barnolas et al. *in press* a y b), diversas columnas estratigráficas y la correlación lateral de las unidades involucradas ilustran la estratigrafía de la zona de estudio. Desde el punto de vista de la estructura de la zona (sección 3.2), los pliegues integrantes del sinclinorio del Sobrarbe son descritos (sección 3.2.2) en relación a los cortes geológicos compensados realizados por diversos autores (Millán, 2006; Soto et al, 2001; Fernánadez-Bellón, 2004) en la sección 3.2.3. A continuación, se describen los trabajos realizados por otros autores en la zona de estudio por medio de métodos afines a los empleados en esta tesis (sección 3.3.). Estos métodos son el paleomagnetismo, tanto su vertiente magnetoestratigrafica (sección 3.3.1.) como la aplicada a caracterizar rotaciones de eje vertical (VAR, sección 3.3.2.), y la anisotropía de la susceptibilidad magnética (AMS, sección 3.3.3.).

Una vez introducido el problema y contexto geológico en cuestión, la segunda parte de la tesis comienza con el capítulo 4 donde se exponen los principios básicos de los métodos aplicados a la zona de estudio. Se abordan aspectos relacionados con el análisis en el laboratorio de las componentes de la magnetización remanente natural (sección 4.2.), pruebas de estabilidad (sección 4.3), aplicaciones del paleomagnetismo para la datación de rocas o como solución de problemas estructurales (sección 4.4.), magnetismo de rocas (sección 4.5.) y la aplicación de la anisotropía de la susceptibilidad magnética (sección 4.6.).

Tal y como se describe en la sección 3.3.1. existen numerosos estudios magnetoestratigráficos en la vertiente surpirenaica, sin embargo la cuenca de Aínsa carecía hasta el momento de una datación independiente que permitiese determinar la edad de los materiales involucrados (capítulo 5). Con este objetivo, se realizó un muestreo de 2450 m de serie (sección 5.2.1.), con una densidad media de una muestra de cada 2.7 m, llevando a cabo 914 desmagnetizaciones con fines magnetoestratigráficos. En

este capítulo se detallan las campañas de muestreo realizadas, las cuales se dividen en tres grandes perfiles denominados río Ara, Coscollar y Mondot. El perfil río Ara se localiza en la porción septentrional, flanco oeste del anticlinal de Boltaña donde puede encontrarse un registro continuo de la serie Ypresiense de plataforma (desde la caliza de alveolinas a la Fm Boltaña). A través de un perfil principal y cuatro subperfiles auxiliares destinados a completar la serie estratigráfica, se cubrieron 1008 m con 347 muestras. El perfil Coscollar está compuesto por ocho subperfiles contiguos (355 muestras) en la parte meridional del flanco este del anticlinal de Boltaña. Este perfil atraviesa 965 m de sedimentos pertenecientes a facies de talud siliciclástico de las Fms San Vicente y Sobrarbe de edad Luteciense. A fin de unir ambos perfiles se realizó una sección de conexión de 90 m abarcando el techo de la Fm Boltaña y la base de la Fm San Vicente en la zona con mejor exposición (perfil de Bal Ferrera). A continuación del perfil Coscollar se muestreó el perfil Mondot, compuesto por dos subperfiles de edad Luteciense superior-Bartoniense inferior, que por medio de 172 muestras abarcaron 417 m se serie estratigráfica. Los materiales muestreados corresponden a la transición marino-continental a través de sedimentos deltaicos (techo de la Fm San Vicente, Fm Sobrarbe y base de la Fm Escanilla). A techo de la serie muestreada, se incluyó y reinterpretó parcialmente el perfil Eripol (Bentham, 1992), constituido por 63 muestras distribuidas a lo largo de 840 m de serie. Este perfil se encuentra integrado en los materiales continentales de la Fm Escanilla.

Las muestras obtenidas fueron analizadas en los laboratorios de paleomagnetismo de la Universidad de Burgos, Institut de Ciencies de la Terra "Jaume Almera" CSIC- Universitat de Barcelona, Universität Tübingen (Alemania), Lehigh University (Pensilvania, USA) e INGV Roma (Italia), consultar la sección 5.2.2. Por medio de estos análisis se ha podido determinar que los principales minerales portadores de la magnetización de las rocas estudiadas son magnetita y contenidos variables de sulfuros, con un contenido creciente de hematites en facies continentales (secciones 5.4.2. y 6.3.1.). El registro del campo magnético Eoceno es estable tal y como indican las tests realizados (secciones 5.4.4. y 6.3.2.). Esta magnetización primaria ha permitido establecer un patrón de 20 magnetozonas identificable y correlacionable con la escala de tiempo de polaridad magnética (GPTS, Gradstein et al., 2004). 15 muestras biostratigráficas conformadas por nummulites y alveolinas, provenientes de estudios previos no publicados, así como una muestra constituida por carofitas, resultado de una campaña piloto de muestreo realizada en la Fm Escanilla, han contribuido a anclar la secuencia de polaridad local obtenida en este trabajo de acuerdo con la GPTS.

Por medio del establecimiento de este marco cronoestratigráfico local, las formaciones involucradas en este estudio han podido ser acotadas con precisión entre el Ilerdiense (Ypresiense) y Priaboniense, crones C24r a C15, abarcando un lapso de tiempo de casi 20 M.a. Esta correlación se encuentra en la figura 27 del capítulo 5. Por medio de este control cronoestratigráfico, se han deducido las tasas de acumulación a lo largo de todo el perfil, pudiendo identificarse tres episodios sedimentarios relacionados con el desarrollo de la plataforma carbonatada Eocena.

Desde el punto de vista de las rotaciones de eje vertical, las investigaciones previamente realizadas en la cuenca de Aínsa (Parés y Dinarès, 1993; Pueyo, 2000; Fernández-Bellón, 2004; Oms et al., 2006) sugerían la actividad rotacional coetánea al plegamiento durante el intervalo Luteciense, tal y como sucede en el anticlinal de Mediano (Fernández-Bellón, 2004). Sin embargo, los resultados obtenidos por medio de campaña piloto de este estudio parecían indicar que en el caso del anticlinal de

Boltaña el crecimiento del anticlinal y su rotación fueron diacrónico (Mochales et al., 2008), alentándonos a intentar determinar con mayor precisión la edad y magnitud de ambos episodios.

Con este objetivo, se consideraron 72 estaciones de rotación (capítulo 6): 34 derivadas de la discretización de los datos magnetoestratigráficos propios, 20 nuevas estaciones localizas en zonas de especial relevancia para la determinación de la rotación del anticlinal, 11 procedentes del reprocesado de cuatro perfiles previos ubicados en el sinclinal de Buil (Bentham, 1992) y 7 estaciones discretas distribuidas en la zona de estudio (Dinarès, 1992; Parés y Dinarès, 1993; Pueyo, 2000), muestreo incluido en la sección 6.2.1. Las estaciones y discretizaciones de los perfiles magnetoestratigraficos proveyeron valores de rotación horaria que oscilan desde 67º (+/- 14.1) a 1º (+/-7.3), con valores promedio de 36º (+/-3.2, datos numéricos en la tabla 1 del capítulo 6). Por medio del conjunto de 791 muestras consideradas (543 desmagnetizadas y 248 reprocesadas del trabajo de Bentham, 1992) y su calibración temporal basada en el estudio magnetoestratigráfico (capítulo 5), se han podido obtener valores de rotación cada 2 M.a muy robustos estadísticamente que oscilan entre 55º (+/- 12.5) y 2º (+/1.5). La evolución temporal de estos valores de rotación agrupados por edades ha permitido detectar varios patrones posibles de descenso de la rotación (sección 6.4.1, figura 15). La evolución de la rotación puede disociarse en una primera etapa de ligera actividad rotacional no significativa durante el Ilerdiense-Luteciense Medio-Superior, con una tasa de 1.2º/M.a. que podría acomodar hasta 15º de rotación. Sin embargo, a partir del límite Luteciese-Bartoniense (41-40 M.a.) se observa un aumento de la tasa de rotación, alcanzando valores de hasta 6.2º/M.a. y extinguiéndose en el Priabonianse medio. Este periodo de rotación significativa acomodaría 37º de rotación horaria y comenzaría en la parte superior de la Fm Sobrarbe para finalizar a techo de la Fm Escanilla.

Teniendo en cuenta esta rotación en el conjunto de la cuenca de Aínsa, las paleocorrientes obtenidas en trabajos anteriores pueden ser restituidas de acuerdo con la configuración previa a la rotación del anticlinal de Boltaña. 170 paleocorrientes compiladas de la literatura (Van Lunsen, 1970; De Federico, 1981; Mutti, 1985; Barnolas et al., *in press* a y b) indican una proveniencia media de dirección SE para las paleocorrientes más antiguas (Luteciense-Bartoniense), que habrían sido rotadas hasta adquirir su configuración N-S actual. Sin embargo, las paleocorrientes más modernas (Bartoniense-Priaboniense) muestran un orientación NW-SE. La restitución de las orientaciones previas a la rotación da lugar a una confluencia de las orientaciones de acuerdo con la geometría del surco turbidítico Eoceno de dirección SE-NW (este análisis es ampliamente detallado en la sección 6.4.3.). Teniendo en cuenta la deformación polifásica que afecta a las estaciones ubicadas en dicho surco turbidítico, en el flanco oeste del anticlinal de Boltaña (la denominada área de San Felizes), se ha desarrollado una restitución secuencial de las direcciones paleomagnéticas. Se ha verificado que esta zona se encuentra afectada tanto por el plegamiento del anticlinal de Boltaña (Luteciense) como por la deformación posterior del sinclinal del Guarga (Olicoceno-Mioceno). La restitución secuencial progresiva considerando ambos episodios disminuye los errores globales y aumenta de la fiabilidad de los resultados obtenidos (sección 6.3.4.).

Por medio de la anisotropía de la susceptibilidad magnética (capítulo 7) y los análisis de magnetismo de rocas realizados en la muestras de edad Ilerdiense-Luteciense (muestreo en la sección 7.2. y mineralogía magnética en 7.3.1.), se ha llegado a la conclusión de que la fábrica magnética refleja la orientación preferente mineral, en particular de los filosilicatos. Esta orientación mineral ha

sido capaz de registrar los efectos de deformación tectónica en un momento inmediatamente posterior al depósito (s.l.), siendo bloqueada en las primeras etapas de diagénesis y comportándose como un indicador pasivo de la deformación posterior. El análisis de la ASM en la etapa pre-tectónica parece registrar la orientación preferente causada por efectos tectónicos lejanos (*far-field*). Las rampas oblicuas del cabalgamiento del Cotiella (situado al NE) dejarían su impronta en la lineación magnética de la etapa Ilerdiense, mientras que los efectos de los cabalgamientos de zócalo (localizados al N) quedarían registrados en las rocas Cuisienses y Lutecienses (sección 7.4.4.). A partir del Luteciense inferior ya se percibirían los efectos del plegamiento del anticlinal de Boltaña *(near-field*), puestas de manifiesto por una orientación preferente mineral marcadamente constante, aunque las evidencias cartográficas parezcan indicar que el plegamiento no comenzó antes del Luteciense Medio.

Con los datos obtenidos en este trabajo por medio de diferentes técnicas y los datos de autores anteriores, se ha desarrollado un capítulo de discusión (capítulo 8) donde se propone un modelo evolutivo para los sucesivos episodios de deformación acaecidos en el anticlinal de Boltaña (sección 8.2., figuras 5 y 6). La rotación registrada en el anticlinal de Boltaña sería posterior a la etapa principal de plegamiento, estando probablemente asociada a una lámina de movimiento inferior y más joven. (Tozal-Alcanadre; Millán, 1996).

En este último capítulo también se lleva a cabo una ampliación de escala y se comparan los datos obtenidos a escala local con aquellos obtenidos en las áreas contiguas (sección 8.3.). En el caso de los resultados obtenidos en el campo de la magnetoestratigrafía, se han comparado las tasas resultantes con las obtenidas por otros autores en cuencas adyacentes (Bentham 1992; Beamud et al., 2003; Oms et al., 2003). Se observa una migración de la subsidencia hacia el Oeste, acorde con el desarrollo de la deformación en el frente surpirenaico, progresivamente más joven hacia el oeste (ver la figura 7 del capítulo 8). Considerando los valores de rotación obtenidos en áreas adyacentes, se observa que la cuenca Surpirenaica sufrió un gradiente moderado de acortamiento, originando rotaciones horarias de baja magnitud durante su deformación (20-30º, ver la figura 8 de este capítulo), detectadas tanto en las Sierras Interiores como Exteriores. Sin embargo en la zona comprendida entre los anticlinales de Mediano, Boltaña y Balzes se llegan a acomodar hasta 50-60º, que no son detectados en las estructuras frontales de la USPC (ver figura 8, capítulo 8). El desplazamiento diferencial (de origen no resuelto hasta el momento) parece condicionado por rampas oblicuas de estructuras extensionales previas y el espesor de sustrato triásico y sería el responsable de la rotación significativa de la zona de estudio.

1. Objectives

1.1. Definition of this research

This work deals with timing, kinematics and origin of oblique structure present in the Southern Pyrenees using as a main tool paleomagnetism in its broadest sense; both as a dating tool and as a way to obtain vertical-axis rotations. Moreover, analyses of the Anisotropy of the Magnetic Susceptibility (AMS) have been performed to decipher additional details of the kinematics of structures. These approaches have been especially focused on the Boltaña anticline and nearby areas. The interest of this structure lies in its present orientation (N-S), oblique* with regard to the dominating Pyrenean trend (ESE-WNW). The location of the Boltaña anticline, at the boundary between the siliciclastic Tremp-Graus Basin and the turbiditic and molasse Jaca basin (the so-called Aínsa basin), as well as its structural position at the western limit of the South Pyrenean Central Unit, add interest to the interpretation of its complex evolution. The implications of the kinematics of the Boltaña anticline in the evolution of the turbiditic Aínsa Basin (that is commonly used as a model of turbiditic deposition in slope areas) has aroused the traditional interest of a broad number of scientists and oil companies. The vast amount of studies here developed allows us for relying on a well-known area whose temporal framework is not yet accurately unravelled.

The arrangement of this report has been done according to the disciplines used to establish the kinematics of the Boltaña anticline and its temporal framework. Chapters two and three focus on the geological setting based on previous investigations. The second chapter explains the geological frame from the plate scale to the scale of thrust sheets. There, the crustal structure and the partitioning of the Pyrenees are detailed. The third chapter is related to detailed stratigraphic and structural features of the Aínsa Basin and the Boltaña anticline. Previous paleomagnetic studies involved in the study area are overviewed in this chapter as well. The fourth chapter deals with the metholodogy applied in this study. Here the paleomagnetic and magnetic fabric principles are centred on the relevant aspects for this work.

Once focused the study area, the main body of PhD is developed in the following chapters. The different kinds of new data produced in this work are described separately. The chapter number five presents the magnetostratographic study carried out in the Aínsa Basin. It is based in the continuous sampling performed throughout the Eocene rocks. It deals mainly with dating questions and therefore paleomagnetism, biostratigraphy and mapping achieved special relevance in this chapter.

The sixth chapter analyzes the problem of the oblique structures of the South-Pyrenean Zone, namely the western boundary of the South Pyrenean Central Unit (SPCU) where the Boltaña anticline is located, from several points of view. From the kinematics point of view, the analysis of the pretectonic, syntectonic and postectonic sequences by means of the study of Vertical Axis Rotations (VAR) is performed.

*Oblique structure is defined as a structure with whose oblique to the main trend of a range.

Deviations with respect to the Eocene reference, are interpreted as VARs. From the methodological point of view, this chapter points the problem of the VAR implications in areas with several deformation stages. A particular area, where the Boltaña anticline and Guarga thrust have strong influence, was selected (San Felizes area at the western flank of the Boltaña anticline). In this section, direct and sequential restorations of complex folding settings are evaluated.

In the seventh chapter, kinematics and internal deformation of the sedimentary sequence is studied by means of AMS. The vast dataset and the continuity of the series allow for deducing the fluctuations of the magnetic fabric throughout the stratigraphic log. By means of this study, far and near tectonic stress fields can be interpreted to influence deformation in relation to the anticline history.

Each chapter presents a discussion dealing with the local implications of the results obtained. Nevertheless, in chapter number eight the applied techniques are put in common and an integrative kinematic model is proposed. Besides the basinal implications and the macro-structures involved in the kinematics of the local features are considered in this chapter.

1.2. Goals of this project

This thesis is the result of almost five years of paleomagnetic studies in the Southern Pyrenees. Nearly five months of paleomagnetic fieldwork (Figures 1 and 2) and nine months of laboratory measurements were accomplished (Figure 3). The project was designed with the following objectives:

- To locate the structural and stratigraphic advances in the knowledge of the Aínsa Basin within an absolute temporal framework by defining the pattern of magnetozones, that reflects the polarity reversals recorded in the strata involved in folds in the sedimentary sequence. Correlation with the Global Polarity Time Scale (Gradstein et al., 2004) will allow to accurately date geological events and temporal boundaries. This could help for future research related to paleogeographical reconstructions at the local (South-Pyrenean basin) or regional (i.e. western Tethys) scale.

- The selection of the best-defined paleomagnetic directions allows for, benefiting from the temporal framework established by means of magnetostratigraphy, determining the magnitude and temporal evolution of Vertical Axis Rotations (VAR) throughout the sequence along the compressional period. The control of the evolving VARs led towards the final objective of understanding the rotational kinematics of the Boltaña anticline.

- The final objective is to build geometric models, using AMS, that provides information about the deformation of sediments, that might be useful to unravel the deformation occurred in the South Pyrenean foreland basin. These goals will help to reconstruct the emplacement of one of the most significant oblique structures of this part of the Pyrenees, the Boltaña anticline. Analysis of the structures whose emplacement pre- and post-date the Boltaña anticline will also help deciphering the structural evolution of the study area.

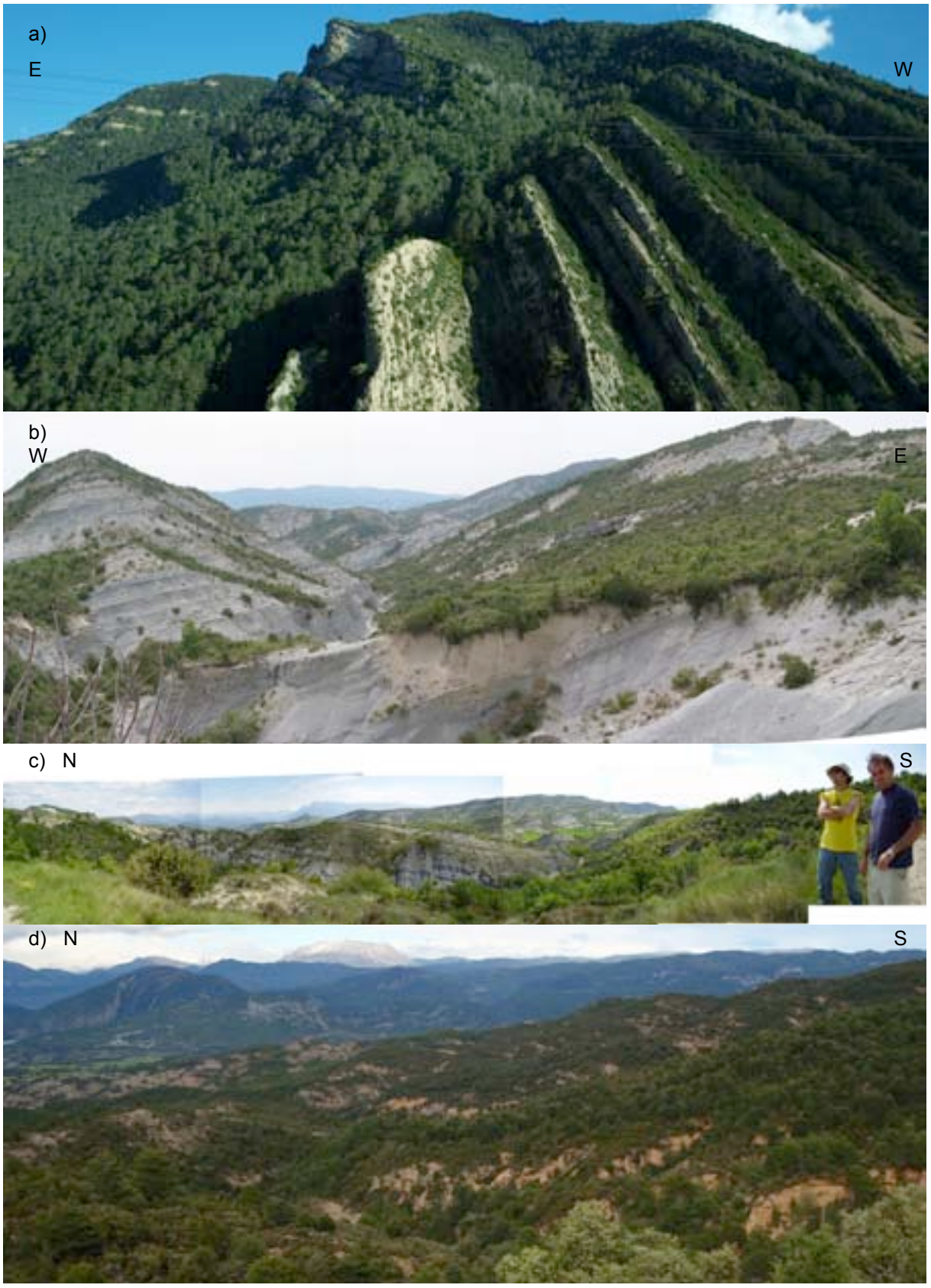

Figure 1. a) Boltaña anticline where the Boltaña Fm is well exposed, near Jánovas. b) Anoxic level at the top of the San Vicente Fm, near Mondot. c) Deltaic progradation of the Sobrarbe Fm, near Castellazo. d) In the foreground the Escanilla Fm and background the Mediano anticline.

Figure 2. Fieldwork during the development of this PhD.

Figure 3. Laboratory of Paleomagnetism of the University of Burgos (shielded 2G Cryogenic) and laboratory of magnetic fabrics (KLY3) of the Geotransfer Research Group, University of Zaragoza.

2. The Pyrenean Orogen

2.1. Introduction

The North Atlantic opening and the subsequent clockwise rotation of the African plate during Cretaceous and Tertiary times produced a general compression along the Tethys margins. In its western side, the Pyrenees, Iberian Range and the Betics-Rift underwent lower shortening related to this geodynamic process in comparison to eastern areas (Alps, Figure 1). During the Alpine orogenic stage, intraplate compressional stresses controlled basin inversion, crustal thickening and lithospheric folding. Variably deep crustal roots characterize the Alpine orogenic chains (Ziegler and Dèzes, 2006).

According to some reconstructions, four hundred km of shortening took place between the Iberian and Eurasian plates in the Pyrenean domain during the opening of the Bay of Biscay (from 118 to 80 M.a., Sibuet et al., 2004). The ECORS seismic reflection profile and teleseismic data show the presence of two distinct slabs dipping to the north. The southern slab is associated to the subduction of the neo-Tethys Ocean, which was formed from late Jurassic to early Aptian (Figure 2). Coevally, elongated back arc basins formed along the future Pyrenean domain (Sibuet et al., 2004). The northern one, active from 85 M.a. is linked to the subduction of the lower continental crust located south of the Pyrenean domain. In the upper crust, normal faults and the north Pyrenean fault became reverse faults and former arc basins were inverted, originating the uplift of the Pyrenees as a double verging wegde (Sibuet et al., 2004), figure 2.

By means of up-to date kinematic data, based on magnetic anomalies in the Atlantic ocean, a geodinamic model of the relative motions of Africa-Iberia and European plates was proposed (Figure 3, Rosenbaum et al., 2002). Convergence of Africa with respect to Europe commenced between 120 to 83 M.a. This motion depended on fluctuations in convergence rates characterised by two periods of relatively rapid convergence (Late Cretaceous and Eocene-Oligocene times) alternated with periods of relatively slower convergence (during the Paleocene and since the Early Miocene). Several stages of Iberian-Europe plate kinematics can be recognised (Figure 3): 1) Left-lateral strike-slip motion in Late Jurassic-Early Cretaceous; 2) Late Cretaceous convergence; 3) Paleocene quiescence; 4) Short period of right lateral strike-slip motion; 5) Final Eocene-Oligocene convergence (Rosenbaum et al., 2002).

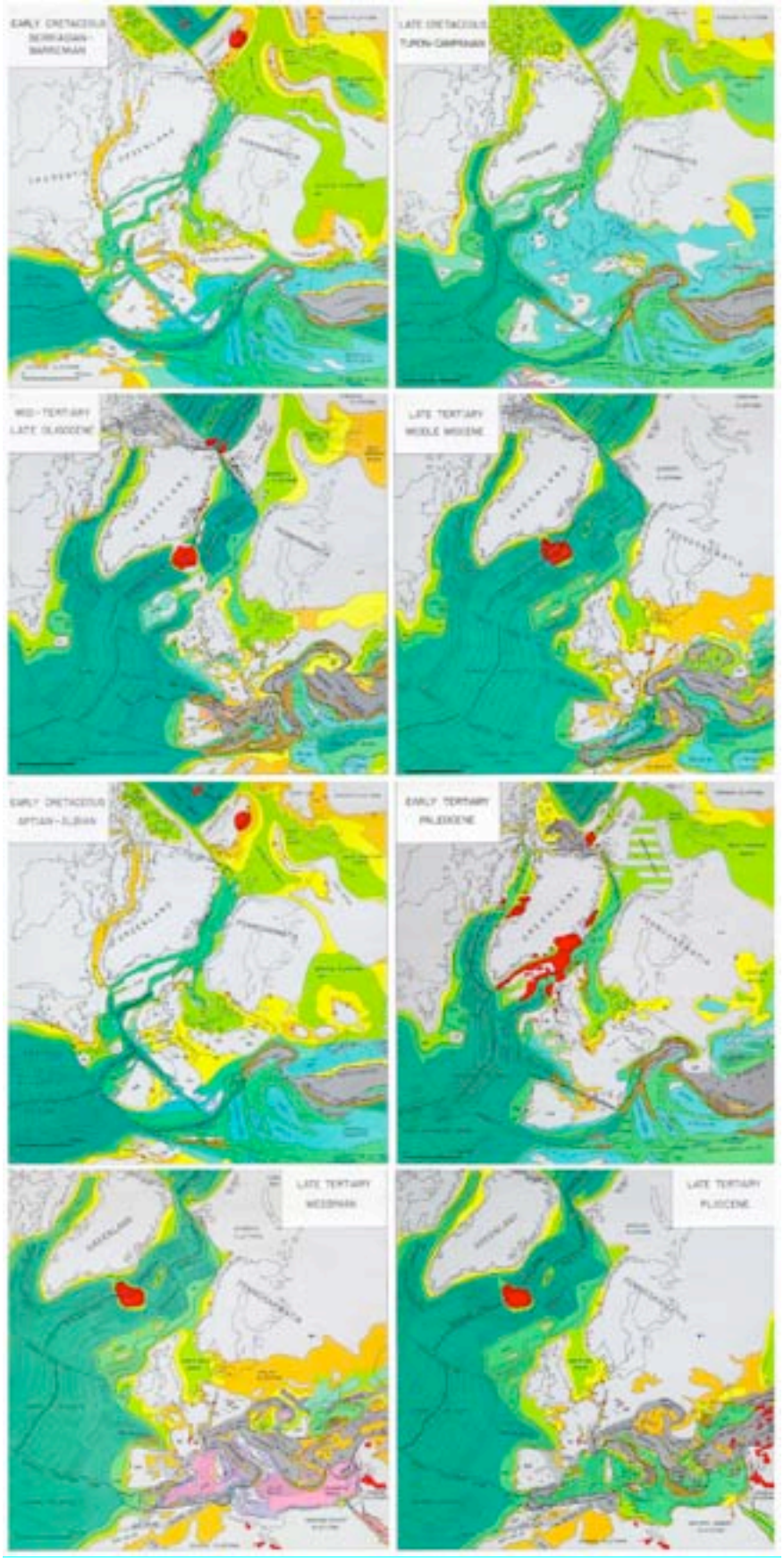

Figure 1. Plate motions, plate-interaction and evolution of rifted basins (Ziegler et al., 2001).

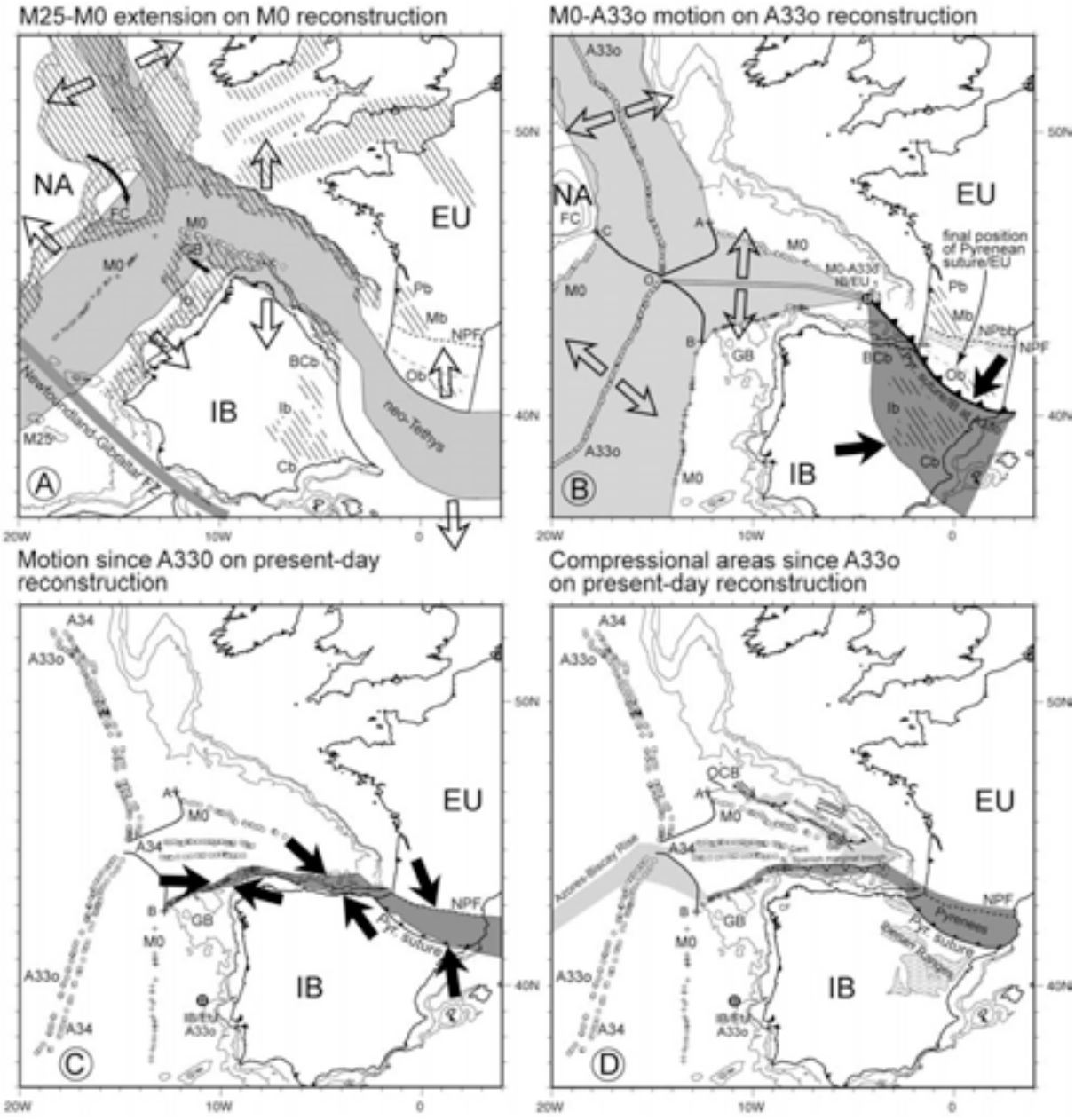

Figure 2. A) Reconstruction of continents at Early Cretaceous where EU (Europe) is supposed fixed. Gray indicates the amount of extension from Late Jurassic to Early Cretaceous. Arrows show the directions of the plate motions. B) Plate reconstruction for Late Cretaceous. Dark grey indicates the amount of convergence in the Pyrenean domain and black arrows convergent motions. C) and D) Plate motion from Late Cretaceous to present. In D light and dark grey represent minor and intense deformation (Sibuet el al., 2004)

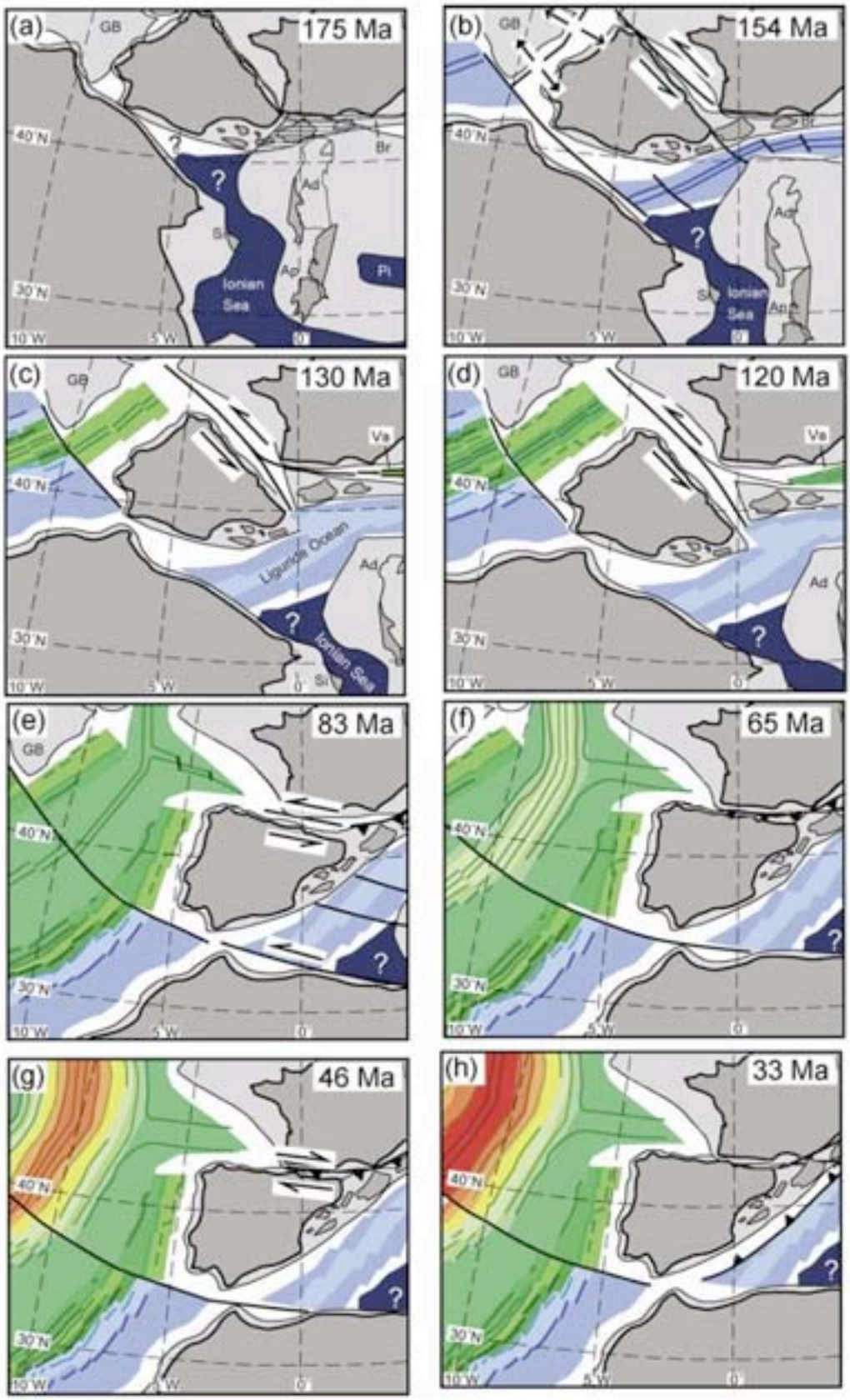

Fig. 3. Reconstruction of the western Tethys since Middle Jurassic using rotation parameters for Africa, Iberia and Europe (after Rosenbaum et al., 2002 and references therein).

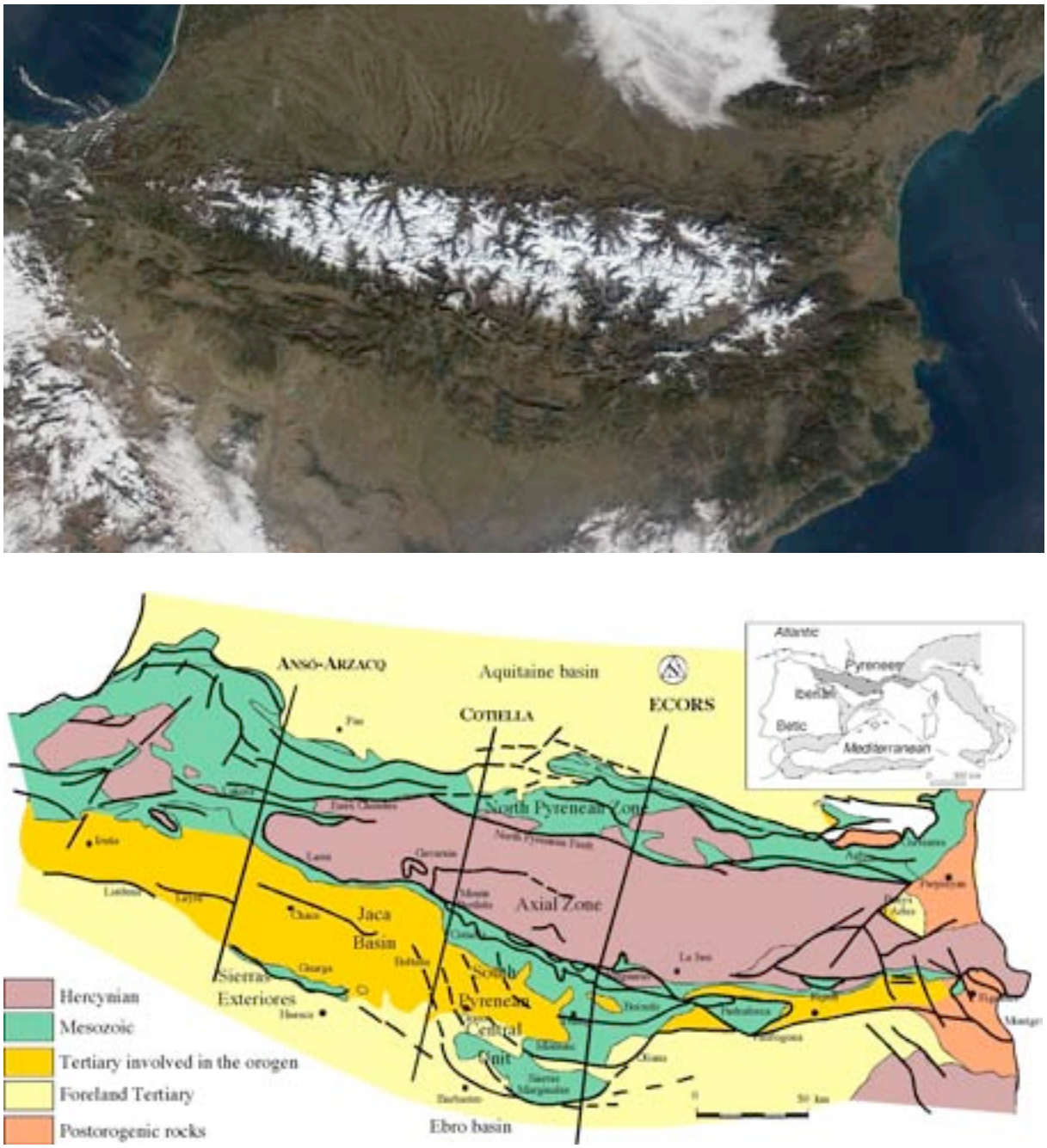

Figure 4. Orthophoto (extracted from http://visibleearth.nasa.gov/) and geological sketch of the South-Central Pyrenees (modified from Pueyo 2000).

2.2. Structural partitioning of the Pyrenean range

The Pyrenees is a double-verging orogenic accretional prism (Olivet, 1996), characterized by fold and thrust systems involving upper crust (Choukroune and Séguret, 1973; Muñoz, 1992). The ECORS-Pyrenees section and subsequent deep seismic profiles performed in the Pyrenean Range (ECORS-Arzac; ECORS-Vizcaya; ESCIN-2, 4) highlighted the continental subduction (Muñoz, 1992;

Teixell, 1996) and the importance of lower crust tectonic indentation (Martínez-Torres et al., 1994) in the configuration of the Pyrenean Range (Figure 4). The Pyrenees spread from the northeast to the northwest corners of the Iberian Peninsula. Its geologic evolution is related to the Iberian plate drifting as well as its interaction with the European plate (Séguret, 1972). Non-unanimous nomenclature has been used regarding its division (Barnolas and Pujalte, 2004). Nevertheless here we use traditional terms that differentiate two main areas: the Pyrenees to the East (where our study area is located) and the Basque-Cantabrian range to the West (Barnolas and Pujalte, 2004). The boundary between them is the Pamplona fault, with poor outcrops expression but significant vertical displacement, considered as a geologic boundary between two areas with contrasting stratigraphy and structure (Razin, 1989; Payros, 1997; Vergés, 2003; Larrasoaña et al., 2003). The study area of this work is placed in the Central Pyrenees, included in the South-Pyrenean zone.

From north to south, three major zones have been defined: i) North-Pyrenean Zone, ii) Axial Zone and iii) South-Pyrenean Zone.

i) The northern and narrower portion of the double-vergent prism of accretion is the **North-Pyrenean Zone**, composed of several thrust sheets, where basement is involved, and most of them tilted towards the north (Séguret, 1972). Its northern limit is established in the North-Pyrenean frontal thrust whereas its southern boundary is not well defined due do the imprecise trace of the North-Pyrenean Fault in some areas. The area of the North-Pyrenean Fault is characterised by thermal metamorphism affecting pre-Albian rocks, presence of mantle rocks (lherzolites) and Cretaceous magmatism in the eastern and central zones (Golberg et al., 1986) and Eocene rocks in the western zone (Choukroune and Séguret, 1973).

ii) The **Axial Zone** is the vast outcrop of uplifted Variscan basement with south verging structures, related to Alpine thrusting (Lakora and Gavarnie thrusts, among others). The Variscan rocks are distributed in large domes with E-W elongation with Proterozoic-Paleozoic cores affected by regional metamorphism. Tight synclinoriums filled by low-grade metasediments rocks separate these domes (Gil-Peña and Barnolas, 2004).

iii) The **South-Pyrenean Zone** comprises post-variscan rocks with south-verging structures, delimited between the north-Pyrenean Fault and the frontal South-Pyrenean thrust. It constitutes the southern portion of the double-vergent prism and is considerably wider than the northern one. Some of the thrust sheets include fragments of Variscan basement (Cámara and Klimowitz, 1985). The South-Pyrenean Zone is divided into Eastern, Western and central Zones.

The **Eastern South-Pyrenean Zone** is comprised between the Mediterranean Sea and the Segre river structural alignment. Here the South Pyrenean Zone is considerably enlarged and composed by four units of Mesozoic-Tertiary rocks (nomenclature from Muñoz et al., 1986): Pedraforca Unit (with two sub-units, the upper one, mainly made of Lower Cretaceous rocks absent in the lower one); Bac Grillera-Biure Unit (made by a Mesozoic-Tertiary cover whose disconnected basal thrust is folded); Figueres-Montgrí (emplacing complete Mesozoic series at its frontal thrust over the continental Upper Eocene rocks); Cadí Unit (Garumn and Eocene lie unconformably on the Variscan basement, and deformation is propagated from Vallfogona thrust to Bellmunt anticline).

The **Western South-Pyrenean Zone** includes the Jaca-Pamplona Basin, bounded by the Pamplona fault (to the W) and the South Pyrenean Central Unit (SPCU, to the E). From north to south several units can be distinguished: Internal Sierras (in contact with the Axial Zone, with materials from Upper Cretaceous to Lower Eocene); Flysch unit or Jaca-Pamplona turbiditic Basin (monotonous thin strata of sandstone/marls belonging to Eocene turbiditic facies with interlayered resedimented carbonates); Val Ancha or Canal de Berdún (correspond to the Arguis-Pamplona marls of Bartonian age); Guarga Synclinorium (Late Eocene and Oligocene continental rocks deformed by the underlying Guarga thrust); External Sierras (hanging wall of the Frontal South-Pyrenean sole thrust, where interference between Eocene deformation with N-S structures and Oligocene deformation with Pyrenean trend appears).

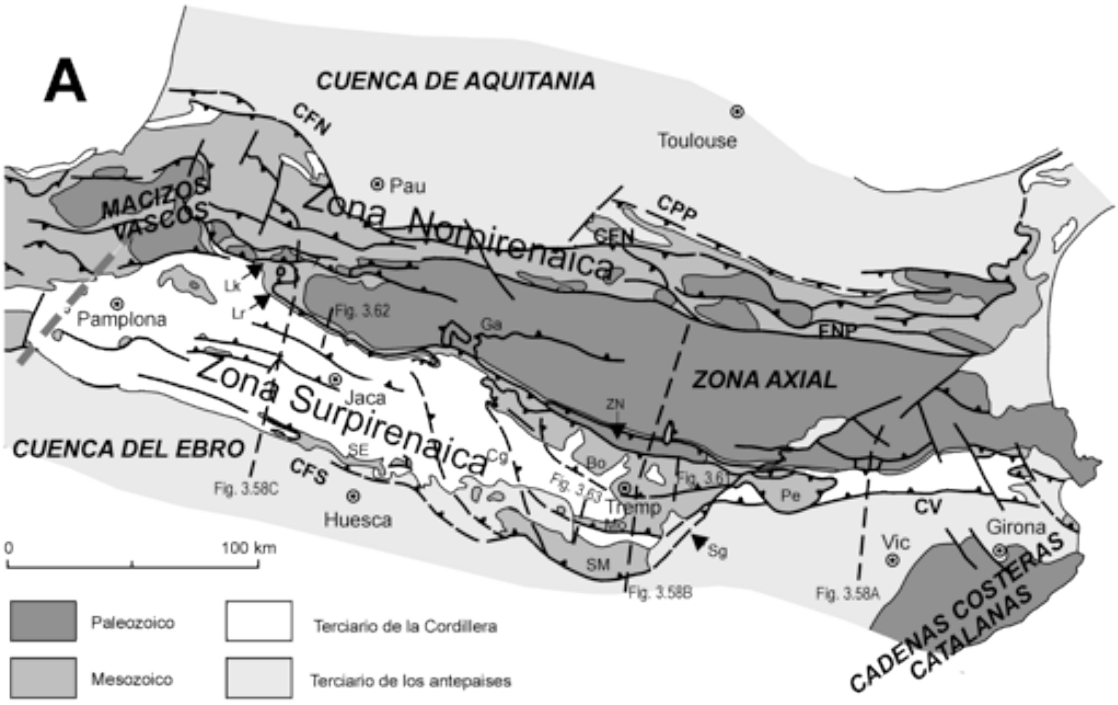

Figure 5. Structural sketch of the Pyrenees (from Barnolas and Pujalte, 2004; Tejero and Fernández-Gianotti, 2004). Main structures: CFS: South Pyrenean Frontal Thrust, CFN: North Pyrenean Frontal Thrust, CPP: *Petites Pyrénées* Thrust, Lk: Lakora Thrust, SE: External Sierras, Ga: Gavarnie Thrust, ZN: Nogueres Zone, Bo: Bòixols Thrust, Mo: Montsec Thrust, SM: Marginal Sierras, Sg: Segre oblique ramps, Cg: Cinca oblique ramps, Pe: Pedraforca sheet, CV: Vallfogona Thrust.

The **Central South-Pyrenean Zone** is comprised between the Segre river structural alignment and the western limit of the SPCU, that is the Cinca river structural alignment (Figure 5). From north to south, Séguret (1972) defined three units that were displaced southwards: the Nogueres Zone, The Gavarnie-Monte Perdido Unit and the South Pyrenean Central Unit (SPCU). The Nogueres Zone is linked to the Axial Zone and presents a succession of allochthonous Variscan units composed by a cover of Upper Carboniferous, Permian and Triassic rocks, tilted toward the south (Séguret, 1972;

Saura, 2004; Saura and Teixell, 2006). They are called the *têtes plongeantes* of the Nogueras zone (Figure 5). The Gavarnie-Monte Perdido Unit comprises paleozoic rocks underlying Cretaceous rocks. Southwards it presents a Cretaceous-Eocene cover detached from the basement at the level of the Upper Triassic. The minor Monte Perdido sheet (equivalent to the Internal Sierras in the western sector) is higher and included into the detached series (Figure 5). The SPCU presents several allochthonous imbricate thrust sheets linked to south verging folds in piggyback sequence. This unit was transported southwards during Eocene times (Puigdefàbregas et al., 1991) producing the partitioning of the southern margin of the Pyrenees. This unit is of special relevance in our study, therefore it will be described in detail in section 2.5.

2. 3. Crustal-scale structure of the Pyrenees

Over the years, several interpretations for the crustal structure of the Pyrenees have been adopted. From the 60s, the generalized allochthonous approach included thick-skinned and thin-skinned models. The thick-skinned model considers the North-Pyrenean fault as the main structure and plane of symmetry of a fan-like structure defined by vertical thrusts in depth (Mattauer, 1968, Séguret, 1972; Choukroune, 1976). The Axial Zone (south of the North-Pyrenean fault) would be the consequence of the thickening of the central part of the Pyrenees, dominated by the Variscan basement. The thin-skinned model considers the Pyrenees as an asymmetric range with thrust sheets predominantly displaced southwards (Hossack et al., 1984; Cámara and Klimowitz, 1986; Muñoz, 1986, Teixel, 1998; among others). The north-verging sheets are considered back-thrusts and the North-Pyrenean fault (inherited from Early-Late Cretaceous sinistral movement of the Iberian plate) would be cut in depth by north-verging thrusts formed in Eocene-Miocene times. According to this model, the Axial Zone would be a tectonic window of an antiformal stack whose thrust sheets moved southwards. The asymmetry of the orogen would be related to crustal subduction of the Iberian plate underneath the European one. Both models consider geophysical studies as seismic profiles and magnetotelluric and gravimetric surveys (ECORS team, 1988; Torné et al., 1989; Pous et al., 1995; Soriau & Granet, 1995; Casas et al., 1997; Vacher & Soriau, 2001, among others). From these studies, thickening of the crust under the Axial Zone, an interruption of the Mohorovicic discontinuity below the North-Pyrenean fault and a reduced crustal thickness of the North-Pyrenean Zone with regards to the South-Pyrenean Zone (Daignières et al., 1982; Choukroune et al., 1989) can be reasonably well established.

Programs as ECORS-Pyrénées and ECORS-Arzacq revealed that the Paleozoic basement is uplifted by thrusts in the Axial Zone and a fan-like thrust pattern in the crust. The Lower crust and the Moho discontinuity (Choukroune et al., 1989; Daignières et al., 1994), placed 33 km below the surface of the South-Pyrenean Front and 55-60 km below the Axial Zone, dip toward the north, deepening under the European Lower crust (where the Moho is 28-30 km deep).

Considering the seismic profiles and other geophysical data, several balanced sections have been performed (Figure 6), integrating surface structures and subsurface data. Thrusting throughout the crust and upper mantle generate the thickening of the Pyrenean crust. From ECORS-Pyrénées section, a total shortening of 100 km (Roure et al., 1989) and 150-165 km (Muñoz, 1992; Beaumont et

al., 2000) has been calculated. On the other hand, 80 km of shortening was deduced from ECORS-Arzacq (Teixell, 1998) in the western sector of the Axial Zone. This disparity is due to diverse interpretations regarding the subcrop of the Mesozoic cover below the South-Pyrenean basement thrusts and the increase of the shortening from E to W (Figure 6, Roure et al., 1989) for instance, or the Iberian continental crust subducted into the mantle (Figure 6b and c, Muñoz, 1992; Berástegui et al., 1993; Teixell, 1998). Teixell (1998) proposed that only the lower crust (mafic and dense) subducted. The collective summary is that the upper-crustal structure is described as a doubled-verging orogenic prism where the North and South-Pyrenean Zones converge at depth (Figure 6).

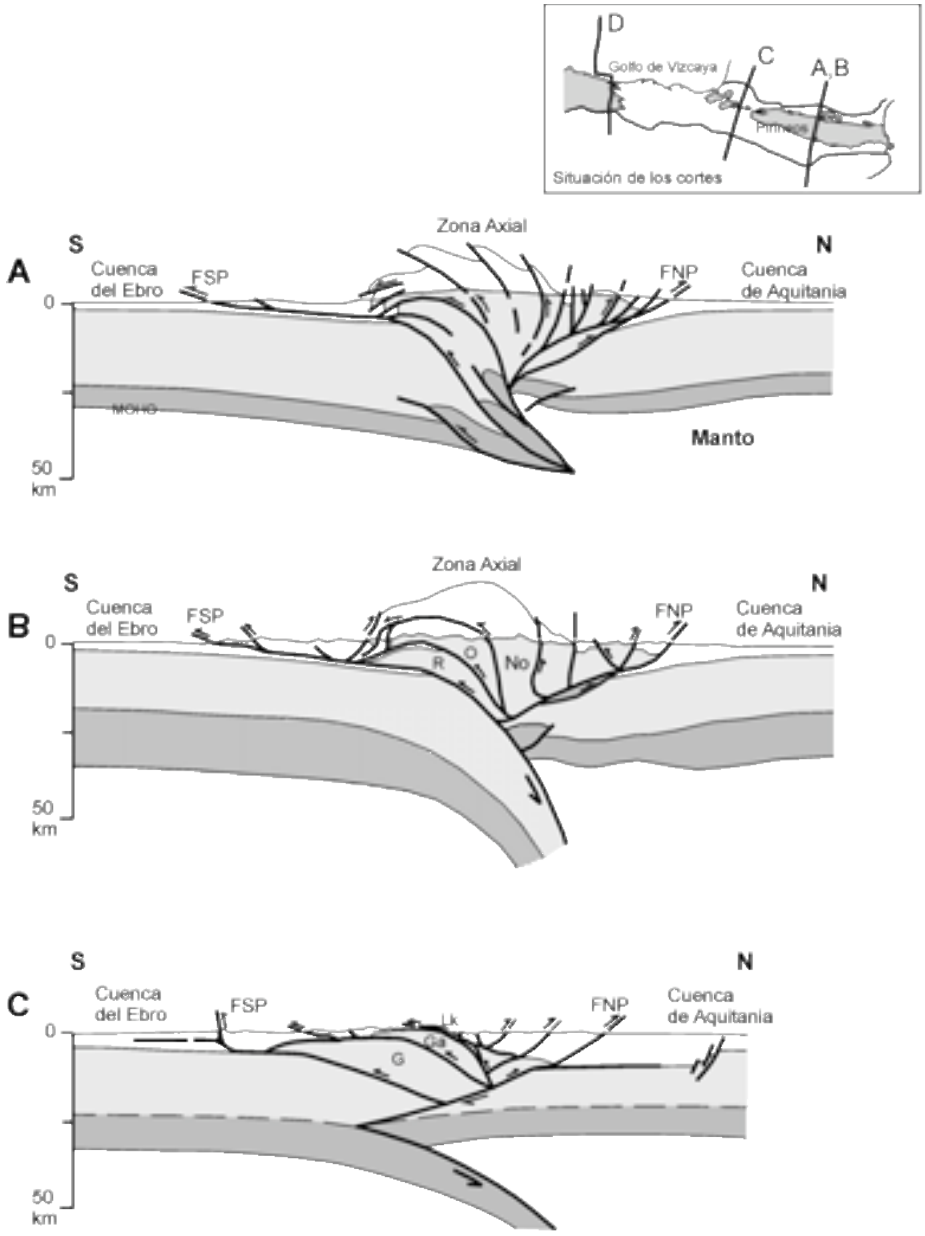

Figure 6. Crustal-scale cross section of the Pyrenees based on seismic data combined with gravity. FNP: North-Pyrenean Front; FSP: South-Pyrenean Front. A) ECORS-Pyrénées (Roure et al., 1989). B) ECORS-Pyrénées (Muñoz, 1992; Berástegui et al., 1993). R, O, No: Rialp, Orri and Nogueres sheets. C) ECORS-Arzacq (Teixell, 1998). The Lower crust interpretation is included. G, Ga, Lk: Guarga, Gavarnie and Lakora sheets. From Teixell, 2004; Tejero and Fernández-Gianotti, 2004.

2. 4. Evolution of the Pyrenees

2.4.1 Paleogeography

The Pyrenean Range originated during the Alpine orogeny in the Western Mediterranean as a consequence of the tectonic inversion of the extensional and transtensional systems developed during Triassic and Cretaceous times. During the Mesozoic period the Pyrenees underwent extensional movements related to the opening of the Atlantic Ocean and the Bay of Biscay. The opening of the Atlantic produced several rifting stages from Late Permian to Early Triassic times (Lucas, 1985; Puigdefàbregas and Souquet, 1986; Ziegler, 1989). However, the South Atlantic opened from Mid-Jurassic to Late Cretaceous and the North Atlantic started at Early Cretaceous (Delfaud, 1969; Peybernès, 1976; Fauré, 1984; Puigdefàbregas and Souquet, 1986). The initial convergence was nucleated in the NW of Spain as early as mid-Cretaceous times (Gibbons and Moreno, 2002) when an accretionary prism resulted of the subduction of the oceanic crust of the Bay of the Biscay beneath Iberia. Nevertheless, wholesale continental collision is considered to start in the eastern Pyrenees, subsequently propagating westwards because of oblique subduction of the Iberian plate below the Eurasian plate (ECORS-Pyrenean team, 1988; Muñoz, 1992; Teixell, 1998; Rosenbaum et al., 2002), and spanned from Late Santonian to Middle Miocene. Subsiding troughs with turbiditic filling were quickly involved in synsedimentary thrusting (Gibbons and Moreno, 2002) in the Iberian side of the orogen. This process enabled a change from generally marine to mostly terrestrial conditions.

In this long-lasting convergence, thrusting was directed north and southwards away from the Axial Zone where Variscan basement rocks crop out and towards its two foreland basins: the Aquitaine basin in France (N) and the Ebro basin in Spain (S), forming an asymmetric, double-verging range (Figure 6). During Early Paleogene, the Pyrenean domain was an east-west trending elongate interplate embayment just connected to the west by the Bay of Biscay and surrounded elsewhere by shallow shelf areas (Figure 7a).

From Paleocene to Middle-Late Ilerdian (see reference time scale by Gradstein et al., 2004, figure 8) a generalized transgression in a large part of the South Pyrenean Basin (Barnolas and Gil-Peña, 2001) took place. Since then, a south Pyrenean channel with siliciclastic feeding from the east (Puigdefàbregas and Souquet, 1986) developed. Further convergence during Eocene, brought about the formation of the emerging orogenic belt and the splitting of the former single basin into northern and southern foreland basins (Figure 7b).

Additional thrusting and uplift during Middle-Late Eocene (Plaziat, 1981) was the cause for retreating marine areas towards the paleo-Bay of Biscay, bounded then by shallow carbonated shelves (Figure 7c). Eventually, the closure of the marine gateway took place during Priabonian times (Costa et al., 2009). After the main convergence stage, during the last Miocene compressional stage, widespread terrestrial conditions with coeval erosion of the original materials (Figure 7d) developed throughout the Pyrenean realm.

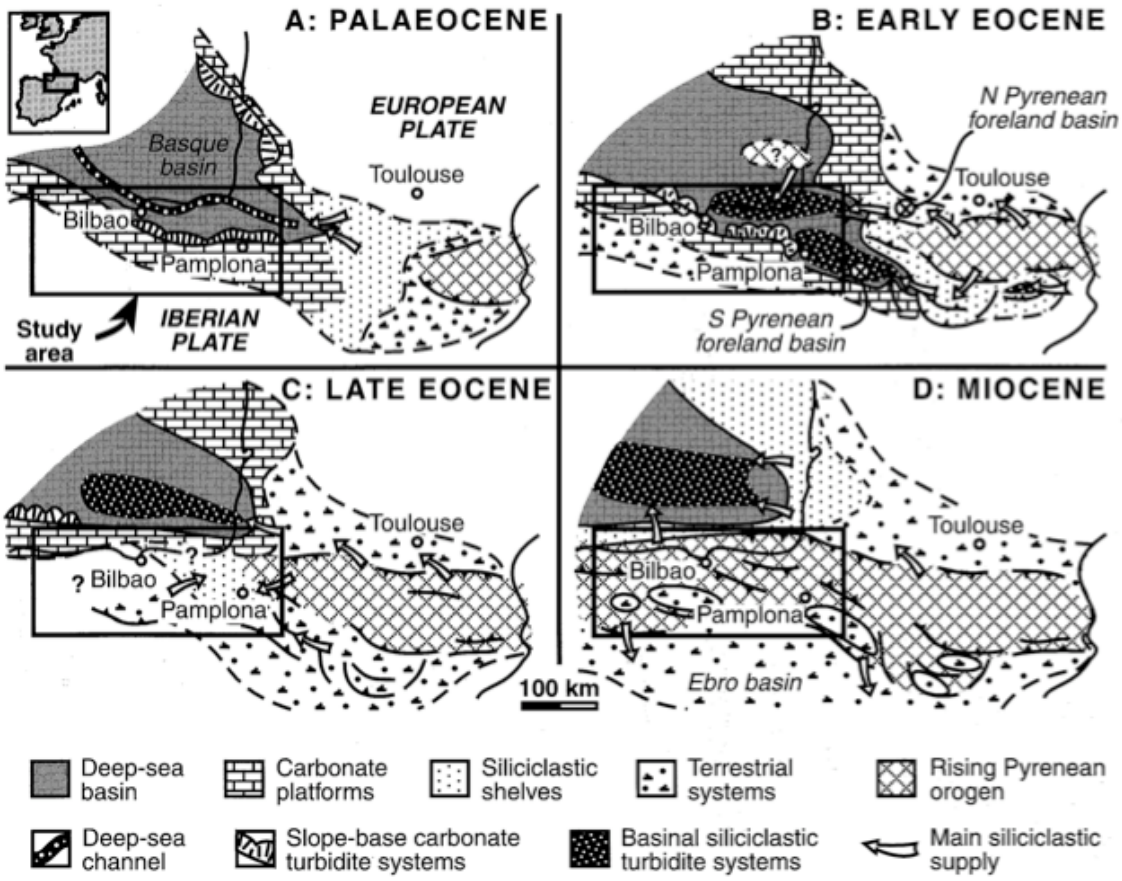

Figure 7. Palaeogeographic evolution of the Pyrenean and Basque-Cantabrian region during Tertiary (from Gibbons and Moreno, 2002, modified from Plaziat, 1981).

2.4.2 Structural evolution

Cámara and Klimowitz (1985) based on an integrative compilation of seismic profiles and wells considered a sequence of footwall cover thrusts. Below this sequence Paleocene-Upper Lutetian rocks lie directly on the Paleozoic basement (Figure 9). Deformation would start in the Late Cretaceous in the east, progressing westwards until Miocene times, with synchronous turbiditic sedimentation in the generated trough. From E to W (see Figure 9), Sant Corneli, Montsec and Cotiella, followed by Monte Perdido, Boltaña, Biniés-Guara are cover thrusts stacking on the allochthonous thrusting over the Ebro Basin. The South Pyrenean Frontal thrust would be a complex set of different imbricate ramps and flats, instead of an only sole thrust front. These N-S structures would represent lateral or oblique ramps of the general movement towards the south. According to Cámara and Klimowitz (1985), the possible dextral strike-slip movement between Iberian and Eupopean plates gave rise to NNW-SSE compression between them, originating the current structure.

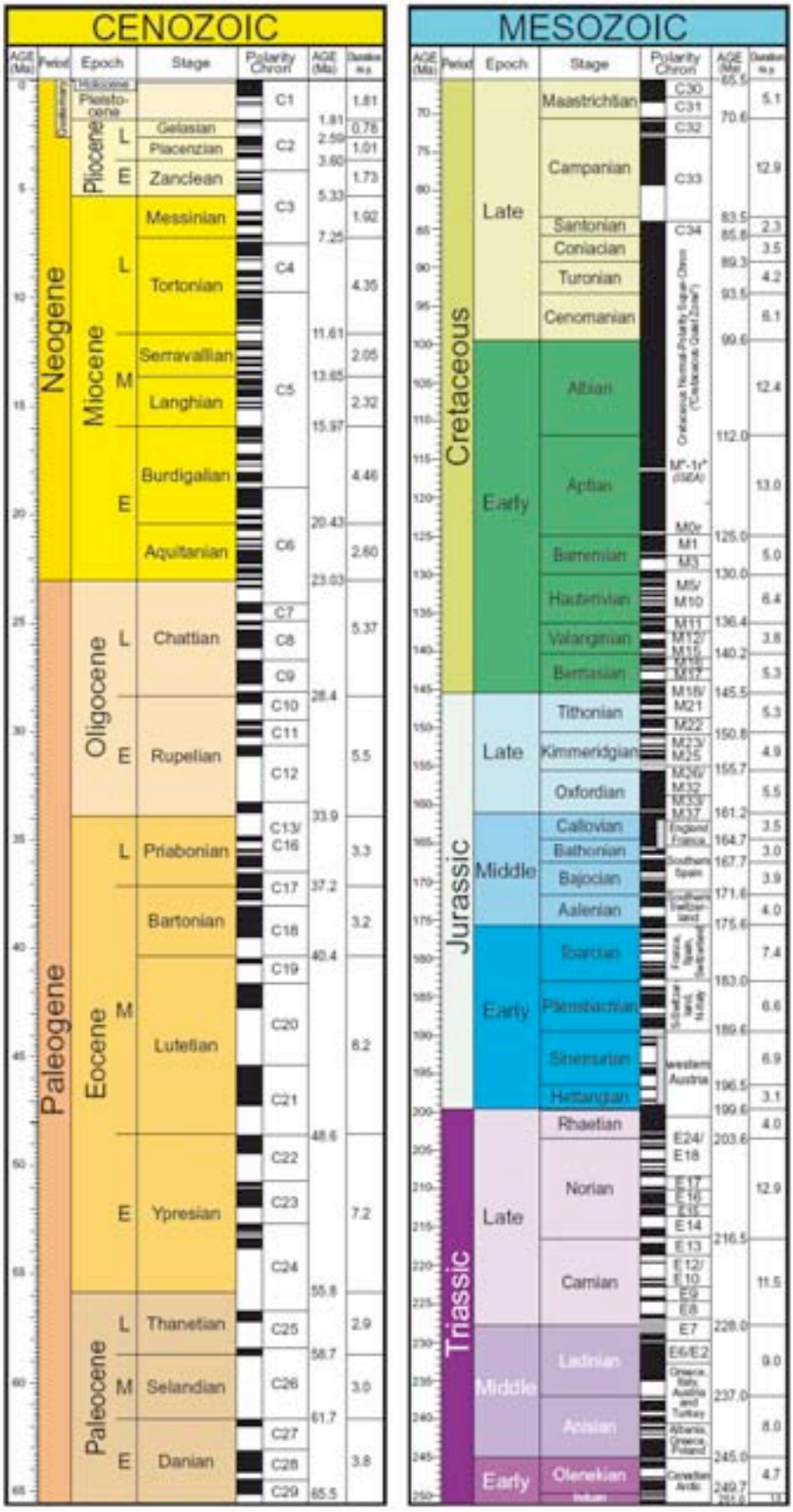

Figure 8. Mesozoic and Tertiary Geological Timescale (Gradstein et al., 2004)

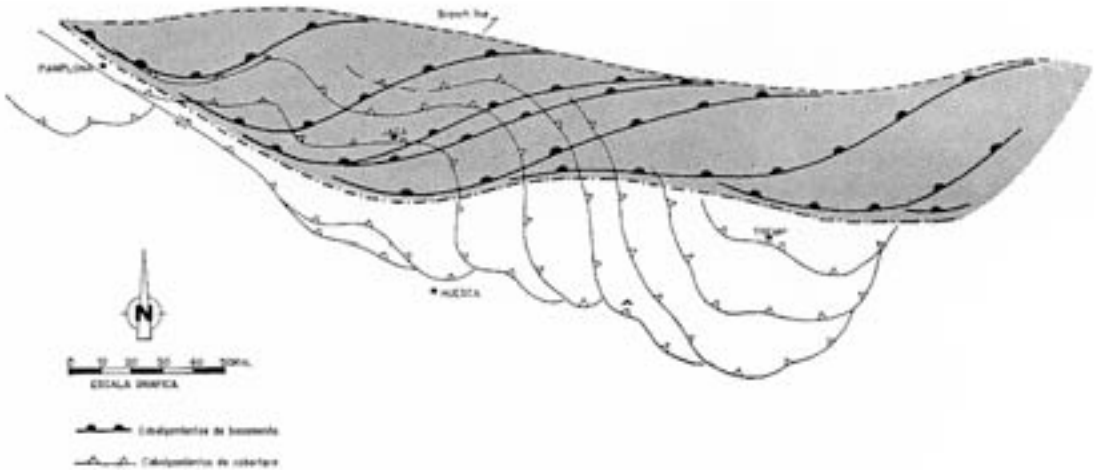

Figure 9. Tectonic model of the South Pyrenean Zone (Cámara and Klimowitz, 1985). This model describes a footwall sequence of cover thrusting propagated from E to W.

2.5. The South Pyrenenan Central Unit (SPCU)

The SPCU is characterised by a set of allochthonous imbricate thrust sheets and associated south verging folds. They were emplaced over the autochthonous rocks of the Ebro foreland basin with thrusting propagating southwards in a piggyback sequence (Séguret, 1972; Garrido-Megías, 1973; Cámara and Klimowitz, 1985; Puigdefàbregas et al., 1991; Muñoz, 1992). These thrust sheets are detached along Triassic evaporites and incorporate Mesozoic and Tertiary cover materials. From Early Cuisian, the emplacement of the South Pyrenean central Unit (SPCU) produced the fragmentation of the South Pyrenean Basin and conditioned subsequent sedimentation. The geometry of these imbricate thrusts is strongly conditioned by the structural inversion of the Cretaceous extensional basin.

In the SPCU, the units of Bòixols, Cotiella, Montsec and Marginal Sierras can be distinguished (Séguret, 1972). Originally, Séguret (1972) included the Pedraforca sheet, which in the present description is included in the Eastern South-Pyrenean Zone. The Bòixols-Turbón Unit has a thick Mesozoic of about 5000 m, including Triassic, Jurassic and Lower Cretaceous rocks and a thin Paleocene and Lower Eocene strata with local Upper Eocene-Oligocene conglomerate cover (García-Senz, 2002), unconformably overlying the previous marine sequence, and subsequent to the main folding stage. Compressive deformation is here recorded from Late Santonian (Late Cretaceous) as a consequence of the inversion of Cretaceous extensional basins (Garrido-Megías, 1973; Simó 1985; Bond and McClay, 1995; García-Senz, 2002). This unit was passively transported southwards on the Montsec thrust sheet, which was active from Ilerdian to Cuisian times (Garrido-Megías, 1972b; Nijman and Nio, 1975; Farrell et al., 1987; Vergés and Muñoz, 1990; Teixell and Muñoz, 2000). The Cotiella Unit present an Eocene footwall with marked NNW-SSE trending cleavage, also present in the Cretaceous marls of the hangingwall (Séguret, 1972). It is detached in the Keuper facies and its origin is likely associated with an oblique ramp (Martínez-Peña, 1991). Several authors consider the emplacement of the Bòixols-Cotiella nappe isochronous during the Late Cretaceous as a consequence

of the positive inversion of lower Cretaceous extensional basins (Garrido-Megías, 1973; Simó, 1985; Berástagui et al., 1990; Bond and McClay, 1995; García-Senz, 2002). The Montsec Unit shows a thin Mesozoic sequence where the Triassic rocks at the bottom are the detachment level and the Upper Cretaceous is relatively thick; Paleocene Garumn facies and the complete Eocene are overlain by Late Eocene-Oligocene conglomerates. Lastly, the ensemble of these units was transported, as a piggyback basin on the Marginal Sierras thrust sheet, during Lutetian and Early Oligocene times (Puigdefàbregas, 1975; Millán, 1996) or the Late Oligocene (Garrido-Megías, 1973; Vergés and Muñoz, 1990; Teixell, 1996; Teixell and Muñoz, 2000). The Marginal Sierras is the lowest and southernmost sheet of the SPCU (Pocoví, 1978a). Its complex internal structure is made up of tectonic units of thin Mesozoic and Tertiary rocks above Triassic evaporites that act as *décollement* level. Wide evaporitic outcrops appear at the basal thrusts evidencing the role of halokinesis on their structuring (Pocoví, 1978b and 1979; Millán et al., 2000). A final ramping of the detachment up to the Eocene evaporites (Barbastro Fm) during Oligocene times is responsible for the southernmost Pyrenean structure. The Barbastro-Balaguer anticline is an arched, 150 km long structure along the southern border of Marginal Sierras (Martínez-Peña and Pocoví, 1988).

The cover thrusts units are also related to the southward transport of the basement units that constitute the Axial Zone antiformal stack (ECORS-Pyrénées and Figure 6). The most important stage of uplift of basement units occurred between Late Eocene and the Oligocene-Early Miocene (Muñoz. 1992; Fitzgerald et al., 1999; Beaumont et al., 2000) on the Guarga – External Sierras thrust sheet (Teixell, 1996). The foreland reflected this shortening by continued thrusting and folding in the Marginal Sierras and External Sierras sector (Vergés and Muñoz, 1990; Anastasio, 1992; Teixell, 1996; Meigs, 1997; Millán et al., 2000; Teixell and Muñoz, 2000) and by reactivations of the Montsec and Bòixols thrusts (Vergés and Muñoz, 1990; Teixell and Muñoz, 2000; Beamud et al., 2001), see figure 10. This deformation affects the hinterlands by backthrusting of the cover thrust over the roof detachment of the basement units (Williams, 1985; Muñoz, 1992; Teixell and Muñoz, 2000; Beamud et al., 2001)

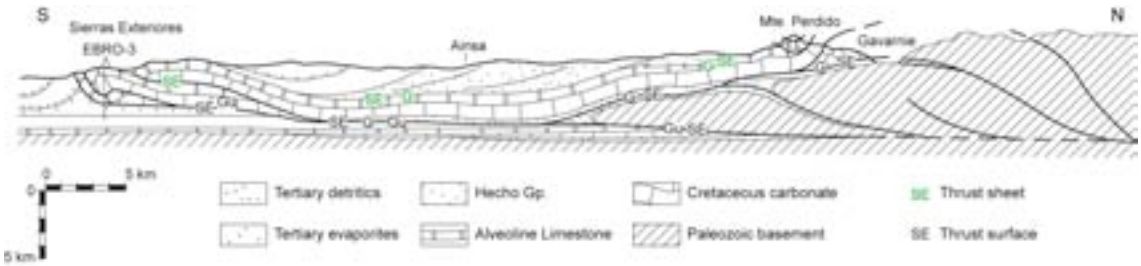

Figure 10. S-N cross section nearby to the Boltaña anticline. G: Gavarnie, Gu: Guarga, SE: External Sierras. Modified from Cámara and Klimowitz, (1985), unit labels from Fernández-Bellón (2004).

Muñoz et al. (1986) defined within the Southern Pyrenees the Upper and Lower sheets according to their structural position, age of emplacement and stratigraphic features. The Upper Thrusting Sheets are mainly composed of Mesozoic carbonate rocks. Its internal structure is characterised by imbricate thrust systems and associated hangingwall folds. They show numerous

structures oblique to the main WNW-ESE Pyrenean trend. Geographically they are equivalents to the SPCU of Séguret (1972) and the units of Marginal Sierras, Montsec, Cotiella, Pedraforca, Bòixols and Figueres-Montgrí are encompassed. The Lower Thrust Sheets are constituted by basement and cover rocks. Usually, the Mesozoic materials are scarce or absent and Paleogene units are relatively thick. They emplaced after the Upper Thrust Sheets and are (from E to W): Cadí sheet, Nogueras Zone and Gavarnie sheet. Their assorted internal geometry varies from imbricate systems in the external areas to duplex and antiformal stack in the internal areas (ECORS-Pyrénées, figure 6).

2.6. The Aínsa Basin

Syntectonic sedimentation occurred in the southern margin of the Axial Zone during the continuous southward motion of the Pyrenean thrusts, shifting the basin depocentres in that direction. In response to the inversion of previous Cretaceous basins, Late Cretaceous compression originated the partial incorporation of the older Pyrenean foreland basin into the Bòixols Unit. A period of relative tectonic quiescence spanned from Maastrichtian to the earliest Eocene (Fernández-Bellón, 2004), with widespread continental and shallow marine sedimentation. Then, thrusting reactivation induced the migration of the depocentre towards the Tremp-Graus Basin, later transported in the hangingwall of the Montsec thrust (Figure 11). This basin opened to the west, over the lateral ramp of the Montsec thrust, into the Aínsa Basin (feeding the turbiditic Jaca-Pamplona Basin). A regional transgression during Bartonian times gave again a unitary character to the South Pyrenean Basin, as proven by biostratigraphic evidences and sedimentary system similarities (Puigdefàbregas, 1975; Barnolas et al., 1992; Barnolas and Gil-Peña, 2001). The Marginal Sierras and External Sierras thrust sheets caused the Graus-Tremp, Aínsa and Jaca-Pamplona Basins southwards displacement as piggyback basins (Middle Eocene – Late Oligocene), leading to major sedimentation in the Ebro Basin. This evolution, coupled with the emplacement of the Basque-Cantabrian unit since Priabonian times, produced a geographic boundary between the Atlantic Sea and the South Pyrenean Basin, beginning a generalized endorheic stage in the Ebro Basin. Finally, continental sedimentation became widespread throughout the southern Pyrenees, sealing the last structures related to Pyrenean thrusting (Coney, 1996; Muñoz et al., 1997; Millán et al., 2000).

Contemporary to the slow westwards propagation of south-transported thrust sheets, numerous structures transverse to the Pyrenean trend (WNW-ESE) were formed West of the SPCU. Among others, structures such as Mediano, Boltaña, Balzes, Pico del Águila anticlines, are understood as oblique ramps of these thrust sheets (Puigdefàbregas, 1975; Poblet and Hardy, 1995; Millán et al., 2000; Soto and Casas, 2001; Fernández et al., 2004). These N-S structures are progressively younger and smaller towards the W (Puigdefàbregas, 1975; Cámara and Klimowitz, 1985; Millán, 1996). Numerous paleomagnetic evidences indicate significant clockwise rotation (30-45°) related to the formation of the N-S structures (Pueyo et al., 2004a an references therein) favouring a clearer interpretation of the paleogeographical distribution of Eocene facies.

Within this frame, the Aínsa Basin originated during Early Eocene as a foredeep southwest of the SPCU, defining the easternmost part of the Jaca-Pamplona undetached basin. During the Middle Eocene, it was included in the Gavarnie-External Sierras thrust front, as a piggyback basin thrusting

towards the foreland (Fernández et al., 2004; Fernández-Bellón, 2004). The Aínsa Basin limits to the west with the turbiditic and subsequently molasse Jaca-Pamplona Basin and with the siliciclastic Graus-Tremp Basin to the East. Basin boundaries generate controversy, although there is a consensus regarding the Boltaña anticline as its westernmost boundary. While some authors consider the Mediano anticline (De Federico 1981; Mutti *et al.* 1988; Barnolas *et al.* 1991), others propose La Foradada Fault as the eastern boundary (Nijman and Nio, 1975; Fernández-Bellón, 2004) of the Aínsa Basin. Probably, none of them were real boundaries of the basin during its formation; they just border the eastern shallow marine and continental deposits of the Tremp-Graus Basin to the western deeper marine sediments of the Jaca-Pamplona Basin.

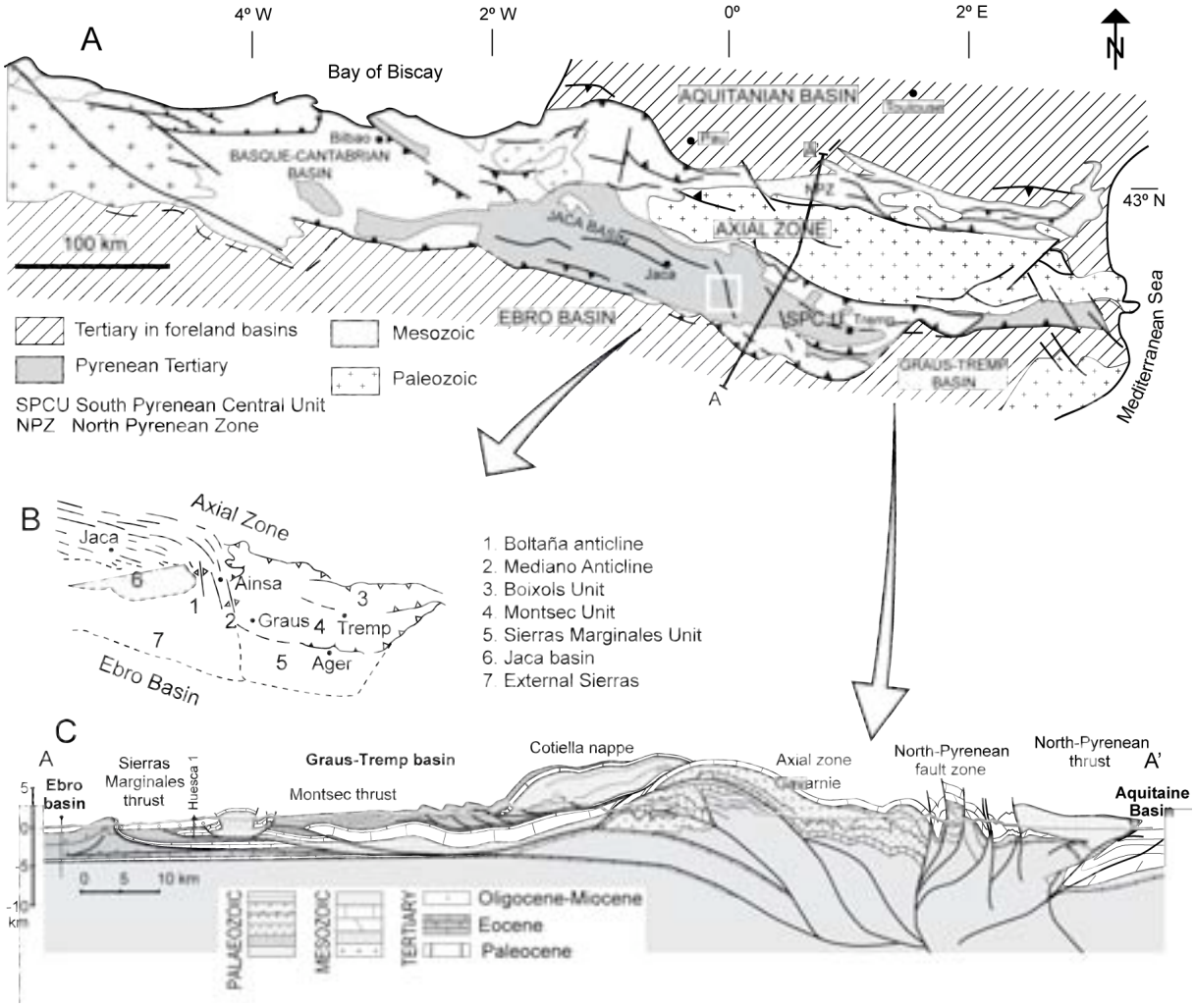

Figure 11. Geological sketch of the Southern Pyrenees. The Jaca-Pamplona Basin to the west and the Graus-Tremp Basin in the east of the Boltaña anticline can be distinguished. Modified from Oliva et al. (2011). b) Simplified structural units in the Southwestern Pyrenees. c) Geological cross-section modified from Martínez-Peña and Casas-Sainz, (2003) of the western boundary of the SPCU.

The substratum of the Eocene Aínsa Basin consists of Upper Cretaceous to Paleocene-Lower Eocene rocks overlying Triassic rocks. The Eocene of the Aínsa basin range from Ypresian (Ilerdian) to Priabonian age (Figure 12). The Lower Ypresian (Ilerdian) is represented by carbonate shelf

limestones (Alveolina Limestone) and marly limestones (Millaris and Metils Fms., Van Lunsen 1970). A deltaic sequence of marls, siltstones and sandstones (Yeba Fm., Van Lunsen 1970), overlies the previous sequence. The Boltaña Fm. represents the upper unit of the Ypresian (Cuisian) succession and consists of shallowing upward heterolithic sequences of sandstones, and bioclastic sandy limestones (Barnolas et al. 1991). These units crop out in the core of the Boltaña anticline (Figure 12). The top of the Boltaña Fm is a flooding surface resulting from a drowning unconformity above the shelf (Barnolas and Teixell, 1994) that preludes the sedimentation of distal carbonate ramp marls of the San Vicente Fm (De Federico, 1981).

The Paules and La Patra Mbs, from the San Vicente Fm, crop out in the western limb of the Buil syncline. The lower part of the Paules Mb (De Federico, 1981) corresponds to a retrogradational ramp, which is evidenced by the abundance of stratigraphic truncations. This retrogradational character turns to progradational in the upper part of the Paules Mb (Barnolas et al., 1992). The transition to La Patra Mb (De Federico, 1981) is located in a flooding surface with glauconite followed by a slope carbonate breccia (Coscollar level, Barnolas et al., 1991). This carbonate breccia slope apron develops at the foot of an erosional truncation in the shallow carbonate Guara Fm (Barnolas et al., 1992), see figure 12.

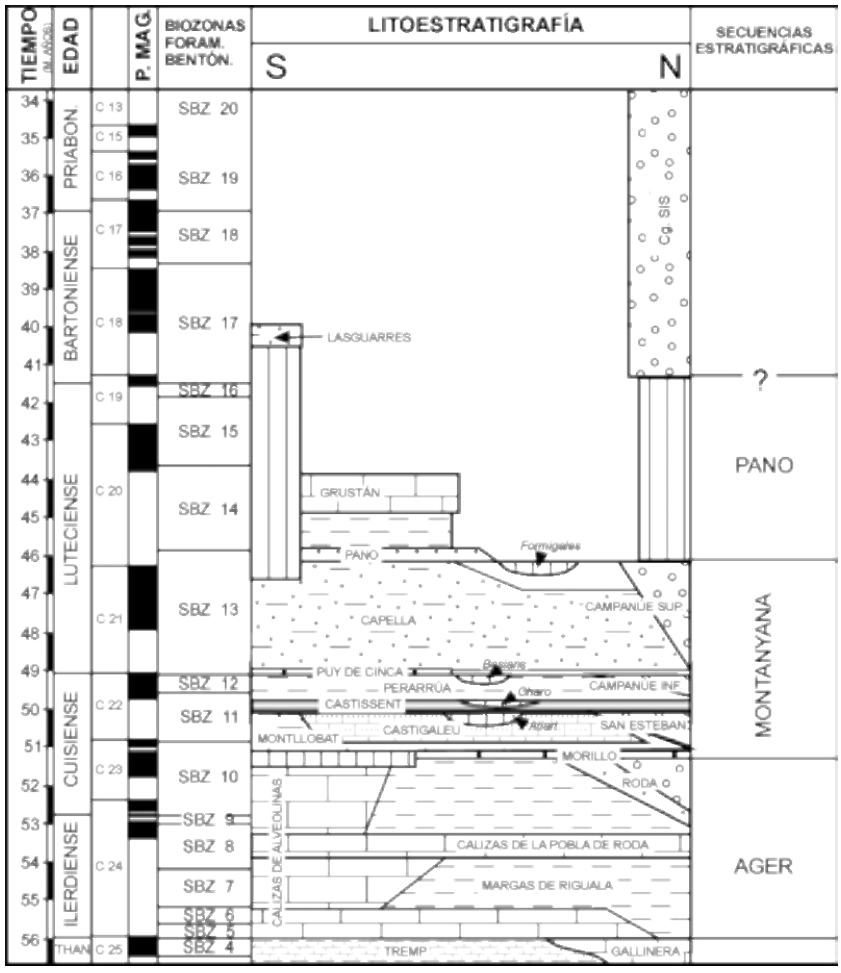

Figure 12a.

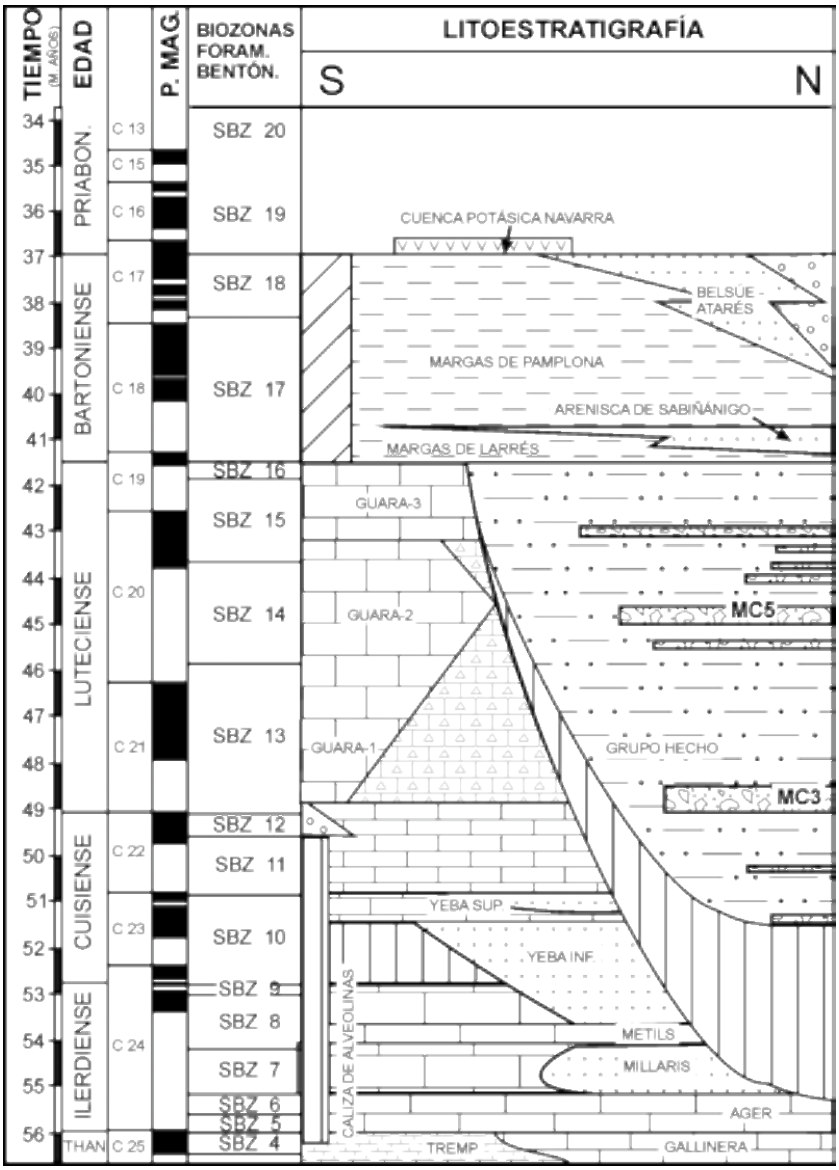

Figure 12. Chronostratigraphic sketch from Ilerdian to Priabonian times (Barnolas and Gil, 2001 and references therein). a) Graus-Tremp Basin. b) From Jaca-Pamplona Basin.

During the foredeep undetached stage (Early - Middle Eocene) a foreland carbonatic margin developed in the south whereas a basin trough filled with turbidites (Hecho Group) was developed in the north (Puigdefàbregas and Souquet, 1986; Barnolas and Teixell, 1994) of the Aínsa Basin (Figures 12 and 13). The morphologic bulges generated as a consequence of growth of the Boltaña and Mediano anticlines, conditioned the geometry and the sedimentary setting of the Aínsa Basin in Middle – Late Lutetian times (Figure 13). The Sobrarbe Fm, with N-NW progradating delta lobes filled this trough (Figure 12). The sharp transition with siliciclastic Sobrarbe Fm is a thin, dark marly anoxic level Barnolas et al., *in press* a). Its age is Middle-Late Lutetian (Muñoz et al., 1998; Barnolas et al., *in press* a). The Escanilla Fm (Garrido Megías, 1968; Bentham, 1992), is Late Lutetian to Middle Priabonian in age (Bentham and Burbank 1996; Mochales et al., 2011a); it corresponds to the lower part of the Campodarbe Gp., sedimented in an alluvial and fluvial system, unconformably lying on the Mediano and Boltaña anticlines (Figure 13).

2.7. Oblique structures of the SPCU

Oblique structures are those with oblique orientation with respect to the main trend of a range or oblique to the main transport direction. They occur in both extensive and compressive regimes, attached to transference zones between adjacent structures (Soto, 2003). The oblique structures in the SPCU setting formed under a compressional stage. The transference areas in thrust and fold belts accommodate displacements between adjacent structures and connect frontal thrusts (Soto et al., 2002). The characteristic transference areas in compressive settings are lateral ramps, oblique ramps and tear faults. A lateral thrust ramp is sub-parallel to the transport direction of the associated thrust sheet (McClay, 1992). When the lateral ramp is vertical it is called a tear fault (parallel to the transport direction and separating two parts with differential displacement). An oblique ramp is a thrust ramp oblique to the transport direction of the associated sheet. Several factors can control the origin of the transference areas in compressive settings (Soto, 2003): i) inherited basement thrust geometries (Kulik and Schmidt, 1988 and references therein). ii) lateral changes of facies or thickness variations (Miller, 1973; Woodward et al., 1988; Calassou et al. 1993; Corrado et al. 1998) associated or not to basement thrusts (Thomas, 1986). iii) Inverted previous extensional faults (Gillcrist et al., 1987; Vergès and Muñoz, 1990; Burbank et al., 1992; Casas-Sainz, 1993). iv) Lateral differences regarding the displacement of the thrust sheet (Elliot, 1976; Allerton, 1998). v) Lateral variations regarding the rheology and thickness of the detachtment level (Liu et al., 1992; Cotton and Koyi, 2000). vi) Lateral variations of the syntectonic sedimentation and erosion rates. vii) Presence of bended folds and thrusts (Marshak et al., 1992). As can be seen, numerous parameters can induce the formation of transference areas in an orogen, for these reasons oblique structures are very frequent in fold and thrust belts.

The Pyrenean range is a fold and thrust belt whose main direction is WNW-ESE (Séguret, 1972; Cámara and Klimowitz, 1985). Nevertheless in the South Pyrenean Zone several compressive structures present an oblique orientation to the main trend. Transverse folds can be found in the eastern and western terminations of the Marginal Sierras thrust (Pocoví, 1978a), in the Cotiella-Bòixols sheet, in the western boundary of the SPCU (Barnolas et al., 1992; Martínez-Peña, 1991) and regularly spaced throughout the External Sierras (Puigdefàbregas, 1975; Millan, 1996; Pueyo, 2000), see figure 13. The study here presented was focused on the structures linked to the western boundary of the SPCU, namely the Añisclo anticline, the Boltaña and Mediano anticlines and the Buil syncline. All of them present N-S trend and conform the Biello-Sobrarbe thrust and fold system (Fernández-Bellón, 2004), located in the western part of the Aínsa Basin (Figure 13). The Boltaña and Añisclo anticlines present some similarities, as it is their relation to west-verging fault-propagation folds related to two blind thrusts (Holl and Anastasio, 1995a, b; Soto and Casas, 2001; Fernández-Bellón, 2004; Tavani et al., 2006). On the other hand, the Mediano anticline is a detachment fold that displays eastwards vergence and northward plunge in its southern sector (Holl and Anastasio, 1993; Poblet et al., 1998). The Buil syncline is located between the Boltaña and Mediano anticlines and covers the Olsón detachment fold, detected in seismic profiles (Millán, 1996; Soto and Casas, 2001).

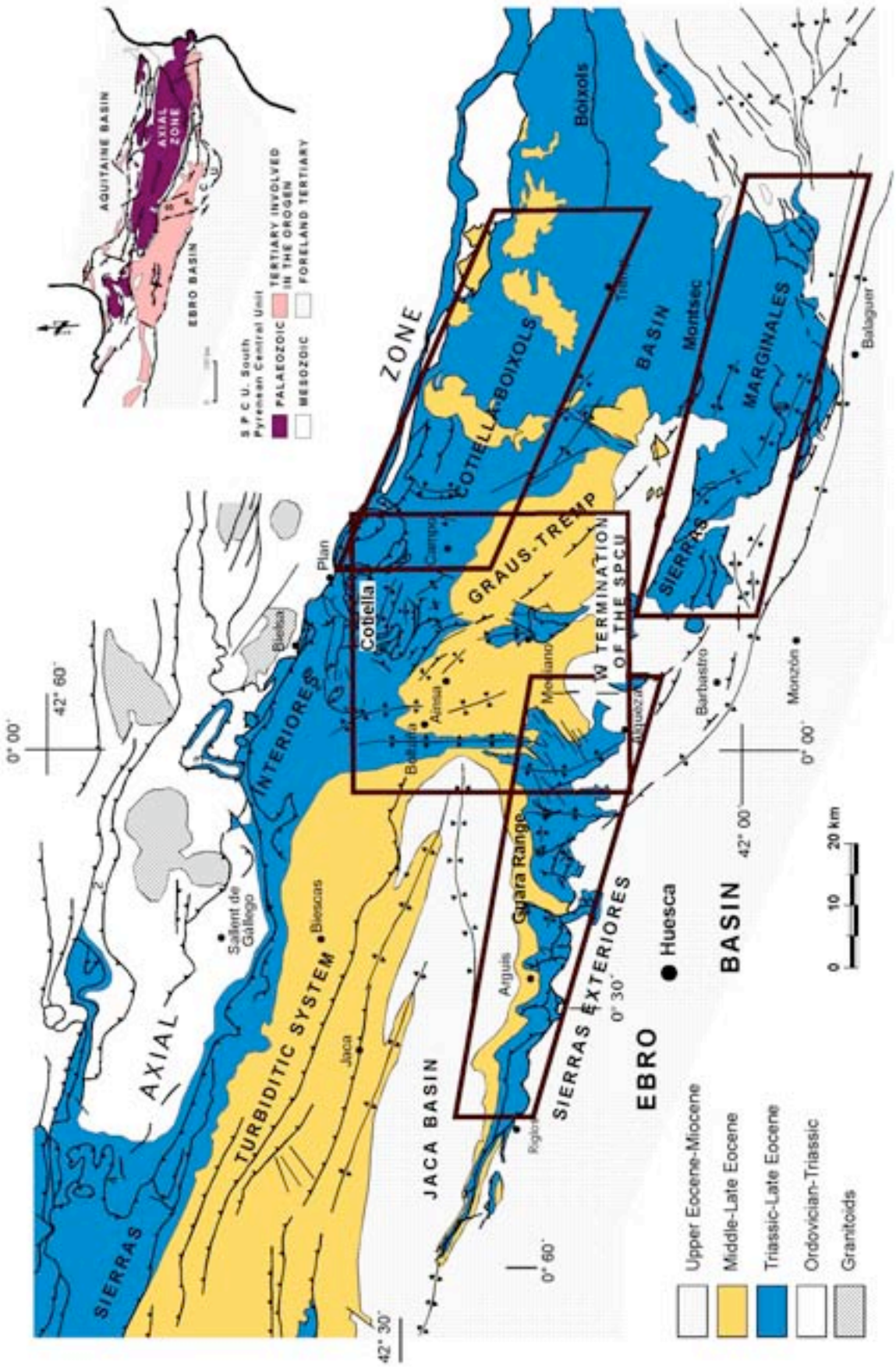

Figure 13. Geologic map Southern Pyrenees where transverse structures are framed. Modified from Puevo et al., (1999) and Millán et al. (2000).

3. Study area

The Southern Pyrenean foreland basin fill records the evolution of the nearby orogenic wedge (Puigdefàbregas and Souquet, 1986; Puigdefàbregas et al., 1991). Extensional normal faults linked to early Cretaceous extension or transtension were inverted from Late Santonian to Maastrichtian times. An E-W elongated turbiditic trough formed ahead the advancing thrust front whose depositional geometries can be related to the continued motion on the Bòixols-Turbón thrust (Puigdefàbregas and Souquet, 1986). The syntectonic character of the continental sedimentation, with respect to late episodes of the Bòixols-Turbón thrust system emplacement, interfered with the shallow marine environments during Late Maastrichtian-Paleocene times. Nevertheless, other authors propose that these syntectonic sediments are linked to the early stages of the Montsec thrust (Arbués et al., 1998; Fernández-Bellón, 2004). Early-Middle Eocene shallow marine and continental environments were controlled by piggyback thrusting propagated southwards into the subsiding foreland basin (Puigdefàbregas, 1975; Nijman and Nio, 1975; Farrell et al., 1987; Puigdefàbregas et al., 1991; Poblet et al., 1998; Teixell and Muñoz, 2000). Sequential lateral and oblique ramps in the main SPCU thrust sheets initiated over inherited Mesozoic extensional faults (Séguret, 1972). Western oblique boundary of the SPCU thrust controlled the lateral transition from fluvio-deltaic systems (Graus-Tremp Basin) to subsiding deep marine (Jaca-Pamplona basin) environments (Puigdefàbregas and Souquet, 1986; Barnolas and Gil-Peña, 2001). This structural control of the sedimentation continued during Late Eocene-Oligocene times with coarse alluvial fans in the hanging wall of the SPCU and across the oblique ramp zone to the west, as a result of a renewed uplift (Bentham, 1992). The southern Pyrenean basin was closed to marine sedimentation at the end of the Eocene (Priabonian times; Costa et al., 2009), that together with a strong subsidence did extend an endorheic lake during Oligocene-Miocene period in the Ebro foreland Basin (Riba et al., 1983; García-Castellanos et al., 2003;).

3.1. Stratigraphy

The pre-tectonic substratum of the Eocene Aínsa Basin consists of Upper Cretaceous to Paleocene-Lower Eocene rocks and Triassic rocks overlying the tectonic detachment surface (Fernández et al., 2004; Fernández-Bellón, 2004); detailed studies describe this pre-tectonic sequence (Van Lunsen, 1970; Garrido-Megías, 1973; Ríos-Aragüés et al., 1982). Once the Aínsa Basin was indirectly involved, as a foreland margin of a foredeep basin, into the hanging wall of the Gavarnie-External Sierras thrust, the sedimentary scenario was completely modified. Several authors have detailed its Eocene stratigraphy (Garrido-Megías, 1973; Van Lunsen, 1970; Puidefàbregas, 1975; De Federico, 1981; Mutti et al., 1985; Barnolas et al., 1991 and 1992; Bentham, 1992; Arbués et al., 1998; Barnolas and Gil Peña, 2001, Fernández et al., 2004; Fernández-Bellón, 2004).

Our study has been focused on the Tertiary sediments cropping out from the core of the Boltaña anticline up to the uppermost sediments of the contiguous Buil syncline. The outcropping rocks range from Ypresian (Ilerdian) to Priabonian (Figure 1) and covers the entire stratigraphic sequence of the Aínsa Basin.

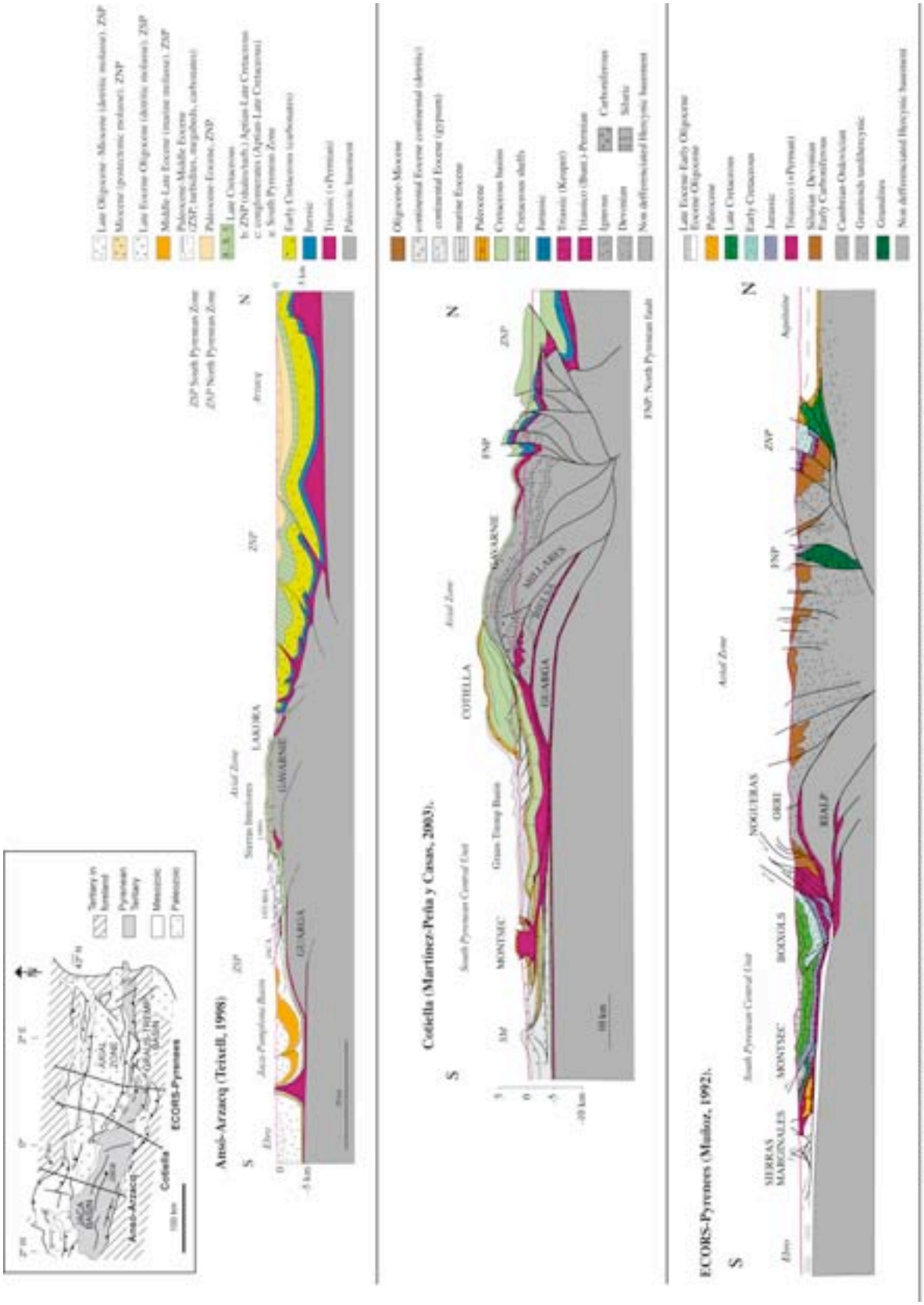

Figure 1. Three main cross-section where the units involved in the southern Pyrenean margin are shown

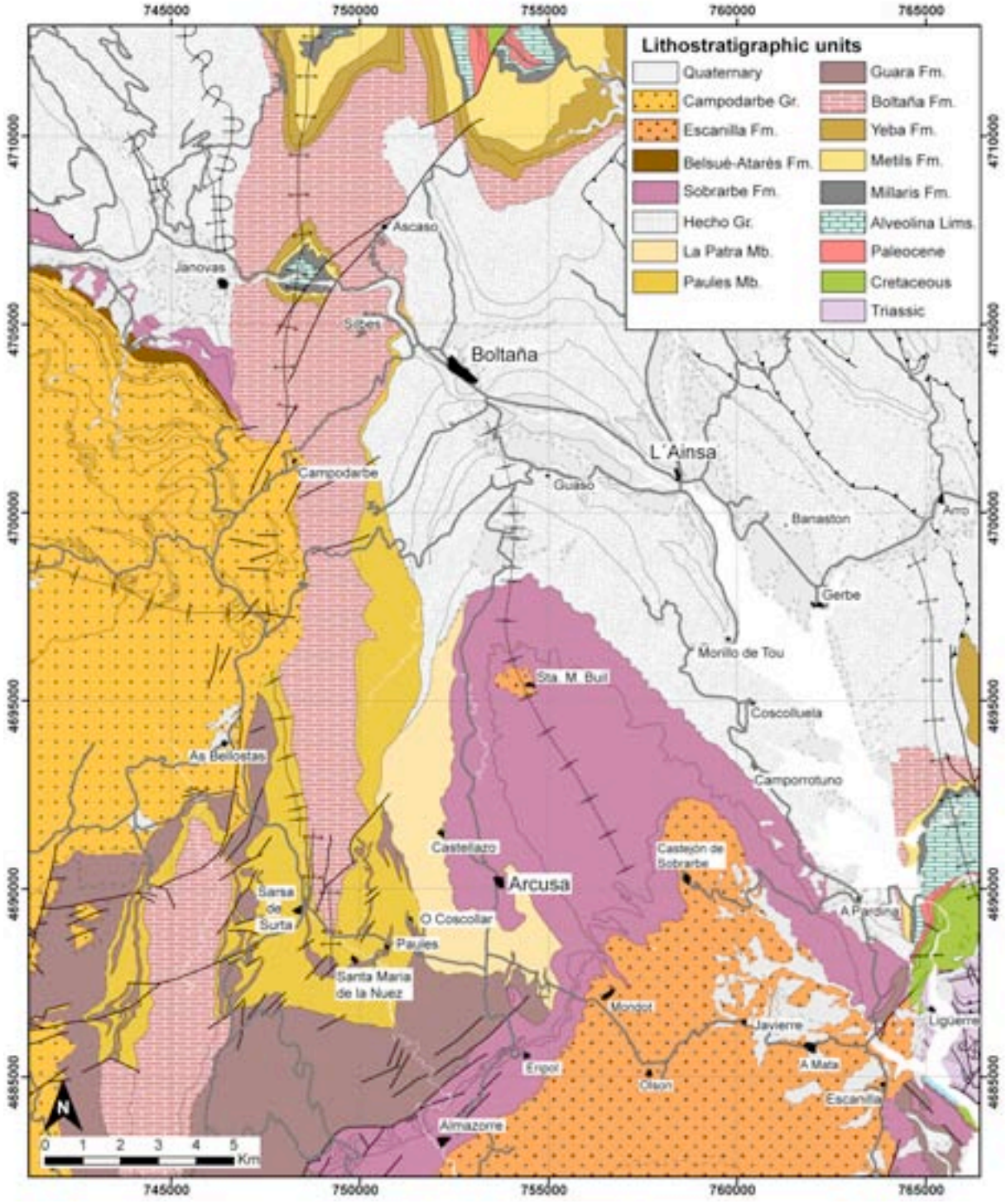

Figure 2. Geological map of the studied area, modified from Barnolas et al. (*in press* a and b). Formal and non-formal units have been individualized according their local use. UTM coordinates European datum ED50, zone 30T.

In the following sections, sampled formations will be marked in bold; nevertheless, we briefly describe all the units represented in the study area. Among them, the pre-tectonic units that can be distinguished are:

Triassic: Middle-Upper Triassic rocks constitute the detachment level for the thrust sheets and associated folds involved in the study area. It consists of shales with thin layers of coastal plain and lagoonal evaporites, limestones and dolostones from shallow marine environments. Its thickness is difficult to determine, Alastrué et al., (1957) estimates around 250 m in outcrops in the core of the Mediano anticline, in the SE corner of the study area.

Cretaceous: Cenomanian-Santonian (Upper Cretaceous) limestones and dolostones lie unconformably over Triassic rocks. A subsequent regional uncorformity evidences the beggining of the tectonic inversion (from extensional to compressive regimes) in the Southern Pyrenees. All this together, with the Campanian-Maastrichtian limestones and sandstones of the Marboré Fm, is almost 400 m thick in the Mediano anticline (Garrido-Megías, 1973) but can reach more than 3 km in the Cotiella unit (García Senz, 2002) in the NE edge of the study area.

Paleocene: It can be found in the north of the study area and locally in the south near the Mediano Reservoir. Dolostones (Fm Salarons, Van der Velde, 1967), limestones and sandy limestones with tidal structures (Fm Gallinera, Van der Velde, 1967) represent the Paleocene

Lower Ilerdian: The **Alveolina Limestones** (Mey et al., 1968), term equivalent to upper Gallinera Fm or Navarri Fm (Garrido-Megías and Ríos-Aragüés, 1972), represents the Lower Ilerdian in the Aínsa Basin. It is the consequence of an extensive transgression in the Pyrenean domain leading to the sedimentation of shelf-carbonated facies, as reflected by the stratigraphic discontinuity pointed by an erosive surface (Robador, 1991). It is composed of quartzite, quartz-gravelly limestones and limestones with chert nodules; its thickness ranges from 70 to 150 m (Fernández-Bellón, 2004). It represents the last quiescence stage before the development of the Aínsa foreland basin in the footwall of the SPCU (Garrido-Megías and Ríos-Aragüés, 1972; Nijman and Nio, 1975; Farrell et al., 1987; Vergés and Muñoz, 1990; Teixell and Muñoz, 2000) or the Montsec thrust sheet (Arbués et al., 1998; Fernández-Bellón, 2004; Fernández et al., 2004). It crops out in the cores of the Boltaña and Mediano anticlines (Figures 3 and 4).

Middle-Upper Ilerdian: The **Millaris Fm** (Van der Velde, 1967; Van Lunsen, 1970) represents distal ramp, deeper facies that conformably overlie the Alveoline Limestones. Marls and marly limestones with thin layers of fine-grained siliciclastic turbidites (tempestites) appear in its upper part (Barnolas and Gil-Peña, 1991). Its age is Middle Ilerdian (Barnolas and Gil-Peña, 2001; Mochales et al., 2011). It crops out in the cores of the Boltaña and Mediano anticlines. Total thickness ranges from 70 to 200 m although the section studied in this work covers 100 m.

The **Metils Fm** (Van Lunsen, 1970) overlies the Millaris Fm and is laterally equivalent to its upper part in some sectors. This unit is Middle Ilerdian in age (Barnolas and Gil-Peña, 2001; Mochales et al., 2011). It represents the progradation of carbonate ramp facies as evinces the decimetric limestone layers interlayered with thinner marl beds with abundant fossils (sponges, bryozoans and echinoderms). It thickens northwards, reaching 180 m in the Ara River section.

Relative deeper siliciclastic sediments evolving towards deltaic facies (**Yeba Fm**, Van Lunsen, 1970) conformably overlie the previous carbonate shelf. In the core of the Boltaña anticline, this unit includes a lower member with marls, siltstones and bioturbated sandstones and an upper member with bioclastic sandy limestone bed followed by two shallowing-upward sequences of marls, siltstones and sandstones. The entire Yeba Fm probably represents an important paleogeographic change to a more pronounced control in the foreland margin sedimentation by the orogenic geometry (Barnolas et al., 2011). The Yeba Fm includes the Ilerdian-Cuisian boundary (Mochales et al., 2011). The thickness of this unit is difficult to measure due to the transitional character of its upper part; an estimate of 170 m has been found for the entire Yeba Fm in the Ara River section (Figures 3 and 4).

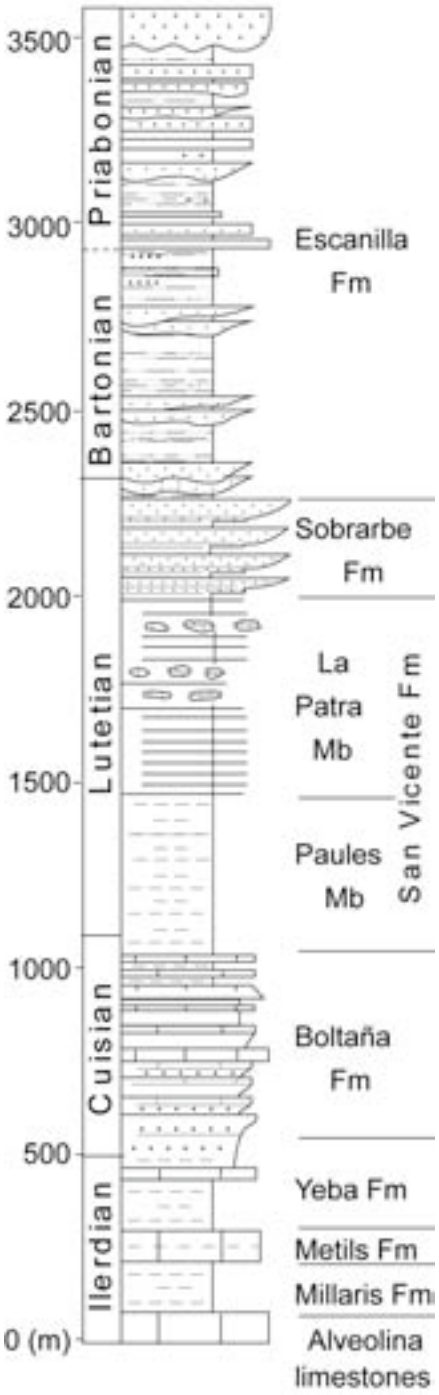

Cuisian: The second main carbonate platform in the Eocene (Barnolas et al., 2011) corresponds to the **Boltaña Fm** (Barnolas et al. 1991), Early-Middle Cuisian (Ypresian) in age, 550 m thick in the Ara River section (Mochales et al., 2011). Barnolas et al. (1991) differentiated three units: lower and upper Boltaña members separated by a double level of limestones with abundant *Assilina* (Ascaso Mb of Van Lunsen, 1970) indicative of a marine transgression (Barnolas and Gil-Peña, 2001). The lower Boltaña Fm corresponds to a mixed shelf (siliciclastic and shallow carbonatic) cropping out in the Boltaña and Mediano anticlines. It is made up of shallowing-upwards sequences with siliciclastic base (marls, siltstones and cross bedded, bioturbated sandstones) including *Assilina*, *Nummulites* and *Discocyclina* whereas its top is shallower, formed by sandy limestones with abundant *Alveolina*. The upper Boltaña Fm presents progressively deeper, shallowing-upward sequences, acquiring therefore a retrogradational character (Barnolas and Gil-Peña, 2001). Its top contains distal ramp carbonates with abundant slump scars and micritic limestones (Figures 3 and 4).

Figure 3. Simplified stratigraphic log where the main units dealt in this work are distinguished.

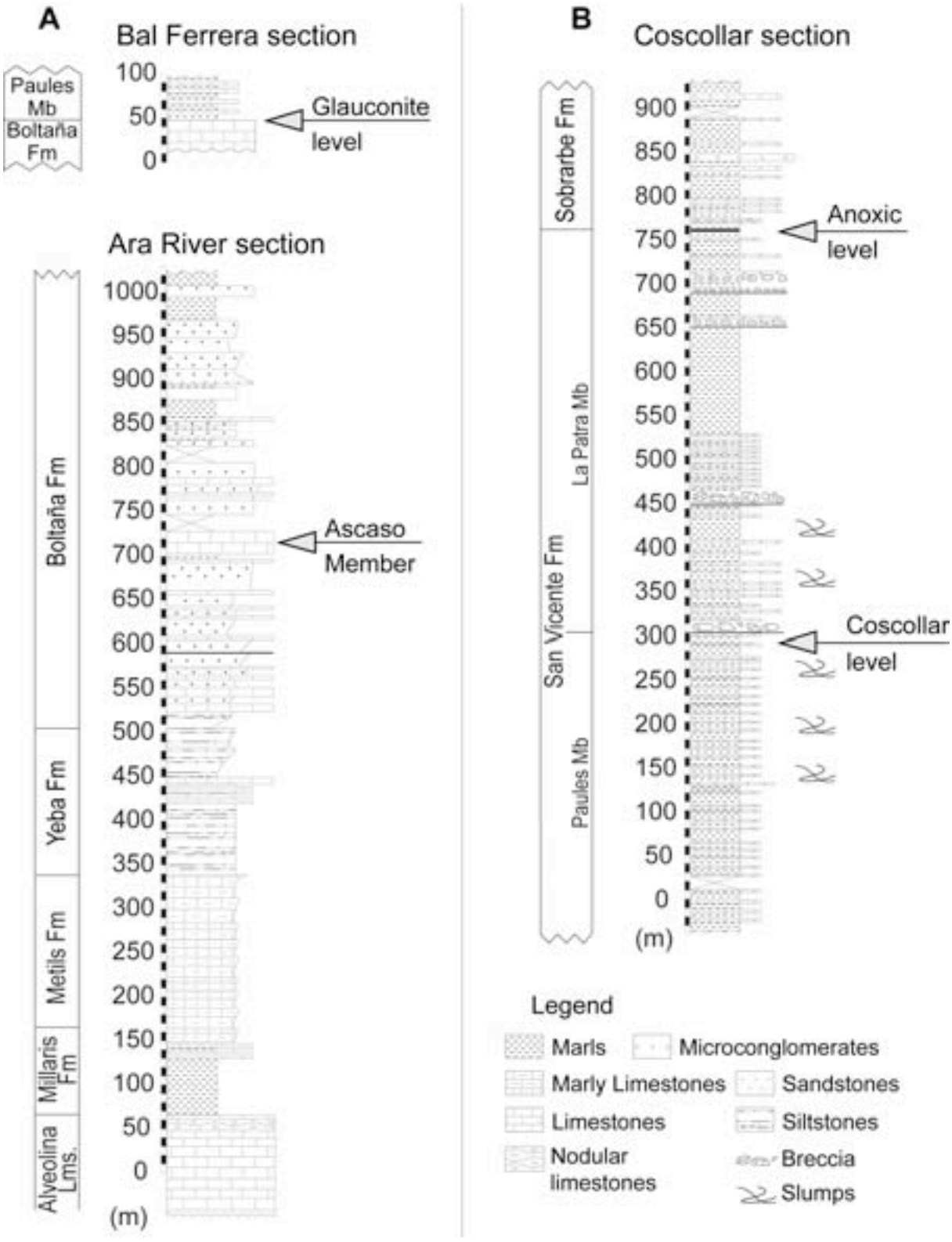

Figure 4. A) Stratigraphic column of the Ara River and Bal Ferrera sections, located in the western and eastern limbs, respectively, of the Boltaña anticline. In this log, the pre-tectonic units sampled in this work and reference levels can be distinguished. B) Stratigraphic column of the Coscollar section (including the Sarsa de Surta section), located in the eastern limb of the Boltaña anticline. This profile represents the the onset of syn-tectonic sedimentation.

In some outcrops a distinctive glauconite level is recognised at its top. All these features point to a flooding surface (Late Cuisian) that represents more than 12 km of the foreland-ward migration of shelf facies (Barnolas et al., 2011). Coeval with this flooding surface a slope truncation is recognized in the north, representing the collapse of the carbonate margin with the later onlap of Lutetian siliciclastic turbidites. (Van Lunsen, 1970; Ríos-Aragüés et al., 1982; Barnolas and Teixell, 1994; Barnolas and Gil-Peña, 2001).

Lutetian: The Early Lutetian is the first syntectonic episode in the Aínsa Basin as evidenced by the interaction between developing structures and depositional systems in the Mediano anticline (Barnolas et al., 1991; Bentham, 1992; Holl and Anastasio, 1993; Teixell and Barnolas, 1995; Poblet et al., 1998; Fernández-Bellón, 2004)

The **San Vicente Fm** (Van Lunsen, 1970) conformably overlies the Boltaña Fm. The contact between both units can be observed in the eastern limb of the Boltaña anticline and in its southern periclinal termination (Bal Ferrera and Sarsa de Surta sections). The San Vicente Fm is used here in the sense proposed by De Federico (1981). In the southern outcrops of the San Vicente Fm, it consists of distal carbonate ramp marl and marly limestones facies (Barnolas and Teixell, 1994), frequently slumped, with some interlayered siliciclastic turbiditic entries from the north and olistostromes of shallow carbonate facies. In this area, two members of the San Vicente Fm were defined by De Federico (1981); the lower, Paules Mb and the upper, La Patra Mb (Figures 3 and 4).

The **Paules Mb** consists of marls and nodular marly limestones (De Federico, 1981). The lowest part of the Paules Mb corresponds to a retrogradational ramp with low sedimentation rate and sedimentary instability which is evidenced by the abundance of internal stratigraphic truncations and glauconite levels. This retrogradational character turns to progradational in the upper part of the Paules Mb (Barnolas et al., 1992) as a result of the increase in sedimentation rate (Mochales et al., 2011). The lowermost part of the Paules Mb contains the Ypresian/Lutetian boundary (Canudo, 1990; Mochales et al., 2011) and the age of this member spans to the Middle Lutetian. Its thickness is strongly variable, interlayering northwards with the Hecho Group (Mutti et al., 1972), see lateral correlations of facies in the figure 5. The sections here studied in the Coscollar area reach 350 m of thickness.

The transition to the **La Patra Mb** (De Federico, 1981, corresponding to the Coscollar Mb by Barnolas et al., 1991) is located in a flooding surface with glauconite, which is followed by a slope carbonate breccia (O Coscollar level). The La Patra Mb corresponds to a base of slope carbonate breccias interlayered with slope marls and scarce distal siliciclastic turbidites from the basin trough (Figure 5). This carbonate breccia slope develops at the foot of an erosional truncation in the shallow carbonate Guara Fm limestone (Barnolas et al., 1992). La Patra Mb also thins northwards, interlayering with the Hecho Group turbidites; in the section studied nearby Castellazo village it reaches 460 m.

The Guara Fm (Puigdefàbregas, 1975), which consists of shallow carbonate shelf limestone with abundant foraminifers (Samsó et al., 1994), crops out in the southern part of the study area (Balzes anticline). In this area its age is Early to Middle Lutetian but westwards, in the External Sierras, it also includes the Late Lutetian (Samsó et al., 1994; Rodríguez-Pintó et al., 2011c). In the Mediano

anticline area Lower and Middle Lutetian (Bentham and Burbank, 1996) shelf and reefal limestones are recognised, distally interlayered with turbiditic sandstones and marls of the Hecho Group. In this area the sedimentation was controlled by the growth of the Clamosa diapir and the Mediano anticline (Garrido-Megías, 1973; Teixell and Barnolas, 1995; Poblet et al., 1998).

The Guara Fm, together with the Paules and La Patra Mbs of the San Vicente Fm represents the distal foreland carbonate margin in Early and Middle Lutetian. Siliciclastic turbiditic complex of the Hecho Group (Mutti et al., 1988; Payrós et al., 1999; Remacha et al., 2003) replace these facies towards the north and northwest (Figure 5). The siliciclastic turbidites and marls of the Hecho Group, cropping out in the Aínsa basin, were named as San Vicente Fm by Van Lunsen (1970).

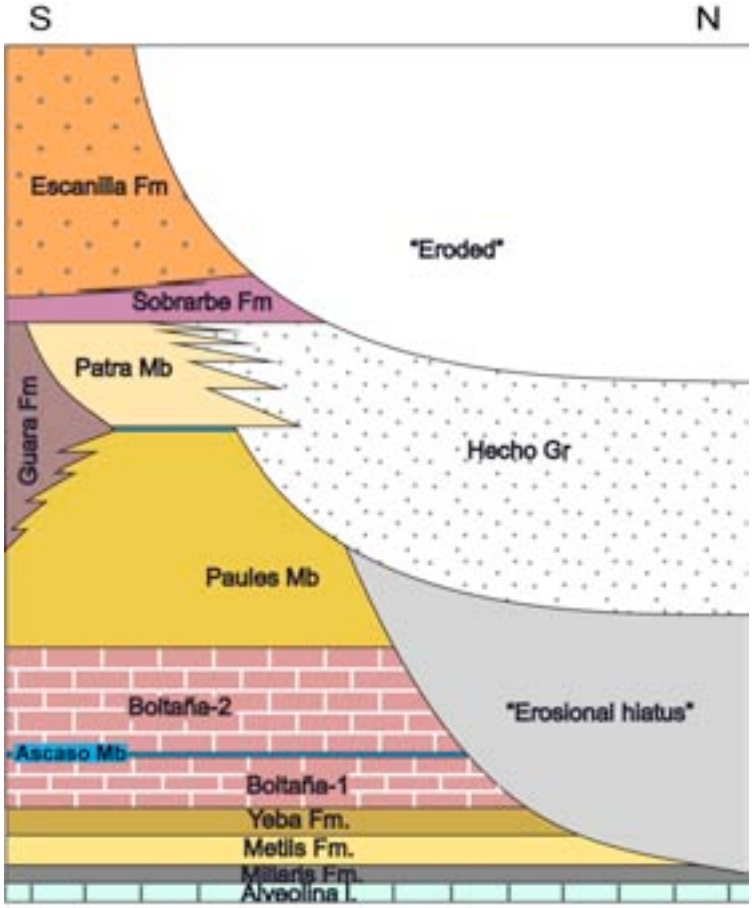

Figure 5. Lateral correlation of facies between the units studied in this work (Mochales et al., 2011). The pre-tectonic sequence is partially eroded. The syn-tectonic sequence is laterally correlated with the turbiditic Hecho Gp to the North and Northwest and with the Guara Fm to the South. The transitional Sobrarbe Fm conformably overlies this section, which together with the Escanilla Fm are subsequently eroded.

As previously mentioned, the transition from shelf to turbidites is recorded by the regional unconformity during Cuisian times that truncated the shelf strata and their onlap with the Hecho Group turbidites. Three main stages of evolution, related to the platform collapse surfaces, can be recognized in the siliciclastis rocks of the Aínsa Basin (Mutti et al., 1985; 1988; Barnolas et al., 1991; Arbués et al., 1998). The first presents a thin interval of fluvio-deltaic rocks (Fígols and Montañana allogroups), the intermediate recorded shallow marine and turbidites (Castissent, Charo, Santa Liestra

and Banastón allogroups), the third stage was deposited contemporary to tectonic deformation (Aínsa allogroups, see Mutti et al., 1985, Remacha et al,. 1998, Soto and Casas, 2001). Each cycle is composed of minor cycles including a basal coarse-grained unit with turbidite system features and a mudstone-rich cover deposited by low-density turbidity currents. The Hecho Group is essentially Lutetian (Teixell and Barnolas, 1995; Barnolas and Gil, 2001), whereas isolated examples testify a possible Cuisian onset (as in the western part of the Basin; Payrós et al., 1999).

Paules and La Patra Mbs are local names and some authors have ommited them, but they are useful for the purposes of this work. According to the allogroups sequence, the lower Las Paules Marls were assimilated to the Banastón allogroup whereas La Patra Marls where assimilated to the Aínsa 1 sequence of the San Vicente allogroup (Soto and Casas, 2001).

A sharp transition between the previous units (La Patra Mb and Hecho Group) with the siliciclastic **Sobrarbe Fm** (De Federico, 1981) occurs over a thin dark marl level (anoxic level of Barnolas et al., *in press* a, see figures 3, 4, 5 and 6). The Sobrarbe Fm is a N-NW prograding deltaic wedge filling the Buil syncline between the growing Mediano and Boltaña anticlines. It includes transgressive bioclastic banks of *Nummulites* between sequences of regressive prograding lobes, conformed by shoreface sandstones regularly interlayered with offshore marls and sandy marls (De Federico, 1981; Barnolas et al., 1992; Muñoz et al. 1998; Dreyer et al., 1999). Its age is Middle-Late Lutetian (Muñoz et al., 1998; Barnolas et al., *in press* a). Sections studied in this work (Mondot section) indicate a thickness of 250 m for the Sobrarbe Fm.

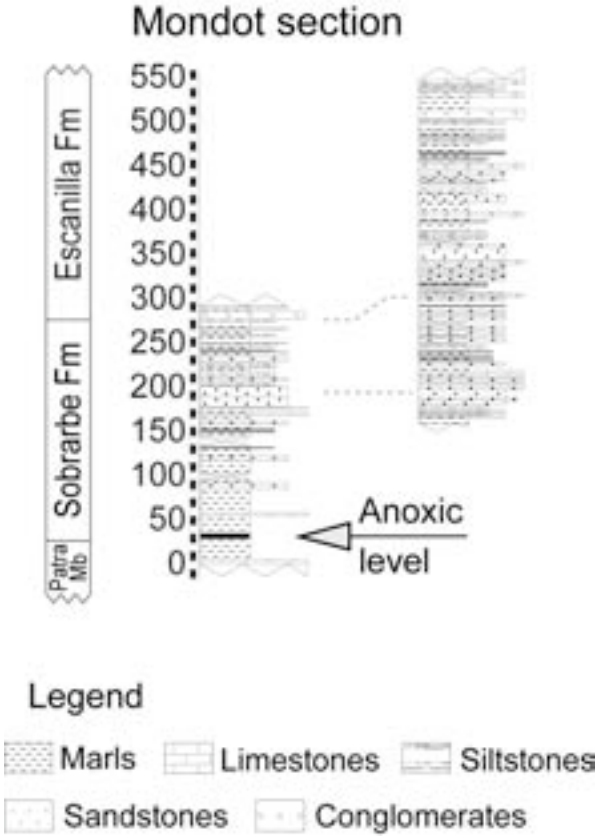

Figure 6. Stratigraphic log of the Mondot section, located in the eastern limb of the Boltaña anticline. Units sampled in this work and a reference level can be distinguished.

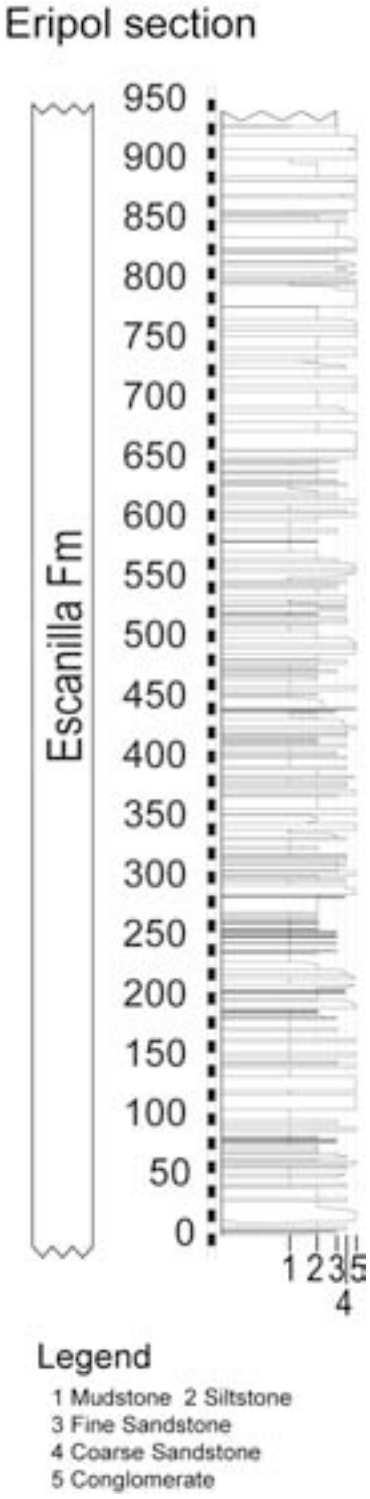

Bartonian-Priabonian: In the south of the Biello-Sobrarbe the upper part of the Sobrarbe Fm crops out in lateral equivalent continental red beds that have been included in our section into the **Escanilla Fm** (Garrido-Megías, 1968). The contact seems to be concordant and diachronous, with lateral equivalences existing between them (De Federico, 1981), figures 3, 5, 6 and 7. The rest of the Escanilla Fm is Bartonian to Priabonian in age (Bentham, 1992; Bentham and Burbank 1996). The Escanilla Fm is interpreted as the record of low-sinuosity stream systems generally flowing axially along the partitioned late Eocene foreland Basin (Garrido-Megías, 1973; Bentham, 1992). Channels of sandstone and conglomerates alternated with progressively redder marls are its main elements. It belongs to the lower part of the Campodarbe Group, consisting of an alluvial-fluvial system.

The Campodarbe Group lies conformably upon the shallow marine and deltaic facies of the Belsué-Atarés Fm in the Jaca basin whereas it lies on a conspicuous unconformity in the western limb of the Boltaña anticline. There is not a consensus regarding the lateral correlation between the Escanilla Fm and the lower part of the Campodarbe Fm. Puigdefàbregas (1975) and De Federico (1981) propose a coeval evolution of both systems (Figure 2). On the other hand, Bentham (1992) proposes an earlier development of the Escanilla Fm whose lower and middle members (Puigdefàbregas, 1975) would be equivalent to the Belsué-Atarés Fm. The upper Mb of the Escanilla Fm would be coeval to the Campodarbe Group in the Jaca Basin (Bentham, 1992). Somehow, both units seem to belong to the same fluvial system regarding the facies-type and the sedimentary environments, deposited during the final stages of deformation of the Aínsa Basin.

Figure 7. Stratigraphic log of the Eripol section (modified from Bentham, 1992), located in the eastern limb of the Boltaña anticline.

Finally, the Sariñena Fm (Quirantes, 1978) unconformably overlies the Escanilla Fm and older sediments. This unit is mainly made up by conglomeratic molasse sourced in the north and northeast, including clasts from the Axial Zone with four stages of development. They evolved from high to low efficient alluvial system, ending in typical marly distal fan environments (Luzón-Aguado, 1999). Its age is Olicocene-Early Miocene (Puigdefàbregas, 1975, Riba et al., 1983) and postdates the later stages of Pyrenean deformation in the eastern External Sierras (Millán et al., 2000).

3.2. Structure

3.2.1. Foreland Basin development

In convergent settings, sediments accumulate in foredeep and thrust sheet top basins in the flexural downward, commonly called foreland basin, ahead of orogenic wedges. Foreland basins develop at the front of active thrust belts where the main transport direction is toward the evolving basin. Basin is underfilled and turbidites generally deposit first. Subsequent deposits are shallow marine or continental as the basin becomes stable or overfilled. The fragmentation or complete detachment of the basin depends on the thrusting propagation rate, presence of underlying detachment horizons or angle of convergence (Allen and Allen, 2005).

The Southern Pyrenees is a complex basin segmented contemporaneously with sedimentation in a piggyback setting. In Late Ilerdian times, the Cotiella nappe emplacement forced the basin break-up in three sub-basins: the Eastern South-Pyrenean foreland Basin, the Tremp-Graus Basin and the Jaca basin. The Eastern South Pyrenean Basin and the Jaca Basin remained as non-detached marine foreland basins, with the same sedimentary model occurring in Ilerdian times. Meanwhile, the Graus-Tremp Basin became a piggyback basin related to the Cotiella thrust, acquiring continental features. Within this frame, a thrust propagated in front of the main thrust along the Triassic evaporites. During Early Paleogene the Graus-Tremp Basis was detached from the Variscan basement and transported southwards by thrusts linked to the emplacement of the SPCU, with piggyback basin features. In earliest Eocene times the Montsec thrust began to develop in front of the Graus-Tremp basin, propagating southwestwards to the Mediano oblique ramp by mid-Cuisian times (Farrell et al., 1987). Growth of the Boltaña anticline to the west of the Aínsa basin indicates that the Aínsa basin was detached as a thrust-sheet-top or piggyback basin in the Lutetian (Farrell et al, 1987).

At present, the Boltaña anticline is a N-S trend anticline, defining the boundary between two structural domains. It separates the Jaca Basin form the Graus-Tremp Basin. Its western boundary is the sub-basin called Aínsa Basin. The Boltaña anticline, as well as the Mediano anticline, deformed and controlled the deposition of the Middle and Upper Eocene sediments in the Aínsa Basin (Puidefàbregas, 1975). In the western margin of the Aínsa basin, shelf and slope facies derived form the eastern Graus-Tremp Basin that in turn would evolve into deeper facies in the western Jaca Basin (Soto et al., 2002). Sharp variations on the accumulations rates and erosive processes affecting the Lutetian slope marls located on the Buil syncline would probably be conditioned by the geometry of the structures in this zone. Subsequently, the southern basin as a whole, formed by the Graus-Tremp, Aínsa and Jaca Basins, was transported southwards and separated from the Ebro Basin by the front thrust of the Marginal Sierras and External Sierras (Vergés and Muñoz, 1990; Anastasio, 1992; Teixell, 1996; Meigs, 1997; Millán et al., 2000; Teixell and Muñoz, 2000).

3.2.2. The Sobrarbe synclinorium

The set of structures of the western sector of the Aínsa basin, included into the Graus-Tramp Basin, conform a complex oblique fault and fold system. The folds here involved are directly related

to underlying faults, associated with their propagation, displacement and the accommodation of deformation between neighbouring faults. These oblique structures are the Boltaña, Mediano and Olsón anticlines and the Buil syncline, located in the hangingwall of the External Sierras-Guarga thrust. They are contemporary with the Eocene sedimentary units.

These oblique structures have a still controversial origin: whereas some authors propose a salt tectonic origin (Holl and Anastasio, 1993), others consider them attached to major oblique ramps (Garrido-Megías and Ríos-Aragüés, 1972; Farrell et al., 1987; Teixell, 2004). Subsequent characterizations of the geometry and kinematics of the western end of the SPCU (Soto and Casas, 2001; Soto et al., 2002) led to propose a pre-tectonic syn-sedimentay wedge thinning towards the west as a main feature conditioning the formation of these structures. Moreover, the Late Triassic viscous material migrated laterally as a consequence of differential overburden of Mesozoic materials. The origin of these oblique structures has been determined to be secondary because of the clockwise rotation responsible for their present configuration (Dinarès et al., 1992; Fernández-Bellón, 2004; Oms et al., 2006). Factors triggering the development of oblique structures in thrust and fold belts might be the positive inversion of preexisting extensional geometries, gradients of shortening along strike, irregular thrust surfaces, differential frictional/thickness features of the detachment layer and cover, changes in sedimentation rates and syntectonic geometries (Soto et al. 2002 and references therein).

3.2.2.1. The Boltaña anticline

The Boltaña anticline is a west-verging, N-S trending (N004, Mochales et al., 2010) 25 km long cylindrical fold (Cámara and Klimowitz, 1985; Martínez-Peña, 1991; Holl and Anastasio, 1995a and 1995b; Millán, 1996; Soto et al., 2003; Fernández-Bellón, 2004). It shows non-significant plunges, except for its southern part where a gentle fold-closure is observed. Its eastern flank shows shallower dips (20-30º) than its western flank (70-80º). The Boltaña anticline has been interpreted to be related to a blind thrust ramp that defines de westward vergence of the fold (Cámara and Klimowitz, 1985; Farrell et al., 1987; Mutti et al., 1988; Martínez Peña, 1991; Holl and Anastasio, 1995; Millán, 1996; Muñoz et al., 1998; Soto and Casas, 2001; Fernández et al., 2004). The thrust-anticline system (Balzes-Boltaña sheet; Millán, 1996) is *décolled* on the Triassic evaporites that form the detachment level to the south Pyrenean thrust system. The thrust that originates the Boltaña anticline presents a displacement of 2,3 km (Soto and Casas, 2001) reaching upwards the San Vicente Fm. This system is located in the hanging wall of the younger Alcanadre-Tozal thrust sheet located in the External Sierras, to the South of the studied area (Millán, 1996, 2006).

Pre-tectonic rocks folded above the evaporitic detachment are mainly of Cretaceous-Ypresian age (as deduced from the Boltaña-1 well data; Lanaja, 1987). Cuisian units thin toward the south, seemingly related to tectonic subsidence associated with the Axial Zone thrust sheet emplacement (Fonnesu, 1984; Puigdefàbregas and Souquet, 1986; Soto and Casas, 2001; Mochales et al., 2010). On the other hand, there is no agreement about the onset of folding in the Boltaña anticline. Several studies suggest that its growth started in Early Lutetian (Arbués et al., 1998; see mapping in Poblet et al., 1998, and thickness variations in depth in Soto and Casas, 2001). Nevertheless, other authors

suggest a younger onset of the deformation, during the Middle Lutetian (Millán, 1996) or at least not before this period (Barnolas et al., 1991). Mapping by Puigdefàbregas (1975) indicates that the deformation might have started as late as the Late Lutetian. The final stages of the Boltaña anticline folding would be bounded at the Late Bartonian times (Puigdefàbregas, 1975; Bentham, 1992; Montes, 1992; Teixell, 1996; Barnolas and Gil-Peña, 2001).

3.2.2.2. The Mediano anticline

The Mediano anticline is a 20 km long detachment fold (Holl and Anastasio, 1993; Poblet et al., 1998). It presents an open and symmetric configuration with a NW-SE trend in its northern part, whereas its southern part shows a narrow, east verging fold with northwards plunge (Poblet et al., 1998). Pre-tectonic sediments are constituted by a thick layer of Triassic shales and evaporites in its core, overlain by Cenomanian carbonates, Garumn facies and Cuisian marls that define the northern termination of the structure. The core of the anticline is cut by several normal faults, as the NE-SW fault responsible for the uplift of its southern block, cropping out the Clamosa dome (Teixell and Barnolas, 1995).

Biostratigraphic and magnetostratigraphic evidences, as well as angular unconformities observed in the Lutetian rocks indicate the onset of Mediano anticline growth, developed from Early Lutetian to Bartonian (Barnolas et al., 1991; Holl and Anastasio, 1993; Teixell and Barnolas, 1995; Bentham and Burbank, 1996; Poblet et al., 1998). Its N-S trend is still under debate: whereas some authors propose a relation with the oblique ramp of Montsec-Peña Montañesa thrust (Farrell et al., 1987; Anastasio, 1992; Bentham, 1992), others consider a linking with the footwall of this oblique ramp (Séguret, 1970; Nijman and Nio, 1975; Cámara and Klimovitz, 1985; Holl and Anastasio, 1993).

3.2.2.3. The Buil syncline

The wider wavelength Buil syncline separates the Boltaña and Mediano anticlines. It shows a general N-S trend with a curved trace towards the east at mapping-scale. It presents a gentle southwards plunge in its southern sector (Fernández-Bellón, 2004). Its growth is linked to the Mediano and Boltaña anticlines. Spatial distribution of paleoflow marks, biostratigraphic and magnetostratigraphic dating in the Mediano anticline bound the age of deformation from Early Lutetian to Bartonian (Bentham, 1992; Bentham and Burbank 1996; Poblet et al. 1998). The Buil syncline acted as a sedimentary trough for the turbiditic and deltaic systems of the San Vicente and Sobrarbe Fms respectively (Mutti et al., 1988; Barnolas et al., 1991; Remacha et al., 1998), defining northwards the periclinal termination of the Buil syncline. Seismic data reveal the occurrence of a secondary and buried anticline, the Olsón anticline, below the Buil syncline. This is a hangingwall anticline related to the Boltaña anticline (Soto and Casas, 2001; Fernández-Bellón, 2004). The thrust responsible for this anticline has a displacement of 1 km (Soto and Casas, 2001) dying out at the base of the Boltaña Fm. The Arcusa anticline is placed between the Boltaña and Olsón anticlines, whose axis trends is NNW-SSE (Soto and Casas, 2001).

3.2.3. Cross-sections

Several authors have attempted to decipher the kinematics of the Aínsa Basin by means of cross sections perpendicular or parallel to the N-S structures (Cámara and Klimowitz, 1975; Holl and Anastasio, 1995 a and 1995b; Millán, 1996; Poblet et al, 1998; Soto and Casas, 2001; Fernández et al., 2004), figure 8. Among them, some were performed using seismic lines, boreholes (Boltaña-1 and Surpirenaica-1) and surface data obtained from fieldwork.

Figure 8. Geological cross sections across the Boltaña anticline and surrounding areas (García-Lobón et al., 2010). Geology by Choukroune and Seguret, 1973. OF (Fernández-Bellón, 2004), SMP, SSI (Séguret, 1972), P (Poblet et al., 1998) M (Millán, 1996), RS (Soto, 2003), T (Tavani et al., 2006) HA (Holl and Anastasio, 1995a, b).

3.2.3.1. Perpendicular crosss-sections

A-A' cross section from Soto and Casas (2001) and Soto (2003) extends from the western flank of the Boltaña anticline to the northern prolongation of the Mediano anticline (Figure 10a). It cuts orthogonally the Buil syncline and obliquely the Boltaña anticline. The structure is mainly defined by two west-verging thrusts that detach in the Mesozoic series and branch at depth. These thrusts are associated with hanging wall anticlines: the Boltaña and Olsón anticlines with 2,3 and 1 km of displacement respectively for their associated thrusts. The former affects the San Vicente Fm whereas the latter dies out in the Boltaña Fm. The cross-section crosses through the periclinal termination of the Buil syncline, defined by the allogroups Aínsa 1 and 2 (La Patra Mb and basal part of the Sobrarbe Fm). In the footwall of the thrust associated to the Boltaña anticline a horse of Cretaceous limestones is observed, as attested by the Boltaña-1 well (Lanaja, 1987). The thickness of the syntectonic units seems to vary laterally. Except for the Upper Triassic, all the units up to the Boltaña Fm remain with constant thickness and thickness variations start from the San Vicente Fm upward. Underlying the thrust system a southwards imbricated sheet of Paleozoic rocks is interpreted. Below, Mesozoic and Tertiary autochthonous rock correspond to the foreland basin (Soto and Casas, 2001), figure 10.

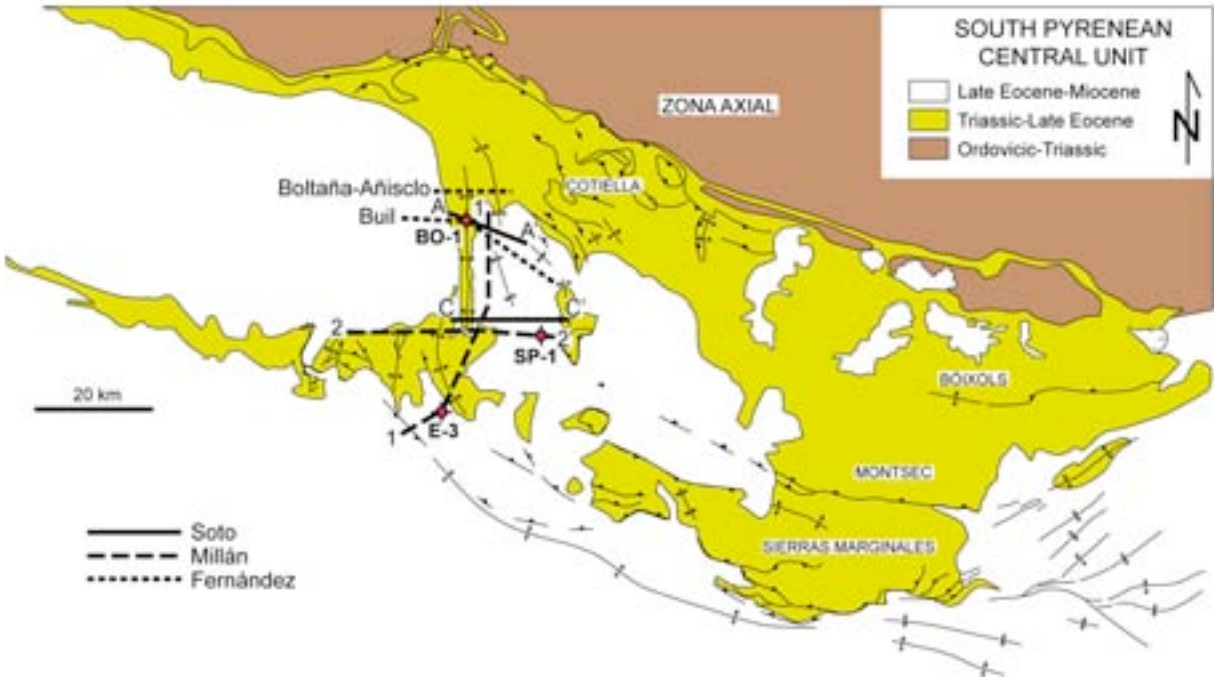

Figure 9. Sketch with the main cross-section in the study area: A-A' and C-C' (Soto el al., 2001; Soto, 2003), 1-1' and 2-2' (Millán, 1996), Buil and Boltaña-Añisclo (Fernández-Bellón, 2004; Fernández et al., 2004). Nearby boreholes are marked in red (Boltaña-1, Surpirenaica-1 and Ebro-3).

Another perpendicular cross-section to the Aínsa basin crosses through the eastern flank of the Balzes anticline, the Arcusa and Olsón anticlines, the Buil syncline and finally reaches the Mediano anticline (C-C' from Soto and Casas, 2001). Two west-verging thrusts detached in the Triassic with

small displacement, reaching the base of the Boltaña Fm., appear in this section. The Mediano anticline is interpreted as a detachment fold, with its core constituted by Triassic rocks. The La Patra Mb and the base of the Sobrarbe Fm are not present in the core of the Buil syncline (Figure 10b).

The 2-2' section (Millán, 1996, 2006) has a N100E orientation and links the western SPCU structures with the northeasternmost structures of the External Sierras (Figure 11, cross section 2-2'). The External Sierras form an imbricate system towards the W, whose thrusts roots in the Basal South-Pyrenean thrust. The eastern part of the section shows that the folds developed during the Middle and Late Eocene (Millán, 1996). From W to E: Balzes, Boltaña and Olsón anticlines, Buil syncline and Mediano anticline. The Tozal-Alcanadre and Balzes-Boltaña blind thrust sheets can be distinguished (Figure 11).

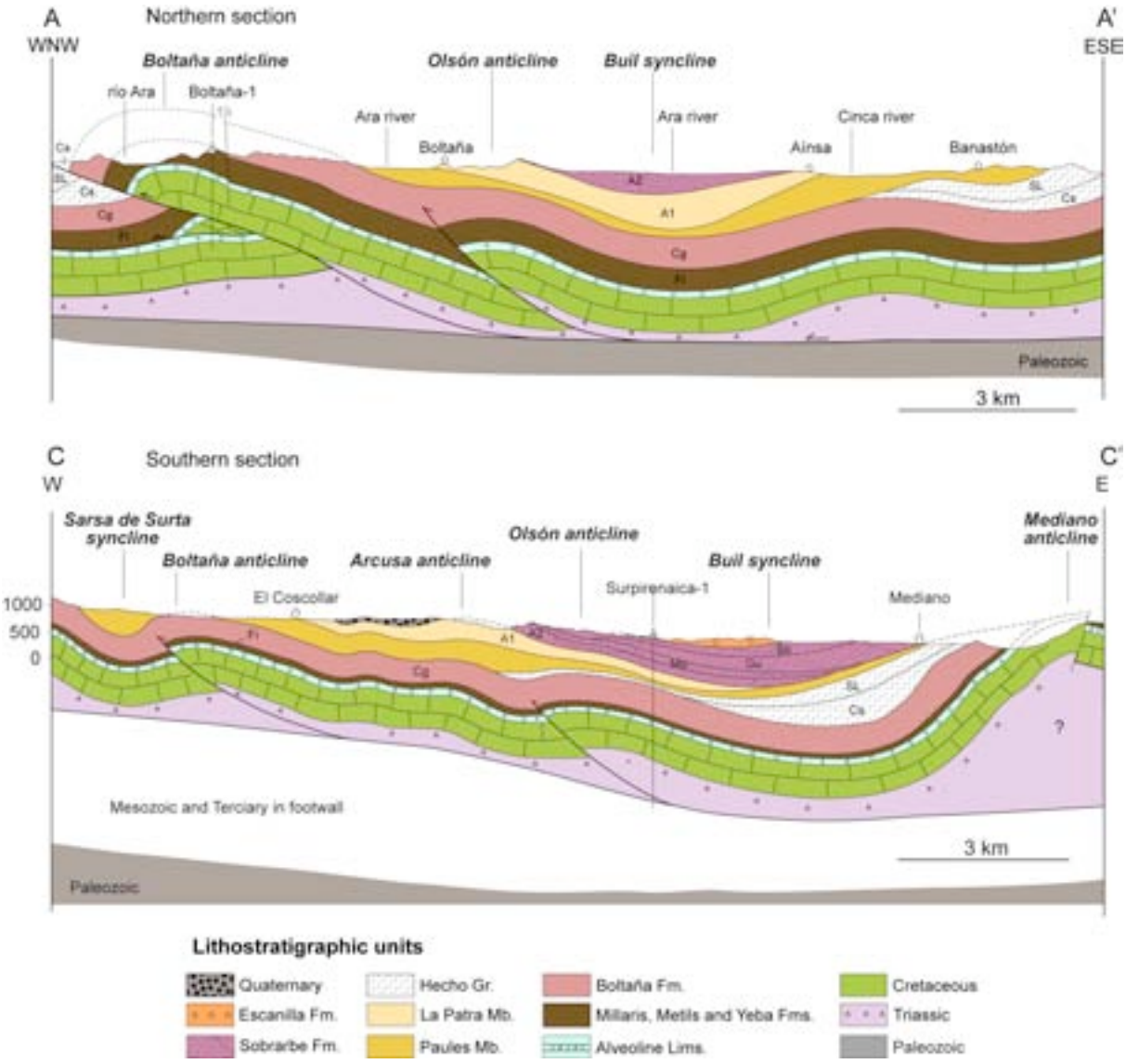

Figure 10. Sections A-A' and C-C' redrawn form Soto et al. (2001). The acronyms of the allogroups used by the author (Fi: Figols; Cg: Castigaleu; Cs: Castissent; SL: Santa Liestra; A: Aínsa; Mo: Morillo; Gu: Guaso; So: Sobrarbe) have been used. Nevertheless the units used in this work are also indicated in the legend. The sections cut the northern and southern part of the Boltaña anticline and Buil syncline.

The Mediano anticline presents a more complete Mesozoic series than the External Sierras, including Cenomanian and Jurassic rocks. The Boltaña thrust continues farther west than the Boltaña anticline, connecting with the Balzes thrust. The Triassic-Cretaceous strata of the Tozal-Alcanadre sheet are located above the authoctonous of the External Sierras and extend sub-parallel eastwards underneath the Boltaña-Balzes sheet. At least from the Boltaña to the Olsón anticlines, the Boltaña-Balzes thrust presents geometry of a hangingwall flat in the Triassic and footwall ramp for the Tozal sheet (Figure 11, cross-section 2-2'). This ramp would be oblique to the NNE-SSW transport direction of the south Pyrenean cover. The Boltaña-Balzes thrust sheet would have been part of the same system for, at least, the Middle Lutetian-Bartonian interval, a period when deformation was shared between both folds (Millán, 1996).

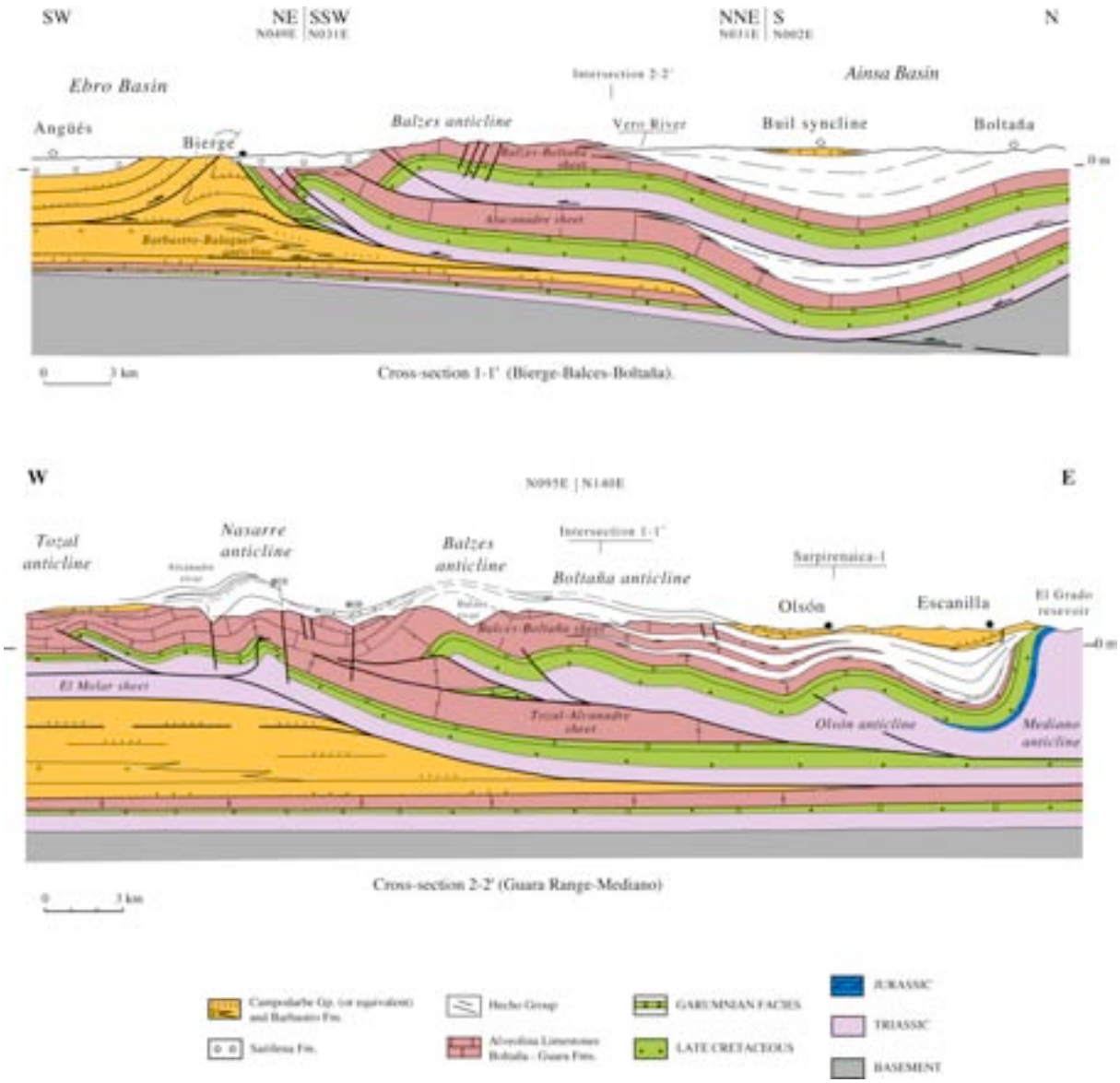

Figure 11. Sections 1-1' and 2-2' redrawn from Millán (1996), units have been modified. The section 1-1' is broadly parallel to the main structures. The section 2-2' is perpendicular to them. From W to E, this section cuts the Tozal, Nasarre, Balzes and Boltaña anticlines, Buil syncline and Mediano anticline, all belonging to the imbricate thrust system extending from the western boundary of the SPCU to the External Sierras.

The W-E to NW-SE cross-section by Fernández et al. (2004) crosses through the Boltaña anticline, Buerba syncline, Añisclo anticline, Buil syncline and the western limb of the Mediano anticline. To the north the Buil syncline opens around the Añisclo anticline to form the Buerba and San Vicente synclines (Figure 12). The Mediano anticline is an east-verging detachment fold (Poblet et al., 1998) that dies out northward below the Aínsa Basin. The Añisclo anticline is a west-verging fault-propagation fold, plunging 25º to the south at its periclinal termination below the Aínsa Basin (Fernández-Bellón, 2004; Tavani et al., 2006). The Boltaña anticline is also a west-verging fault-propagation fold, with a sub-horizontal fold axis that extends beyond the Aínsa Basin both to the north and south (Fernández et al., 2004).

a) Buil cross-section

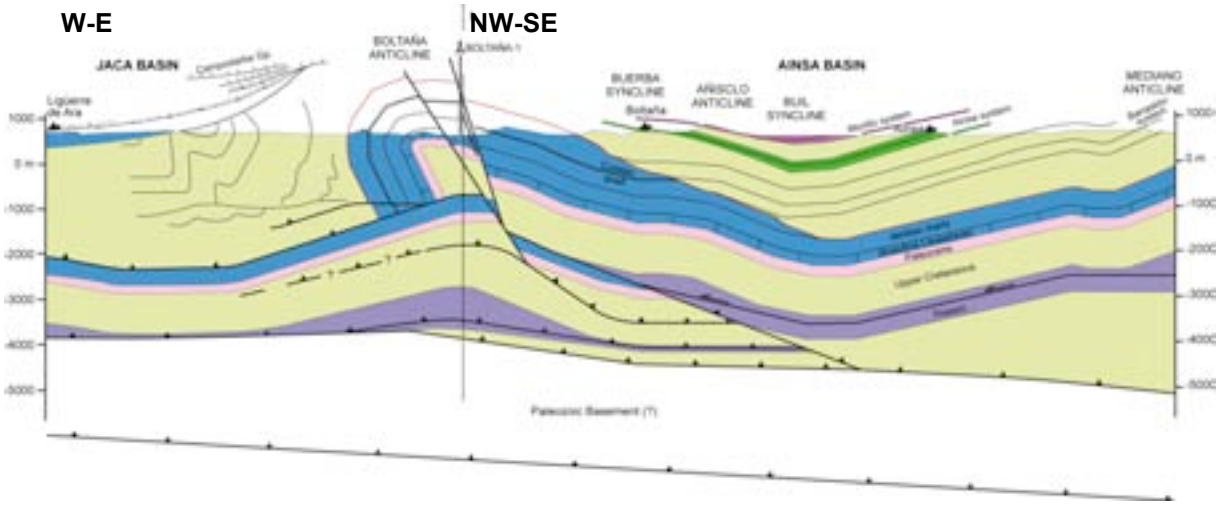

b) Boltaña-Añisclo cross section

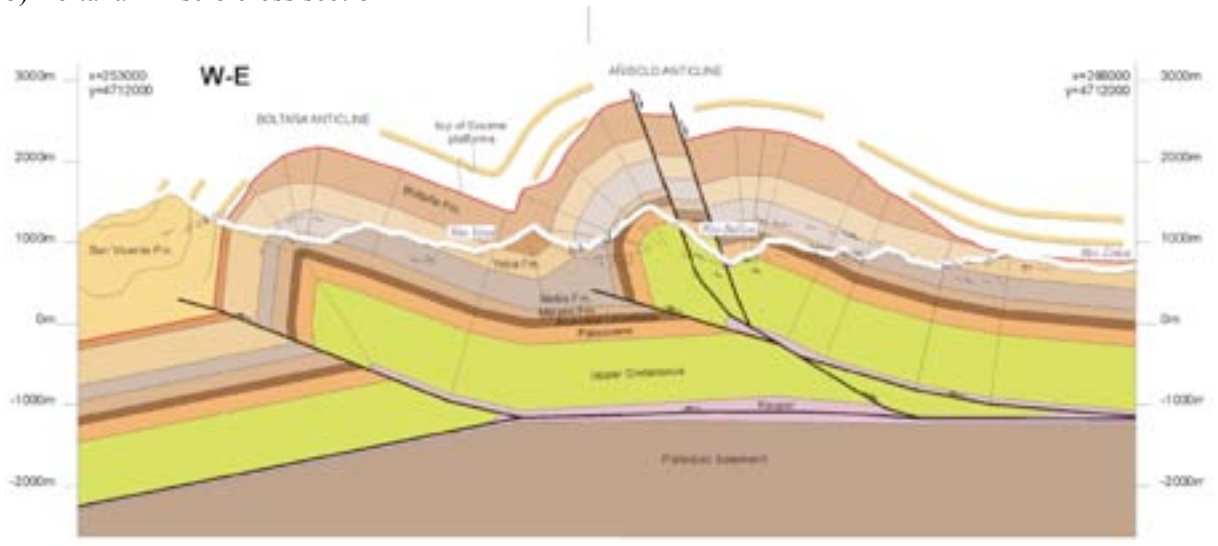

Figure 12. a) W-E to NW-SE Buil cross-section from Fernández et al. (2004). The main N-S structures of the Aínsa Basin as well as the Boltaña thrust can be observed. Eastwards, the Hecho Gr turbidites eroded the Ilerdian shelf strata. Westwards, the strata of the Hecho Gp underlie the Campodarbe Gp. b) W-E Boltaña-Añisclo cross-section across the northern sector of the Boltaña anticline and its relation with the Añisclo anticline (Fernández-Bellón, 2004)

3.2.3.2. Along-strike cross-sections

The 1-1' Bierge-Balzes-Boltaña cross-section by Millán (1996) (Figure 11a) extends from the Aínsa to the Ebro Basins, going through the External Sierras. It cuts obliquely the Balzes anticline and is sub-parallel to the Boltaña anticline. This section shows three thrust sheets: the southern one represents a ramp on the Campodarbe Gp that produces a detachment fold (Barbastro-Balaguer) within the gypsiferous Barbastro Fm. Northwards, two superposed thrust sheets, the upper, Boltaña-Balzes, the lower, Alcanadre sheet and a third one that represents a part of the Tozal sheet. The three units have SW vergence and detach in the Triassic. The space between the basement and the Boltaña-Balzes thrust is here interpreted as the autochthonous footwall of the Alcanadre sheet (Millán, 1996). The shelf limestones crop out in the southern sector whereas in the northern sector the Hecho Gp turbidites and the continental rocks of the Escanilla Fm (Campodarbe Gp) appear.

The Boltaña-Balzes thrust presents a hangingwall flat located in the Triassic that becomes a thrust ramp in the southern boundary of the sheet (W limb of the Balzes anticline). In the northern sector, the Boltaña-Balzes thrust sheet presents a wide syncline below the Aínsa Basin (Millán, 1996). On the other hand, the Alcanadre thrust sheet presents a wide flat in Triassic strata. Most part of the footwall of the Alcanadre sheet is constituted by the autochthonous of the External Sierras (Figure 11, cross-section 1-1'). The Alcanadre sheet is folded in its northern sector. Under this fold, there is a structural bulge that responds to the stacking of the basement thrust sheets. This geometry corresponds to those detected below the Guarga synclinorium (Cámara and Klimowitz, 1985). The tilting observed in the conglomerates of the Sariñena Fm with regard to the Guara Fm suggests a re-activation of the structures during the deposition of the Sariñena Fm in Miocene times (Figure 11, cross-section 1-1').

3.3. Previous paleomagnetic and AMS studies

Paleomagnetism has been applied in the Pyrenees and the Aquitaine and Ebro foreland basins since the 60s. Pioneer works of the Utrecht Universiteit (Van der Lingen, 1960; Schwarz, 1962) are located in the Western Pyrenees (Canfranc and Hecho valleys). Similarly, earliest studies on AMS by Girdler (1961) where conducted in schists from the northern Pyrenees and by Gleizes and Bouchez (1989) in the Mont Louis granitic body. More than 200 peer-reviewed papers (about 80 paleomagnetists from more than 40 institutions worldwide) attest for the still growing interest in the Pyrenean paleomagnetism. In total (see compilations by Pueyo et al., 2005b, 2006; López et al., 2008 and San Miguel et al., 2010), there are already more than 21,000 demagnetizations from 1,700 sampling points, 170 of them are magnetostratigraphic profiles covering more than 74 km of sections. This unique density of paleomagnetic data is due to several reasons: a) availability of synorogenic materials, b) the excellent outcrop conditions, c) the occurrence of well-exposed oblique structures (López et al., 2008 and San Miguel et al., 2010).

Magnetostratigraphic studies have mostly devoted to syntectonic deposits and the foreland Tertiary sequences clarifying substantially the Pyrenean geochronology. The inherited geometry of the Mesozoic basins, the distribution of detachment levels, the diachronism of deformation, gradients of shortening, etc. have produced numerous oblique structures, a perfect target for paleomagnetic studies

focused on the characterization of vertical axis rotations. Currently over 1,500 paleomagnetic sites attest this interest, although their distribution is not homogeneous and reflects especial attention in certain units or structures. The Central Pyrenees (especially the Aínsa and Jaca basins) concentrates more than one third of the data since the early 90s. The combination of rotation and magnetostratigraphic studies, has not only characterized the magnitude of rotation but also its chronology, kinematics and the relationship with folding and thrusting (San Miguel et al., 2010).

3.3.1. Magnetostratigraphic studies

Starting with pilot studies by Burbank et al. (1987), several magnetostratigraphic studies have been performed in the South-Central Pyrenean basins. Hogan (1993), Hogan and Burbank (1996), Oms et al. (2003), Rodríguez-Pintó et al., (2008, 2011c, d), Kodama et al. (2010) improved the chronostratigraphy of the Jaca Basin whereas Pascual (1992), Pascual et al., (1990, 1992), Bentham (1992), Bentham and Burbank (1996), Serra-Kiel et al. (1994) and Beamud et al. (2003) focused on the Aínsa and Graus-Tremp Basins (Figure 13).

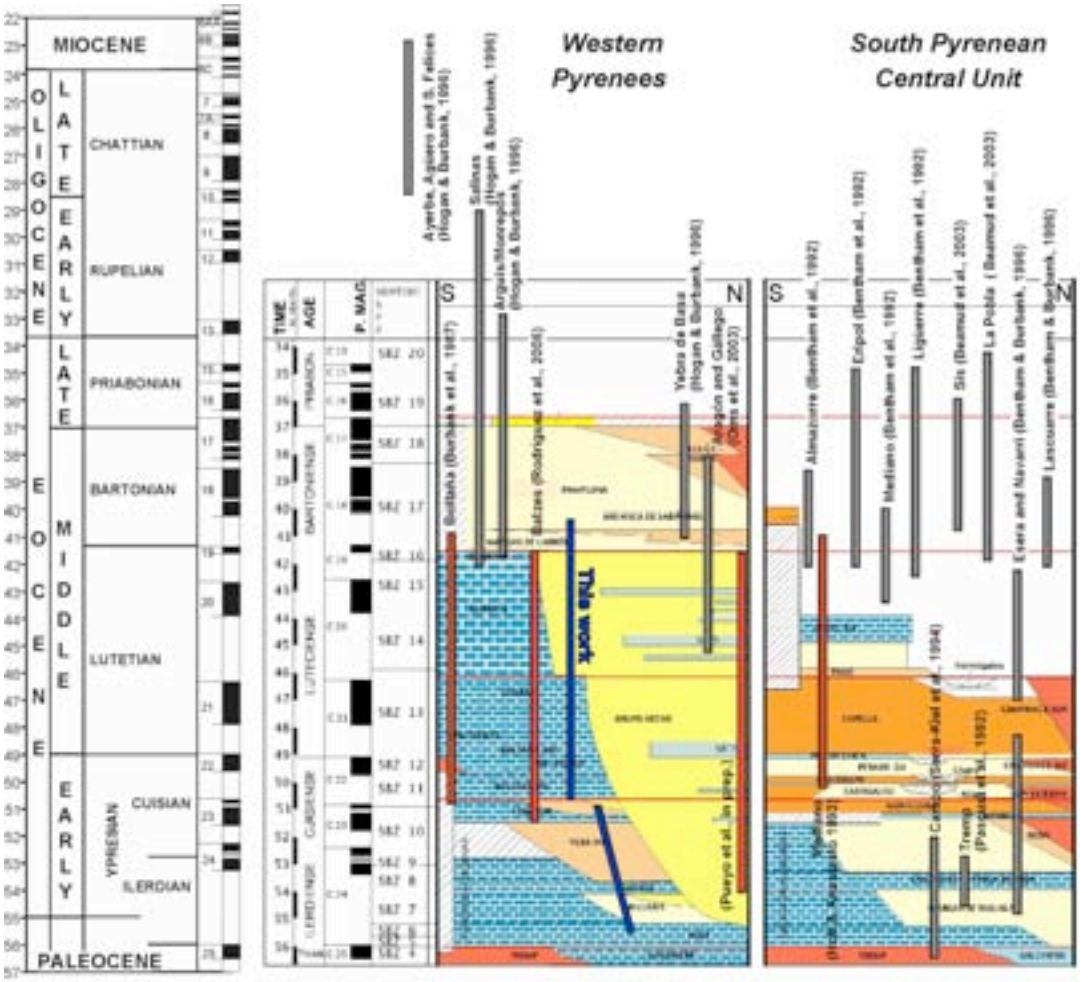

Figure 13. Stratigraphic correlation sketch of the Western and Central South Pyrenean Basin (Barnolas and Gil, 2001) comprising all magnetostratigraphic studies performed (modified from Pueyo, 2008). Within this frame, the study carried out in this work is located.

Hogan (1993) and Hogan and Burbank (1996) approached to the shallow marine–continental transition by several magnetostratigraphic sections (≈ 10 km sampled) located in the Jaca molassic Basin (Figure 14). Among them, three sections started at top of the Guara Fm (Late Lutetian) and continued across the continental rocks of the Campodarbe Fm, some of them reaching the Rupelian (Salinas section).

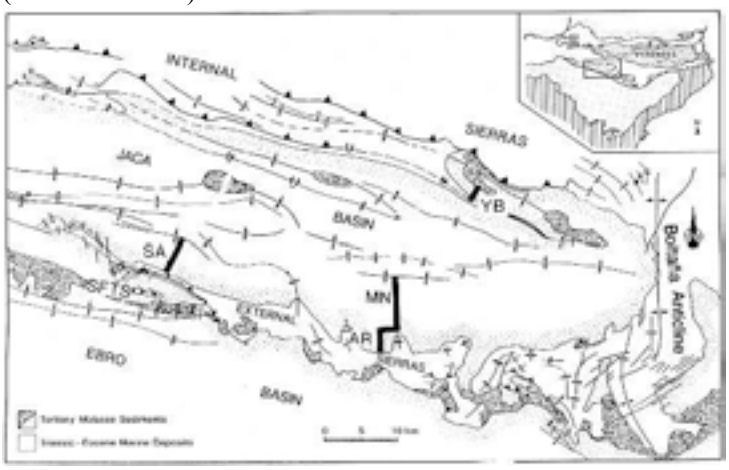

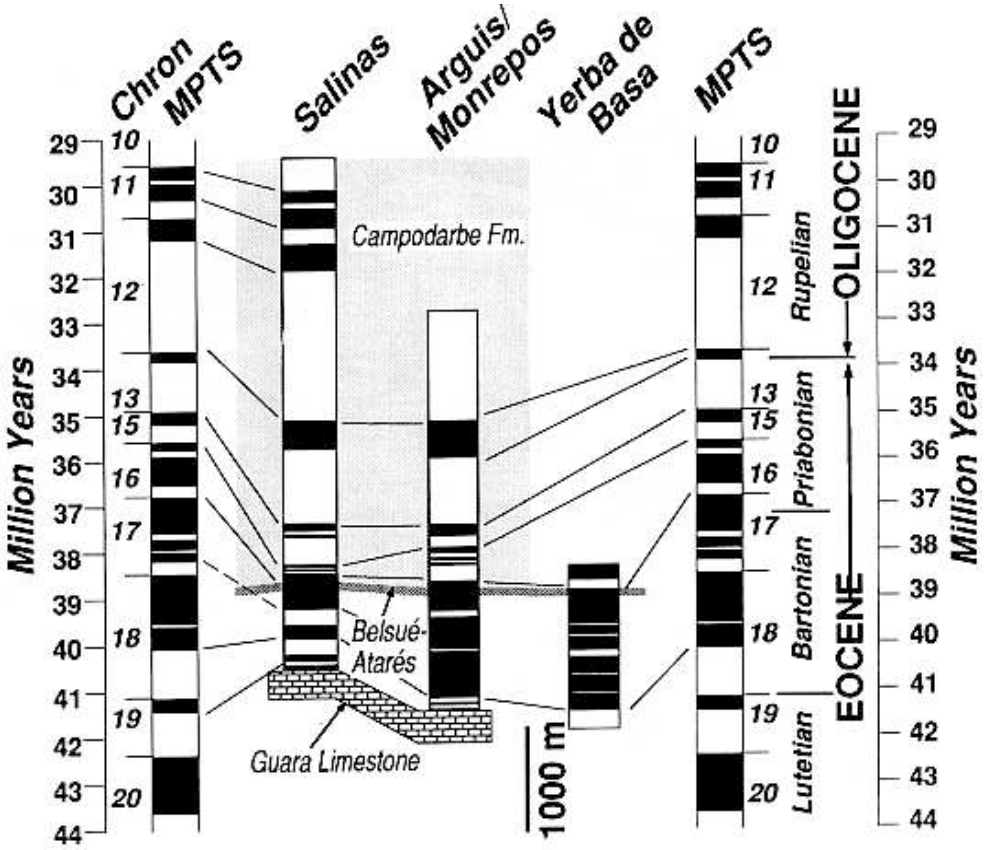

Figure 14. Mapping location and time span of the Jaca Basin sections performed by Hogan and Burbank (1996).

Several short sections were successfully focused on the C13N magnetozone allowing for an isochron across the basin to be tracked. Further improvements on the Arguis-Monrepós profile have been recently done by Kodama et al. (2010), in the Arguis marls (Bartonian), and Rodríguez-Pintó et al. (2011c, d) in the Guara limestones (Lutetian).

Oms et al. (2003) dealt with the chronology and correlation of the northern flank of the Jaca Basin. They built a composite section with two new profiles (Gállego and Aragón) and a third one (Yebra) by Hogan and Burbank (1996), gathering more than 2 km of stratigraphic sequence. The lower and middle parts of the studied section represent the turbiditic sedimentation of the Jaca-Pamplona Basin whereas the upper one includes the transition to the continental molasse. The pile is dated from Lutetian to Bartonian (Figure 15).

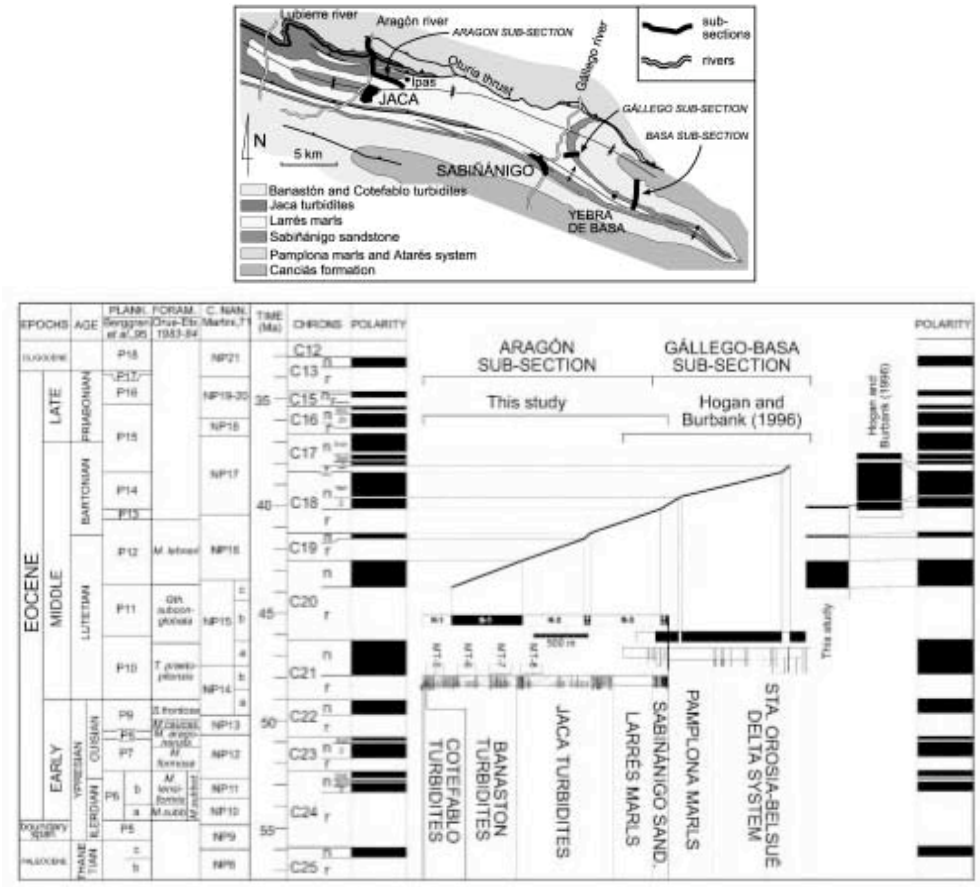

Figure 15. Location of the Aragón and Gállego sub-sections (Oms et al., 2003) and Yebra de Basa section (Hogan and Burbank, 1996). Correlation with the Global Polarity Time Scale established by Cande and Kent (1995) and biozonation by Berggren et al., (1995).

Bentham (1992) and Bentham and Burbank (1996) correlated four sections in the Aínsa Basin (both flanks of the Buil syncline) with two composite sections located between the Ésera and the Isábena valleys (Graus-Tremp Basin), see figure 16. The rocks recorded in the Graus-Tremp Basin were dated as Ypresian-Lutetian (Navarri, Figure 17). The most relevant sections for this work are those placed in the Aínsa Basin (Figures 16 and 17). They belong to transitional and continental environments, covering from the Hecho Gp turbidites (only Mediano section) to the Escanilla Fm. The Almazorre, Eripol, Mediano and Ligüerre sections span from Lutetian to Priabonian times. They partially overlap (Mediano) or complement (Eripol) the data obtained in the present study.

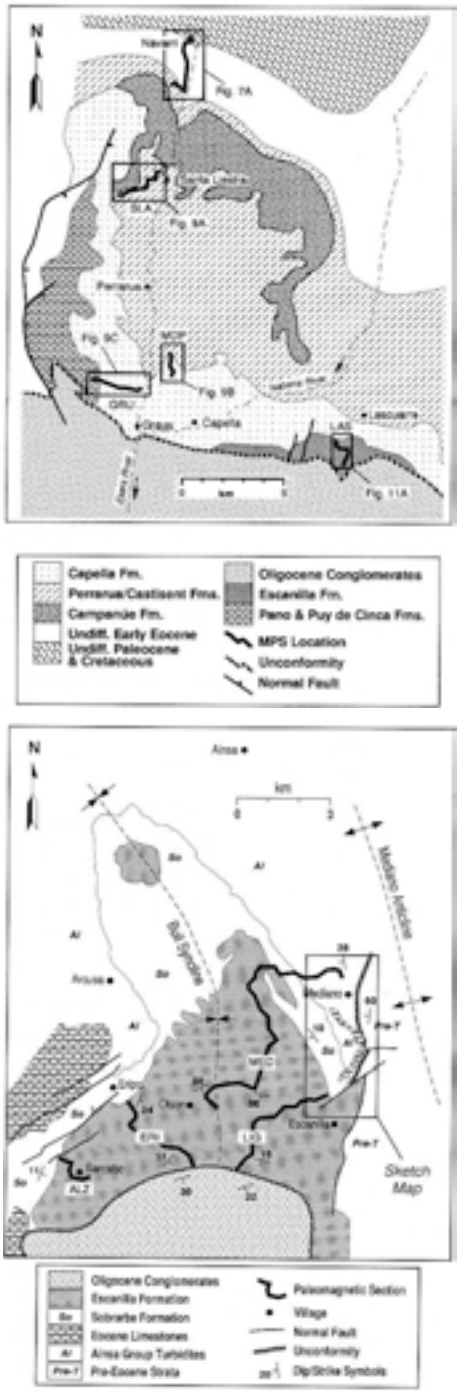

Figure 16. Simplified geologic map of the western Graus-Tremp and Aínsa Basins showing the location of the sections studied by Bentham (1992), Bentham and Burbank (1996).

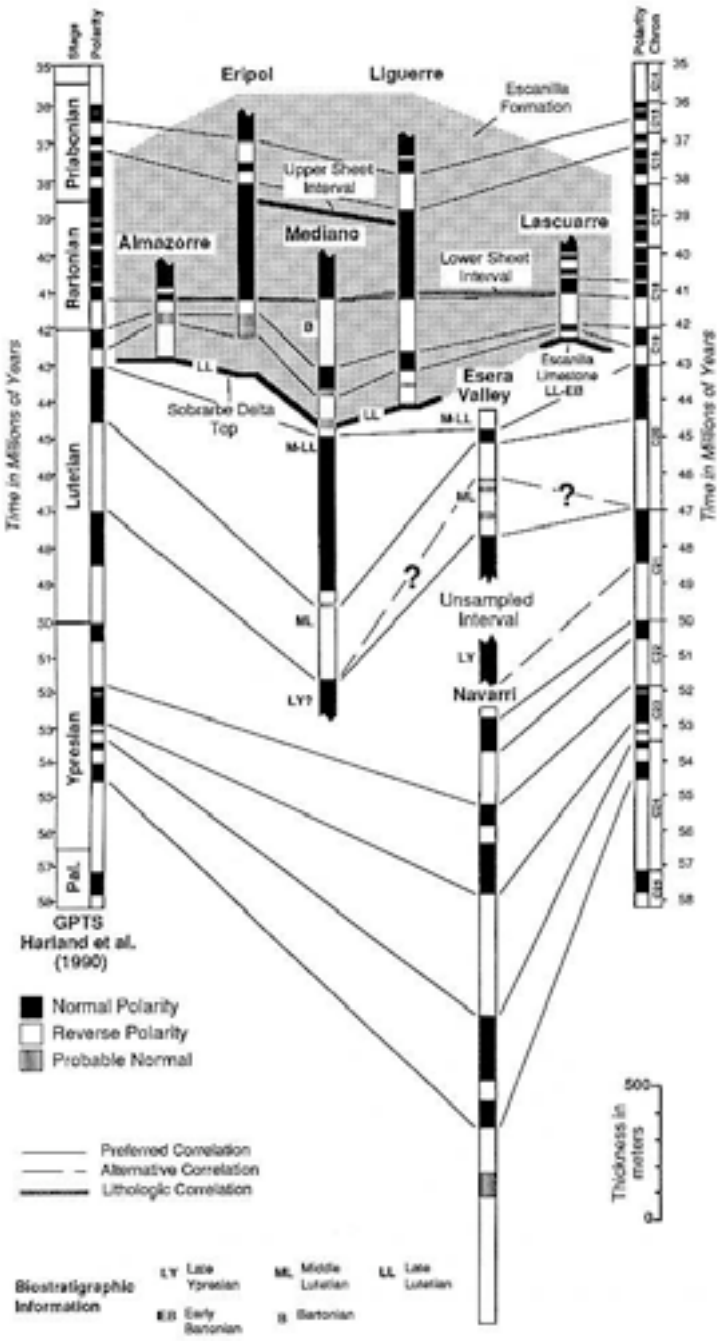

Figure 17. Correlation of the local magnetic polarity sequences from the Graus-Tremp Basin (Lascuarre and Ésera sections) and the Aínsa Basin (Ligüerre, Mediano, Eripol and Almazorre) with the magnetic polarity timescale (Harland et al., 1990 at that time). From Bentham (1992), Bentham and Burbank (1996).

Beamud et al. (2003) performed a marine-continental correlation by means of magnetostratigraphic series in continental sediments (mostly conglomerates) and anchored them by means of charophyte and mammal assemblages (Figure 18). Two magnetostratigraphic sections at the Eastern part of the Graus-Tremp Basin (Sis and Pobla de Segur) were dated as Bartonian-Priabonian in age (Figure 19).

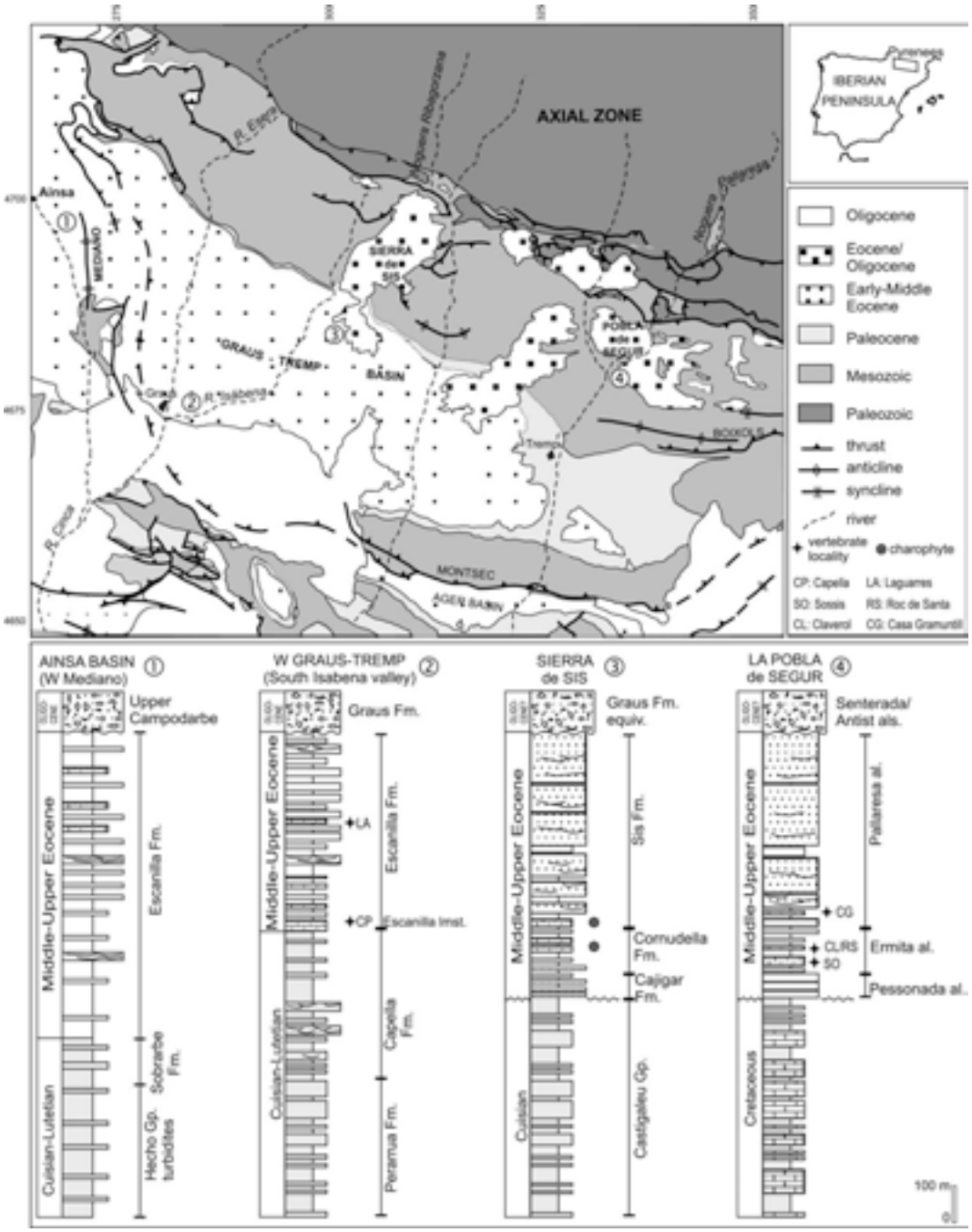

Figure 18. Geological map of the south-central Pyrenees showing the location and stratigraphy of the Aínsa, Graus-Tremp, Sis and La Pobla de Segur sections with indication of the charophyte assemblage (Beamud et al., 2003)

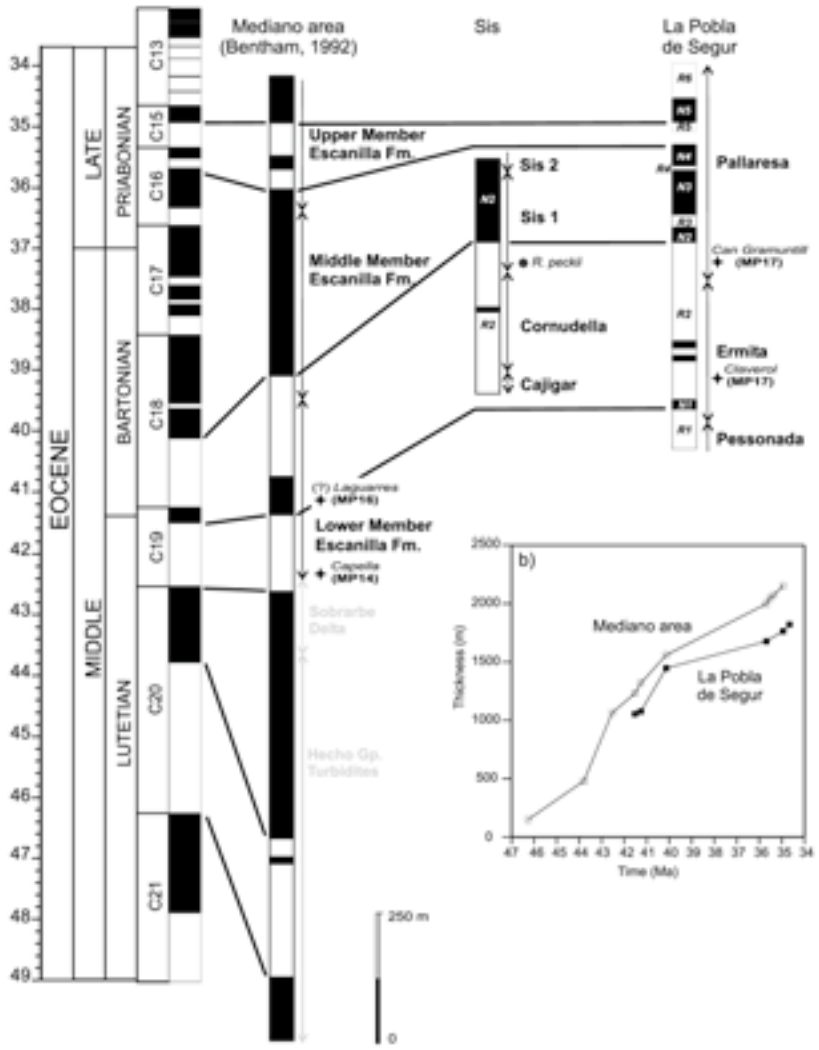

Figure 19. Correlation of the Pobla de Segur and Mediano magnetostratigraphic profiles (Beamud et al., 2003). The Mediano area log is a composite section from the Mediano and Eripol magnetostratigraphic sections.

Serra-Kiel et al. (1994) defined the chronostratigraphy of the marine sediments corresponding to the lower Tertiary in the Graus-Tremp Basin. The established magnetostratigraphic frame (Pascual et al., 1991; Molina et al., 1992; Pascual, 1992) and the numerous biostratigraphic references (Serra-Kiel et al., 1994 and references therein) allowed for dating the Ilerdian stratotype at Tremp and the parastratotype at Campo as well as several control-sections located in between across the Paleocene-Ilerdian (Ypresian) interval (Figure 20).

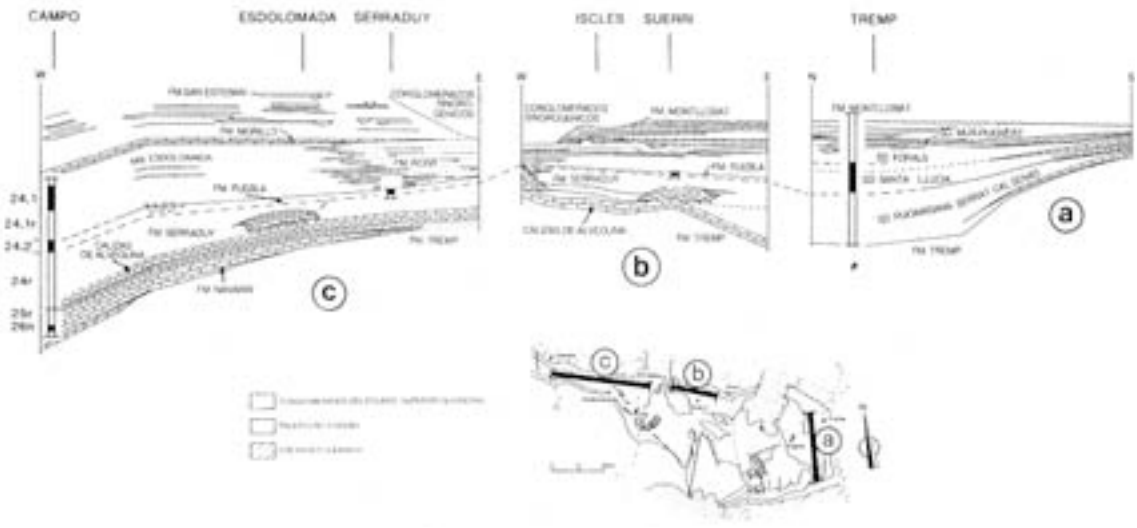

Figure 20. Magnetostratigraphic sketch of the Graus-Tremp Basin (Serra-Kiel et al., 1994)

3.3.2. Vertical Axis Rotations (VAR) studies

Paleomagnetism has been revealed as an efficient tool to characterize vertical-axis rotations in thrust belts (McCaig and McClelland, 1992; Allerton, 1998; Pueyo, 2010). Applications to Pyrenean problems (Pueyo et al., 2003a; Oliva-Urcia and Pueyo, 2007a; Oliva-Urcia et al., 2010) allow for shortening correction in cross-sections (Millán et al., 1996; Oliva-Urcia and Pueyo, 2007b) and map-view restorations to be established (Pueyo et al., 2004a) as in the Andes (Arriagada et al., 2008) or as in the Rocky Mountains (Sussman et al., 2011).

The entire Southwestern-central Pyrenean area is affected by clockwise rotations as shown by numerous palaeomagnetic studies, both in the Aínsa Basin and in the External Sierras, (Dinarès, 1992; Bentham, 1992; Parés and Dinarès, 1993; Hogan, 1993; Pueyo, 2000; Fernández-Bellón, 2004; Oms et al., 2006; Rodríguez-Pintó et al., 2008, 2010; Mochales et al., 2008, 2011b, figure 21). An on-line database, at the Spanish Geological Survey (http://www.igme.es/infoigme/aplicaciones/paleomag/), will allow a quick view of the paleomagnetic data compiled in the Pyrenees during the past seven years (San Miguel et al. 2010 and references therein, figure 22).

As in other South Pyrenean structures (i.e. Pico del Aguila; Pueyo et al., 2002), clockwise rotations explain the current oblique orientation of the N-S trending folds in the studied area with respect to the main WNW-ESE Pyrenean trend (Fernández-Bellón, 2004; Oms et al., 2006; Mochales et al., 2008; Mochales et al., 2011b). These rotations are related to differential displacement in the hanging-wall of the South Pyrenean sole thrust (Nichols, 1989; McElroy, 1990; Millán, 1996) and they are caused by the slow westwards lateral propagation of the imbricate system (Pueyo et al., 1999 and 2004; Oliva-Urcia and Pueyo, 2007b).

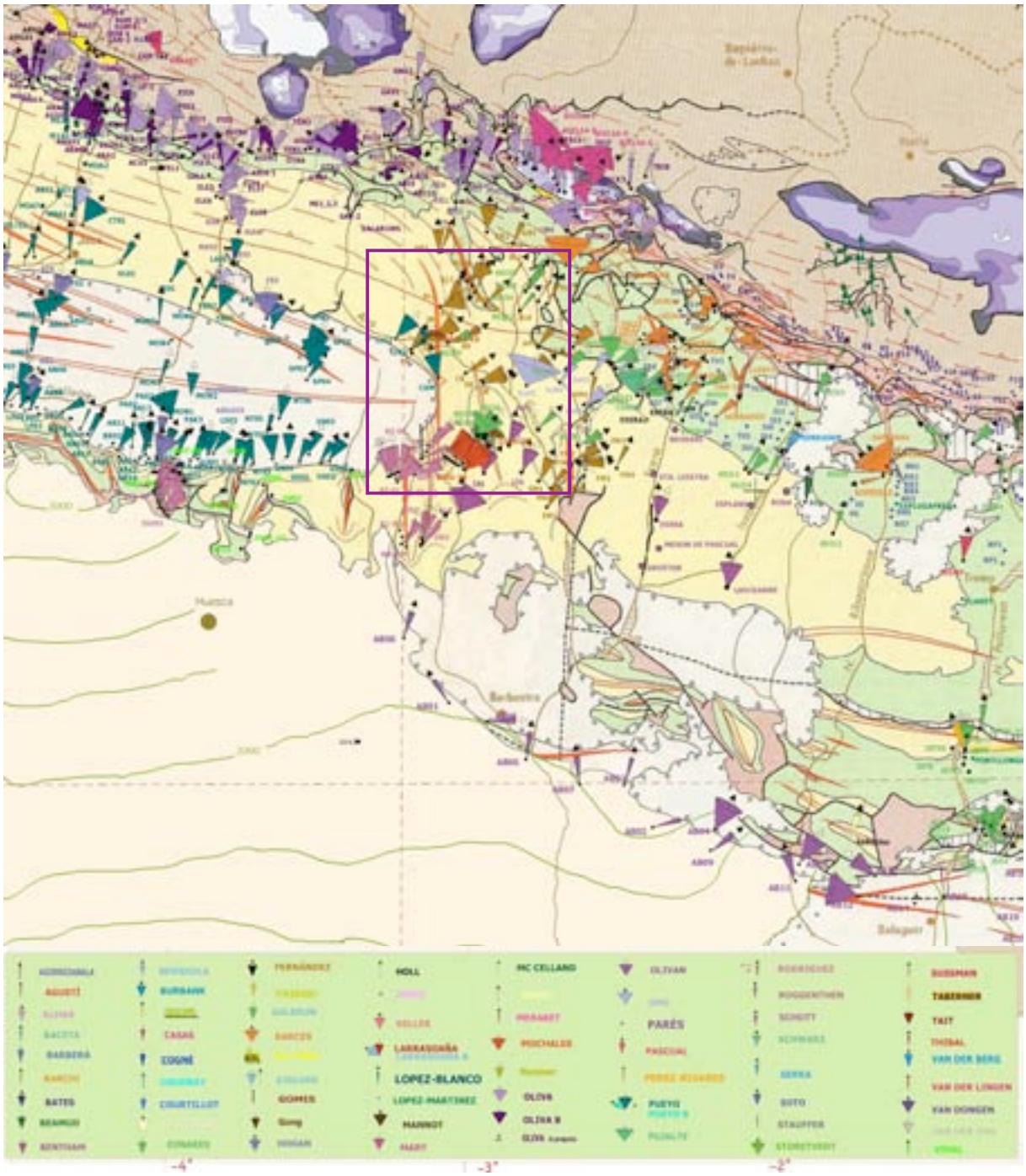

Figure 21. Database of the paleomagnetic data of the Pyrenees (López et al., 2008) in the surroundings of the Aínsa Basin. The study area is framed (Figure 13).

A considerable amount of studies focused on the study area aiming to clarify the kinematics of oblique structures west of the SPCU. Holl and Anastasio (1993) estimated the age of onset of folding for the Mediano anticline by means of the integration of the analysis of geometry of unconformities and magnetostratigraphic studies. They established the onset of the folding growth at 42 M.a. Poblet et al. (1998) accurately determined the age of folding at 47.90 ± 0.1 M.a. through integration of biostratigraphic data and previous paleomagnetic data (Bentham, 1992 [Mediano section]; Holl and Anastasio, 1993). Well-exposed growth strata in the Mediano anticline are attributed to coeval rotation of the structure (Poblet et al., 1998) with rates of limb tilting of 2.2º to 4.2º/M.a. (Holl and Anastasio,

1993).

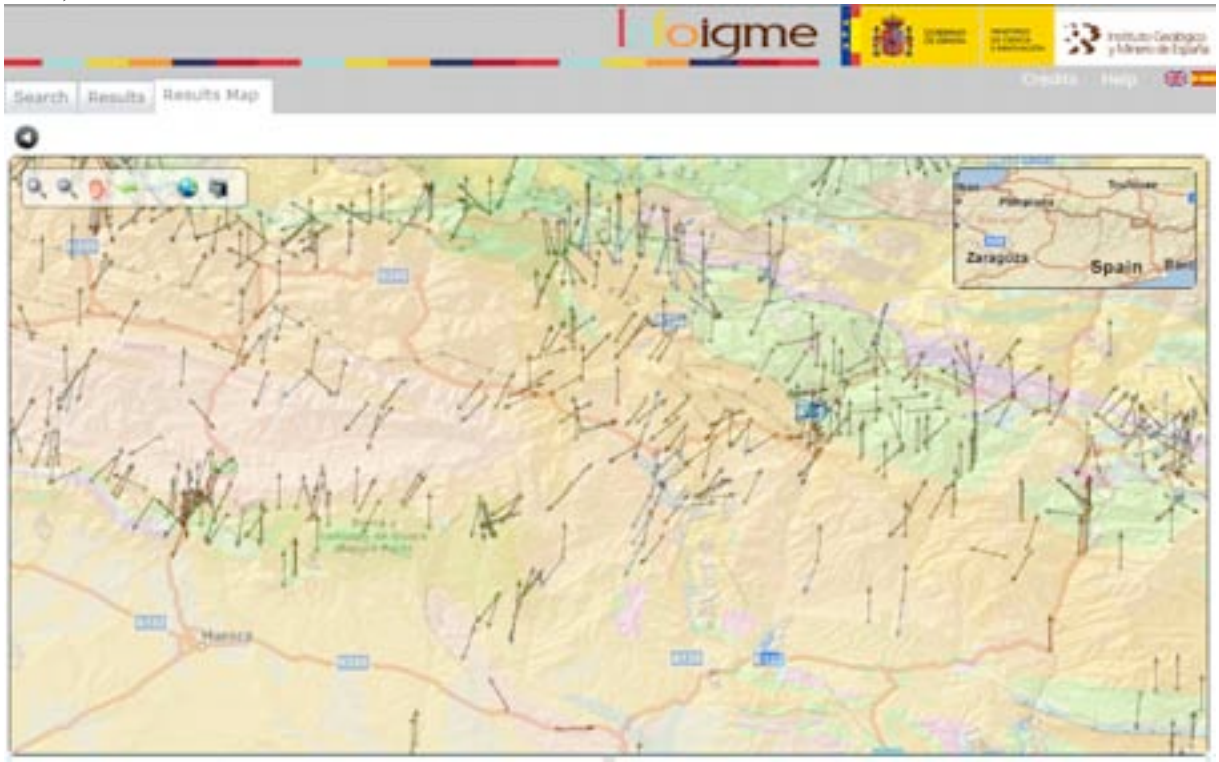

Figure 22. On-line visualization of Pyrenean paleomagnetic data. Vectors are magnetic declinations after restoration to the paleo-horizontal and represent the VAR at that point. http://www.igme.es/infoigme/aplicaciones/paleomag/ (San Miguel et al., 2010).

Discrete VAR sites placed on the Mediano anticline (90J31 and 90J30) by Dinarès (1992) and Parés and Dinarès (1993) revealed values of declination between 50° and 61º (α_{95}: 14.6); in the Buil syncline (90J25, 90J36, 90J38), sites located in Lutetian rocks recorded VAR values of 42º (α_{95}: 38.8), 46º (α_{95}: 9.3) and 44º (α_{95}: 23) respectively. Five discrete sites located in the northern part of the Aínsa Basin (Oms et al, 2006) show assorted declination deviations; SO01, 40º (α_{95}: 8.1), SO02, 36º (α_{95}: 10.2), SO04, 57º (α_{95}: 16.6), SO05, 21.8 (α_{95}: 89.5) and SO06, 39º (α_{95}: 12.2). Another four VAR magnitudes placed on the Bartonian-Priabonian rocks of the Aínsa Basin can be considered as derived from mean values of magnetostratigraphic studies (Bentham, 1992; Bentham and Burbank, 1996). The ALM, ERI, LIG and MED profiles displayed quite divergent polarities (non antipodal): ALM(N): 2º (α_{95}:25) and ALM (R): 218º (α_{95}: 32); ERI(N): 34º (α_{95}: 8) and ERI(R): 184º (α_{95}: 21); LIG(N): 12º (α_{95}: 12) and LIG(R): 209º (α_{95}: 15); MED(N): 12 (α_{95}: 6) and MED(R): 209º (α_{95}:15). Three discrete sites (LIG1, LIG2 and CAM1) by Pueyo (2000) scattered in the transition to the Campodarbe Gp on the western limb of the Boltaña anticline, Bartonian in age, recorded 222º (a_{95}: 22), 225º (α_{95}: 20) and 346º (α_{95}: 21) in declination. Rodríguez-Pintó is performing a vast survey about VAR sites in the contiguous Balzes anticline. It is worth mentioning that the Lutetian series record VARs from 25 to 55º CW rotations (Rodríguez-Pintó et al., 2010) in the eastern limb of the Balzes anticline, whereas the carbonated rocks of the western limb present a marked overlapped character showing spurious CCW rotations (Rodríguez -Pintó et al., 2011a, b).

Discrete VAR data derived from seven previous sites (90J sites by Dinarès, 1992; Parés and Dinarès, 1993; and LIG1&2 and CAM1 sites by Pueyo, 2000) are shown in the table below. They are located in the study area, near the studied profiles and sites, and, due to their relevance, have been taken into account in the present study (Table 1 and figure 21 and 23).

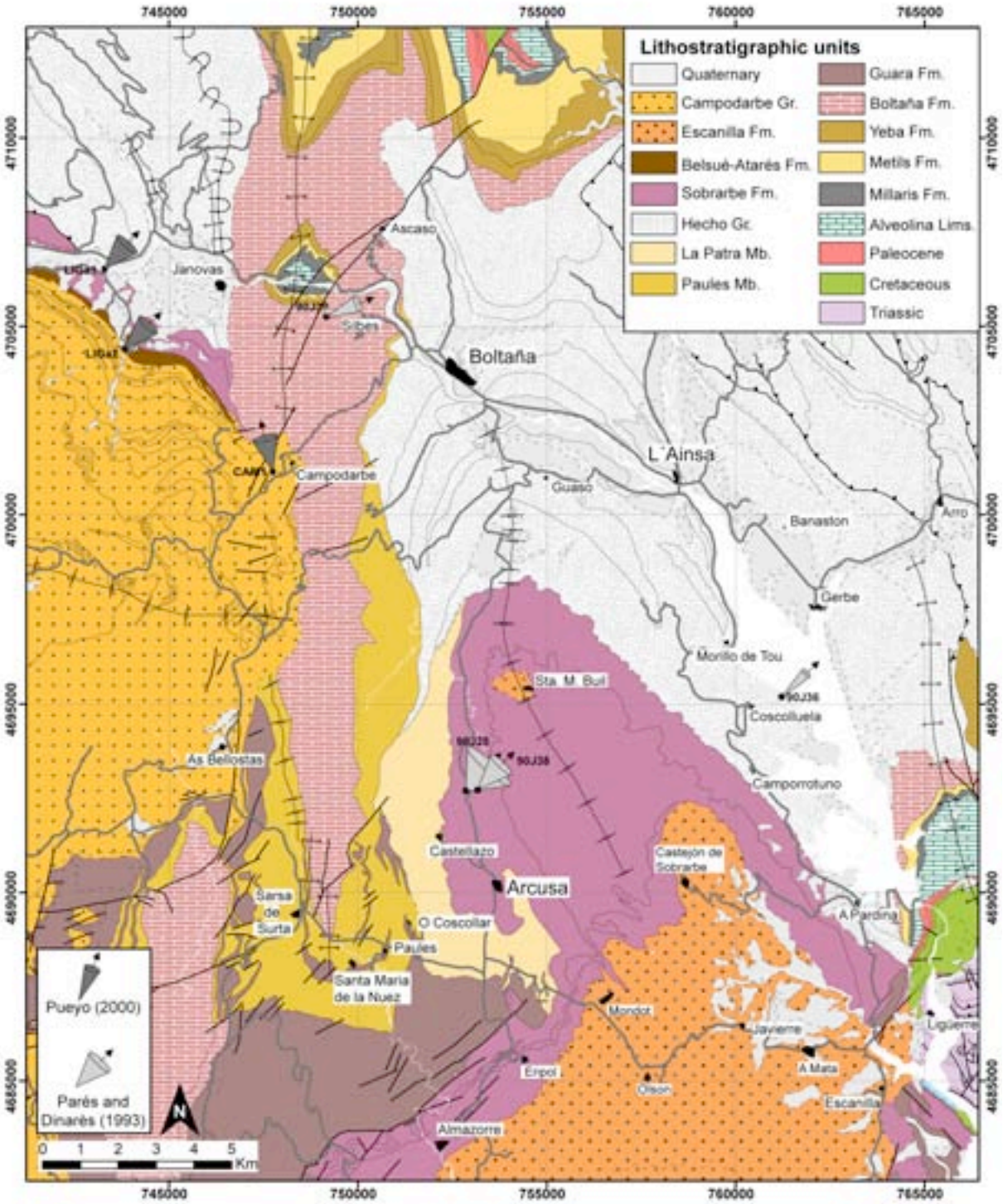

Figure 23. Mapping of the study area with the paleomagnetic studies performed by other authors.

Site	Pol.	n/N	Z	UTM-X	UTM-Y	Strike	Dip	DD	Dec	Inc	α95	kappa	Dec'	Inc'	α95'	k'	Unit
LIGa1	R+N	10/10	30T	743317	4706473	146	68	W	226	29	22	5	222	-38	22	5,0	3
LIGa2	R	10/10	30T	743823	4704271	154	54	W	230	18	20	6	225	-34	20	6,0	4
CAM1	N	6/7	31T	254105	4101043	150	20	W	5	37	21	9	346	45	21	9,0	5
90J25	N	4/4	31T	258700	4692000	155	7	SW	45	42	38,8	6,6	42	49	38,8	6,6	3
90J36	N+R	5/5	31T	268000	4694000	143	17	SW	48	38	8,8	76,3	46	55	9,3	69,0	2
90J38	R	2/2	31T	259100	4692000	351	40	E	161	-66	23	120,5	224	-48	23	120,4	3
90J39	R	5/7	31T	255900	4705000	17	15	SW	233	-57	14,1	19,2	247	-47	14,1	19,3	1

Table 1. Previous VAR discrete sites used in this work. LIG and CAM by Pueyo (2000) and 90J from Parés and Dinarès (1993). Pol. Polarity; Dec, Inc a95 and kappa (in situ), Dec', Inc', a95' and kappa' (after bedding correction). Units: 1 Boltaña Fm, 2 Hecho Gp, 3 Sobrarbe Fm, 4 Belsué-Atarés Fm, 5 Campodarbe Gp.

Several unpublished sites studied by Fernández-Bellón (2004) and Fernández et al., (2003 and in review) have not been considered in this work. 38 VAR sites were distributed thrououth the Aínsa Basin to deduce the kinematics evolution of the structures involved (Table 2 and Figure 24).

a)

						bedding		ChRM										
										in situ				bedding corrected				β (net
site	X	Y	Z	unit	age	dip dir	dip	N	type	dec	inc	k	α_{95}	dec	inc	k	α_{95}	rotation)
AB	251535	4704356	825	Ar	L. Lutet	171	82	8	R	023	22	55	8	**029**	**44**	58	7	**26**
BB	257560	4705951	628	SM-Si	U. Cuis	121	29	6	R	028	55	41	11	**061**	**46**	30	13	**58**
CB	258408	4701832	650	SV	L. Lutet	159	29	7	R	022	46	42	9	**056**	**60**	42	10	**53**
GB	260682	4700467	700	SV	L. Lutet	203	19	9	N	063	42	32	9	**074**	**52**	27	10	**71**
JB	253031	4705874	700	SV	L. Lutet	258	85	6	R	069	43	17	17	**070**	**40**	15	18	**67**
SB	260560	4700852	670	SV	L. Lutet	222	12	7	N	069	40	10	22	**075**	**48**	9	23	**72**
YB	254488	4706261	640	Yb	U. Ilerd	269	54	8	R	061	10	7	22	**055**	**35**	7	22	**52**
BL1	264043	4713214	978	Yb	U. Ilerd	068	33	10	N	024	39	276	3	**034**	**12**	219	3	**31**
BL2	255208	4710255	1216	Yb	U. Ilerd	274	83	3	R	057	58	27	24	**073**	**19**	27	24	**70**
BL3	255847	4710475	1280	Yb	U. Ilerd	092	17	6	R	016	25	132	6	**023**	**20**	131	6	**20**
BL4	260898	4710445	984	Mt	M. Ilerd	200	20	9	R	**041**	**23**	48	8	045	40	45	8	**42**
BL5	259503	4712061	1062	Mt	M. Ilerd	081	90	11	R	**024**	**26**	85	5	319	30	73	5	**21**
BL6	267643	4710863	759	Yb	U. Ilerd	146	4	11	N	033	30	582	2	**036**	**33**	504	2	**33**
BL7	256609	4711485	1160	Yb	U. Ilerd	110	26	7	R	018	28	42	10	**031**	**25**	42	10	**28**
BL10	258686	4713538	1148	Yb	U. Ilerd	090	10	5	R	**049**	**43**	15	20	053	35	15	20	**50**
BL11	259195	4712972	1118	Mt	M. Ilerd	080	84	11	R	**019**	**15**	36	9	329	25	33	9	**16**
BL12	268580	4710575	969	Yb	U. Ilerd	030	20	11	N	027	36	104	5	**029**	**16**	100	5	**26**
AN1	255461	4717875	1244	Mt	M. Ilerd	095	45	6	R	327	26	24	14	**358**	**42**	24	14	**-5**
AN2	261380	4720904	1635	MI	L. Ilerd	006	9	4	R	008	45	13	22	**007**	**38**	14	22	**4**
AN3	264261	4719592	1170	MI	L. Ilerd	144	5	12	R	024	17	33	8	**025**	**16**	37	7	**22**
AN4	255359	4717714	1139	Mt	M. Ilerd	040	5	11	N	021	33	60	6	**021**	**28**	60	6	**18**

b)

						bedding		ChRM											
										in situ				bedding corrected					β (net
site	X	Y	Z	unit	age	dip dir	dip	N	type	dec	inc	k	α_{95}	dec1	dec2	inc	k	α_{95}	rotation)
AP1	266540	4698290	665		M. Cuis	234	15	6	R	239	-40	35	12	240	**240**	**-55**	35	12	**47**
AP2	267580	4705000	810		M. Cuis	061	20	7	R	208	-54	75	11	**217**		**-36**	52	13	**34**
BA1	266600	4701670	595		U. Cuis-L. Lut.	213	27	12	N	46	29	4	23	53	**52**	**55**	27	9	**49**
EM1	268630	4684920	530	Es	U. Lutet	186	9	7	R	216	-34	24	13	220	**220**	**-42**	24	13	**37**
FM1	272800	4690350	600	Sam	L. Lutet	138	21	7	N	45	65	24	13	84	**84**	**59**	24	8	**81**
FM2	273030	4690520	580	Sam	L. Lutet	003	5	7	N	33	44	60	8	**35**		**40**	60	8	**32**
FM3	273040	4690520	580	For	L. Lutet	185	11	8	N	52	40	98	6	60	**59**	**47**	98	6	**56**
FM4	277560	4689660	820	For	L-M. Lutet	355	15	8	N	40	58	52	8	**27**		**46**	52	8	**24**
HM1	274350	4696290	650	Castnt	M. Cuis	090	32	7	R	175	-24	95	6	189	**193**	**-23**	115	6	**10**
MM1	271670	4695020	755		M. Cuis	003	18	8	R	233	-62	114	5	**238**		**-44**	109	5	**55**
OA1	272090	4705040	1160		L-M. Cuis	193	11	5	R	236	-50	21	17	**223**		**-55**	19	18	**40**
PM1	269100	4687090	560	Camptno	M. Lutet	248	14	7	N	46	41	41	10	40	**40**	**54**	28	12	**37**
SM1	267530	4688130	570	Sobr	M. Lutet	264	12	6	N	30	32	20	15	23	**23**	**38**	20	15	**20**
YM1	270700	4689190	610	Yb	U. Ilerd	278	42	10	N	90	18	38	9	**82**		**60**	56	6	**79**
YM2	272400	4690650	550	Yb	U. Ilerd	080	34	8	N	11	77	22	12	**61**		**49**	29	11	**58**

Table 2. ChRM directions for each site and derived rotation (b) for the Boltaña and Añisclo anticlines (a) and Mediano anticlien (b) by Fernández-Bellón (2004). UTM in zone 31

In spite of the abundant existing data, several aspects are far from being solved. According to Fernández-Bellón (2004) sedimentation and fold formation were coeval during Early Lutetian times, with a progressive decreasing of the vertical axis rotation. Decreasing of the rotation value eastwards is explained by the synsedimentary character of rotation, as in Mediano anticline (see figure 25 from Fernández-Bellón 2004), or due to deposition of progressively younger sediments placed in less oblique positions (Pueyo, 2000; Fernández-Bellón 2004; Oms et al., 2006). Conversely, Mochales et al. (2008) propose a non-steady scenario and a younger Bartonian-Priabonian main rotational event. The accurate chronological frame of rotation of structures and the exact amount of rotation (Fernández-Bellón, 2004; Mochales et al., 2008) are not solved before this work, becoming key questions for the complete understanding of the kinematics of the South Pyrenean Zone and of this study.

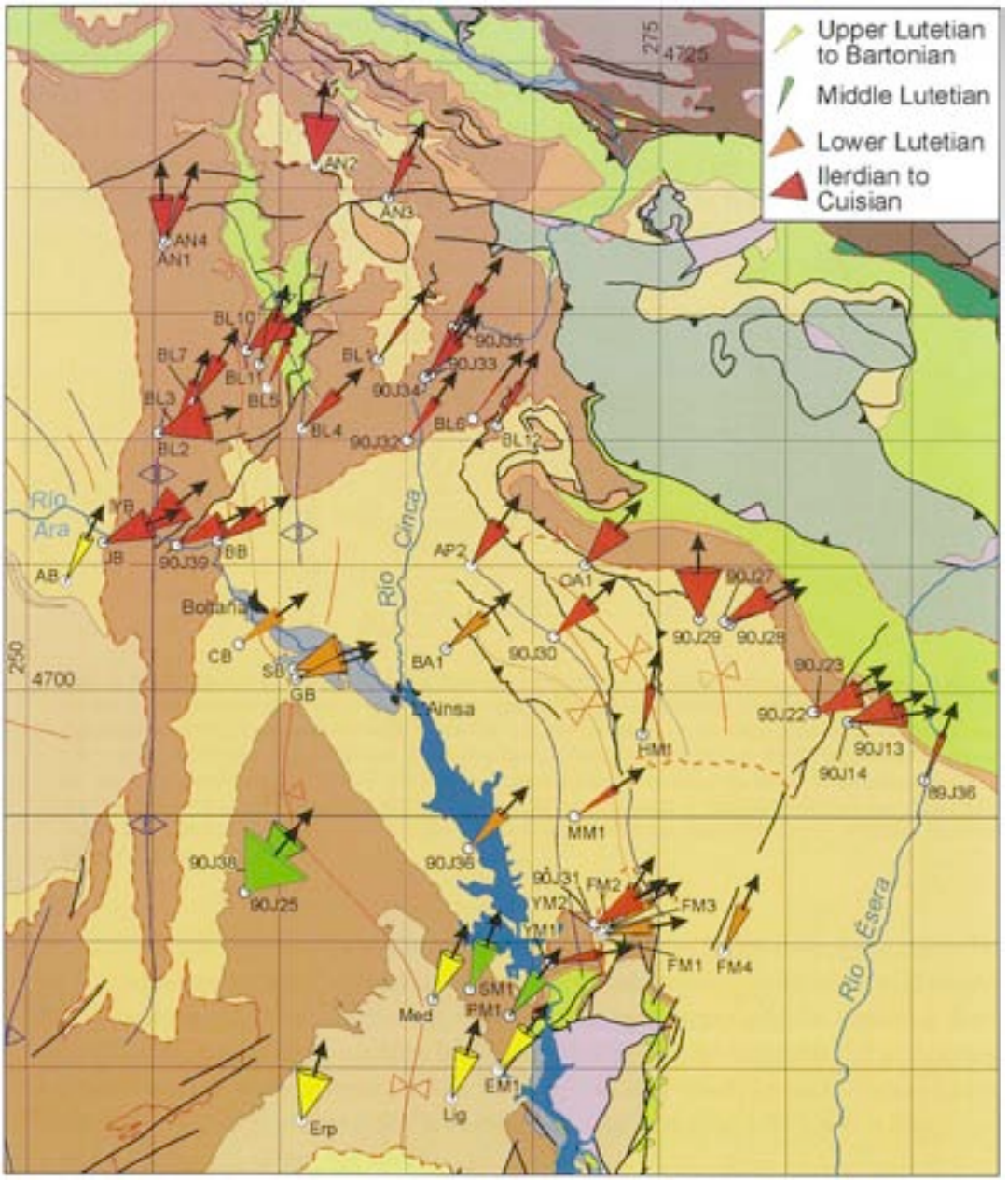

Figure 24. Map of the Aínsa Basin with VAR sites considered by Fernández-Bellón (2004). Confidence angles are included (a_{95}). Sites 90J (Dinarès-Turell, 1992), Med, Lig and Erp (Bentham, 1992) and ages are included.

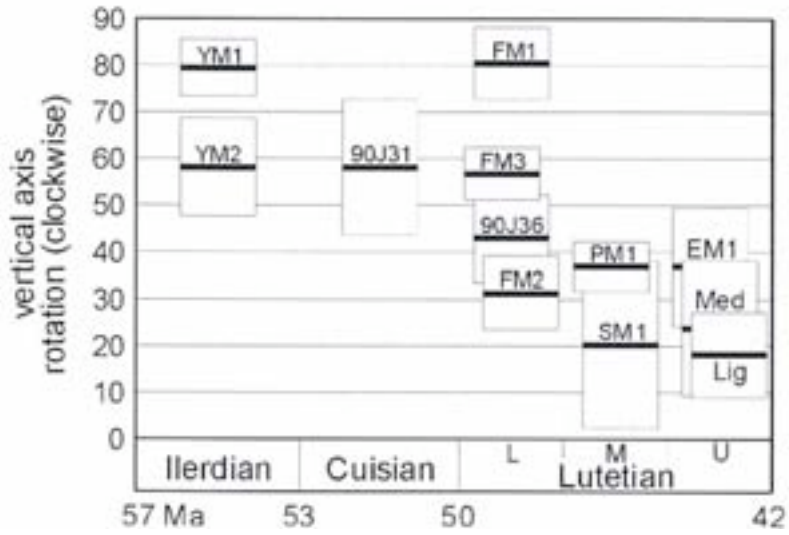

Figure 25. CW rotation for the Mediano anticline. Rotation is represented by a bold line and a95 by an encompassing box. Highest amounts of rotation were recorded in Ilerdian and smallest in Late Lutetian.

3.3.3. Anisotropy of the Magnetic Fabric (AMS) studies

Anisotropy of magnetic susceptibility (AMS) is a sensitive recorder of fabric orientation (mineral preferred orientation) in weakly deformed rocks (see e.g. Parés and van der Pluijm, 2002 and references therein). It becomes a useful tool in the absence of other strain indicators, as occurs in the Pyrenean foreland basin. Magnetic fabric is expressed as an ellipsoid, which can be compared with the finite strain ellipsoid, at least in a relative sense, to ascertain the degree of convergence between both indicators. In compressive settings and appropriate rock magnetic content (i.e. pure paramagnetic signal), the axis of maximum elongation of the ellipsoid would approximately correspond to the stretching direction.

Regarding the Pyrenean pioneer research in Anisotropy of the Magnetic Fabric (Girdler, 1961), Dinarès-Turell et al (1991) studied several localities of the SPCU. They interpreted as sedimentary magnetic fabrics those contained in non-deformed rocks. On the other hand, in deformed rocks the magnetic ellipsoid may mimic the ellipsoid of deformation. Subsequently, the Aínsa Basin was subjected to further AMS analysis (Dinarès and Parés, 1992). A change of directional data and shape of the ellipsoid was observed when approaching to the cleavage front. Some mineral magnetic lineation was observed in non-apparently deformed rocks.

In the Jaca-Pamplona Basin the method became quite sensitive to infer the strain of rocks where classic structural methods are not effective (Larrasoaña et al., 1997). A preliminary estimation of the deformation mechanism to explain the structural features of the study area was possible. Buckling and flattening dominated as folding mechanisms in the Hecho Gp turbidites, whereas the upper sequence was deformed by a flexural slip-flexural flow combination at the limbs and tangential-longitudinal deformation at the hinges (Figure 26). The first stages of folding seem to obey to pure

shear parallel to bedding (layer parallel shortening), although fabrics near faults would be associated with simple shear (Larrasoaña et al., 1997).

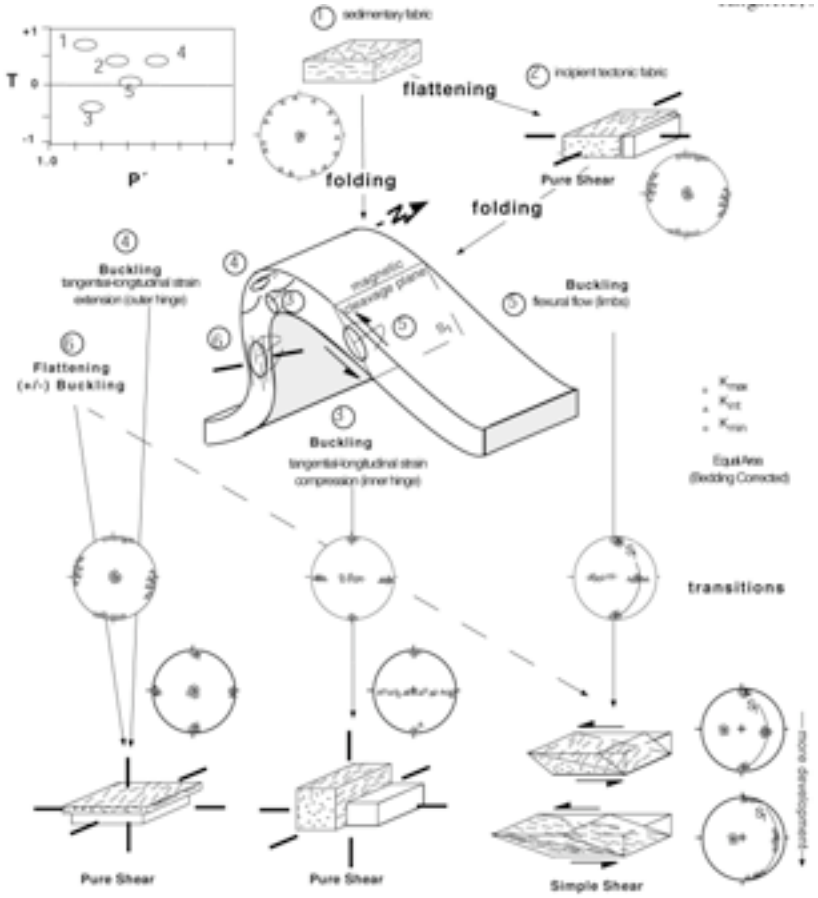

Figure 26. Sketch showing the evolution of an initial fabric in the different parts of a fold deformed by buckling and/or flattening, as well as the expected AMS directional results. Each folding mechanism is related with its corresponding type of deformation (Larrasoaña at al., 1997).

Subsequently, Larrasoaña et al. (2004) integrated AMS, structural, palaeomagnetism and rock-magnetism in the Eocene marine marls of the Jaca-Pamplona Basin. The comparison between different methods allowed for detecting a tectonic overprint, affecting the phyllosilicate matrix of the mudrocks but not the remanence carriers. A relative chronology was established between sedimentation, blocking of the magnetic fabrics, acquisition of the magnetic remanence and deformation. Early stages of deformation (LPS or coetaneous sedimentation) that affected the Jaca-Pamplona basin (Mid-Late Eocene) favoured the blocking of the magnetic fabrics and simultaneous lock-in of the remanence, bracketed to a very short time span (<15? K.y.) after the sedimentation (Figure 27), They therefore validated the use of magnetic fabrics as passive indicator of the deformation (Larrasoaña et al., 2004).

Meanwhile, Pueyo et al. (1997) determined the folding mechanism at the Pico del Águila anticline (External Sierras) by means of AMS. The location of the sites in the synclines is close to the hinges of the folds formed in deep marine and transitional rocks, confirming the expected parallelism between the axis of the initial fabric and the deformed one. The degree of anisotropy increases with

the depth along the stratigraphic pile as a consequence of the higher shortening experimented by the lower units. It seems that a parallelism exists between the magnetic anisotropy and the shortening. The folding mechanism was of tangential-longitudinal deformation at the hinges and flexural flow at the fold limbs (Pueyo et al., 1997), figure 28.

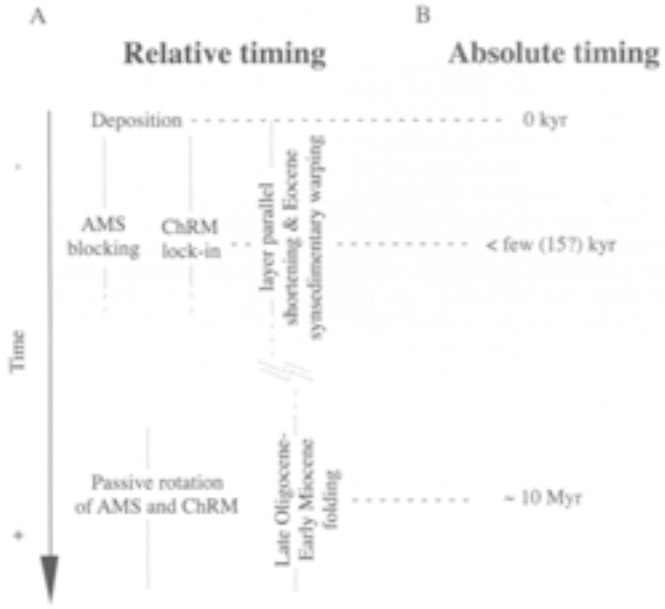

Figure 27. A) Relative chronology between deposition, blocking of the magnetic fabrics, remanence lock-in and deformation. B) Estimated absolute time for the process involved. From Larrasoaña at al., 2004.

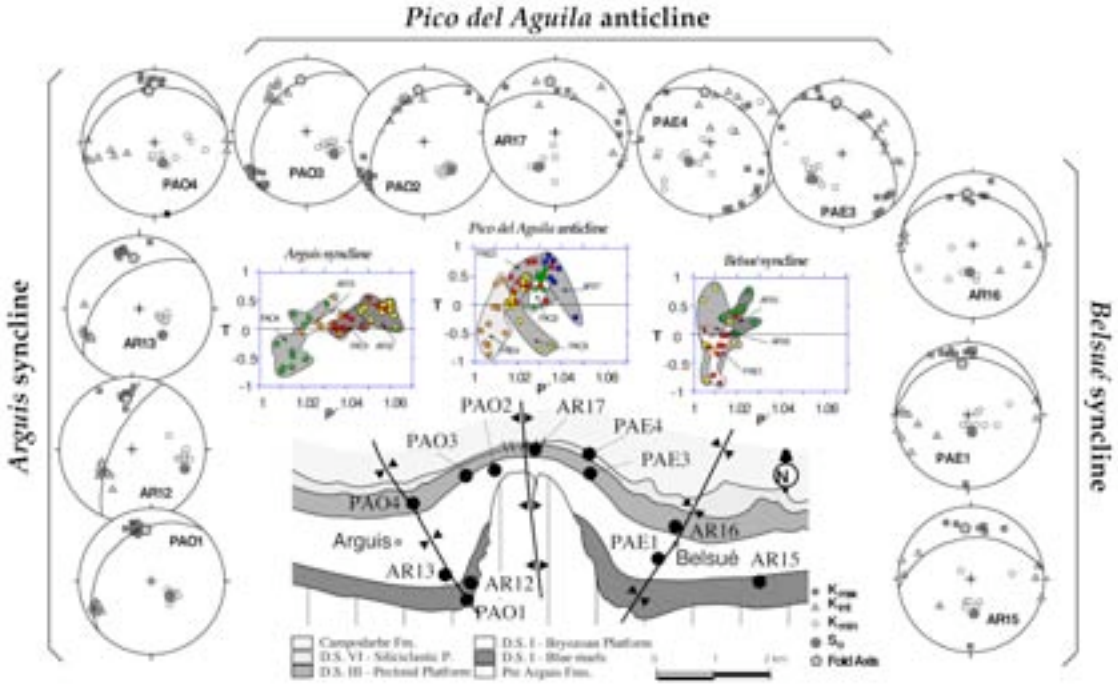

Figure 28. Detailed map of the Pico del Aguila anticline showing the location of the studied sites. Equal area projection of the magnetic fabrics and the T-P´ diagrams are shown (Pueyo et al., 1997).

In the Internal Sierras and the Jaca-Pamplona Basin, Upper Cretaceous to Eocene rocks have been surveyed aiming to correlate AMS and other deformation indicators (Pueyo-Anchuela et al., 2007; Oliva et al., 2009). Two main types of stretching lineation have been interpreted from AMS fabrics: the first one is defined by a magnetic lineation parallel to the major structures interpreted as LPS-associated. The second one is normal to the bedding-cleavage intersection lineation, therefore coinciding with the regional tectonic transport direction. Pueyo-Anchuela et al. (2010) identified magnetic fabrics that were grouped into (1) fabrics related to layer parallel shortening (LPS) acquired in pre-folding conditions, (2) fabrics related to cleavage development and (3) fabrics related to shear parallel to the thrust movement and intermediate cases (Figure 29). The magnetic fabric contained in the bedding plane and tilted by the folding suggests an acquiring fabric previous to folding. On the other hand, AMS was revealed as a sensitive method to detect VAR in fold and thrust systems (Pueyo-Anchuela et al., 2008 and 2011).

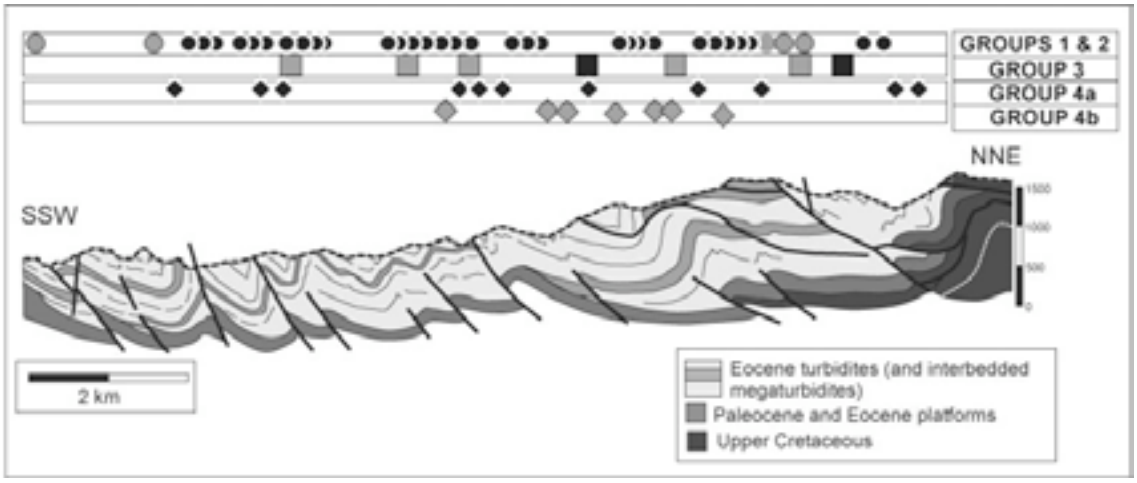

Figure 29. Cross-section from the central studied zone and distribution of the defined fabric groups (cross-section based on Teixell 1992) by Pueyo-Anchuela et al. (2010).

In the SPCU, a relationship between the AMS and the superimposed folding was detected (Soto, 2003; Soto et al., 2003). The weakly deformed Upper Cretaceous marine marls from the hanginwall and footwall of the Cotiella-Bòixols nappe were surveyed in this study. These rocks presented a well developed compactional magnetic foliation and lineation interpreted as the result of Layer Parallel Shortening (LPS). Two non-coaxial fold-and-thrust events (Cretaceous and Early Eocene in age) with approximate N-S and WNW-ESE respective orientations were detected. The N-S stage is linked to the emplacement of oblique ramps, pre-dating the main WNW-ESE Pyrenean stage (Eocene-Oligocene, see figure 30).

South of the Marginal Sierras, a study of the southernmost structure of the Central Pyrenees in Priabonian rocks, the Barbastro-Balaguer anticline, allowed detecting maximum elongations of the magnetic ellipsoid parallel to the axis of the local structures (Oliván et al., 2008, figure 31). Here, the magnetic fabric blocking suggests an early diagenesis stage according to LPS and previous to folding (Late Oligocene). The wide scatering of the lineation (of 60º) might be associated to secondary nature of the fold curvature (i.e. VARs).

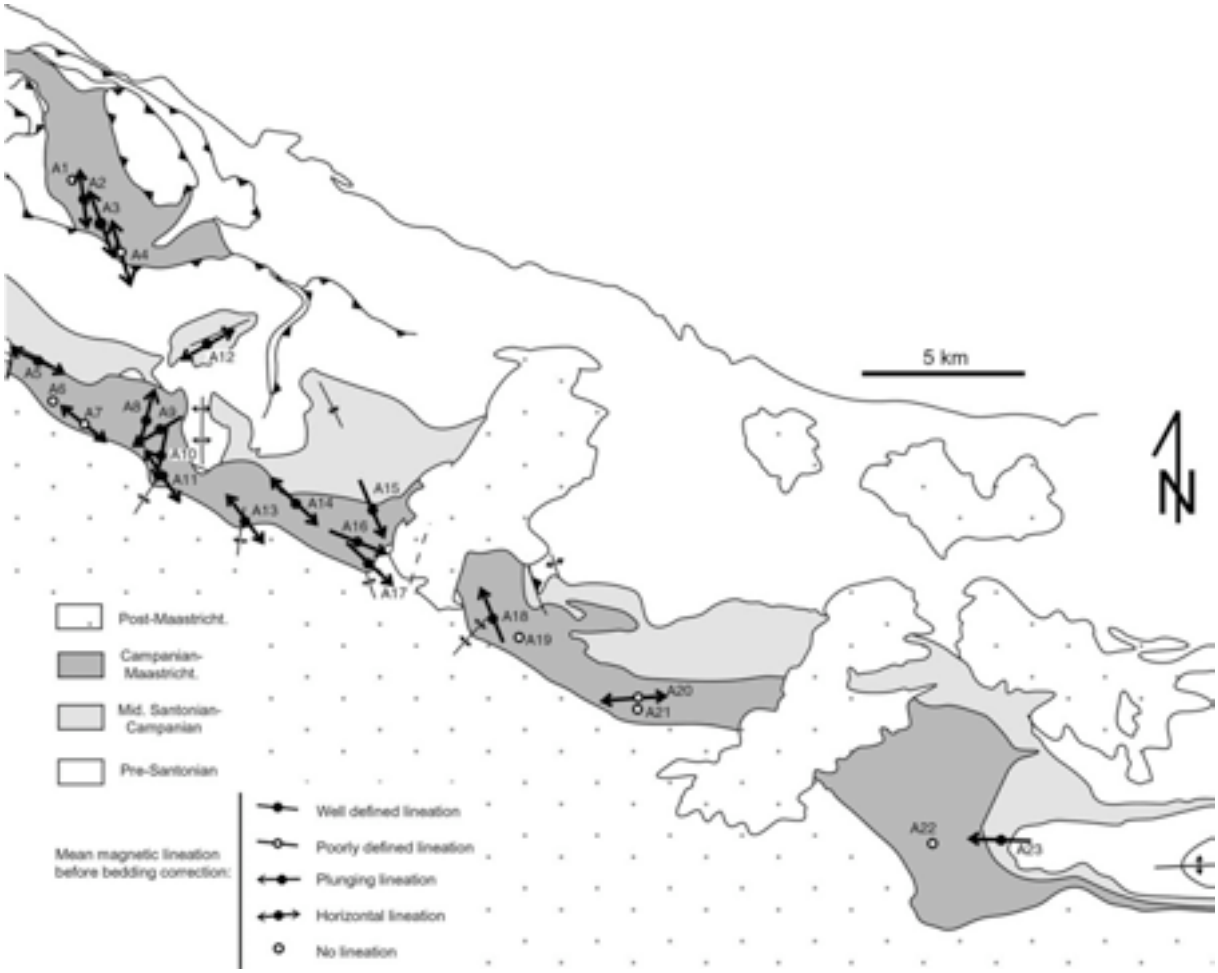

Figure 30. Summary of orientation of the magnetic lineation in the northern sector of the SPCU map view (Soto et al., 2003).

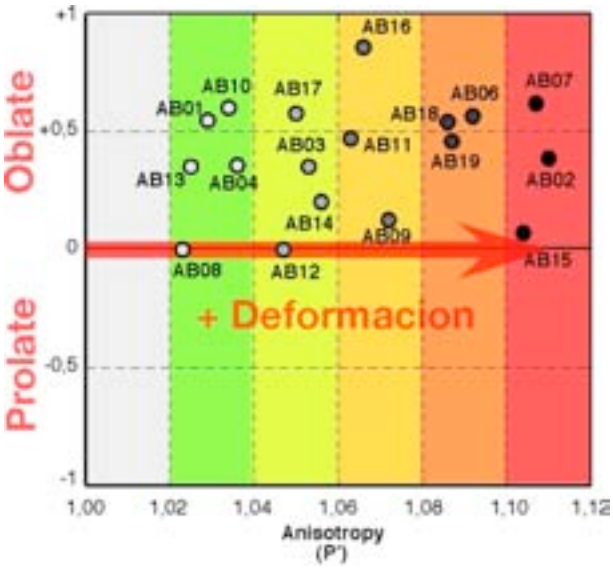

Figure 31. Mean T-P' (shape and anisotropy) diagram of the studied sites in the Barbastro anticline. Anisotropy degree increases with the degree of deformation, although the shape of the ellipsoid remains oblate in most cases (Oliván et al., 2008)

In the Internal Sierras, several AMS analyses have been performed (Oliva-Urcia et al., 2006; Oliva-Urcia et al., 2009). Triassic rocks included in the Bielsa basement thrust sheet, belonging to the Axial Pyrenees, presented a non-sequential pattern of AMS-ellipsoid related to flexural deformation and flattening (Figure 32). Therefore the clustering of the magnetic lineation does not respond to an increasing degree of the flexural deformation. One possible explanation is that the original lineation is strongly marked (Oliva-Urcia et al., 2006). Upper Cretaceous siltstones, affected by pressure-solution cleavage shows variable orientation, not conforming the typical cleaved sedimentary rock pattern suggested by Parés et al (1999). Nevertheless, the paramagnetic subfabric (Low Temperature-AMS) shows remarkably constant directional properties, clustering the maximum axes of the ellipsoid parallel to the intersection lineation. By means of LT-AMS, preferred orientations of the phyllosilicates seems to be related to Late Cretaceous compressive stage, not altered by subsequent deformation occurred during Late Eocene-Early Oligocene times when the pressure-solution cleavage took place (Oliva-Urcia et al., 2009), figure 32.

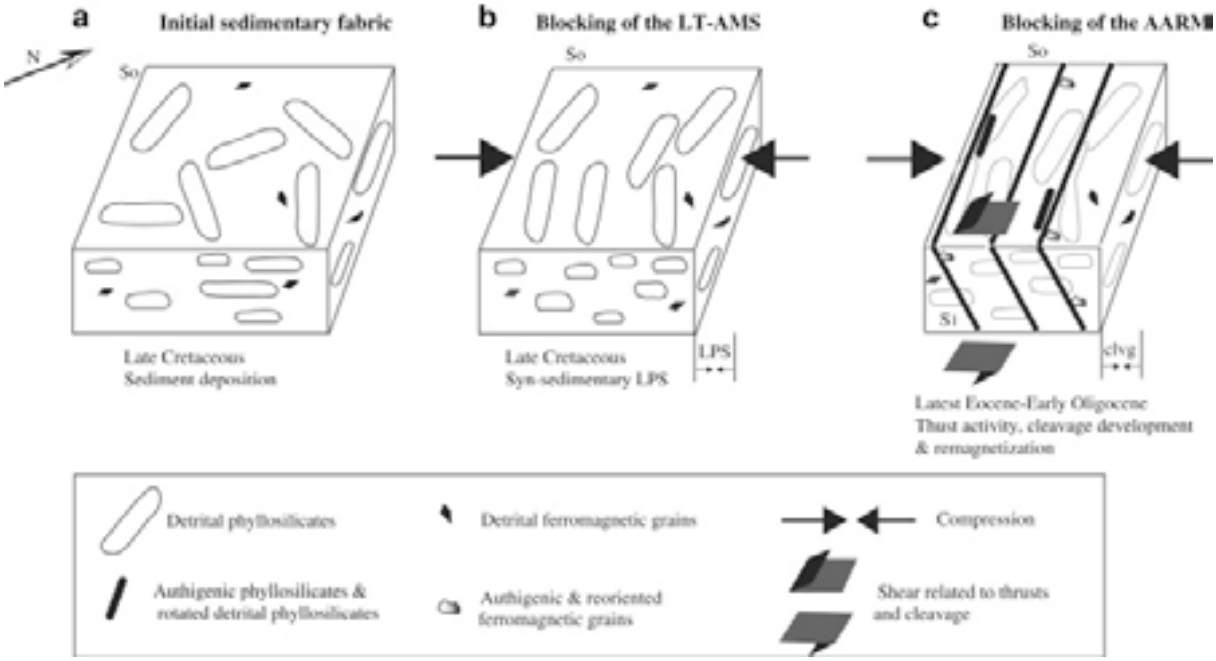

Figure 32. Sketch showing the evolution of the magnetic subfabrics in connection with the tectonic evolution of the Internal Sierras. a) Campanian-Maastrichtian initial sedimentary fabric. b) Campanian-Maastrichtian tectonic overprint (by LPS) causing the orientation of the phyllosilicates and the LT-AMS blocking. c) Late Eocene-Early Oligocene tectonic overprint caused by thrust activity and cleavage formation (Oliva-Urcia et al., 2009).

4. Methods applied to the study area

4.1. Introduction

Paleomagnetism is based on the record of the Earths's Magnetic Field (EMF) in crustal rocks (Figure 1). A primary magnetization takes place during rock formation (consolidation, diagenesis, cooling, etc) by means of several acquisition mechanisms (detrital, thermal, chemical). Nevertheless, rocks can undergo subsequent processes of magnetization called secondary magnetizations o remagnetizations. The Natural Remanent Magnetization (NRM) is the addition of all magnetizations of a rock. For chronological or structural interpretations it is key to determine the primary or secondary character of magnetizations and their relation to other geological processes (folding, metamorphism, etc.).

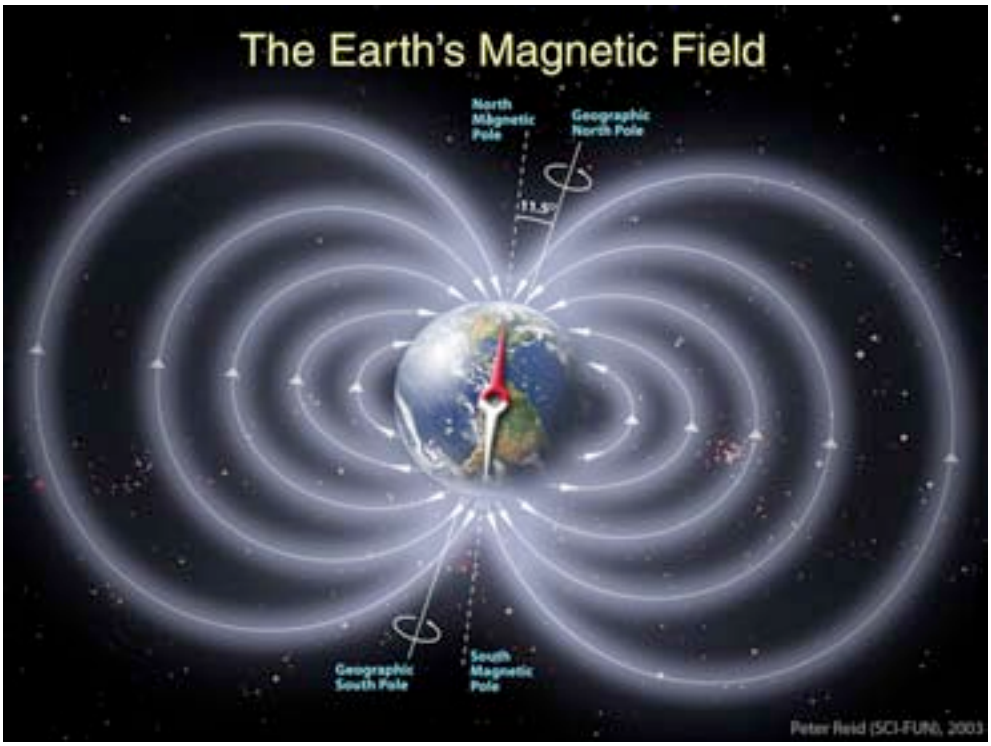

Figure 1. The external core generates a dipolar magnetic field that currently forms an angle of 11.5º with respect to the rotation axis.

Since the 80s, paleomagnetism has become a useful tool in regional tectonics because it is one of the best indicators to quantify vertical axis rotations between different structural units (Klootwijk, et al., 1986; McClelland and McCaig., 1988; Van der Voo, 1990; Butler, 1992; McCaig and McClelland, 1992; Kissel et al., 1993; Mattei et al., 1995; Allerton, 1998; Speranza et al., 2002, among others). Indeed, it is the sole technique that allows for determining motions from an absolute, external and global reference system, as the EMF. For these reasons, paleomagnetism has become an essential tool to understand thrust and belt systems in three dimensions.

Paleomagnetism entails the assumption of certain methodological hypotheses. The first one assumes that the magnetization acquired by a rock during its formation (cooling, diagenesis in a widest sense), the so-called primary component, has to be oriented parallel to the direction of the EMF at that time (geological sense). This primary magnetization can be stable along the geologic time, although the rock may be subsequently exposed to different magnetic fields. In a particular study, it is possible to demonstrate this hypothesis by means of stability tests (fold, reversal, conglomerate, baked contact tests). The second hypothesis assumes that the rocks were magnetized under the effect of a dipolar magnetic field centred on the Earth's rotation axis. If the secular variations of the EMF were averaged for about 10,000 years, that mean would fulfil those premises. This is de so-called GAD hypothesis (Geocentric Axial Dipole).

The first hypothesis is usually not fully accomplished because of the rocks can experiment thermal or chemical processes that modify, or even remove, the primary magnetization. Nevertheless, these processes may be linked to a stable secondary magnetization (remagnetization) that can accomplish the aforementioned stability conditions, being considered for secondary structural interpretations. Remagnetizations can be partial or total, deleting completely the original magnetization. The main goal is to decipher which is the primary or secondary imprint and to associate it with the structural frame in force during the acquisition period.

4. 2. Demagnetization

The relaxation time (t) is the required time to reorient the magnetic moment of a given single domain magnetic carrier (coercive force [Hc] and saturation magnetization [Js] with a given volume [v]) under a new external magnetic field. τ diminishes when temperature is higher, overcoming energetic barrier that maintains the magnetic moment aligned to a previous determined orientation, according to the equation:

$$\tau = \frac{1}{C} \exp\left(\frac{v\,Hc\,Js}{2\,k\,T}\right)$$

Where τ is the relaxation time, T the temperature, C the frequency factor ($\approx 10^{-8}$ sg^{-1}) and k the Boltzmann constant ($1.38 \cdot 10^{-16}$ erg/ºK)

The artificial modification of τ at the laboratory for a given rock allows unravelling the magnetic history of that rock and is the physical basis of demagnetization.

Characteristic Remanent Magnetization (ChRM) is the most stable magnetic component identified in a given rock. The main objective of demagnetizations is unravelling the NRM (addition of all components), especially the ChRM. The progressive thermal demagnetization (TH) involves heating to progressively higher temperatures and cooling in null external field. The orientation and intensity of the vectors are measured at every step as magnetization is being gradually removed thus decomposing vectorially the NRM. Minerals with lower unblocking temperature give randomly oriented signals (auto balanced in the zero field) whereas minerals with higher unblocking temperature still contribute to the magnetic signal. They should be progressively deleted by increasing the temperature up to the unblocking temperature of each magnetic mineral, ultimately the magnetization

will be totally removed. Magnetizations are usually more stable at higher temperatures (as deduced from the relaxation time equation). TH demagnetization allows for characterizing the orientation of the magnetic components; nevertheless it has the disadvantage that the temperature usually causes chemical changes in the rock, leading to the growing of new magnetic minerals (usually very unstable and viscous) that may mask the original signal if the zero field at the oven is not properly setup, or in the absence of shielding rooms. Magnetic susceptibility is controlled in every temperature step to recognize these mineral changes.

On the other hand, by means of the alternating field (AF) demagnetization, the sample is subjected to progressively higher alternating magnetic fields and the magnetization vector is measured at every step (as in the TH method). Vectors related to coercivities bellow 10-20 mT are usually related to imprints of the current EMF or other viscous components (sampling, storage, etc.). Higher coercivities may be related to older geological times, more stable and are used to calculate the ChRM of the sample. However, in sedimentary rocks AF frequently shows additional problems (overlapping of components, gyro-remanences, etc.) when compared to the more stable and suitable TH demagnetization (Ouliac, 1976).

Fitting the ChRM

Regarding the calculation of characteristic components from the demagnetization diagrams, the software used were Paldir (University of Utrecht) and VPD (IGME, Unit at Zaragoza, Ramón et al., 2011a). Due to the differential stability of the magnetic carriers, the demagnetization of the NRM offers a three-dimensional image that informs about the magnetic history of the rock. The representation of the progressive demagnetization evolution is the orthogonal diagram (Zijderveld, 1967), a valuable tool to determine the magnetic components of a rock (Figure 2). Eyeball selection of demagnetization points (sample level) and the fitting by Principal Component Analysis (Kirschvink, 1980) will derive in a population of vectors (site/profile level) representing the record of the paleomagnetic field.

The population of vector is statically associated to a scattering of points in a sphere (Fisher, 1953) where the density of points ($P_{\delta A}$) is ruled by:

$$P_{\delta A} = \frac{k}{4\ senh\ (k)} \exp\ (k\ cos\ \psi)$$

Where $P_{\delta A}$ is the probability to find a datum into an area (δA) and an angular distance ψ from the measured direction. $P_{\delta A}$ is maximum at ψ=0. The precision parameter *k* described the scattering of points, where *k*=0 reports random distributions throughout the sphere. If *k* is high, the data clusters around the resultant mean direction. *k* is calculated as (N-1)/(N-R), where R is the resultant vector sum of N vectors.

The summary vector of all directions is the resultant mean direction. The unitary vector that defines the direction of magnetization in a Fisher distribution is dependant on the declination (Dec), inclination (Inc), number of observations (N), and length of the resultant vector (R). The α95 parameter is widely used, which is calculated according to the following development:

The angle $\psi_{(1-P)}$ with a density P, is defined as (McFadden, 1980):

$$\cos \psi_{(1-P)} = 1-(N-R)\left[\left(\frac{1}{P}\right)^{\frac{1}{N-1}}-1\right]$$

The angle formed by the mean direction with the 95% of the directions is approximately (in degrees):

$$\psi_{95} = \frac{140^{o}}{\sqrt{k}}$$

Based on this mathematical development, it was demonstrated that for $k>3$ the mean direction will be into a semi-apical angle $\alpha_{(1-P)}$ around the resultant vector R according to:

$$\cos \alpha_{(1-P)} = 1-\frac{N-R}{N}\left[\left(\frac{1}{P}\right)^{\frac{1}{N-1}}-1\right]$$

Normally P is assumed as 0.05 to draw the 95% confidence circle around the mean (Van Der Voo, 1990). When α is low, the following approximation is used (McElhinny and McFadden, 2000):

$$\alpha_{95} = \frac{140^{o}}{\sqrt{kR}}$$

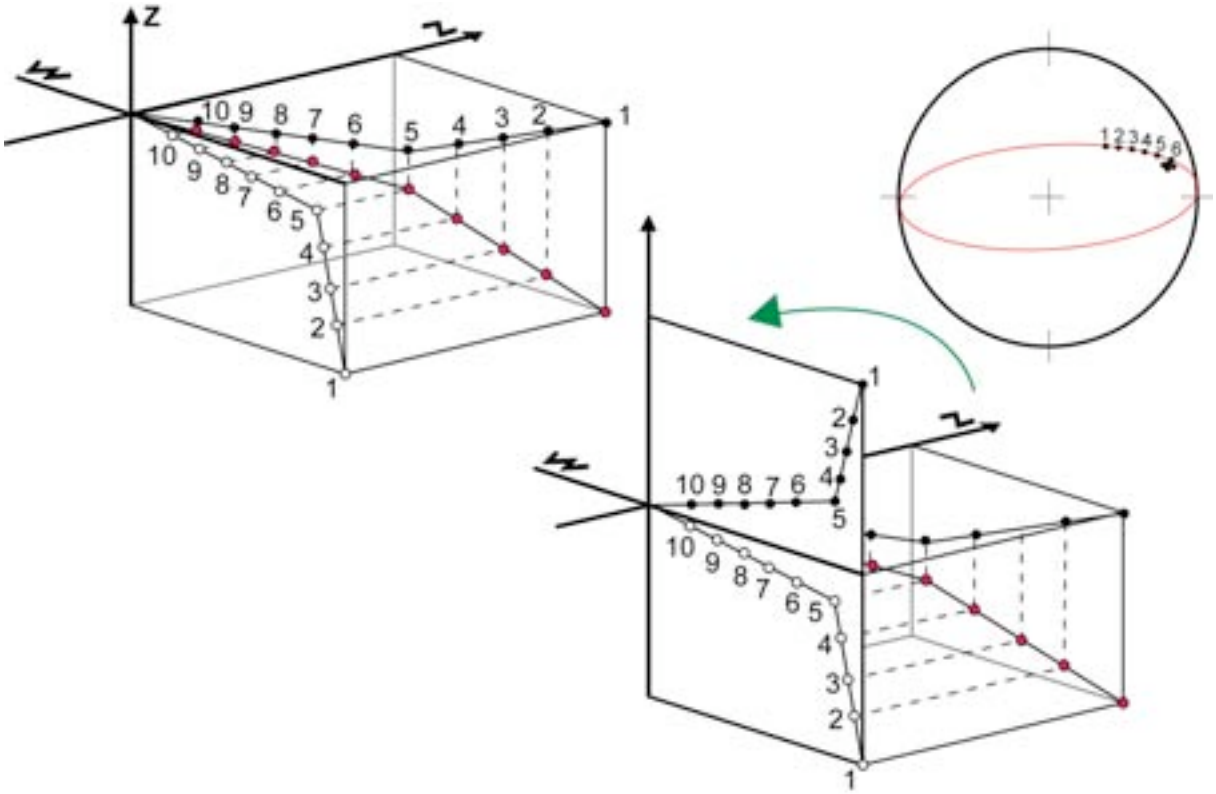

Figure 2. Enveloppe of orthogonal diagrams (Zijderveld, 1967) during demagnetization. Each red point represents a vector to the origing during progressive demagnetization (1 to 10). Declination is expressed as black points and inclination as white points. Representation in stereoplot of the demagnetization evolution. Modified from Lowrie (1997).

Other "non-fisherian" approaches have been obtained to calculate the paleomagnetic averages (Bingham, 1974; Kent, 1982; Tauxe et al., 1991) being the Fisher distribution widely used as basis for statistical treatment of the paleomagnetic data (Van der Voo, 1990). In this work we have used the "Stereonet 6.3.3" software (Allmendinger, 2006) that allows for calculating a mean for each set of samples (site/profile level) by means of Fisher's statistics.

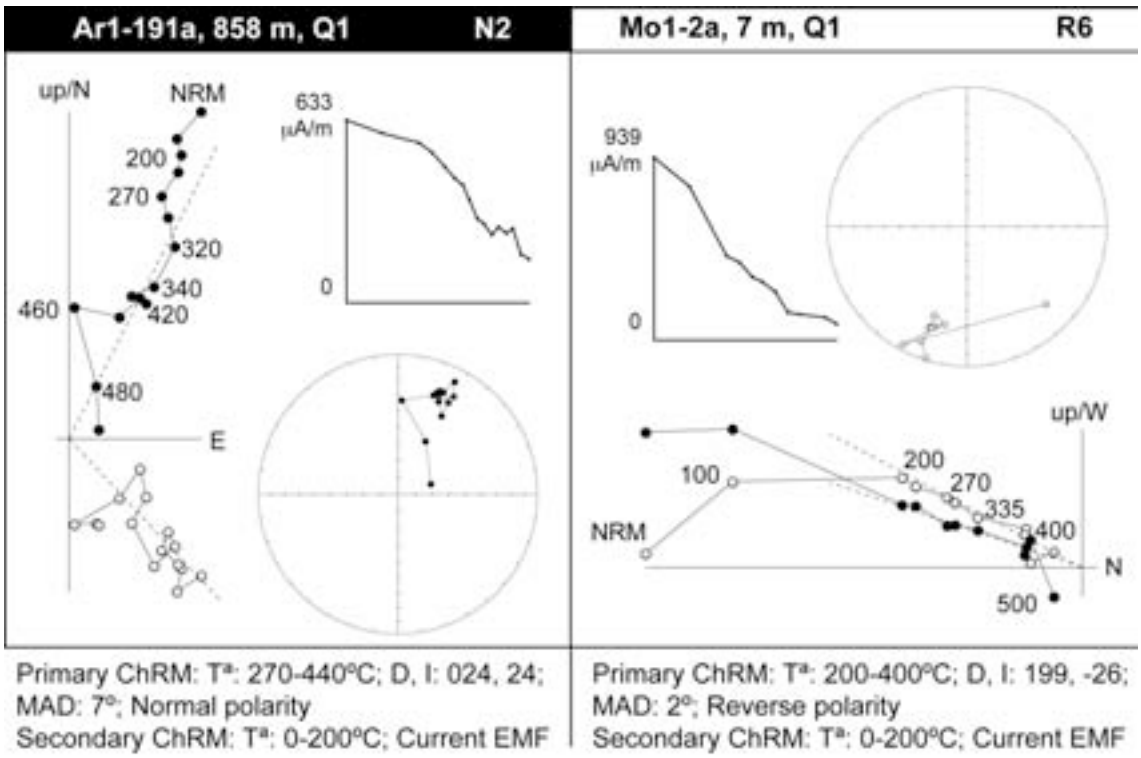

Figure 3. Examples of orthogonal diagrams, intensity decay and stereoplots form thermal demagnetizations of this work. Every step represents the magnetization vector at a given temperature (T °C). Fitting of directions. D: Declination, I: Inclination, MAD: confidence angle. Besides, Intensity decay is also shown, stratigraphic height (m), quality (Q) of the sample and magnetozone where it is located.

4.3. Stability tests

There are several tests allowing to check the stability (relative age) of the magnetization with respect to other geological processes. The most popular are the fold and reversal tests. The fold test (Graham, 1949) consists in comparing the spatial scattering of mean magnetic directions from some sites before any correction (*in situ, geographic system, bac* in this work) and after bedding correction (restored, *paleogeographic system*, *abc* in this work). If magnetization predates deformation, the population of vectors will show a better clustering after total restoration (positive test) whereas if the magnetization postdates folding, the clustering occurs before tectonic correction in present geographic coordinates (Figure 4).

Remagnetizations may also take place during folding. Synfolding magnetizations have relevant structural implications (snapshots of orogenic processes, basin reconstruction, etc…).

Therefore, the fold tests must evaluate the degree of clustering during stepwise unfolding. The software used in this work has been the SuperIAPD (Torsvik et al., 1992).

Reversal test is based on the dipolar nature of the EMF, averaged in long terms, and the polarity inversions. Therefore, normal and reverse records of the paleomagnetic field (i.e. along a stratigraphic section) should display an antipodal character on the stereoplot. A positive test indicates the primary origin of the magnetization (Figure 5).

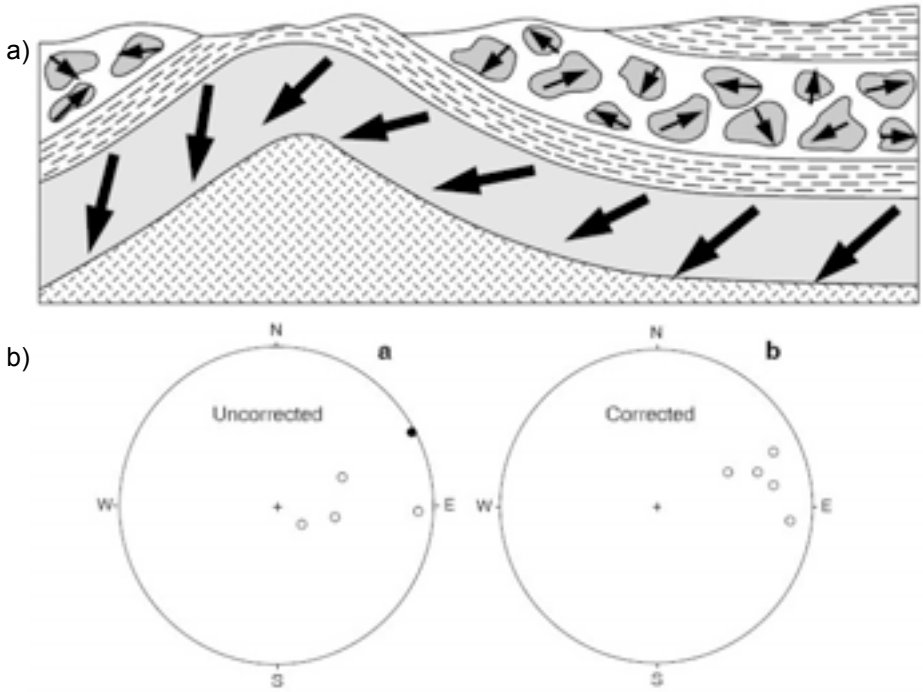

Figure 4. a) Sketch of the fold and conglomerate tests. Bold arrows are directions of ChRM in the limbs of the fold and in pebbles of the conglomerate. Random distribution of ChRM directions in pebbles indicates that ChRM was acquired prior to formation of the conglomerate. b) Equal-area projections show mean ChRM directions. Solid circles indicate directions in the lower hemisphere of the projection; open circles indicate directions in the upper hemisphere. Improved grouping of ChRM upon restoring the limbs of the fold to horizontal indicates ChRM formation prior to folding (modified from Butler, 1992).

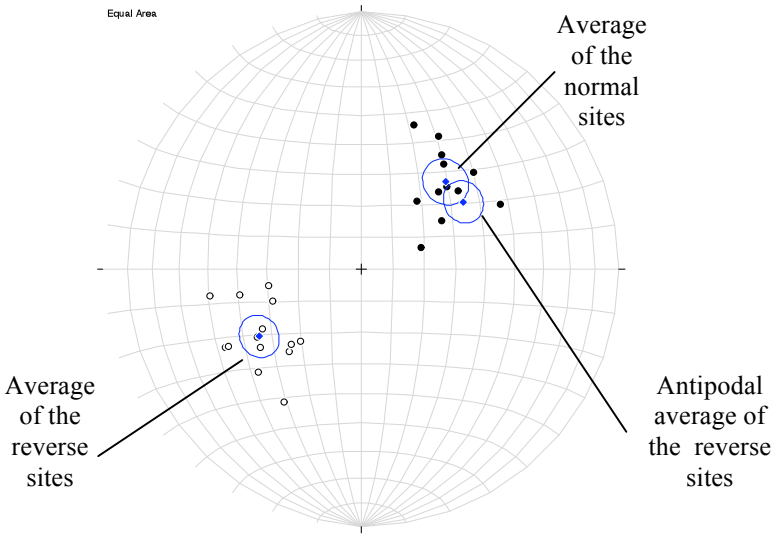

Figure 5. Hypothetical reversal test of two group of samples with normal and reverse antipodal directions. Their confidence angles are overlapped, being a positive test.

The conglomerate test (Graham, 1949) consists of measuring the magnetization in the pebbles and matrix of a conglomerate. The magnetization of the matrix can be acquired during or after the deposition; nevertheless the pebbles provide some additional information. If their directions are randomly distributed, it can be interpreted that the magnetization has remained stable, at least from the moment of conglomerate formation. In this case, the test is positive (Figure 4). On contrary, if the pebbles present parallel magnetizations, the original magnetization has been modified after the conglomerate formation. The contact test (Everitt and Clegg, 1962) consists of comparing the magnetization of an igneous body with the host rock aiming to establish a relation between the emplacement of the igneous body and the acquisition of the magnetization. Since in this work we deal with sedimentary rocks this kind of analysis was not performed. We could not apply the conglomerate test as well since the studied lithologic types are fine-grained.

4.4. Applications of paleomagnetism

4.4.1. Magnetoestratigraphic dating

Magnetostratigraphic dating is a technique based on the reconstruction of the local pattern of polarity reversals and its comparison with the global polarity time scale. The local polarity sequence derives from demagnetized samples along a stratigraphic pile. Individual ChRM (primary) directions are converted (present longitude and latitude are known), to the orientation of the Virtual Geomagnetic Pole (VGP) by means of the GAD model; normal polarity displays positive and high VGP latitudes (regularly around 90°) and reverse polarity the opposite position (-90º). The comparison of the local pattern of magnetozones with the Geological Timescale (GPTS) will allow for age deductions, where each reversal boundary will be an isochron.

This technique is widely developed owing to the establishment of trustworthy global scales (Bergreen et al. 1985; Harland et al., 1990; Cande and Kent, 1992 and 1995; Gradstein et al., 2004), which calibrate the reversal boundaries by alternative dating methods, normally stable isotopes. The referential GPTS used in this study was Grandstein et al. (2004), Figure 8, section 2.4. The suggested calibration is based on data that follow the quality criteria proposed by Opdyke and Channell (1996): Availability of biochronologic data constraining the age of the profiles involved; Stratigraphic control of the basin development and field data that unambiguously confirm the lateral relation between two studied profiles; Detailed stepwise demagnetizations carried out to successfully isolate the different magnetic components; Fitting of ChRM directions using PCA (Kirschvink 1980); Magnetostratigraphic data presented in full detail (VGPs, inclinations, declinations, and statistics); Magnetic carriers qualitatively identified by means of magnetic mineralogy experiments; Fold and antipodal tests that prove the stability of the magnetization and confirm the primary character of the ChRMs.

4.4.1.1. Laboratory and processing procedures

The NRM analysis aims at the isolation of the primary and secondary components responsible for the rock magnetization. It is composed of different analyses detailed below:

1. Pilot paleomagnetic analysis of representative samples from characteristic outcrops that helps taking further decisions regarding demagnetization routines. With this objective, the samples are subjected to detailed and progressive thermal and alternating field demagnetizations. Thermal demagnetization is usually the most effective method to analyze sedimentary rocks (Ouliac, 1976). All demagnetizations were performed with a Cryogenic Magnetometer (2G) and several models of ovens (detailed below)

2. Depending on the rock type, pilot demagnetizations help choosing the most adequate demagnetization routine of the NRM (sequence of steps). In the case of TH demagnetization, an exhaustive control of the magnetic susceptibilityis was done at every thermal step to recognize any mineralogy alteration. These measurements were taken by means of a Kappabridge susceptometer (KLY2 and KLY3, Agico)

3. The fitting of the different components of the ChRM can be done by means of the analysis of the demagnetization results. The isolation of the primary and secondary components allows detecting possible remagnetizations (McCabe and Elmore,1989; Jackson, 1990; Menard and Rochette, 1992; Housen et al., 1993; Katz et al., 1998).

4. Stability analysis. Normally the fold and reversal tests will help supporting the primary character of the ChRM, which is a critical keystone in magnetostratigraphic studies.

5. Once the primary character is demonstrated, a Local Polarity Sequence (LPS) is built. To do so, the site location (longitude and latitude) together with the primary magnetic vector (declination and inclination after bedding correction) will allow, by means of the GAD hypothesis, calculating the expected paleolatitude of the Virtual Geomagnetic Pole, which in turns gives the polarity of the magnetic field at the time of rock formation.

6. Alternative chronostratigraphic data (biostratigraphy, isotopes, etc.) allows anchoring the LPS to the Global Polarity Time Scale. The final result (and the great advantage of magnetostratigraphy) is a continuous dating along the studied profile with a number of isochrones equal to the number of recognized polarity reversals.

4.4.2. Structural Geology and Tectonics

The EMF has a global character, thus a direction recorded by a rock in a particular time depends of the latitudinal position in which the rock was formed (as a consequence of the GAD hypothesis). Hence the use of the paleomagnetism as one of the basis of plate tectonics since it can determine the latitudinal position of continents and their relative (latitudinal) motion along time. Early paleomagnetic studies were focused on paleogeographic reconstructions and still continue nowadays

(Torsvik el al., 2008). Nevertheless, since the early 60s (Norris and Black, 1961) paleomagnetism has been applied to regional tectonics since it is able to detect anomalous directions in deformed areas.

These deflected directions (i.e. vertical axis rotations, VAR) are related to the kinematics of certain folds, thrusts and directional faults. Therefore, paleomagnetism (sometimes called magnetotectonics in this particular application) is the sole technique that allows for an absolute determination of rotation magnitudes, thus opening new insights towards the understanding of three-dimensional kinematics of deformed areas. To refer few works among many, magnetotectonics has been of great help to decipher kinematics of oroclinal bends (Grubbs and Van der Voo, 1976; Stamatakos et al., 1996; Weil, 2006), thrusting emplacement (Osete et al., 1989; Channel et al., 1990; Allerton, 1998; Oliva-Urcia and Pueyo, 2007a) and strike-slip faults (Garfunkel, 1988; Little and Roberts, 1997; Larrasoaña et al., 2003a).

The main goal of a magnetotectonic study is to determine vertical axis rotations (VAR) undergone by a structural unit during its deformation. To detect them, a difference between the paleomagnetic direction and the reference (obtained form the expected paleomagnetic pole of the closer stable plate) has to be established.

A paleomagnetic investigation focused on the characterization of vertical axis rotations in deformed areas (i.e. fold and thrust belts) should honor some specific reliability criteria (Pueyo, 2010) additionally to those suggested by Van der Voo (1990) for the evaluation of the quality of paleopoles:

1) Rock deformation (folding, thrusting and rotation) and magnetization ages must be known.

2) A minimum of 5 sites (10 is desirable) per thrust or structural unit (10-15 specimens per site). Site means characterized by $\alpha 95 \leq 10°$ (never >15°) and $k > 20$ (never <10).

3) Detailed demagnetization that guarantees the isolation of all magnetization components and allows for a reliable calculation of directions and demagnetization circles. Directions and/or circles should be fitted by PCA (Kirschvink, 1980). Combined use of difference and resultant vectors are always preferable to detect instrumental problems. More than 4 steps involved in the calculation (vectors and planes) and MAD<10° (never >15°);

4) Field test and error-control techniques. Conglomerate, reversal or fold test (including the small-circle intersection method by Waldhör and Appel, 2006) must be performed to support the magnetization age. Additional strike vs. declination and dip vs. inclination diagrams should be achieved to avoid errors in case of synfolding remagnetizations.

5) Structural control. Fold and thrust geometry and kinematics should be known to avoid restoration errors and subsequent alteration of the fold test.

6) The origin of the inclination error should be identified among its three major sources; compaction, internal deformation and overlapping of directions.

7) Rotations have to be contrasted to an appropriate reference in the undeformed foreland (absolute VAR) or in the nearest footwall (relative VAR).

4.4.2.1. Laboratory and processing procedures

1. The laboratory procedures carried out for magnetotectonics are similar to those performed for magnetostratigraphy, except for the quality of data used. Usually, in magnetostratigraphic studies the ChRMs are classified according to different qualities. High quality ChRMs (Q1) entails unequivocal and straight to the coordinate origin directions. In the intermediate quality (Q2), the ChRMs unambiguously allow polarity recognition, although secondary processes distort the quality of the directions. In the low quality ChRMs (Q3), directional data are of very poor definition. Whereas Q1 and Q2 were used for magnetostratigraphic aims, just those Q1 ChRMs have been considered in magnetotectonic analysis in this work.

2. The high quality directions derived from magnetostratigraphic data in this work were gathered according to several criteria. These criteria include the geographical proximity, to belong to the same section, chron and formation and the need of having a minimum number of samples that ensures the statistical quality of the derived mean. Apart from the gathering of the samples derived from magnetostratigraphic profiles, twenty additional sites have been sampled to obtain supplementary rotation magnitudes. These sites are sampled according to the classic concept of "locality"; a) covering a reduced stratigraphic length (a few meters ≈5-20m), b) within the same sedimentary unit (similar expected rock magnetic response) and c) with a constant bedding attitude.

3. The reference used in this work has been calculated for the Aínsa Basin using the stable data from the Eastern Pyrenean foreland basin during Eocene times (profiles La Rovira and Grau de Sunyer of Vic area, Easterm Pyrenees); Declination: 004º, Inclination: 53º, a_{95}: 4.6°, k: 9.6 (Taberner et al, 1999). This sector (S in figure 6) is determined by the data:

-Geographic coordinates (stable data); Latitude: 41° 55' N (41.92°), Longitude: 2°, 15'E (2.25°)

-Paleomagnetic mean: n:110 (67N+43R) N+(-R); Dec: 004.2; Inc: 52.6; α_{95}: 4.6°, k: 9.6 (Taberner et al, 1999).

The Virtual Paleomagnetic Pole calculation was done by means of the program VGP.exe (University of Utrecht) based on of the algorithm expressed in figure 6. The VGP coordinates of the pole of the Vic area is: PLat: 80.7; PLong: 155.6E

The expected direction at the Aínsa Basin from the this stable Lutetian Pole would be conditioned by the geographical data of the point S' (Figure 6):

-Geographic coordinates; Latitude: 42° 21' N (41.35°), Longitude: 0°, 04'E (2.07°)

This position represents the central part of the studied area, which is located between the Sarratillo and Castellazo villages. The reference palomagnetic direction of the study areas is therefore: n:110 (67N+43R) N+(-R); Dec: 004.6; Inc: 53.2; α_{95}: 4.6°, k: 9.6

The angular differences between this local reference and our sites are interpreted as Vertical Axis Rotations (VAR; β) undergone by the structural unit in question (Figure 7).

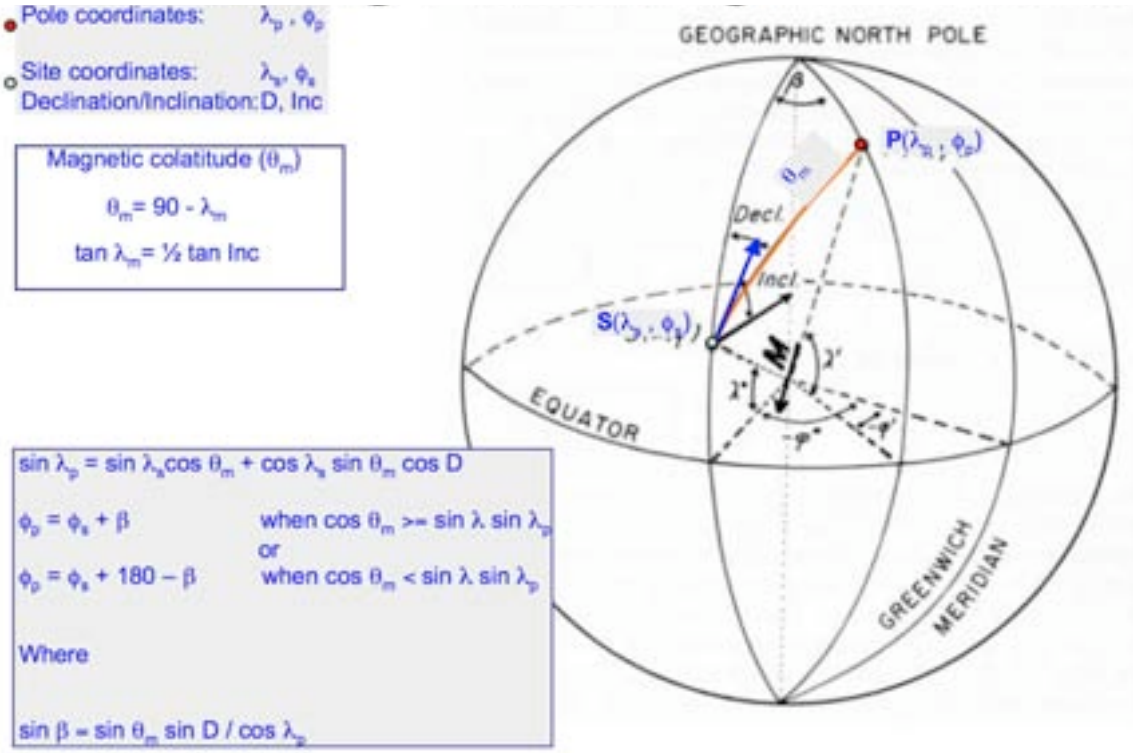

Figure 6. Mathematical development to calculate a local paleopole from data for stable portions of the plate (Butler, 1992). By courtesy of Miguel Garcés Crespo.

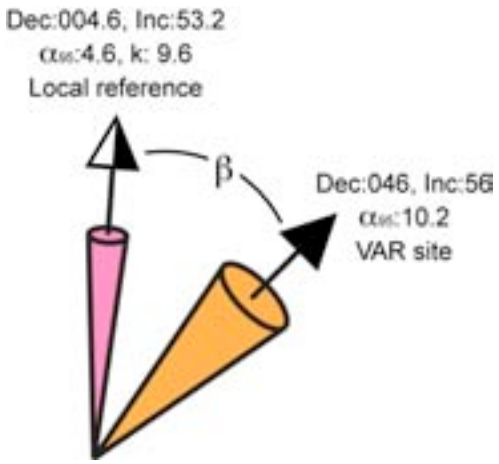

Figure 7. Difference between the Eocene reference and the local vector is interpreted as VAR.

4.5. Rock magnetism

Rock magnetism comprises several kinds of analyses focused on the study of the magnetic carriers of the rocks. Its main purpose is to determine the magnetic minerals present in the rock, their relative concentration, fabric, etc. These techniques are usually employed to support paleomagnetic interpretations since the recognition of rock magnetism allows for determining the meaning and

stability of the NRM. Physical response of the minerals in variable temperature and/or external fields is the basis of rock magnetism.

The thermal demagnetization of the NRM is, in fact, an excellent approach to rock magnetism since the unblocking temperatures of the ChRM indicates the thermal range of the magnetic carriers. Nevertheless, minerals with common unblocking temperatures as well as additional factors as grain size, concentration, crystallization, etc. lead us to perform detailed and specific analysis aimed to determine precisely the magnetic bearers of the rocks. AF demagnetization also provides information about rock magnetism based on the ranges of coercivity that it offers. For example, both iron sulphides and magnetite display low coercivity (*soft minerals*), being more restrictive for magnetite (below 0.3T) with wider range for the iron sulphides (up to 0.5 T, Lowrie, 1990). On the other hand, *hard minerals* present coercivity values not measured by common instruments used in most paleomagnetism laboratories (1-2 T). They are goethite (≈ 1.2T) and hematite (≈ 6T), often identified by incomplete saturation of the magnetization.

4.5.1. Laboratory and processing procedures

There are many rock magnetism analyses, and below we only describe those performed in this study:

1. Isothermal remanent magnetization (IRM): by means of a Pulse magnetizer (details below) a direct magnetic field is applied at room temperature. Then, the remanent magnetization is measured. Progressively increasing fields and subsequent measurement of the magnetization in each step (with the cryogenic magnetometer, explained below) will describe the acquisition curve of the rock that help to qualitatively discriminate between *hard* and *soft minerals.* More sophisticated post-processing of data, based on the coercivity spectrum analysis, allows more quantitative details (Kruiwer et al., 2001). IRM analyses were performed in the laboratories of Tübingen (Germany) and Lehigh (PA, USA).

2. Lowrie's test (Lowrie, 1990) or thermal demagnetization of three axes IRM: This technique provides information about the unblocking temperature of the magnetic carriers taking advantage of a sorting based on their coercivities. The routine applies different magnetic fields along different axes of the sample: 1.2 Tesla (hard fraction) field to z-axis, 0.3 T (intermediate fraction) to the x-axis and 0.1 T (soft fraction) to the y-axis. Subsequently the thermal stepwise demagnetization is applied with 35° to 50ºC increments, up to 600ºC. Thermal demagnetization allows analyzing the three-axes intensity decay curves and sorting the present minerals depending on their unblocking temperatures and coercitivities. The devices used are pulse magnetizers, ovens and cryogenic magnetometers. These analyses were performed in the laboratories of Tübingen (Germany), Lehigh (PA, USA) and Rome (Italy).

3. Hysteresis loops: Analysis related to an intrinsic property of ferromagnetic minerals. When a magnetic field is applied to a non-magnetized sample, starting at the origin in a magnetic intensity (J) versus magnetic field (H) diagram (figure 8), the hysteresis curve describes the curve *a, b, c*. By increasing H, the saturation is reached at J_{S1}. When decreasing H the magnetization describes the *b*

curve, preserving certain magnetization at H=0, called remanent magnetization (Jr). When J is completely removed, negative values of H determine Hc, called coercitivity (coercivity force). The hysteresis loop will be completed by the *c* segment and never comes back to the coordinate origin (0,0) if the sample is not fully demagnetized. The hysteresis parameters allow classifying the magnetic content of the rock. *Soft minerals* describe narrow and elongated hysteresis loops with low-density energy stocked, easily magnetizable and little remanent magnetization. *Hard minerals* present short and wide loops, stocking high-density energy and remanent magnetization. From hysteresis loops we can deduce saturation magnetization (J_{S1}), remanent magnetization (Jr) and coercive force (Hc). These analyses were performed at the Tübingen laboratory (Germany), by means of AGFM 2900 (Princeton Measurements Corp).

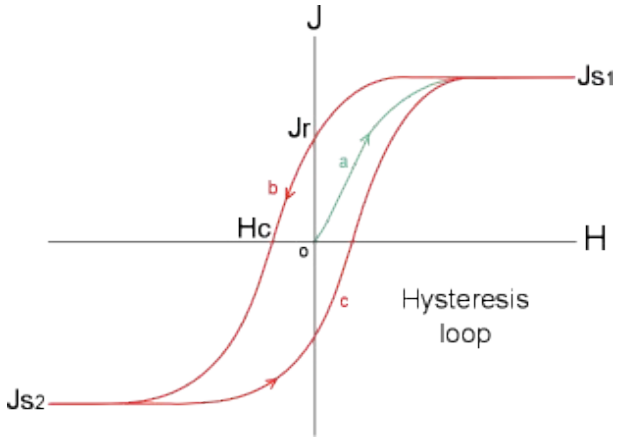

Figure 8. Hysteresis loop (De Miguel, 1974)

4. Low temperature measurements: Most ferromagnetic minerals experiment crystalline changes at low temperatures (between 20°C and 4 K [-296º C]). These crystalline transitions lead changes in the magnetic properties characteristic of each magnetic mineral. For example magnetite displays the Verwey's (1939) transition at 100º K, hematite has one at 262º K (Morin, 1950), pyrrhotite displays it at 30-34 K (Rochette et al., 1990). The detection of these transitions assumes a mineralogical diagnostic evidence that compares to the, always difficult, optical recognition. In this work, we have measured the evolution of magnetic susceptibility at low temperatures They were taken by means of the KLY3 susceptibility bridge (Agico) with the CS3 furnace attached in the Geotranfer laboratory at the University of Zaragoza.

5. Low field / High field susceptibility measurements (LF/HF): Analyses aimed to establish precisely the paramagnetic and ferromagnetic contributions (Rochette, 1987; Hrouda and Jelinek, 1990; Pueyo et al., 2005a). Measurements were carried out with the MPMS-XL SQUID magnetometer (Quantum Design Ltd.) of the ICMA Service (Universidad de Zaragoza - CSIC). The steps followed are: Centring in Direct Current (DC); Susceptibility measurement in LF, Alternating Current (AC), 4 Oe, 920 Hz and 0.4 mT (similar conditions to KLY-3S); HF susceptibility measurements and DC at 1T, 1,5T and 2T. Since the high field susceptibility can be considered only paramagnetic (providing a

complete saturation of any ferromagnetic mineral), any deviation of the LF susceptibility with respect to the HF susceptibility will be the ferromagnetic contribution.

4.6. Anisotropy of Magnetic Susceptibility (AMS)

The measurement of the Anisotropy of the Magnetic Susceptibility (ASM) is a non-destructive technique of rapid application to determine the features of the magnetic fabric of the rocks. AMS is a useful tool in structural analysis. Under appropriate conditions (dominant paramagnetic content) it can be considered a reliable approach of the preferred mineral orientation. In these conditions, AMS can be used to describe the deformation undergone by weakly deformed sedimentary rocks when other markers are not present (Tarling and Hrouda, 1993; Borradaile and Henry, 1997; Mattei et al., 1997; Speranza et al., 1997; Bouchez, 1997; Parés et al., 1999; Latta and Anastasio, 2007; Oliva et al., 2009)

The magnetic susceptibility (k) is an intrinsic property of the matter and represents the ability of a solid to be magnetized under an external magnetic field under a given temperature (Jelinek, 1981). k is a second rank tensor and it can be represented by an ellipsoid defined by three axes (Figure 9). The magnetic fabric is the result of the intrinsic (crystalline and shape anisotropies) and extrinsic (resulting from the physical orientation of the minerals) factors.

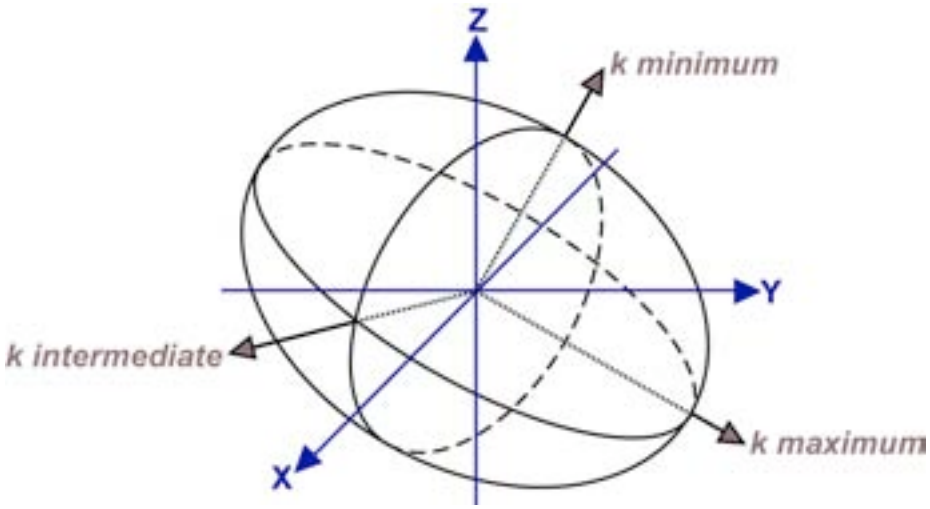

Figure 9. AMS ellipsoid graphically expressed by three axes where the principal susceptibility direction (k_{max}), intermediate (k_{int}) and minimal (k_{min}) are involved (from Gil-Imaz, 2001).

Depending on k there are three types of substances:

i) Diamagnetic materials do not present unpaired electrons at atomic-scale and their response is thus opposite to an external field, with much weaker intensity. Therefore k in diamagnetic materials is weak, negative ($k<0$) and independent of the temperature. Apart from water and air, most rock forming minerals are diamagnetic: quartz, calcite, gypsum, potassic feldspar, etc. with k values around $-14\ 10^{-6}$ S.I. (Rochette, 1987).

ii) Paramagnetic substances present unpaired electrons and their response face an external field is favourable and proportional to the applied field. K is therefore positive (k>0), weak and dependent on the temperature (Curie-Weis law, Nagata, 1961)

$$J = k \cdot H$$

Clay minerals, phyllosilicates as biotite, muscovite and chlorite (Martín-Hernández and Hirt, 2003) and other silicates as olivine, pyroxene and amphiboles (Rochette, 1987; Bouchez, 1997) are paramagnetic with k around 10^{-5} - 10^{-4} S.I.

iii) Ferromagnetic materials (s.l.) present unpaired electrons in their structure and magnetically coupled with adjacent atoms. Their magnetic dipoles are parallel giving rise to a strong spontaneous magnetization in the absence of an external field. K is very high (k>>>0) as occurs in iron, cobalt and nickel (e.g.). Ferromagnetics subjected to an external field describe the hysteresis loop magnetizations (Figure 8). Once ceased the external field, ferromagnetics preserve a residual or remanent magnetization (Jr).

During the last decades, the advances in rock magnetic mineralogy have allowed to find out that not only ferromagnetic minerals but also the paramagnetic minerals contribute to the bulk susceptibility of rocks, which can be determinant in AMS studies. In rocks with dominant paramagnetic minerals, AMS reflects the orientation of phyllosilicates (Rochette, 1987) and is an indicator of the mineral preferred orientation.

4.6.1. Laboratory procedures

1. A standard sample is inserted at room temperature in the susceptometer (KLY3) that applies a very low magnetic field (0.4 mT) and measures the induced magnetization of the sample. Jelinek's (1977) method integrates the magnetic ellipsoid from these measurements. Magnetic ellipsoids can be classified according to their shape; three kinds of extreme cases (fabrics) can be observed: oblate ($k_{max} \approx k_{int} >> k_{min}$), prolate ($k_{max} >> k_{int} \approx k_{min}$) or triaxial ($k_{max} > k_{int} > k_{min}$).

2. The degree of anisotropy of the ellipsoid is represented by P' and the shape parameter by T. Oblate ellipsoids present $0<T\leq1$ and prolate ellipsoids $-1<T\leq0$. The L parameter describes the magnetic lineation and F the foliation. The shape and orientation of the ellipsoid characterize the magnetic fabric of a rock, in a similar way to Flinn's, diagram (1962).

3. In sedimentary rocks, where susceptibility is controlled by paramagnetic minerals, the anisotropy is the result of deposit, subsequent compaction of the sediments and possible records of far-field effects of tectonic deformation processes (i.e. layer parallel shortening). Anisotropy is dependant of the grain size, therefore it is important to focus the sampling in finer lithologies to avoid the effect of tractive currents during deposition. In tectonically deformed rocks, the ellipsoids of magnetic susceptibility are usually associated with the ellipsoid of finite strain (Hrouda, 1982; Borradaile, 1988; Dinarès-Turell et al., 1992)

4.7. Instruments

The measurement of magnetic properties of the samples obtained in this work has been performed in several paleomagnetic laboratories: Zaragoza, Burgos, Barcelona (Spain), Tübingen (Germany), Lehigh (Pennsylvania, USA) and Rome (Italy) by means of the following instruments:

MMTD (Magnetic Measurement) and TSD (ASC) ovens

These ovens are used in thermal demagnetization to heat and cool the samples in the absence of magnetic field (Figure 10). By means of the ovens we can find out the unblocking temperature as demagnetization advances. The laboratories of Burgos, Barcelona and Tübingen have the MMTD60 model and the laboratories of Bethlehem and Rome have the TDS-48 model.

SQUID Magnetometer 755R (2G)

Superconducting properties of particular materials at low temperatures (≈ 4 K) allow the measurement of very weak magnetic flows (≈ 10^{-12} Am^2). Cryogenic magnetometers were adapted to paleomagnetic standards some decades ago, These instruments include three-axes SQUIDs (superconducting quantum interference device) consisting in a sophisticated coil system immersed in liquid helium (4ºK, -269ºC) that behave as superconductors. The magnetic flow (Am^2) caused by the samples can be transformed to magnetic moment (A/m) in each axis (x, y and z) considering the rock volume (m^3). Magnetization (addition of magnetic moments) is obtained in core-coordinate system (sample axes) and can be easily transformed to geographic or paleogeographic reference systems by using the field orientation data (sample core orientation and bedding plane). All measurements in this report were taken in this kind of magnetometers (2G), some of them placed in shielded rooms (Bethlehem and Rome) and others under Helmholtz coils (Figure 11).

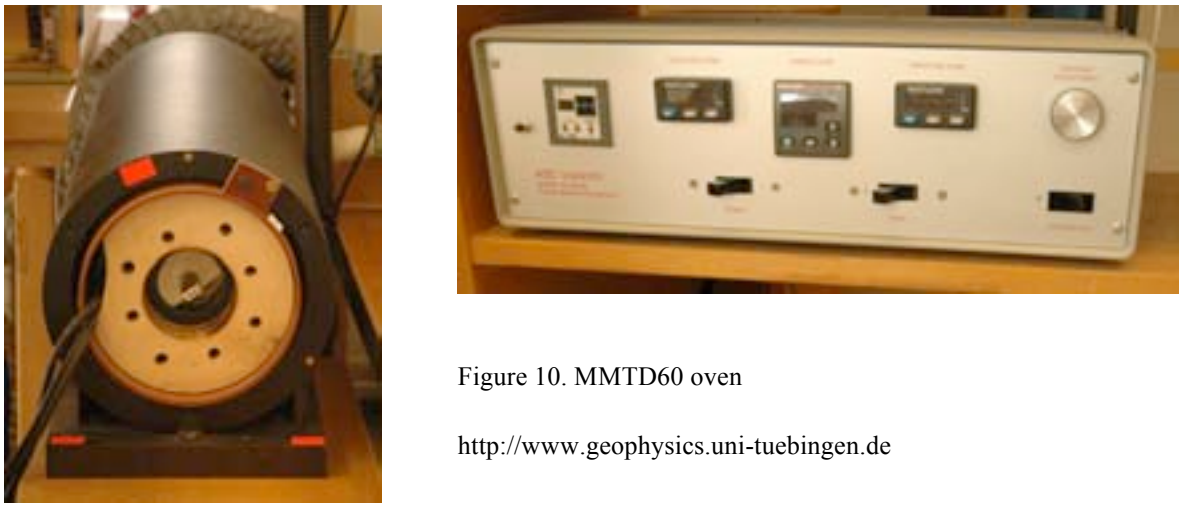

Figure 10. MMTD60 oven

http://www.geophysics.uni-tuebingen.de

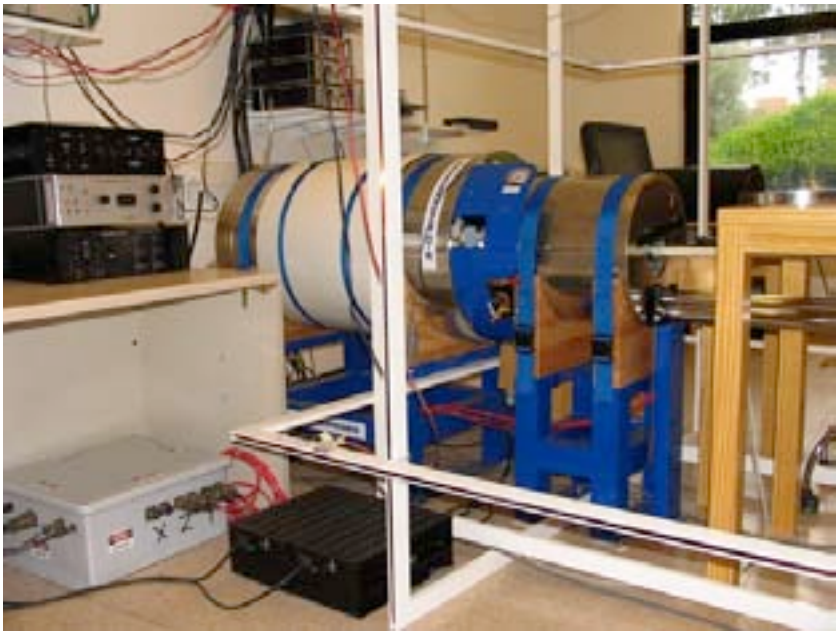

Figure 11. SQUID Magnetometer 755R (2G), http://www.ubu.es.

Kappabridge KLY2 and KLY3 (Agico)

Apart from AMS measurements, these instruments can provide data on the evolution of the magnetic susceptibility during TH demagnetization in relation to mineral neo-formation (Figure 12). The CS2 and CS3 models from AGICO Inc. allow performing susceptibility measurements at low and high temperature, respectively. These analyses allow observing the dependence of the susceptibility and finding out some mineralogical transitions. It was used to control mineralogical changes during demagnetization in all the laboratories. All room-temperature and low-temperature AMS measurements were taken in the Geotransfer laboratory (Internal Geodynamics, U. Zaragoza).

Figure 13. AGICO KLY-3 Susceptibility Bridge
http://wzar.unizar.es/perso/geotransfer027/

MMPM9 Pulse-Magnetizer:

This instrument is used to induce a magnetic field on the sample and to obtain the IRM progressive acquisition curves. IRM is the saturation magnetization that a sample is able to hold after being exposed to an external magnetic field. The IRM curve gives an approach to the coercivity spectrum of the magnetic minerals present in the rock (Figure 13). It was used in the laboratories of Tübingen, Lehigh and Rome.

Figure 13. MMPM9 Pulse Magnetizer. http://www.geophysics.uni-tuebingen.de

Alternating Gradient Force Magnetometer AGFM 2900 (Princeton Measurements Corp.):

It is used to discriminate between para- and ferromagnetic contributions from the minerals contained in the rocks, comparing high and low magnetic field measurements (Figure 14). Moreover, hysteresis loops (see figure and description of hysteresis loop in 4.5 section and figure 8) allow us to deepen in the nature of the magnetic carriers. Parameters as remanence and saturation magnetizations as well as characteristic coercivity (Hc), and remanent coercivity (Hcr) can be obtained with this instrument. Hysteresis loops were performed in the laboratory of Tübingen.

MPMS Cryogenic magnetometers (Quantum Design Ltd.):

Equipment that allow for determining the magnetization, permeability and susceptibility in alternating or direct magnetic fields with great precision. It is here used to compare susceptibilities obtained at Low and High fields; if both measurements (K_{LF} and K_{HF}) are similar, a dominant paramagnetic contribution will be proven. Otherwise, if the measurement at HF differs significantly from measurement at LF, an important ferromagnetic contribution can be inferred (Figure 15).

Figure 14. a) MicroMAG (Princeton AGFM 2900) reaches 2 Teslas. b) Holder sampling of AGFM. http://www.geophysics.uni-tuebingen.de; http://www.irm.umn.edu.ind

Figure 15. SQUID Magnetometer, MPMS-5S (left) and MPMS-XL5 (right). ICMA Service (UZ - CSIC). http://www.unizar.es/icma/depart/O5_msi.htm

5. Magnetostratigraphy of the Boltaña anticline and the Aínsa Basin

5.1. Chonostratigraphic frame and need of this work

The importance of this area lies in the oblique configuration of its structures, involved in a syntectonic genesis and the good record of Eocene sedimentation. Besides, oil companies (Conoco-Phillips, Norsk-Hydro-Statoil, Shell, Repsol-YPF, Elf-Total, etc..) have focused their interest in the Aínsa Basin due to the analogue-model reservoir that constitutes its turbiditic sequence.

Magnetostratigraphic studies have been carried out in adjacent areas (see detailed description in section 3.3). In the Jaca Basin, the Guara Fm records the Ypresian/Lutetian boundary (at its base) and spans along the entire Lutetian interval (Rodríguez-Pintó et al., 2006, 2011c, d). The interval covered from the top of the Guara Fm to the Campodarbe Fm has been characterized as Late Lutetian–Oligocene in age (Hogan, 1993; Hogan and Burbank, 1996; Kodama et al., 2010). In the Graus-Tremp Basin, surveys were focused in the Paleocene-Eocene boundary in Tremp (Ilerdian Stratotype) and Campo (Ilerdian and Cuisian Parastratotypes) (Pascual et al., 1991 and 1992; Pascual, 1992; Molina et al., 1992; Serra-Kiel et al., 1994; Pujalte et al., 2003). Moreover, a detailed study was performed to the East in the Sis and la Pobla de Segur conglomerates whose ages range from Late Lutetian to Priabonian (Beamud et al., 2003). The only study placed in the Aínsa Basin dealt with the continental strata of the Escanilla Fm (Bentham, 1992; Bentham and Burbank, 1996), which ranged from Late Lutetian to Priabonian.

As can be noticed, the age of the materials involved in the Aínsa basin has been interpolated from adjacent areas by means of stratigraphic or biostratigraphic criteria. Usually, it is a feasible method to partially define the chronology of a moderately large area. Nevertheless, several factors contribute to preclude a definitive chronostratigraphic frame in the Aínsa Basin from stratigraphic criteria alone: 1) Spatial changes in the sedimentary pile are complex and prevent an unambiguous interpretation (Almela et al., 1958; Puigdefàbregas, 1975; Nijman and Nio, 1975; Soto and Casas 2001; Barnolas et al., *in press* a, b). 2) In spite of the abundance of micropaleontologic studies, most biostratigraphic data are not published so far (Barnolas et al., *in press* a and b). 3) The scarce paleomagnetic data directly obtained in the basin are focused mostly in the upper part of the sedimentary pile (Escanilla Fm; Bentham, 1992 and Bentham and Burbank, 1996) or has low resolution (Mediano section by Bentham, 1992; Holl and Anastasio, 1993).

In marine settings, shelf environments experiment quickly and continue sedimentation, taking place an early blocking of the magnetization and avoiding reworking of sediments and fossils. Since ambiguous interpretations can be minimized, this sort of settings reveals themselves as suitable for bio- and magnetostratigraphic studies. In this sense, the Boltaña-Balzes anticlines provide a near N-S complete transect of the foreland carbonate margin of the Western South Pyrenean Basin in its eastern part (Barnolas and Gil-Peña, 2001; Barnolas et al., 2011). The development of this study was favoured by the continuous sequence located in the core of the Boltaña anticline. In this place, conformable

contacts characterize the Ypresian sedimentary record and covered stretches were sampled in nearby areas. Two of the three main Eocene carbonate shelves (Barnolas and Gil-Peña, 2001; Barnolas et al., 2011) can be recognized in the Ara River section, surveyed in this work. The lower one includes an Early to Middle Ilerdian shallow platform (Alveoline Limestones) and the second one corresponds to the Boltaña Fm, Cuisian in age (Barnolas and Gil-Peña, 2001; Mochales et al., 2011; Barnolas et al., 2011). The last carbonate shelf is Late Cuisian to Middle Lutetian in age (Guara Fm, Samsó et al., 1994; Barnolas and Gil-Peña, 2001; Rodríguez-Pintó et al., 2006; Barnolas et al., 2011). Their carbonate slope is well exposed south of the Boltaña anticline, constituting the Paules and La Patra Mbs, sampled in this work as Coscollar section. The subsequent and conformable sedimentary record of the Sobrarbe Fm is the optimal way to reach the previously dated Escanilla Fm (Bentham, 1992; Bentham and Burbank, 1996). The Mondot section cuts across these formations. The new 2.5 km of stratigraphic sequence sampled in this work represents a continuous and dense sampling design to establish an accurate chronostratigraphic frame in the Aínsa Basin. The Eripol section (Bentham, 1992; Bentham and Burbank, 1996) was integrated in this work (840 m). Age determinations and subsequent inferences are exposed in such way that they can be re-used and re-interpreted in the future (see Appendixes 1 and 3).

The final goal is to place this sedimentological evolution within an absolute temporal framework (Gradstein et al., 2004) by constructing a pattern of magnetozones where units at both limbs of the Boltaña anticline are involved. Moreover, the absolute ages and sedimentary evolution will allow us for defining reliable accumulation rates. Once compiled, ages and accumulation rates may be compared with adjacent sub-basins within the southern Pyrenean foreland system.

5.2. Paleomagnetic methods.

5.2.1. Sampling

Fieldwork and sampling were founded on a compilation of detailed geographic information (mapping, 1:40000 topographic maps and 1:25000 from IGN, 1:33.000 aerial photos and and 1:5.000 orthophotographs from http://sitar.aragon.es). Sampling was designed depending on their geologic and stratigraphic relevance. This work and the construction of the stratigraphic logs were possible thanks to the help and experience of Antonio Barnolas, Josep Serra-Kiel and Josep Mª Samsó.

Paleomagnetic samples were extracted by means of a bit connected to a petrol-powered portable drill cooled by water (Figures 1 and 2). The cores were oriented *in situ* with a magnetic compass and cut in the laboratory (Geotransfer group, University of Zaragoza) according to standard dimensions (21 x 25 mmØ), figure 3. Sample spacing was 2.7 m in average. A detailed mapping and stratigraphic study were carried out to ensure reliable correlations among profiles (Figure 4 and Appendix 1).

Two pilot profiles were performed (June 2006) in the southern termination of the Boltaña anticline (which form part of the Coscollar section) to define the magnetic carriers and demagnetization procedures. The samples extracted revealed primary magnetizations and agree with

the expected polarity pattern of the GPTS, giving new expectations to develop longer sections. Then, three long magnetostratigraphic profiles (Ara River, Coscollar and Mondot, Figure 4) were drilled in different structural positions to entirely cover the pre- and syntectonic sequences involved in the Boltaña anticline and the Buil syncline. The uppermost section, Mondot, was designed to joint the Eripol section by Bentham (1992) in the Escanilla continental formation. Altogether it constitutes a complete section throughout the marine to continental rocks of the Aínsa Basin.

Figure 1. Fieldwork; drilling and orientation of paleomagnetic samples

Figure 2. Drilling equipment.

Figure 3. Labeled standard specimens of the Coscollar section.

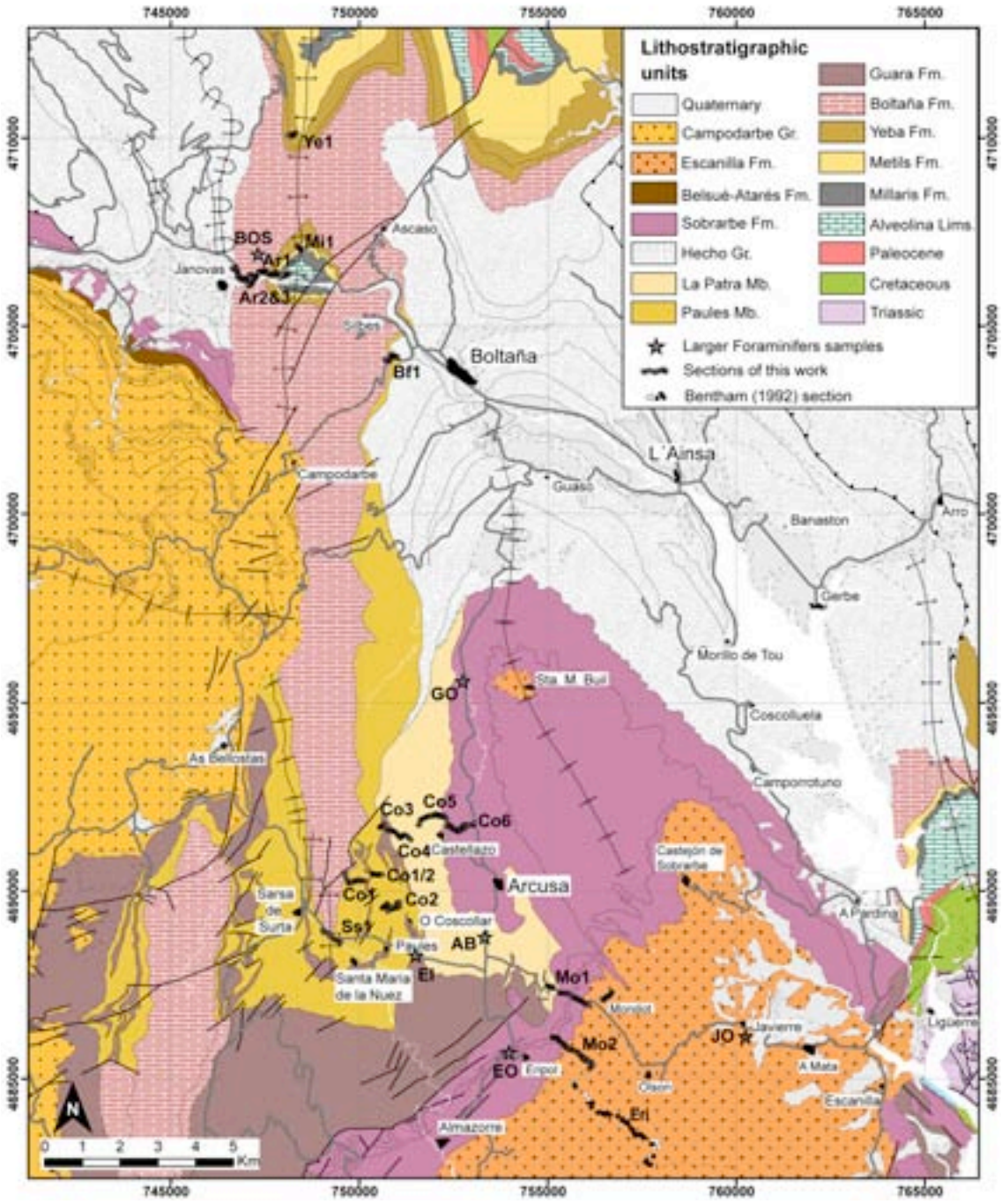

Figure 4. Geological map of the studied area, modified from Barnolas et al. (*in press* a and b). Formal and non-formal units have been individualized according their local use. Magnetostratigraphic sections and Larger Foraminifers fossil localities are located as well. UTM coordinates European datum ED50, zone 30T (see higher resolution in Appendix 1).

5.2.1.1. Ara River and Bal Ferrera sections.

The first profile (Ar1) is located in the western flank of the Boltaña anticline (road section over the Ara River, Figure 5 and 6). The section starts in the Alveolina Limestone and ends near the

top of the Boltaña Fm. In this section the top of the Boltaña Fm was eroded (erosional truncation) previously to the onlap of the Hecho Gp turbidites.

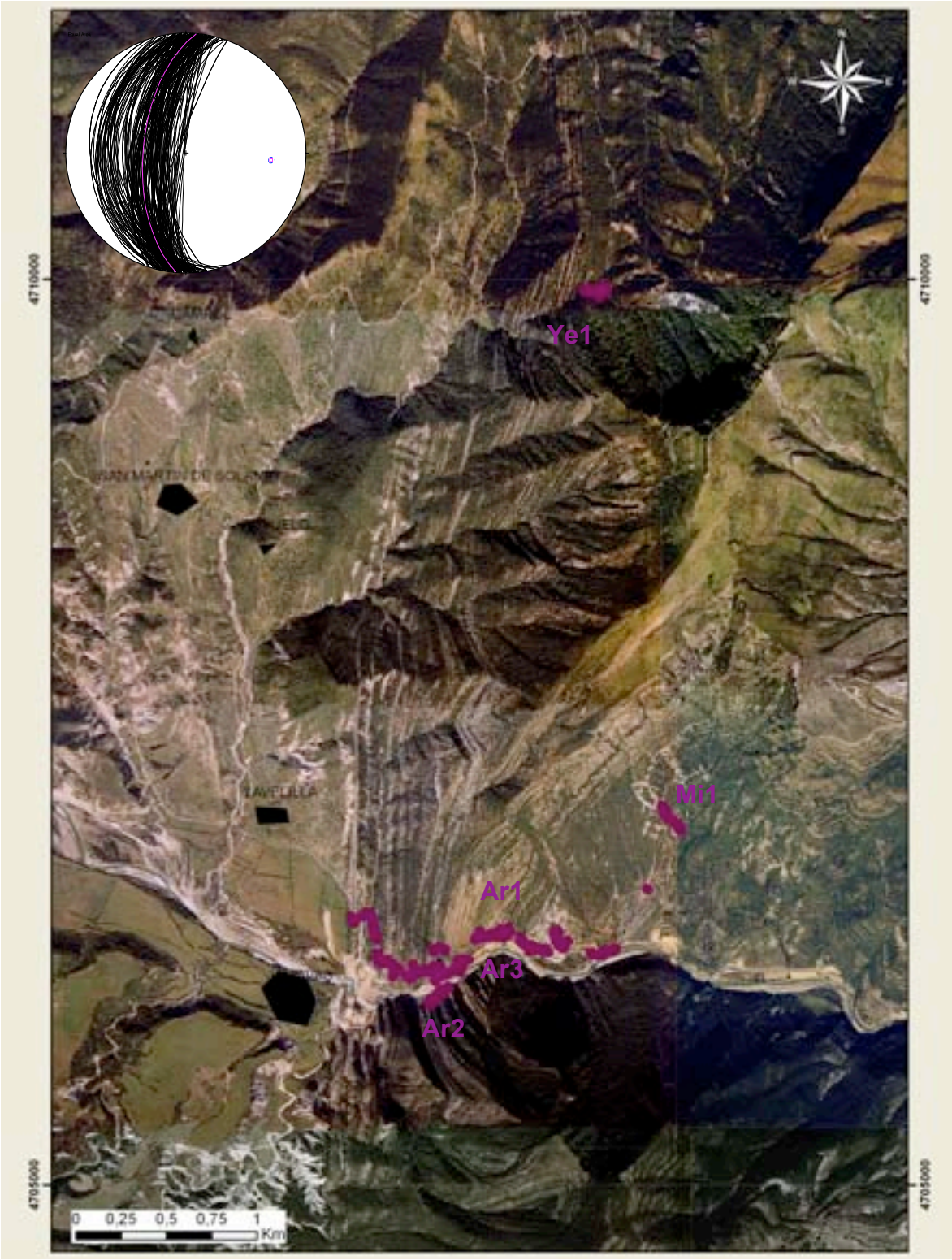

Figure 5. 1:25000 orthophoto mosaic of the Ara River section in ArcGIS (original 1:5000 photos from http://sitar.aragon.es). Samples were georeferred in the field with a GPS Map 76CSx by Garmin (UTM coordinates European datum ED50, zone 30T). Equal area stereoplot of the Ara River section beds.

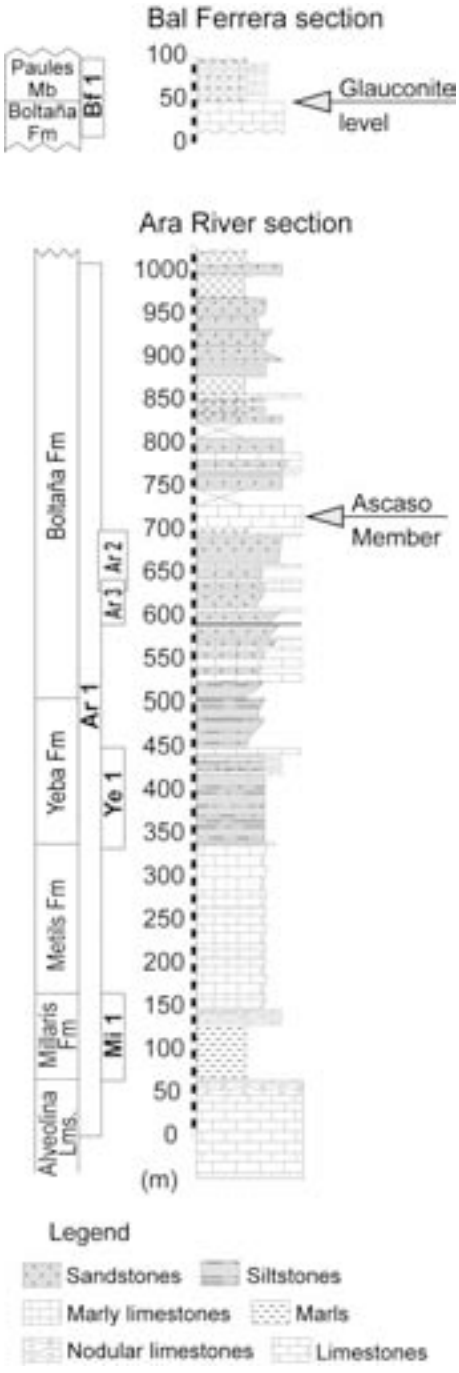

Figure 6. Stratigraphic log and extension of the sub-sections in the Ara River section.

Four supplementary sections (Mi1, Ye1, Ar3 and Ar2), in alternative tracks and dirft roads complete the sequence. 222 sampled layers, all of them analyzed by thermal demagnetization procedures, comprise the Ar1 sub-section. Besides, 29 sister samples were demagnetized by alternating fields. The sub-section Ar2 was placed in the opposite bank of the Ara River, following the PR-HU-40 footpath. The Ar3 sub-section was placed in the ancient road of the Ara River section. 22 and 14 cores respectively compose them, of which one specimen per layer was thermally demagnetized. The Mi1 sub-section is located upstream of a left tributary of the Ara river (Los Basones, figure 7). 32 layers were drilled and samples thermally demagnetized (3 sister samples by alternating fields). The Ye1 sub-section is located in the core of the Boltaña anticline, in a lateral gully between the villages of Campol and Yeba. It is conformed by 23 cores, from them 23 samples were thermally demagnetized and 3 sister samples by alternating fields.

Totally, it comprises a thickness of 1000 m, with 347 samples (one sampled level every 2.9 m). The mean bedding orientation is 005,60W, although a great variability has been observed (Figure 5)

The rest of studied profiles correspond to the eastern flank of the Boltaña anticline. The Bal Ferrera section (Bf1) intermediate profile between the Ara River and Coscollar sections was sampled because of the good exposure of the Boltaña Fm to Paules Mb continuous transition and because of the observed erosion of the top of the Boltaña Fm in Ar1. Bf1 comprises a thickness of 90 m with 25 cores (figures 5, 6, and 8); all of them thermally demagnetized. The average bedding is 007,25E.

Figure 7. Topographic map 1:25000 (IGN) of the northern sector of the Boltaña anticline.

5.2.1.2. Coscollar section.

The Coscollar composite section, south of the Bal Ferrera section, cuts the Paules and La Patra Mbs of the San Vicente Fm (De Federico, 1981) and the lower part of the Sobrarbe Fm. The Ss1 section cuts the concordant Boltaña Fm – Paules Mb contact. Eight partial sections form the composite Coscollar profile (Ss1, Co1, Co1/2, Co2, Co3, Co4, Co5 and Co6). The Ss1 sub-section is located in the southern periclinal termination of the Boltaña anticline, in the left bank of the Vero River (Figures 5, 9, 10 and 11). 13 cores, all of them demagnetized by thermal procedure, compose it. The Co1 and Co2 sub-sections were the pilot prospecting of this work, all the samples being thermally demagnetized. The Co1 sub-section departs from the north of Coscollar, it has 32 samples distributed in 107 m of sequence. Co2 was placed eastwards, covering 162 m of series with 48 cores.

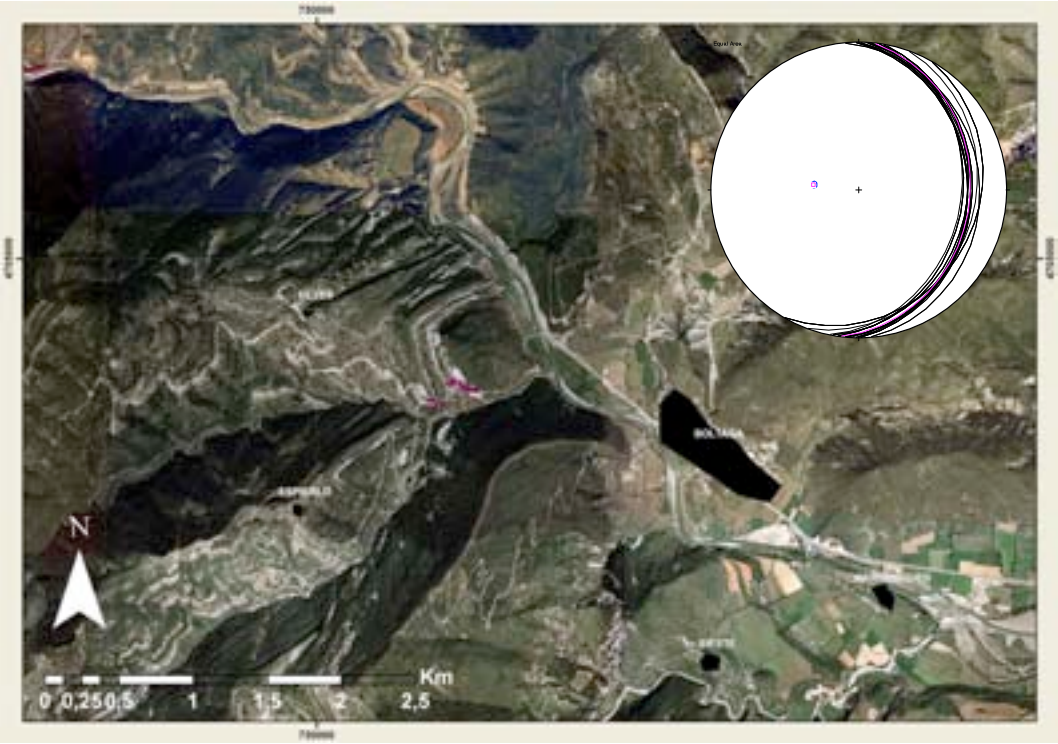

Figure 8. 1:25000 orthophotograph mosaic of the Bal Ferrera section in GIS (original 1:5000 photos from http://sitar.aragon.es). Samples are georeferred in the field by UTM coordinates European datum ED50, zone 30T. Equal area stereoplot of the Bal Ferrera section beds.

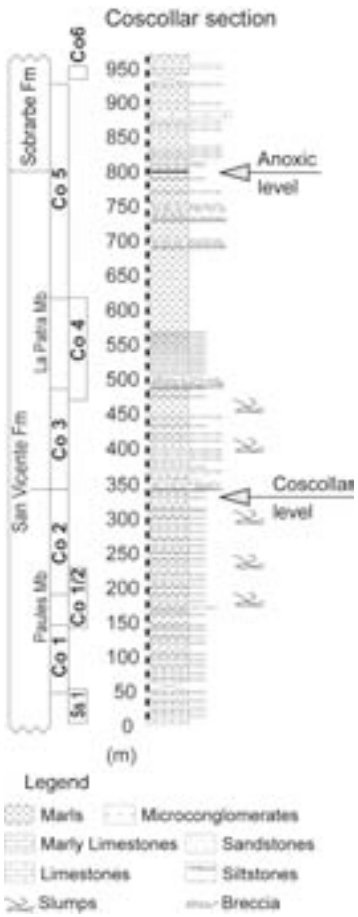

A characteristic glauconitic level indicates the boundary between the Paules and La Patra Mb (Coscollar level, at the top of Co2, figure 9). The Co1/2 sub-section was performed to connect Co1 and Co2 through the Comechazos gully (Figure 10). It is composed by 31 samples in 74 m of stratigraphic sequence. They were demagnetized by thermal procedure. The Co3 sections links with the top of Co2 south of Castellazo, and 44 cores along 133 m of series compose it. All of them were thermally demagnetized and 10 sister specimens by alternating fields. Co4 covered the southwestern track of Castellazo; it is formed by 48 samples covering 140 m of sequence, all of them thermally demagnetized plus 10 by alternating fields.

Co5 surrounds northwards the Castellazo gully to link with eastwards Co6, which ends in the A-2205 road. 102 and 7 samples composed them, covering 303 and 16 m of stratigraphic sequence, respectively (all thermally demagnetized, 18 and 1 respectively, by alternating fields).

Figure 9. Stratigraphic log and extension of the sub-sections in the Coscollar section.

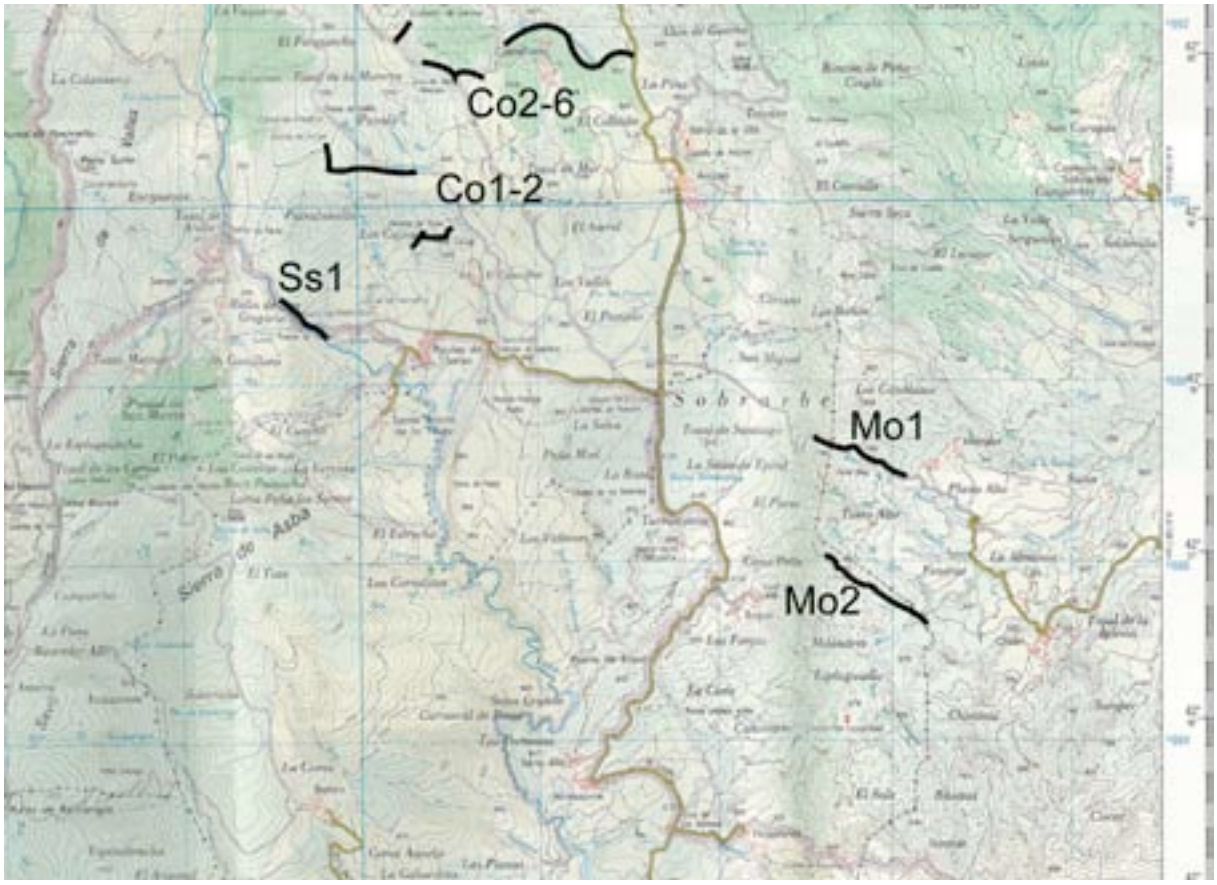

Figure 10. 1:40000 topographic map (Ed. Pirineo) of the southern sector.

All in all this profile covers 965 m of sequence with 355 cores (one sampled level every 2.7 m). The average bedding attitude is 177,23E. There are two main stratigraphic reference levels within this sequence; the first is the Coscollar level that corresponds to a flooding surface indicating the Paules-La Patra Mbs transition. The second one is a regional reference anoxic level in the transition between the La Patra Mb and the Sobrarbe Fm. This level has been used to correlate the Coscollar and Mondot profiles.

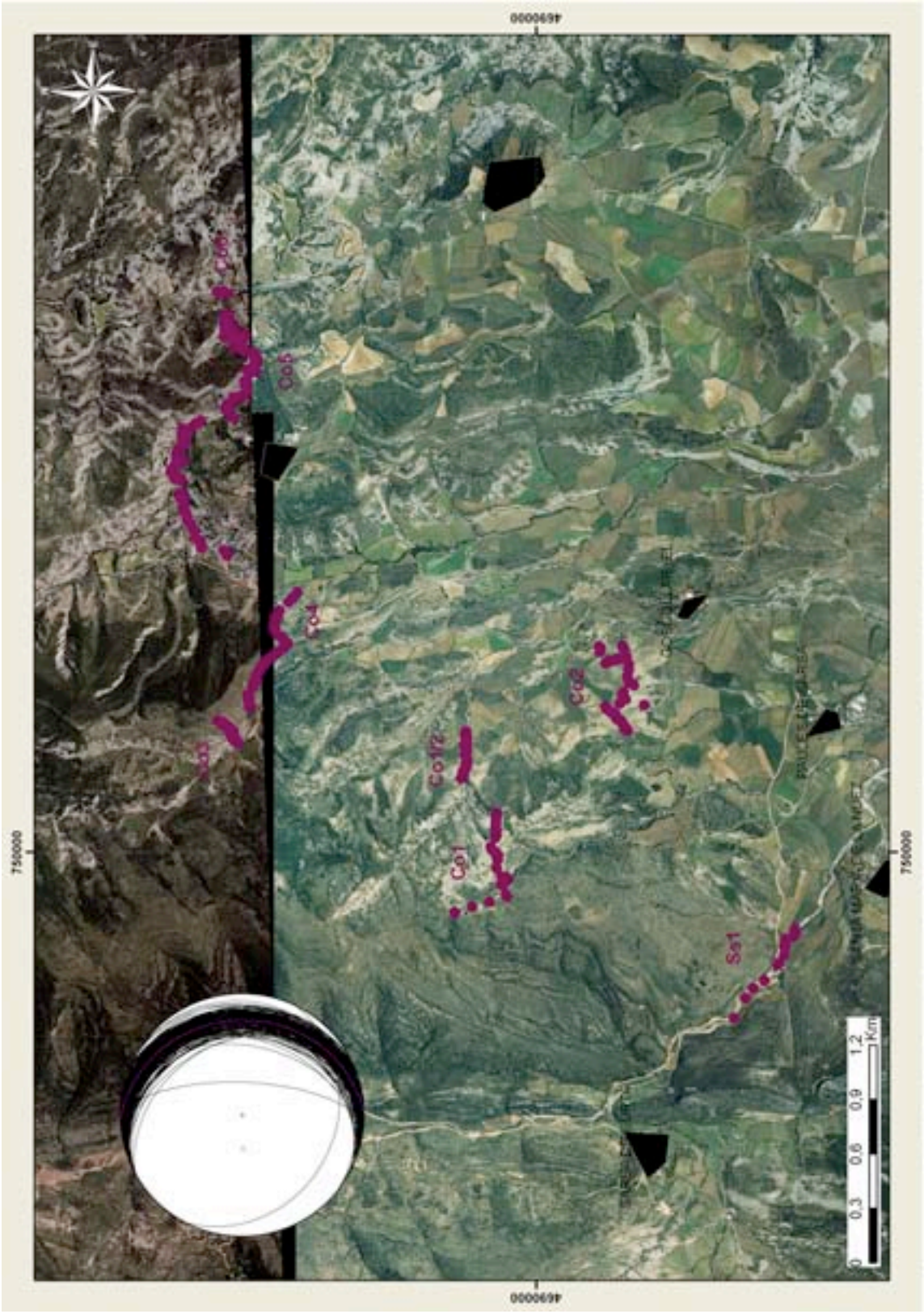

Figure 11. 1:25000 orthophotogrph mosaic of the Coscollar section in ArcGIS (original 1:5000 photos from http://sitar.aragon.es). Samples are georeferred in the field (UTM, ED50, zone 30T). Equal area stereoplot of the Coscollar section bedding.

5.2.1.3. Mondot section.

The Mondot section comprises the upper part of the La Patra Mb, the Sobrarbe Fm and the lower part of the Escanilla Fm including two overlapped sub-profiles (Figure 12). Lateral correlation between them was established by tracking (in the field or in the ortophotos) some reference conglomerate beds.

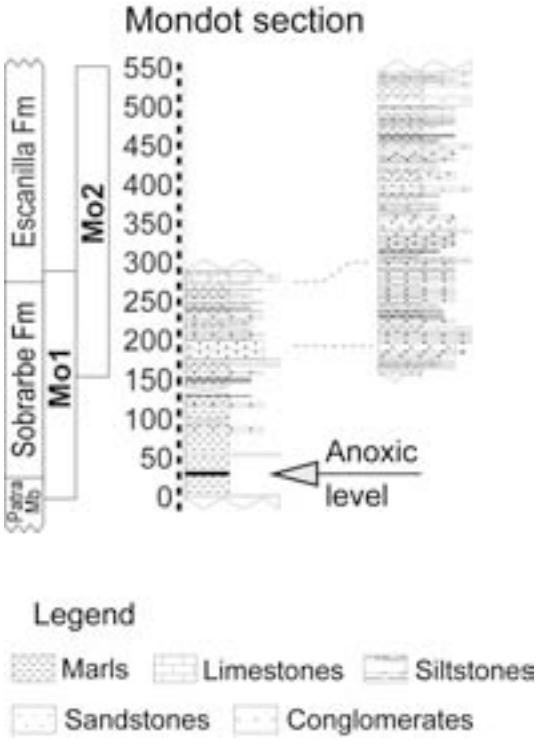

Figure 12. Stratigraphic log and extension of the sub-sections in the Mondot section.

The Mo1 sub-section begins in the road westwards of Mondot and ends in the neighbourhood of Mondot (Figures 10 and 13). It is formed by 85 sampled levels (covering 278 m of sequence) that were thermally demagnetized (and 7 samples by alternating fields). Mo2 sub-section is located westwards of Olsón. It is composed by 79 samples covering 395 m, all of them thermally demagnetized. The complete Mondot section includes 172 samples, covering 539 m along the expected Lutetian-Bartonian boundary (one sampled level every 2.4 m). The upper 250 m belong to the Escanilla Fm in sub-section Mo2. Mean bedding orientation is 023,19E. The rocks sampled range from marls to fine-grained sandstones.

Figure 13. 1:25000 orthophotograph mosaic of the Mondot (violet) and Eripol (B&W, from Bentham, 1992) sections in GIS (original 1:5000 photos from http://sitar.aragon.es). Samples are georeferred by UTM coordinates, ED50, zone 30T in the field. Equal area stereoplot of the Mondot section beds.

5.2.1.4. Eripol section from Bentham (1992)

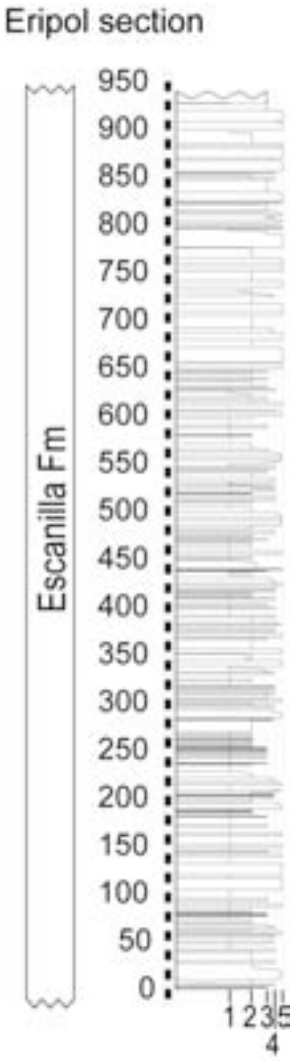

Figure 14. Stratigraphic log of the Eripol section.

The Eripol section performed by Peter Bentham (University of Southern California) in the early 90's covers the entire Escanilla Fm and could be properly georeferred taking advantage of the detailed geographic description of this section in his PhD report (Bentham, 1992). The Eripol section covers 840 m, with 63 analyzed sites (Figure 13). Although the sampling density in the Escanilla Fm (every 18.4 m in average) was lower than the standards of this PhD, the integration of these data has allowed us to complete the paleomagnetic study of the whole sedimentary record of the Aínsa Basin. The correlation between Mo1 and Mo2 sections and Eripol section is assured by good reference levels at the outcrop scale.

All profiles together (17 sub-sections) represent a continuous stratigraphic succession (≈3.300 m) deposited from Ilerdian to Priabonian times. This large dataset provides an accurate frame to establish a reliable chronology of the entire Aínsa Basin record during the Eocene.

5.2.2. Laboratory procedures

The demagnetization of the natural remanent magnetization (NRM) was done in several paleomagnetism laboratories at the Universities of Burgos and Barcelona (Spain), Tübingen (Germany), Bethlehem (Pennsylvania, USA) and Rome (Italy). However, all magnetization measurements were always taken by means of the same instrument, a 2G DC-SQUID cryogenic magnetometer. Some of the magnetometers were placed in shielded rooms (Bethlehem and Rome), and others under Helmholtz coils. The noise level in all magnetometers was always below 5 x 10^{-6} A/m. The ovens employed were the model MMTD60 (Magnetic Measurement) in Burgos and Barcelona, and model TSD-1 (Schonstedt) in Barcelona, Tübingen, Bethlehem and Rome laboratories.

Several demagnetization strategies were adopted due to the assorted rock types involved. Although several pilot alternating field (AF) demagnetizations were performed in detail, the thermal treatment revealed most efficiently the Characteristic Remanent Magnetization (ChRM) directions. As a general rule, progressive thermal demagnetization (TH) was performed by means of, at least, 14

steps (sometimes 19), with 20° increments (or smaller) in key intervals. Demagnetizations were run up to 580° (except for the upper part of Mondot section where evidences of hematite forced us to reach 695°C with key intervals of 5ºC). In the case of AF demagnetizations, measurements were carried out in geometrically increasing steps to reach 100 mT. Sub-sections were entirely measured in the same laboratory, to avoid instrumental variations.

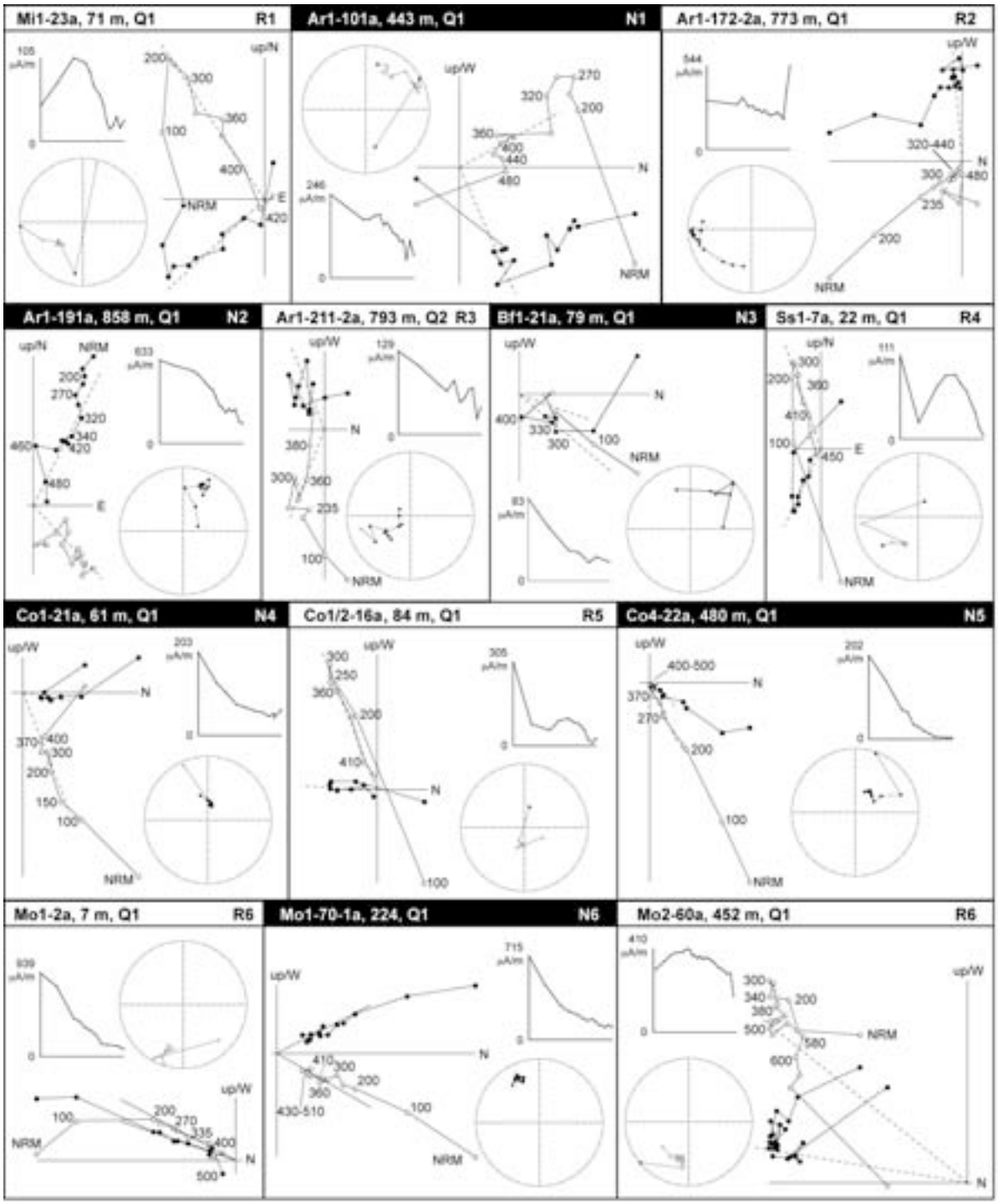

Figure 15. Representative Zijderveld's (1967) diagrams (thermal demagnetizations), stereoplots and intensity drops corresponding to each local magnetozone are presented. NRM is 10^{-6} A/m magnitude. Diagrams are plotted *in situ*, stratigraphic height (m) and quality of the ChRM (Q) are shown for every sample.

Demagnetization data were plotted on orthogonal demagnetization diagrams (Zijderveld, 1967), equal-area projections and intensity decay curves (see Figure 15). ChRM directions were fitted in the orthogonal diagrams using the principal component analysis method (Kirschvink, 1980), by means of the programs *Paldir* (University of Utrecht) and *VPD* (IGME, Unit of Zaragoza; Ramón and Pueyo, 2008; Ramón et al., 2011a; http://www.igme.es/internet/zaragoza/aplicaInfor.htm). Virtual Geomagnetic Field latitudes (VGP) of the ChRMs were calculated by means of the geocentric and inclined dipole model and considering the specific geographic locations of the sampling points.

ChRMs were classified according to different levels of quality. High quality ChRMs (Q1) entail unequivocal and straight to the coordinate origin directions. The intermediate quality (Q2) directions unambiguously allow polarity recognition, although secondary processes distort the quality of the directions. In the low quality ChRMs (Q3), some directional data can be extracted, although they are not reliable because of: 1) poor definition (very few steps point to the coordinate origin), 2) anomalous inclinations or 3) anomalous magnetic intensities. Therefore, they were not considered to build the local sequence of magnetozones.

Fold tests were conducted using the super IAPD software (Torsvik et al.,, 1986), which follows the criteria by McElhinny (1964). Correlation of the local magnetostratigraphic sequence and the geomagnetic polarity timescale (GPTS) was done using Gradstein et al. (2004) scale. The correlation obtained by Bentham (1992) was based on the Standard Geological Time Scale of Harland et al. (1990) and was accordingly corrected to Gradstein et al., (2004) scale. Magnetic chron extension were used as the major reference to calibrate both scales.

Some rock magnetism analyses were performed to control the carriers of the paleomagnetic signal. By means of the pulse magnetizer (MMPM9 at the Tübingen University, ASC at Lehigh University and a 2G at the IGNV in Roma) and 2G cryogenic magnetometer, 68 analyses of the coercitivity spectrum of the isothermal remanent magnetization (IRM) were carried out. Between 24 and 30 increasing fields up to 1.8 Tesla were applied. Moreover, 87 samples were thermally demagnetized following Lowrie's test (1990) rules; a 1.2 Tesla field was applied to z-axis, 0.3 T to the x-axis and 0.1 T to the y-axis. Subsequently the thermal stepwise demagnetization was applied with 35° to 50ºC increments, up to 600ºC. Finally, 51 hysteresis loops were obtained in the Alternating Gradient Force Magnetometer AGFM 2900 (Princeton Measurements Corp.) at the Tübingen University.

5.3. Biostratigraphic methods

5.3.1. Sampling

Geological mapping studies performed by the Spanish Geological Survey (IGME) during the 90's in the Aínsa Basin (Barnolas et al. *in press*), were accompanied by systematic biostratigraphic researches leaded by Josep Serra-Kiel,Josep Mª Samsó and collaborators. Larger foraminifers, nummulitids and alveolinids, were systematically sampled from bottom to top of the Ara River section during the MAGNA series construction (Barnolas et al, *in press* a). They were revised and accurately

located for this work. Previous prospected outcrops of nummulitids were laterally correlated to the levels of the Coscollar and Mondot sections, (samples GO, EI, AB and EO), see figure 4. Within this PhD, in collaboration with Nieves López† and Geosfera (María Presumido and Juan Antonio Cárdaba), a pilot biostratigraphic prospect was conducted in the continental Escanilla formation. This campaign provided positive results in 7 out of 17 prospected levels (see table 2 and figure 17), 4 of them were rich in micro-vertebrates or charophytes. The richest level holds abundant gyrogonites (sample JO and figure 16) and could be correlated with Eripol section.

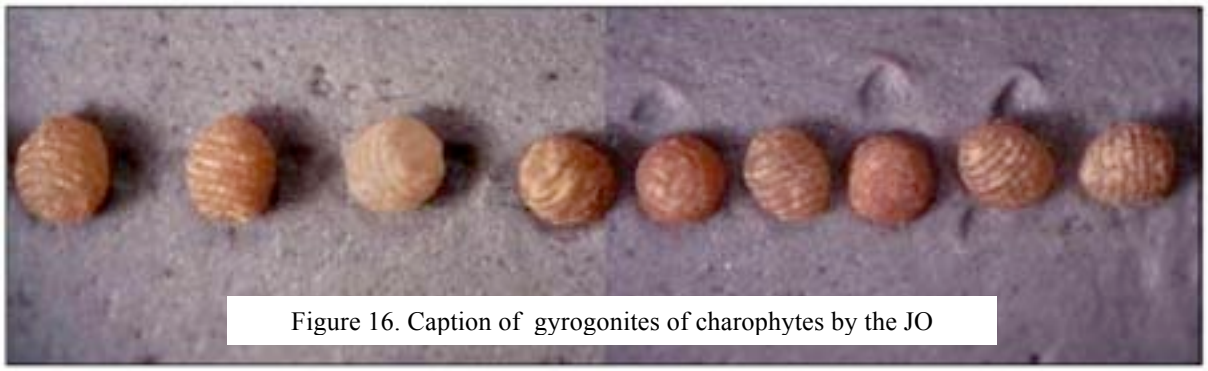

Figure 16. Caption of gyrogonites of charophytes by the JO

The biostratigraphic sites collected are summarized in the next table:

Section	Site	Fossil Remains	Zone	UTM-X	UTM-Y
Ara River	BOS1	Alveolina	30T	748211	4706330
Ara River	BOS2	Nummulites-Assilina	30T	747649	4706342
Ara River	BOS3	Nummulites-Assilina	30T	747486	4706373
Ara River	BOS4	Alveolina	30T	747411	4706360
Ara River	BOS5	Alveolina	30T	747385	4706351
Ara River	BOS6	Nummulites-Assilina	30T	747334	4706293
Ara River	BOS7	Nummulites-Assilina	30T	747250	4706294
Ara River	BOS8	Alveolina	30T	747197	4706298
Ara River	BOS9	Assilina	30T	747045	4706157
Ara River	BOS10	Nummulites-Assilina	30T	746871	4706226
Ara River	BOS11	Nummulites-Assilina	30T	746710	4706468
Coscollar	EI (Ermita San Isidro)	Nummulites	31T	256998	4687999
Coscollar	AB (Arcusa Breccia)	Nummulites	31T	258837	4688313
Coscollar	GO (Gorgos outcrop)	Nummulites	31T	259226	4685285
Mondot	EO (Eripol outcrop)	Nummulites	31T	258690	4695350
Eripol	JO (Jabierre outcrop)	Charophytes	31T	265658	4685323

Table 1. Biostratigraphic sites, section sampled or laterally correlated, dominant fossil assemblage, UTM coordinates (ED50)

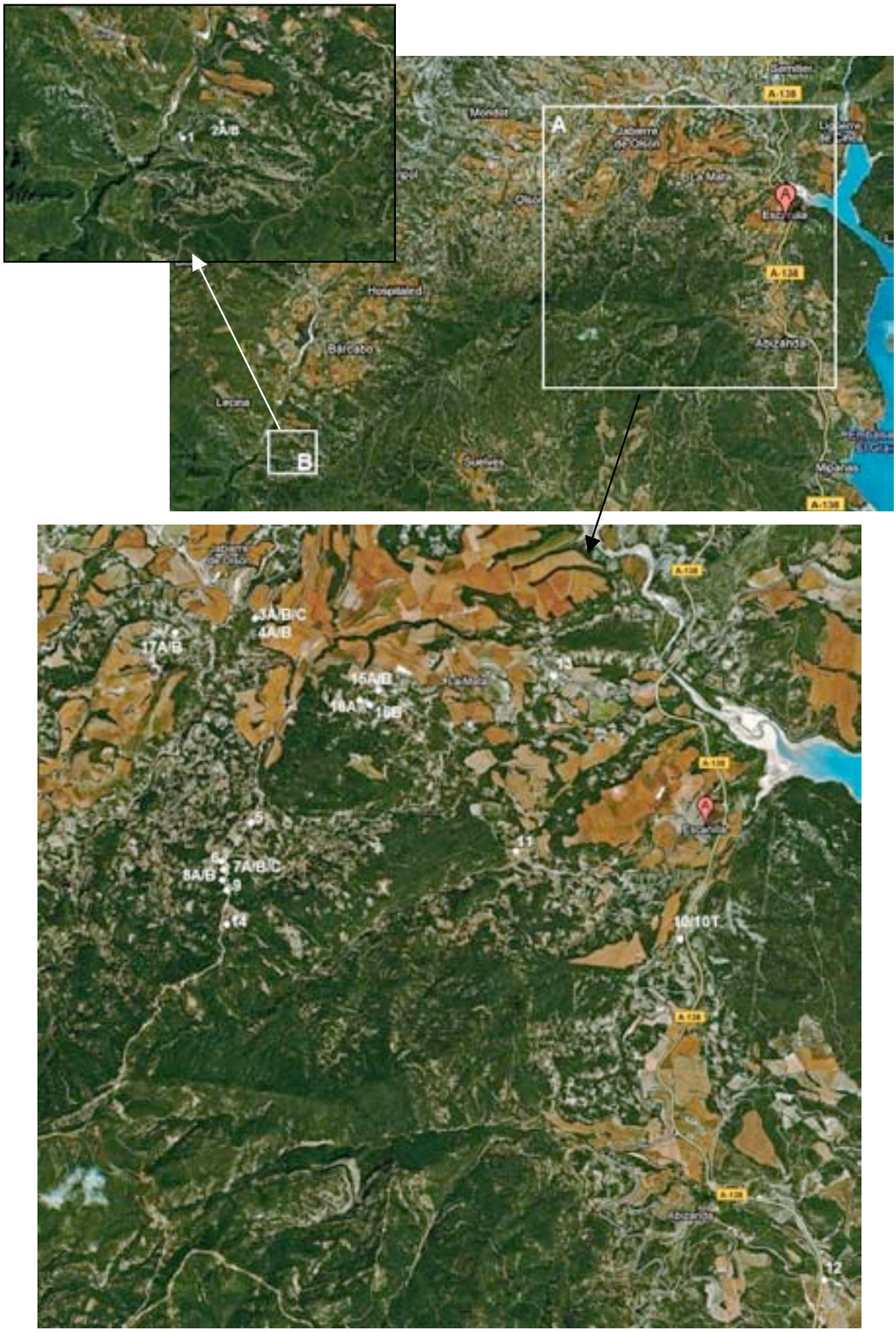

Figure 17. Collection of samples belonging to the Escanilla Fm (www.maps.google.com).

Sample	Weight (Kg)	UTM-X	UTM-Y	RESULT
1	50	256249	4678575	Two rodent incisor, bones of indeterminate vertebrae, teeth of rays, foraminifers, molluscs…
2a	50	256680	4678747	Bones of indeterminate vertebrae, teeth of indeterminate fish, foraminifers, molluscs, echinoderms, gyrogonites…
2b	40	256698	4678730	Negative
3a	50	265639	4685319	Negative
3b	50	265639	4685319	Fragment of indeterminate mollusc, carbonate rest
3c	50	265639	4685321	Fragment of indeterminate mollusc
4a	50	265658	4685323	Bones of indeterminate vertebrae and abundant gyrogonites
4b	25	265658	4685322	Fragment of indeterminate gastropod, two foraminifers
5	100	265550	4683812	Negative
6	50	265332	4683500	Negative
7a	100	265344	4683425	Fragments of carbonate rest
7b	25	265344	4683425	Fragments of carbonate rest
7c	25	265344	4683425	Fragment of indeterminate gastropod
8a	25	265334	4683373	Negative
8b	25	265334	4683373	Negative
9	2	265367	4683293	Negative
10	25	268780	4682851	Negative
10T	3	268780	4682851	Negative
11	50	267526	4683516	Negative
12	50	269743	4680162	Two rodent incisor, bones of indeterminate vertebrae, foraminifers, gastropods, echinoderms …
13	25	267899	4684784	A foraminifer and a gyrogonite
14	50	265287	4683035	A fragment of foraminifer and a fragment of indeterminate vertebrae
15a	25	266521	4684748	Negative
15b	25	266521	4684745	Negative
16a	50	266398	4684673	Tooth and fragments of bones of indeterminate vertebrae
16b	50	266457	4684649	Fragment of indeterminate gastropod
17a	25	265013	4685218	Fragment of teeth of macromammal
17b	25	265015	4685217	Negative

Table 2: Biostratigraphic prospecting at the Escanilla Formation (Geosfera)

5.3.2. Laboratory procedures

The nummulitids and charophytes were studied in isolated specimens. The rocks with these fossils were disaggregated in water, oxygen peroxide and Na_2CO_3 solution and later sieved with mesh apertures of 1.0, 0.5 and 0.2 mm. The *Alveolina* genus was studied in thin sections. The larger foraminifers and charophytes were picked out under a light microscope and measured at 40x magnification. The material is housed at the Departament d'Estratigrafia, Paleontologia i Geociències Marines, Universitat de Barcelona and was studied by Josep Serra Kiel (foraminifers), Josep Sanjuan and Carles Martín Closas (charophytes). Remaining prospects from the Escanilla Fm are storaged at IGME (Unit of Zaragoza).

5.4. Results

5.4.1. Paleomagnetic directions

5.4.1.1. Ara River and Bal Ferrera sections

A highly variable Natural Remanent Magnetization (NRM) has been observed through the Ara River section and the connecting Bf1 sub-section (Table 3) ranging from 10 to 1000 10^{-6} A/m, within the typical marine rock values (Channell, 2007).

Formation	Mean NRM ($\cdot 10^{-6}$ A/m)	NRM Standard Error	Mean Susceptibility ($\cdot 10^{-6}$ S.I.)	Susceptibility Standard Error
Alveoline Lms.	446	± 55.4	16	±7.4
Millaris Fm	140	± 38.9	90	±18.6
Metils Fm	714	± 73.8	33	±4.7
Yeba Fm	293	± 82.8	73	±11.7
Boltaña Fm	192	± 16.9	61	±6.9
Ascaso Mb	93	± 27.3	8	±3.2
Paules Mb	102	± 7.2	20	±2.5
La Patra Mb	356	± 46.9	57	±9.6
Sobrarbe Fm	232	± 105.0	86	±10.9
Escanilla Fm	1100	± 264.4	112	±8.4

Table 3. Detailed NRM intensities ($\cdot 10^{-6}$ A/m S.I.) and bulk susceptibilities (10^{-6} S.I.) of the formations involved in the study.

In spite of the relatively scattered behavior found in many samples from the Boltaña Fm, the ChRM could be successfully isolated in most of them. The unblocking intervals were 320º-500ºC and 25-100 mT (AF in sister samples). AF analysis did not offer reliable ChRMs in most analyzed samples. Viscous components, below 200ºC and below 10 mT, were either randomly distributed or close to the present geomagnetic field and hence not considered (Figure 15).

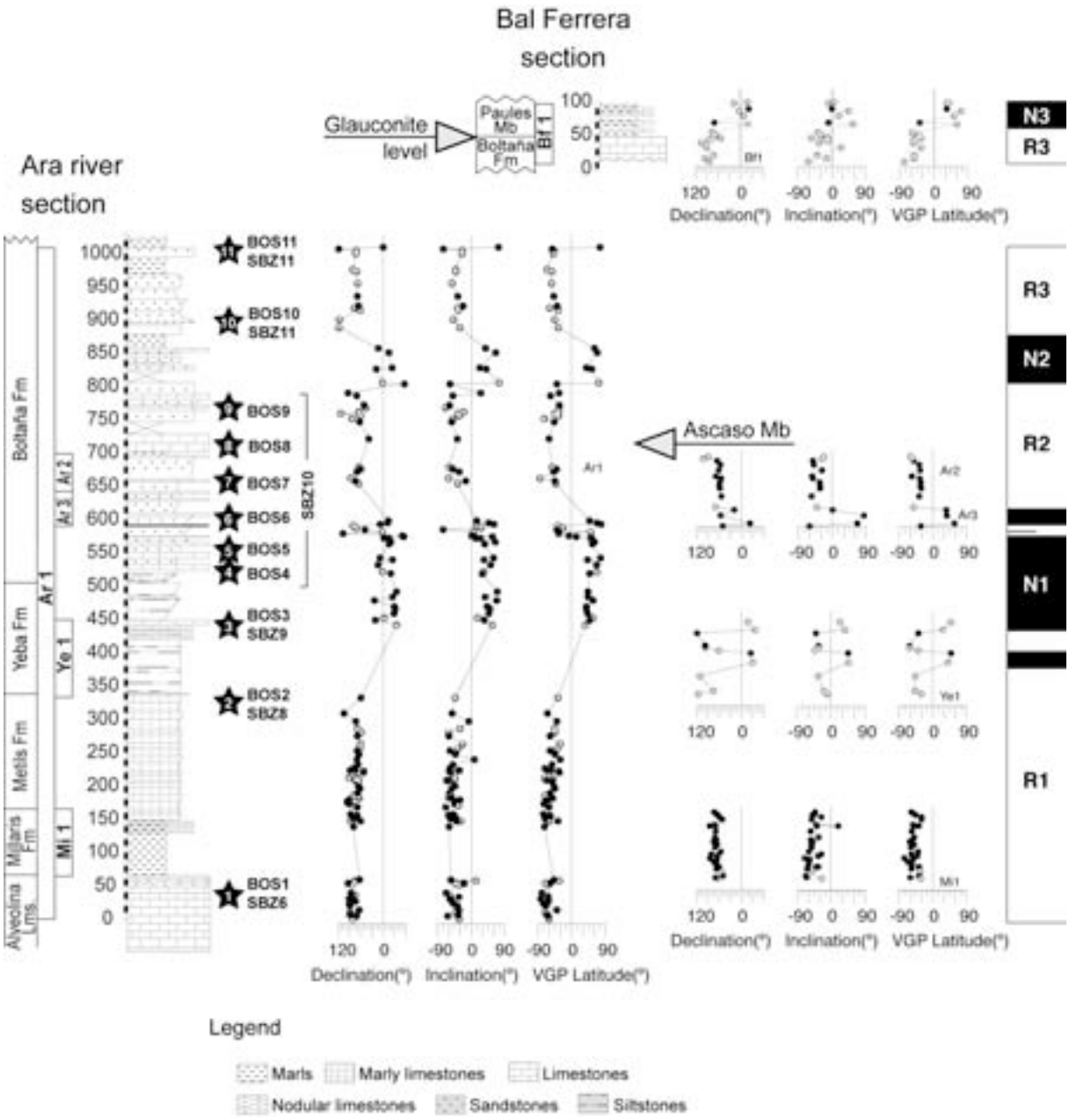

Figure 18. Stratigraphic columns (Ara and Bal Ferrera sections) with the magnetostratigraphic data (right); Declination, Inclination and VGP Latitude of the ChRM are expressed in degrees. Black dots represent high quality paleomagnetic directions (Q=1) and grey ones are intermediate vectors (Q=2). New biostratigraphic data (black stars) are placed in the sections.

The VGP latitudes evaluated from individual ChRMs define a clear succession of magnetozones during Ypresian times (magnetozones have been numbered from bottom to top; Figure 18, for detailed numerical data see Table 4 and Appendix 2). The R1 reverse zone characterizes the lower 375 m of section. Several magnetozones have been recorded along the upper 600 m of section; they are collectively gathered into N1 (375 to 610m, Yeba Fm and Lower Boltaña Fm). The sub-sections Ar1 and Ar3 bound the last N1 zone, whereas the sub-section Ar2 is characterized by reversal polarity (R2). On top of this section, three long local magnetozones can be delimited: R2, N2 and R3. They are located within the Upper Boltaña Fm. An undetermined stratigraphic gap from the eroded

top of the Ara River section to the bottom of Bf1 prevents us to determine the complete R3 zone. The Boltaña Fm-Paules Mb concordant contact was recorded in the Bf1 sub-section which includes the R3/N3 inversion in the Paules Mb (Figure 18).

Section	n/N	Polarity	Dec (bac)	Inc (bac)	α95 (bac)	k (bac)	Dec (abc)	Inc (abc)	α95 (abc)	k (abc)	Strike (rhr)	Dip
Ar1-1	56/58	R	231,7	-23,2	6,8	11,1	207,0	-48,9	5,0	15,5	182	40
Ar1-2	31/37	N	49,1	4,4	12,3	5,0	20,1	49,2	11,1	6,7	185	68
	30/30	R	60,2	-4,6	18,6	3,2	213,8	-49,4	10,3	7,4	185	68
	61/67	N+(-R)	57,2	2,5	8,9	5,2	27,1	49,5	7,5	7,1	185	68
Ar2	12/18	R	253,5	22,6	6,7	46,4	246,7	-41,0	8,0	33,5	189	71
Ar3	7/10	N	59,8	10,1	49,0	4,2	337,6	59,8	-	3,9	178	71
	2/5	R					236,5	-52,6	74,5	26,9	178	71
	5/5	N+(-R)	59,8	10,1	49,0	4,2	18,4	63,0	47,4	4,5	178	71
Mi1	31/32	R	240,2	-43,4	5,9	20,0	234,1	-47,8	6,1	18,7	190	7
Ye1	10/11	N	95,3	-30,2	21,5	6,7	94,9	41,4	21,2	6,8	187	73
Ss1	5/6	R	209,7	-54,8	8,4	77,4	234,9	-57,1	11,8	53,4	76	9
Co1	6/6	N	2,0	60,4	16,8	20,3	30,4	49,4	17,9	18,0	353	22
	16/19	R	217,4	-68,8	9,0	17,8	237,2	-55,1	10,3	13,8	353	22
	22/25	N+(-R)	25,5	67,4	8,0	15,9	49,2	54,1	8,9	13,1	353	22
Co1/2	24/26	R	193,1	-62,9	4,4	46,7	221,8	-46,9	4,7	39,9	350	26
Co2	41/42	R	195,4	-67,0	4,1	30,5	223,9	-52,6	4,5	25,4	357	25
Co3	13/15	N	20,1	51,9	11,8	14,4	46,2	39,0	12,9	12,3	355	25
	29/30	R	209,5	-71,5	8,9	10,0	237,5	-52,5	9,3	9,3	355	25
	42/45	N+(-R)	25,0	65,4	7,4	9,7	53,3	48,4	7,6	9,4	355	25
Co4	26/30	N	15,9	66,0	11,4	7,1	47,0	55,5	11,0	7,6	1	21
Co5	43/52	N	15,3	61,8	9,4	6,3	45,6	50,6	9,4	6,4	358	24
	38/45	R	209,3	-54,8	8,0	9,4	226,6	-39,5	8,0	9,4	358	24
	81/97	N+(-R)	22,8	58,6	6,2	7,4	46,1	45,2	6,2	7,4	358	24
Co6	5/7	R	203,8	-54,6	13,0	44,3	222,8	-40,8	12,9	45,2	354	22
Mo1	25/29	N	82,2	71,9	16,5	4,1	91,4	51,8	16,6	4,0	15	20
	44/49	R	189,2	-48,5	6,9	10,8	211,8	-44,7	6,6	11,5	15	20
	69/78	N+(-R)	20,6	59,1	8,2	5,3	48,2	50,2	8,2	5,4	15	20
Mo2	48/53	R	215,2	-47,0	12,8	3,7	232,7	-45,0	12,5	3,7	47	23

Table 4. Paleomagnetic mean data in the studied sub-sections. n/N: number of samples considered/analyzed. Dec, Inc, α95 and k: Declination, Inclination, semi-apical angle of the confidence cone and concentration factor, *in situ* (bac) and restored (abc)..

5.4.1.2. Coscollar section

A weak intensity of the NRM has been observed in the Coscollar section and in the connecting Ss1 sub-section (Table 3). However, both sections systematically yielded a stable and measurable remanent magnetization. Apart from a viscous component below 200ºC and 10mT, the ChRM was frequently isolated in the 250-500ºC interval and occasionally at 350-580ºC when the detrital content was higher, as in the Co4 sub-section. Some AF demagnetizations display ChRMs in the 25-80 mT field interval. Again, thermal demagnetizations defined better the ChRMs.

The derived VGP latitudes allow building a well-defined succession of magnetozones (Figure 19). The Ss1 sub-section has recorded the N3-R4 reversal and the Co1 sub-section the R4-N4 reversal. The N4-R5 reversal was identified at Co1/2 and Co2 recorded the R5 zone. The Paules Mb included the R3/N3 reversal and spans to the bottom of the R5 zone. The Co3 sub-section starts above Coscollar level (La Patra Mb) and records the R5-N5 reversal. The turbidites in Co4 provide low angle individual VGP latitudes, especially in its sandy upper part. Nevertheless, they show a clear normal polarity within the N5 magnetozone. Co5 sub-profile reveals the N5-R6 reversal. The anoxic level found in the central portion of the sub-section evinces the beginning of the Sobrarbe Fm, close to the N5-R6 reversal but still with normal polarity. The top of the Coscollar section is the Co6 sub-section that remains in the R6 magnetozone (see Figure 19 and Table 4 for detailed numerical data).

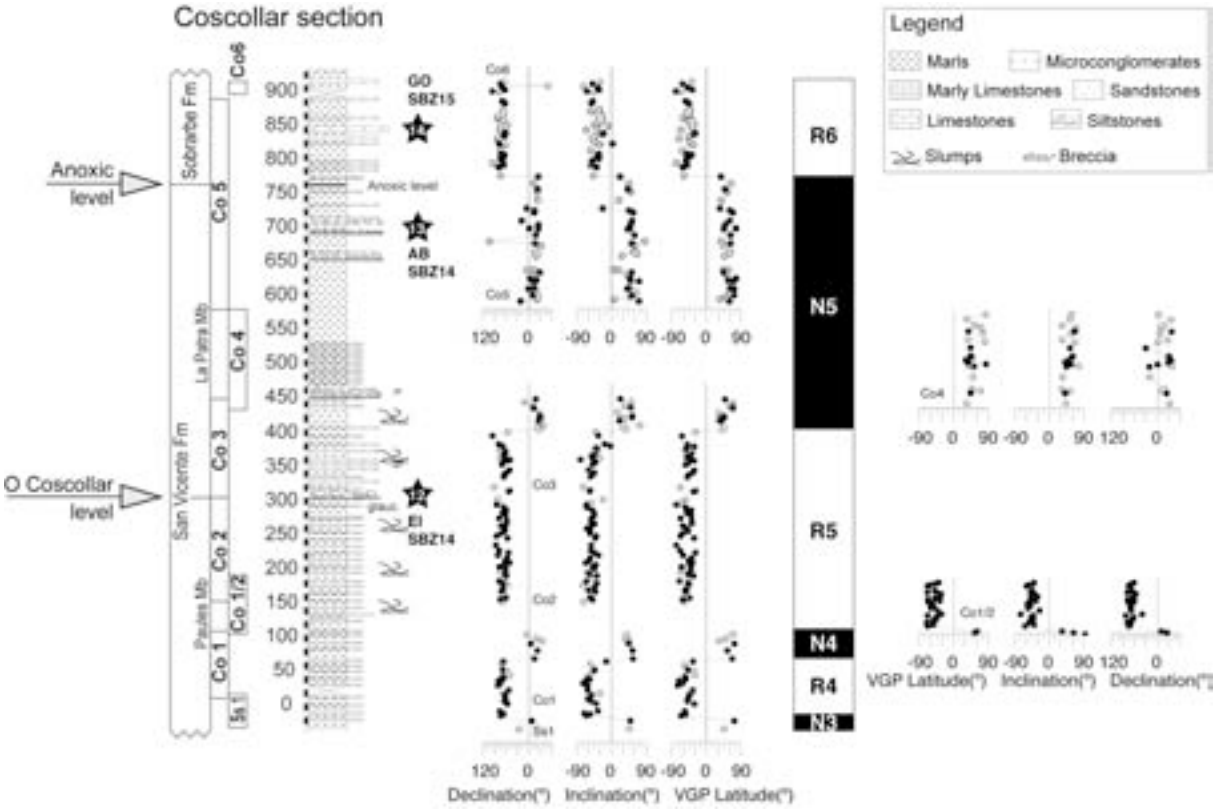

Figure 19. Stratigraphic columns (Coscollar section) shown at the left together with the magnetostratigraphic data (right); Declination, Inclination and VGP Latitudes of the ChRM are expressed in degrees. Black dots represent high quality paleomagnetic directions (Q=1) and grey ones are intermediate vectors (Q=2). New biostratigraphic data (black starts) are placed in the sections.

5.4.1.3. Mondot section

Weak and constant NRM values were observed in the lower part of the Mondot section included in the Sobrarbe Fm, whereas NRM values in the Escanilla Fm were variable and much higher (Table 3) according to the typical behavior of continental rocks. The deltaic deposits of the Sobrarbe Fm frequently offered consistent ChRMs in the 300-500ºC temperature range and in the 25-60 mT field interval. In the fluvial deposits of the Escanilla Fm, ChRMs were isolated between 360-580ºC. A high temperature ChRM was isolated in 12% of the base of the Escanilla Fm samples (500-695ºC), usually related to coarse-grained levels or red beds. Thermal analyses provide a low-temperature component unblocking below 200ºC and a low-field component below 10 mT in the AF analysis, which were discarded.

VGP latitudes define a clear succession of three magnetozones for the lowermost 400 m (Mo1 and lower part of Mo2), while in the uppermost 100 m (upper part of Mo2) only a few samples with coherent magnetization allow constraining the local magnetostratigraphy (Figure 20, Table 4). Despite this low resolution, the Mo1 sub-section is well defined, successfully identifying the N5-R6 boundary within the Sobrarbe Fm. The anoxic regional supposedly isochronous level found in the Co5 and Mo1 sub-sections, makes the N5-R6 a solid boundary. The bottom of the Escanilla Fm. can be included toward the upper part of the R6 magnetozone (last samples of Mo1 and first 150 m of Mo2). The increase in siliciclastic contents in the Escanilla Fm, and subsequent randomly distributed ChRMs, forced us to remove a considerable amount of samples (47%). Concerning the Mo2 sub-profile, the local polarity scale begins in the magnetozone R6. The uppermost 150 m of Mo2, although less densely sampled, allow constraining the R6-N6 and the N6-R7 polarity reversals (Figure 20).

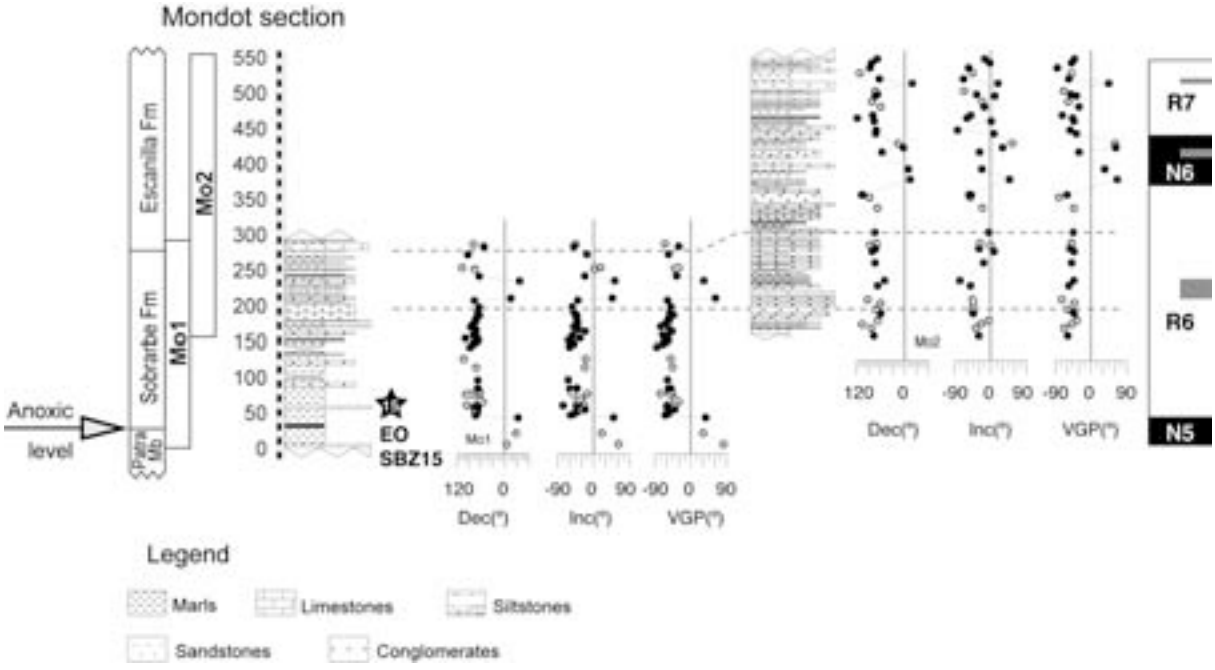

Figure 20. Stratigraphic columns (Mondot section) shown at the left, together with the magnetostratigraphic data (right); Declination, Inclination and VGP Latitudes of the ChRM are expressed in degrees. Black dots represent high quality paleomagnetic directions (Q=1) and grey ones are intermediate vectors (Q=2). New biostratigraphic data (black star) are placed in the sections.

5.4.1.4. Reprocessing of the Eripol section

The uppermost part of the Mo2 sub-section overlaps with the lowermost part of the Eripol section studied by Bentham (1992), figure 21. This basal part of the section is included within the R7 chron. From here, Bentham (1992) defined a succession of magnetozones (N7, R8, the long N8, R9, N9, R10 and N10), some of them recorded by very few sites (N7, R8 or N9).

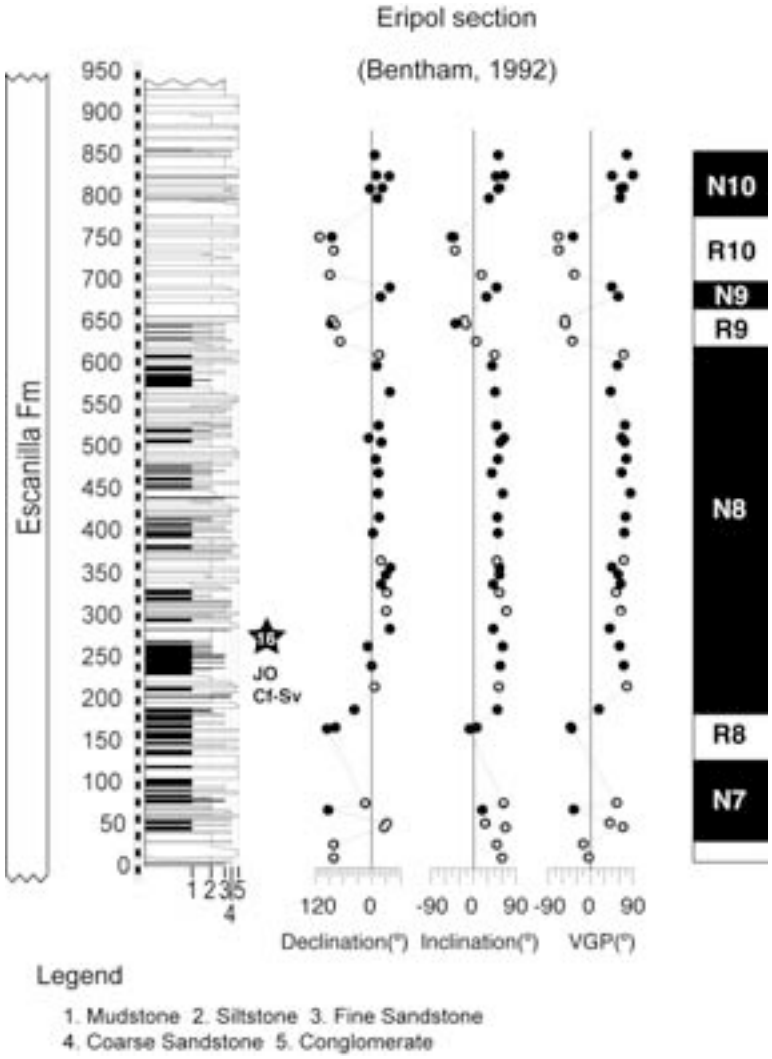

Figure 21. Stratigraphic columns (Eripol section) and magnetostratigraphic data (right); Declination, Inclination and VGP Latitude of the ChRM are expressed in degrees. Black dots represent high quality paleomagnetic directions (Q=1) and grey ones are intermediate vectors (Q=2), classified by Bentham (1992). New biostratigraphic data (black star) are placed in the sections.

5.4.2. Rock magnetic properties

The vast dataset of rock magnetism analyses (especially thermal demagnetizations of three components IRM's or Lowrie's, 1990, tests) allows us classifying the samples according to their main magnetic carrier. Thus, samples with unblocking temperatures of 580ºC have been classified as Type

I- mainly magnetite (Figure 22a). Variable magnetite/sulphide ratios, with temperature drops at 580ºC and 350-400ºC respectively, were classified as Type II (Figure 22b, c, d). Samples with dominant iron sulphides content (unblocking temperatures at 350ºC) are of Type III. More complex combinations of magnetite (580ºC), iron sulphides (350-400ºC) or hematite (upper than 600ºC) are classified as Type IV (Figure 22e).

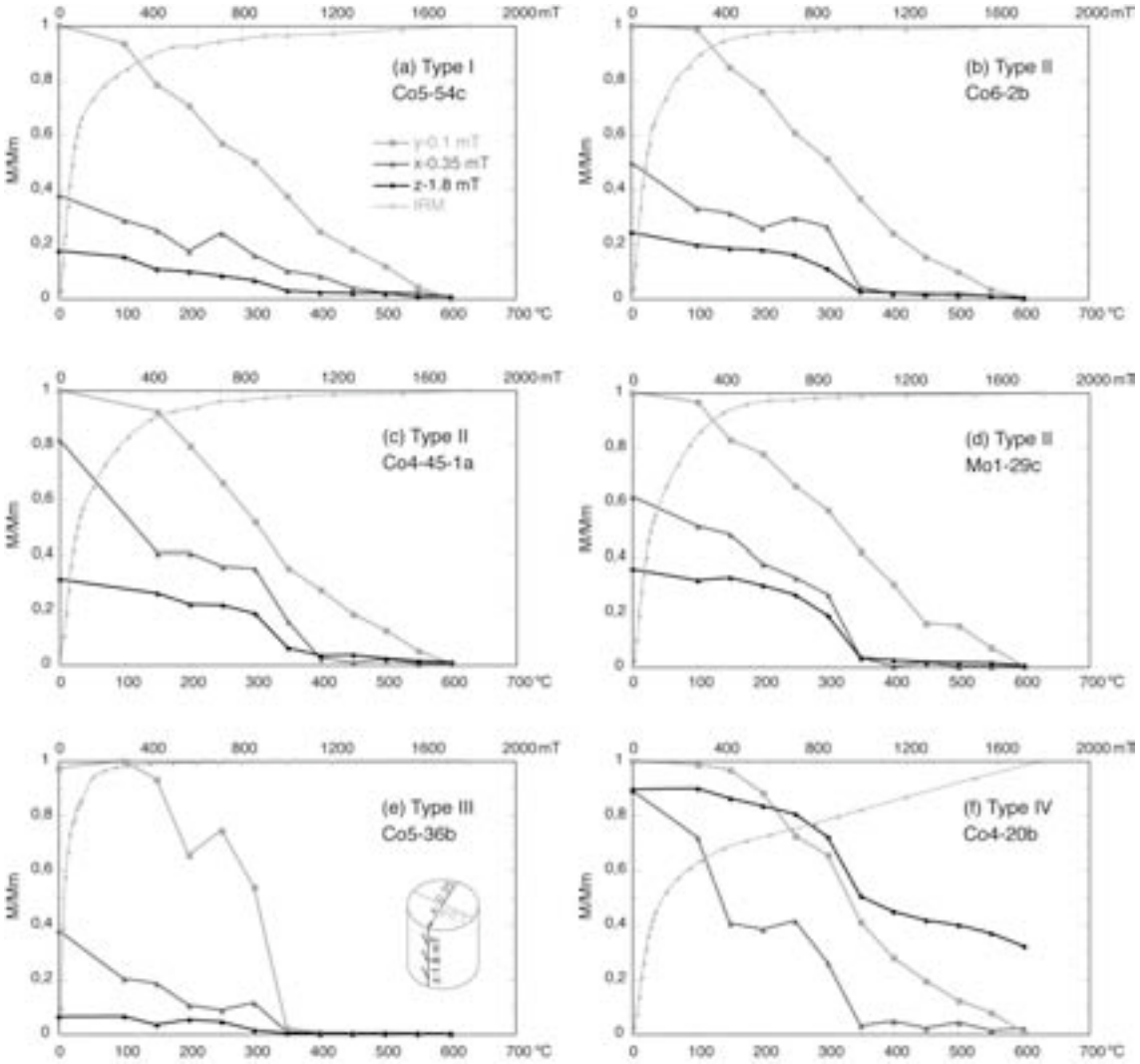

Figure 22. Lowrie (1990) test analysis and IRM acquisition curves. In down abscissas (lower line) demagnetization temperatures are represented, in upper line abscissas increasing field (mT) applied to IRM in ordinates normalized remanent magnetization intensity.

Regarding the Ara River section, 21 Lowrie (1990) tests and 17 IRM analyses were performed. In short, the Alveolina Limestone, Metils Fm and Upper Yeba Fm have magnetite as the main carrier (small contributions of sulphides and hematite cannot be ruled out) (Type I). In the case of the marly units (Millaris and Yeba Fms.), where the phyllosilicate content is higher, the iron

sulphides ratio is also higher (Type II). The main magnetization carrier in the Boltaña Fm is magnetite, although variable amounts of iron sulphides (Types I and II) and rare evidences of high coercivity minerals (Type IV) are observed as well.

In the Coscollar section, rock magnetism analyses (47 Lowrie tests and 43 IRMs) point to Type II carriers in the Paules Mb. In La Patra Mb, at the Co3/Co4 boundary, assorted mineralogy has been observed: magnetite, iron sulphides and a higher proportion of hematite (Type IV), and hematite as the only magnetic carrier in some cases. The rest of La Patra Mb showed abundance of Type II magnetic mineralogy and isolated cases where magnetite (Type I) or iron sulphides (Type III) are the main carriers. With regard to the Sobrarbe Fm, magnetite and iron sulphides are the responsible for magnetization (Types I and II).

The Mondot section (8 IRM and 19 Lowrie tests) displays assorted magnetic mineralogy; at the bottom of the Mo1 sub-section (Sobrarbe Fm) variable ratios of magnetite and iron sulphides dominate the magnetic signal (Figure 22, Type II). Nevertheless, towards the top of the Sobrarbe and its transition into the Escanilla Fm, an increasing proportion of high coercivity minerals are observed (Type IV). At the base of Mo2 (Sobrarbe Fm) magnetite and iron sulphides coexist. Similar to Mo1, samples obtained from the Escanilla Fm present a variable ratio of magnetite, iron sulphides and hematite.

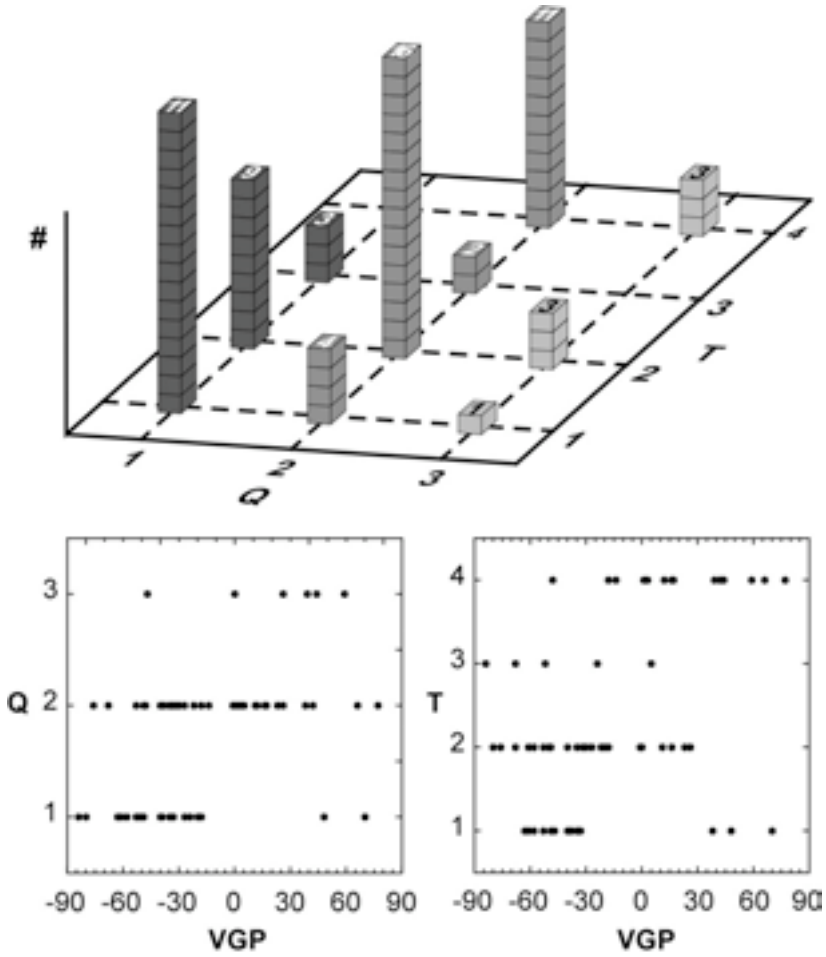

Figure 23. Relations between the rock magnetic carriers (T), the quality of the ChRM (Q) and the VGP paleolatitude.

This rock-magnetism classification (T) has been related to the quality of the directional data (ChRMs of the demagnetized sister samples; Q factor, Figure 23). A histogram with the three variables (T, Q and number of occurrences) reveals that high quality ChRMs were mainly carried by magnetite, and magnetite with some content of iron sulphides. Medium–quality ChRMs and, to a lesser extent, the lower quality ones, are related to samples with mixture of magnetite and iron sulphides, as well as variable ratios of hematite. Therefore, correlation between high quality ChRMs directions and magnetite content can be established.

T and Q parameters were plotted against the VGP paleolatitudes derived from the ChRM. Magnetite and high quality ChRMs show unambiguous VGP values since higher content on iron sulphides and/or hematite are responsible for most anomalous VGP latitudes (-30º<VGP<30º). This evidence supports the filtering of low angle VGPs in order to reduce noise.

5.4.3. Origin of magnetic noise

The Aínsa basin rocks display a slightly noisy paleomagnetic signal. This seems to be partially due to the occurrence of magnetic sulphides, as can be inferred from the relation between the quality factor of the paleomagnetic directions (Q) and the rock magnetic classification (T): a higher content in sulphides (TII or TIII) is clearly correlated (Figure 23) with a lower quality of the direction (Q≥2). Sulphides in the South Pyrenean Basin are formed from detrital magnetite during the early diagenesis (Larrasoaña et al., 2003a). The lock-in of this stable chemical magnetization may last several thousand years depending upon the accumulation rates and the *redox* equilibrium. This gap can be variable and cannot be accurately estimated, but the range of variation allows for suitable magnetostratigraphic studies to be performed (Larrasoaña et al., 2003a). In fact, this small delay in the acquisition may affect the primary direction in a syntectonic pile, since the rock may record the external field during earlier stages of folding (for a given bed). These dip angles are variable and depend on lock-in times, folding rates, etc. Besides, variable grain size distributions (i.e. delta entries within the talus) as well as overlapping with younger (postfolding) components in the platform facies (Rodríguez-Pintó et al., 2011b) may additionally contribute to the noise caused by sulphides. Finally, deflection of the primary declination and inclination could be caused by internal deformation related to the Boltaña anticline that may accommodate some flexural flow at the fold flanks in the thick mudstone sequence.

In any case, the fisherian (Fisher, 1953) distribution of data, displaying almost antipodal means (Figure 24), together with the similarity of the reverse and normal mean directions to the expected Eocene inclination (local reference: Dec, Inc: 005, 53; α95: 4.6º; k: 9.6, see chapter 4), allow us rejecting any major cause of noise deflecting the original VGP.

Therefore, only intermediate and high-quality ChRMs were used to construct a reliable local polarity scale. In this sense, the lower latitudes (< 30°) of the VGP, mostly related to poor quality samples or high sulphide contents (Figure 23), were removed from the dataset aiming to avoid this unnecessary noise. In total 29% directions were rejected (being sandstones half of the samples). Finally, the unusually large number of samples in this study (≈ 1.000) allows us to do this kind of treatment and still permits to build a robust and trustable local polarity sequence.

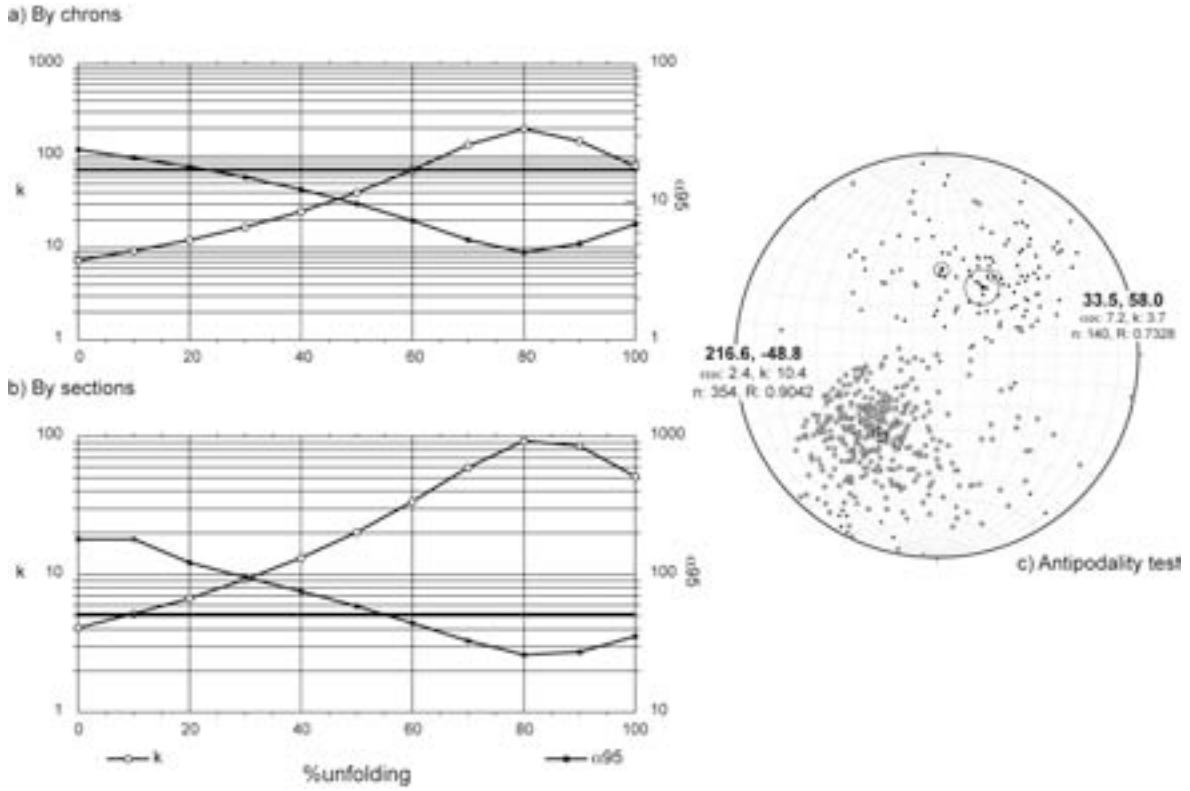

Figure 24. a and b) Fold test in the Aínsa Basin (McElhinny, 1964 run under SuperIAPD) point to a prefolding character of the ChRMs. c) Stereoplot of high quality individual directions (after bedding restoration). The antipodal nature of the normal and reverse means also supports the primary origin of the magnetization (dashed circle represents the normalized reverse mean).

5.4.4. Paleomagnetic stability

Two different kinds of data grouping for the fold test were done to check the magnetic stability in the samples obtained. Firstly, paleomagnetic mean directions were calculated for every chron (normal and reverse polarities were treated separately). Besides, a macro-fold test was done using the section means (Figure 24, Table 5), of the Ara River and Coscollar-Mondot sections. Only well-characterized ChRMs (with inclinations comprised between 40 and 60º and $a_{95} \leq 10º$) were considered for the fold test by chrons. In the case of fold test by sections, high and medium quality ChRM vectors were computed in the mean.

The slightly synfolding (80%) and non-significant character is likely caused by the aforementioned sources of noise, which are known to produce apparent syntectonic magnetizations (Pueyo, 2010). Moreover, the slight obliquity between the Boltaña fold axis (N004E, Mochales et al., 2010) and the mean Eocene magnetic record in the Aínsa Basin (DEC: 035, figure 24c) could reduce the accuracy of the fold test. However, this apparent synfolding magnetization is non-significant with respect to the total restoration (100%). Both fold tests performed confirm therefore a significant prefolding character of the ChRM component, allowing us to be confident with the primary origin of the magnetization as attested in numerous paleomagnetic works in the South Pyrenean basin (Bentham, 1992; Dinarès, 1992; Hogan, 1993; Pueyo 2000; Larrasoaña 2000; Oliva, 2004).

	Declination (bac)	Inclination (bac)	α95	Strike (rhr)	Dip	Declination (bac)	Inclination (bac)
By sections:							
Ara River	25	69	4	358	22	56	54
Coscollar-Mondot	60	16	11	185	54	29	53
By chrons:							
N1	64	8	10	184	64	31	56
R1	57	34	6	181	25	41	53
R3	71	16	7	190	73	8	62
R5	21	63	7	25	15	49	60
R6	15	66	3	354	24	47	51
N6	11	61	7	360	24	41	50
R7	12	56	4	3	21	37	48

Table 5. Numerical data used in the fold test.

Finally, the stereoplot of the whole dataset (only Q=1 vectors) reveals two pseudo-antipodal directions (Normal: n=140, Dec: 034, Inc: 58, a95: 7.2°, k: 3.7, R: 0.7328 and Reverse: n=354, Dec: 217, Inc: -49, a95: 2.4, k: 10.4, R: 0.9042) also pointing to a primary origin of the magnetization.

5.4.5. Biostratigraphic data

Biostratigraphic sites systematically collected in the Ara River section and isolated samples correlated laterally with the Coscollar, Mondot and Escanilla sections (see figures 4 and 25 for all biostratigraphic sites and figure 26 for the range of larger foraminifers). They helped to constrain the pattern of magnetozones (Figure 18, 19, 20 and 21) into the GPTS (Figure 27) by Gradstein et al. (2004).

5.4.5.1. Ara River section

Sample BOS1, collected in the Alveolina Limestone, contains the association of *Alveolina ellipsoidalis* SCHWAGER 1863, *Alveolina vredenburgi tumida* HOTTINGER 1960, *Alveolina dolioliformis* (SCHWAGER 1863), *Glomalveolina lepidula* (SCHWAGER 1863) and indicates an Early Ilerdian (Biozone Alveolina ellipsoidalis) according to Hottinger (1960) or SBZ 6 according to Serra-Kiel et al. (1998). At the top of the Metils Fm the sample BOS2 contains the association composed by *Nummulites pernotus* SCHAUB 1951, *Nummulites atacicus* LEYMERIE 1846, *Assilina leymeriei* (D'ARCHIAC & HAIME 1853), *Assilina pustulosa* DONCIEUX 1926, *A. canalifera* (D'ARCHIAC 1853) indicating a Middle Ilerdian 2 (Biozone Nummulites exilis) according to Schaub (1991) or SBZ 8 according to Serra-Kiel et al. (1998). The Late Ilerdian or SBZ9 is represented by the sample BOS3, located in the limestones that belongs to the middle part of the Yeba Fm, with the association *Nummulites subramondi subramondi* DE LA HARPE *in* SCHAUB 1951 and *Assilina pomeroli* SCHAUB 1981.

In the lower part of the Boltaña Fm, the sample BOS4 contains *Alveolina schwageri* CHECCHIA-RISPOLI 1905, *Alveolina oblonga* D'ORBIGNY 1826, *Alveolina foranasinii* CHECCHIA-RISPOLI 1909, *Glomalveolina minutula* (REICHEL 1936); sample BOS5 provided *Alveolina ruetimeyeri* RUETIMEYERI 1960, *A. oblonga* D'ORBIGNY 1826, *A. foranasinii* CHECCHIA-RISPOLI 1909, *A. schwageri* CHECCHIA-RISPOLI 1905, *G. minutula* (REICHEL 1936); sample BOS6 yielded *Nummulites burdigalensis burdigalensis* DE LA HARPE *in* SCHAUB 1951, *Assilina placentula* (DESHAYES 1838); sample BOS7 is characterized by *Nummulites subramondi thalmanni* SCHAUB 1951 *N. burdigalensis burdigalensis* DE LA HARPE *in* SCHAUB 1951 and *Assilina placentula* (DESHAYES 1838); sample BOS8 (Ascaso Mb) contains *A. oblonga,* D'ORBIGNY 1826, *A. schwageri* CHECCHIA-RISPOLI 1905, *A. ruetimeyeri* RUETIMEYERI 1960. The sample BOS9, collected overlying the Ascaso Mb, contains *Assilina placentula* (DESHAYES 1838) and *Assilina plana* SCHAUB 1951. All these associations indicate an Early Cuisian age (Biozone Alveolina oblonga) according to Hottinger (1960), Biozone Nummulites planulatus according to Schaub (1981) or SBZ 10 of the Serra-Kiel et al. (1998).

The samples located in the uppermost Boltaña Fm, such BOS10 and 11 yielded *Nummulites leupoldi* SCHAUB 1951, *Nummulites burdigalensis cantabricus* SCHAUB 1981, and *Assilina laxispira* DE LA HARPE 1926 *in* SCHAUB 1955, which indicate a Middle Cuisian Biozone Nummulites praelaevigatus according to Schaub (1981) or SBZ 11 of Serra-Kiel et al. (1998).

5.4.5.2. Coscollar section

Ermita San Isidro outcrop (EI)

Outcrop located to the south of the Arcusa village (Figure 25) that belongs to the Coscollar level of the Co2 sub-section (EI in Figures 27). Sample EI contains *Nummulites beneharnensis* DE LA HARPE 1926 and *Nummulites boussaci* ROZLOZSNIK 1924. This association indicates a Middle Lutetian 1 according to Schaub (1981) or SBZ 14 of Serra-Kiel et al. (1998).

Arcusa breccia outcrop (AB)

Outcrop located to the south of the Arcusa village (AB in Figure 25 and 27), correlated with Co5 sub-section, in the La Patra Mb. The sample contains *Nummulites discorbinus* (SCHLOTHEIM, 1820), *Nummulites boussaci* ROZLOZSNIK 1924, *Nummulites beneharnensis* DE LA HARPE 1926 and *Nummulites* aff. *millecaput* BOUBÉE 1832. This association indicates a Middle Lutetian 1 according to Schaub (1981) or SBZ 14 of Serra-Kiel *et al.* (1998).

Los Gorgos outcrop (GO)

Los Gorgos outcrop located in the Sobrarbe Fm above the regional anoxic level and correlated with the Co5 sub-section (GO in Figures 25 and 27). This sample contains *Nummulites crassus* BOUBEE 1831*, Nummulites lorioli* DE LA HARPE 1879 and *Nummulites sordensis* HERB & SCHAUB 1966. This association indicates a Middle Lutetian 2 age according to Schaub (1981) or SBZ 15 of Serra-Kiel et al. (1998).

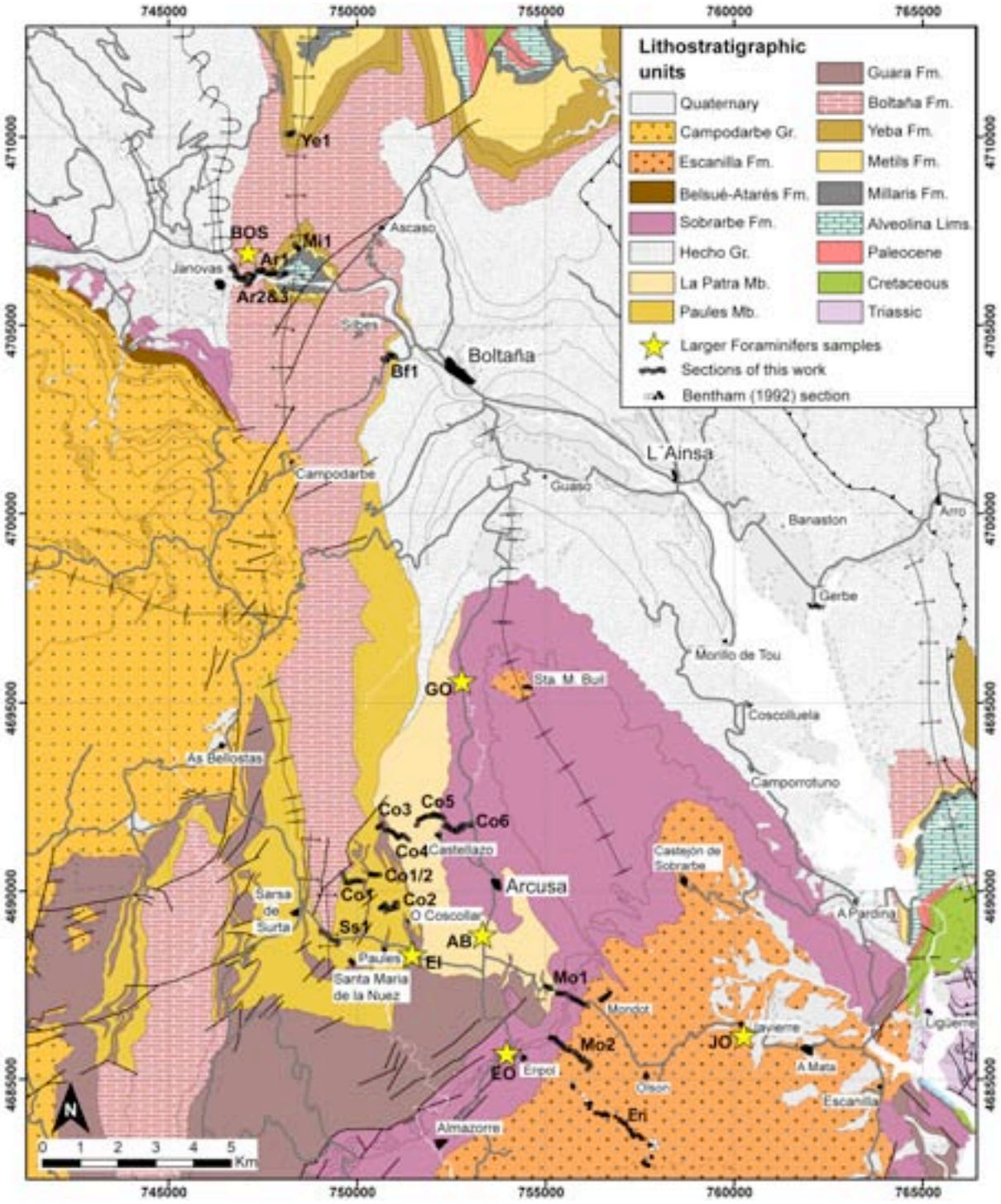

Figure 25. Geological map of the studied area, modified from Barnolas et al. (*in press* a and b). Larger Foraminifers fossil localities are highlighted. UTM coordinates European datum ED50, zone 30T.

5.4.5.3. Mondot and Eripol sections

Eripol outcrop (EO)

The Eripol outcrop is located near Eripol village (EO in Figures 25 and 27) at the base of the Sobrarbe Fm (above the anoxic level). This sample contains *Nummulites crassus* BOUBÉE 1831 and *Nummulites sordensis* HERB & SCHAUB 1966. This association indicates a Middle Lutetian 2 according to Schaub (1981) or SBZ 15 of Serra-Kiel et al. (1998).

Barranco de Jabierre de Olsón outcrop (JO)

This outcrop is located near Jabierre de Olsón, in a ravine (JO in Figures 25 and 27), to the SSE of the village. Brown claystones belonging to the Escanilla Formation delivered an abundant assemblage of charophyte gyrogonites dominated by *Harrisichara lineata* GRAMBAST 1957 with a few gyrogonites of *Maedleriella* sp. and *Gyrogona* sp. This assemblage indicates a Middle Bartonian to Middle Priabonian age according to Riveline (1986) and range from biozone Chara friteli, to the basal part of the biozone Stephanochara vectensis of the European charophyte biozonation of Riveline et al. (1996) and Hardenbol et al. (1998).

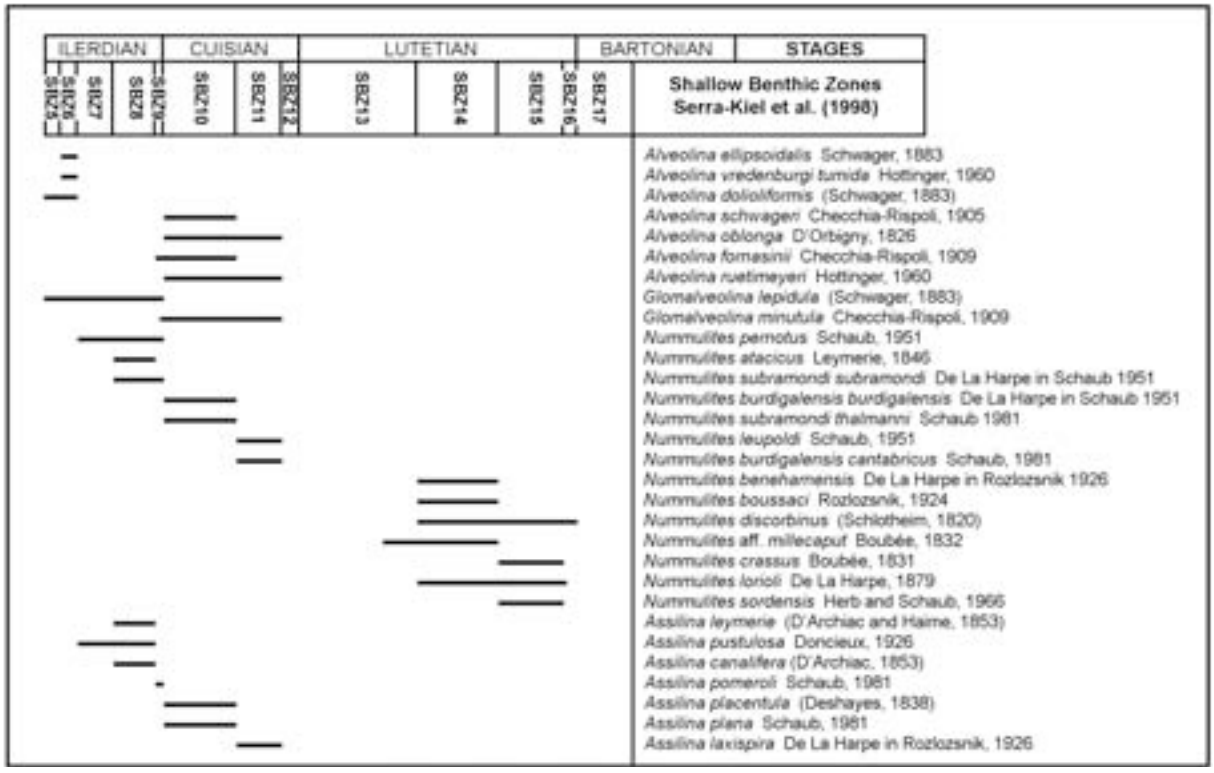

Figure 26. Biostratigraphical range of the larger foraminifers according to Serra-Kiel et al. (1998) present in the gathered samples.

5.5. Interpretation

5.5.1. Correlation with the GPTS.

In this work we propose a new chronostratigraphic frame for the Aínsa Basin that allows for characterizing orogen-scale sedimentary and tectonic processes. The magnetostratigraphy described in this work allows establishing some global correlations for the Aínsa Basin, supported on benthic foraminifera (Ara River, Bal Ferrera, Coscollar and Mondot sections) and charophyte gyrogonites (Eripol section), according to the following considerations (Figure 26):

The first reverse-polarity zone R1 found in the lowermost 375 m of the Ara River section, is correlated with the polarity chron C24r, in agreement with the corresponding SBZ6 and SBZ8 associations. The normal N1 zone is collectively linked to the C24n due to the lack of magnetic resolution in this part of the profile (Figures 27 and 28). The fossil assemblages found in the Yeba Fm correspond to the Late Ilerdian or SBZ9 (Serra-Kiel et al., 1998). This means that the Ilerdian/Cuisian boundary occurs within the upper part of the Yeba Fm, in the C24n chron. This constitutes a special relevant issue of this work since it helps to determine the Ilerdian-Cuisian boundary in the Ara River section.

We agree with Pascual et al., (1992) and Serra-Kiel et al. (1994) where they link the first normal zone found in the Tremp and Campo sections (stratotype of the Ilerdian and parastratotype of the Ilerdian and Cuisian, respectively) to C24n.3n (considering the conversion between Harland et al., 1990 and Gradstein et al., 2004, scales). The integration of the results obtained in the Tremp and Campo sections with the Ara River section here presented, together with the original biostratigraphic source (Molina et al., 1992) and future recalibrations, will provide a more accurate definition of the biozone boundaries.

The R2 zone is related to C23r, according to the SBZ 10 biozone (Figure 26). Around meter 800 of the succession, the N2 normal-polarity zone is correlated with C23n, being impossible to identify in the local sequence the expected short chrons located at its top. The subsequent R3 is hence matched to C22r, according to SBZ11.

In Bal Ferrera section the zone R3 was attributed to C22r and N3 to C22n, identifying the contact between the Boltaña Fm and the Paules Mb within.

In the lowermost part of the Paules Mb (Ss1 sub-section), we find the C22n/C21r boundary. According to the current time scale (Gradstein, et al., 2004) it could represent the Ypresian-Lutetian boundary. Previous studies based on planktonic foraminifers (Canudo, 1990) and nummulitids (Schaub, 1981) corroborate the correlation between these two events in the Boltaña anticline.

The local pattern of magnetozones allows for correlating R4 to C21r and N4 to C21n. The Coscollar level is Middle Lutetian 1 or SBZ 14 in age and is located in the upper part of C20r (R5). The stratigraphic continuity of sub-sections allows correlating N5 with C20n. The Middle Lutetian 1 or SBZ 14 is at higher stratigraphic positions than expected (AB outcrop), as recently proposed in the Agost (Larrasoaña et al. 2008) and the Isuela sections (Rodríguez-Pintó et al., 2011c).

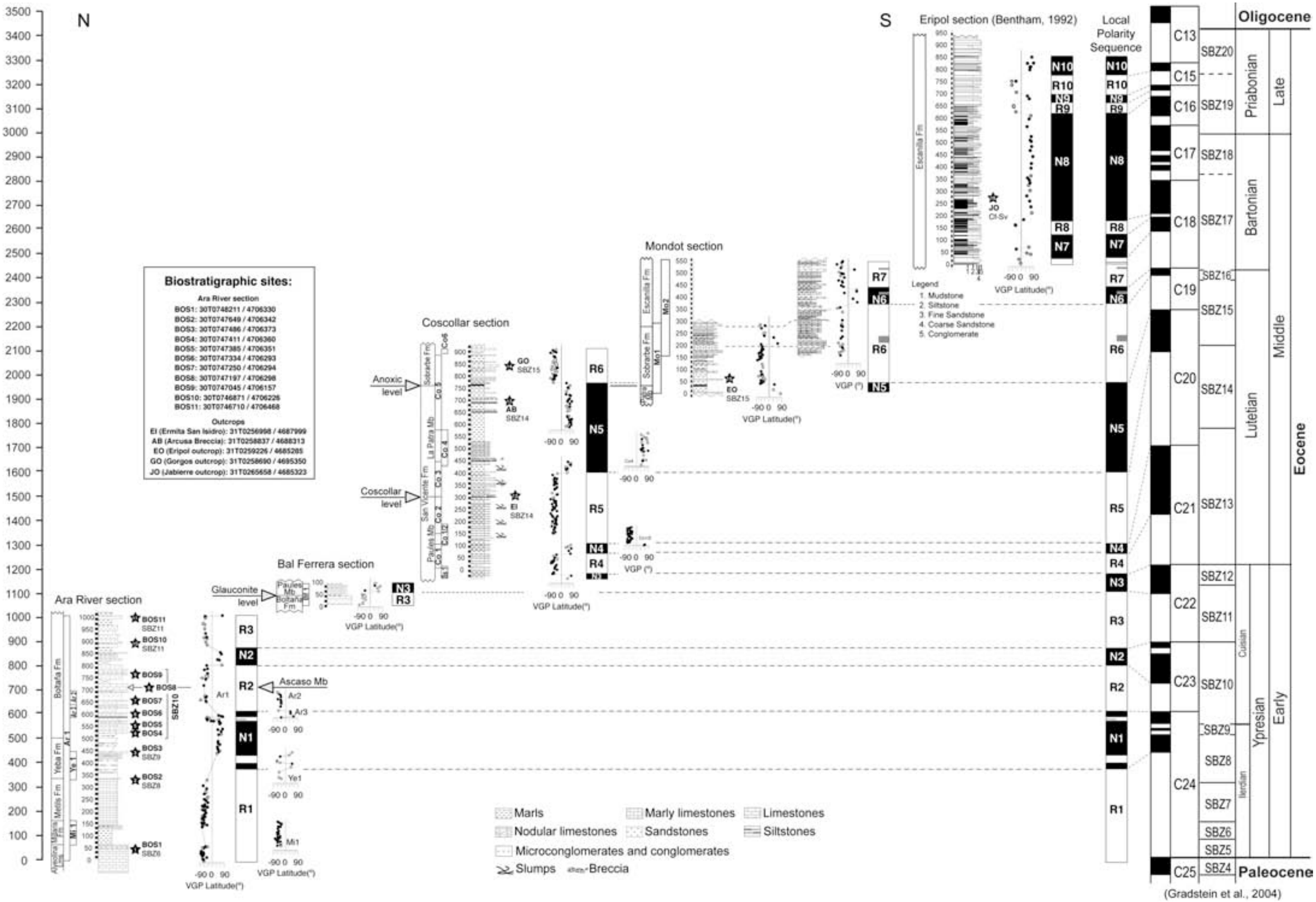

Figure 27. Integration of all the stratigraphic and magnetostratigraphic sections together with local biostratigraphic data based on SB Zonig (Serra-Kiel et al., 1998). Besides, the correlation with the GPTS (Gradstein, et al., 2004) is presented. Derived absolute aging of the formation tops and reference levels are placed to the left to each section.

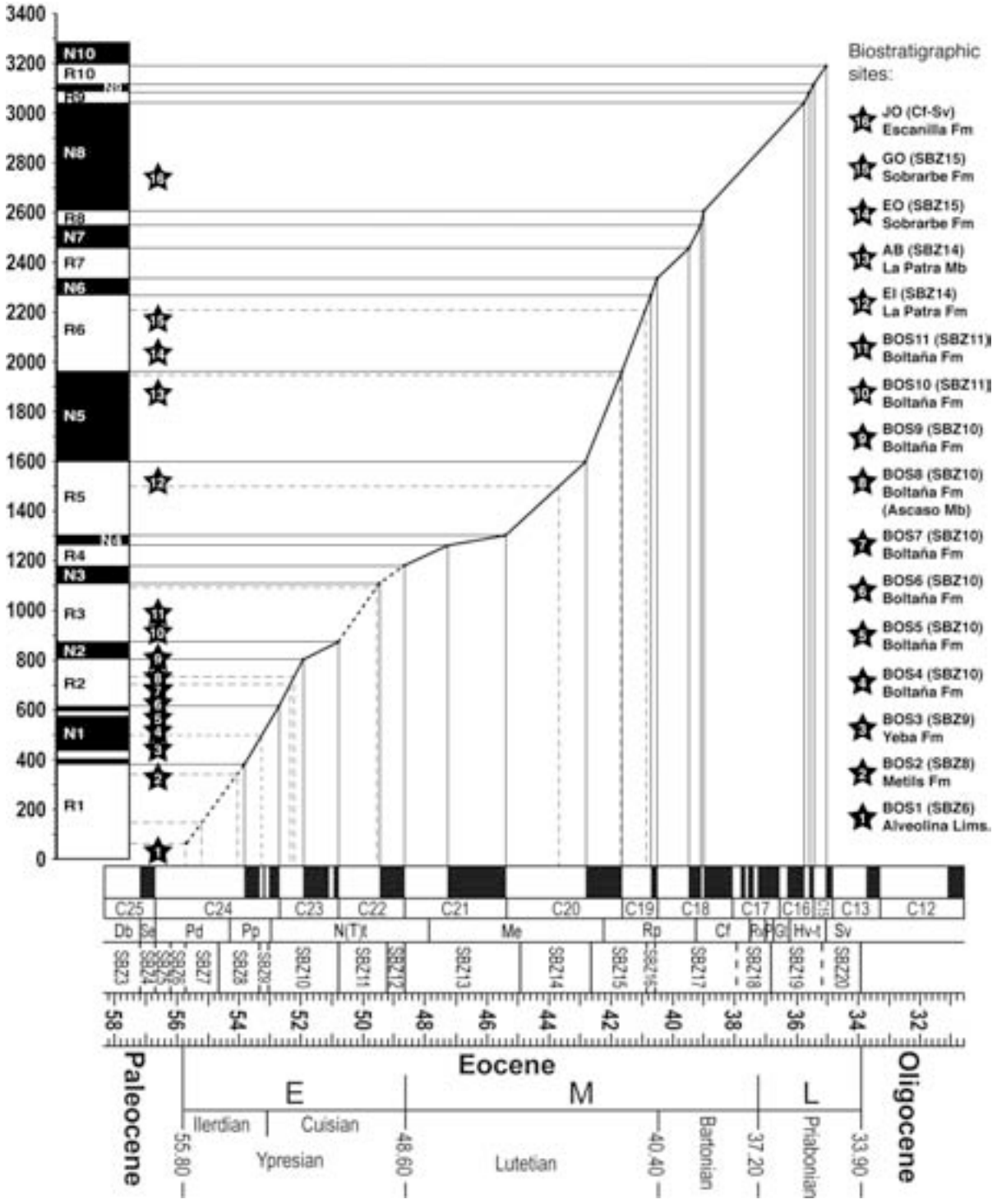

Figure 28. Correlation between the local polarity sequence (ordinates in meters) and the Global Polarity Time Scale (abscissa in My.) by Gradstein et al. (2004). Biostratigraphic sites (and their attributed SBZ) are also shown. Continuous lines indicate the magnetozones correlation with the GPTS proposed in this study. Dashed lines bound the formations tops. The bold line represents accumulation rate, the dashed bold lines indicate undetermined accumulation rates. SBZ (Serra-Kiel et al., 1998) and charophytes (Riveline et al., 1996) scales are included. Charophyte biozones (Db: Dughiella bacillaris; Se: Sphaerochara edda; Pd: Peckichara disermas; Pp: Peckichara piveteaui; N(T)t: Nitellopsis (Tectochara) thaleri; Me: Maedleriella embergeri; Rp: Raskyella pecki; Cf: Chara friteli; Rv: Raskyella vadaszi; P: Psilochara repanda; Gt: Gyrogona tuberosa; Hv-t: Harrisichara vasiformis-tuberculata; Sv: Stephanochara vectensis).

This shows the need to recalibrate the current SBZ scale (Serra-Kiel et al., 1998) around the SBZ 14 –SBZ 15 boundary. The R6 zone is correlated with C19r. The Paules Mb covers therefore from C22n to C20r and La Patra Mb from C20r to the end of C20n. In this section we can consider that the anoxic level at the bottom of the Sobrarbe Fm is the base of the Middle Lutetian 2 or SBZ 15 and the boundary between C19r and C20n.

The Mondot section covered from the uppermost C20n (N5) to C18r (R7). The previous interpretation of the Eripol section (Bentham, 1992) does not match within this frame and has to be reinterpreted; the lower normal polarity found by Bentham (1992), here labeled as N7, was attributed to chron C19n. Nevertheless, we attribute this interval to C18.2n. R8 is linked to C18r.1r. The top of N8 defined in Bentham (1992) remains as the top of C16n.2n, because of the lack of resolution within the short Bartonian-Priabonian reversals.

The Escanilla Formation at Jabierre de Olsón provided a charophyte assemblage characteristic of the Middle Bartonian to Middle Priabonian interval (Biozones Chara friteli, Raskyella vadaszi, Psilochara repanda, Gyrogona tuberosa, Harrisichara vasiformis-tuberculata and base of biozone Stephanochara vectensis) according to Riveline (1986), Riveline et al. (1996) and Handerbol et al. (1998). This biostratigraphic data is the only available information allowing for a reliable correlation of the local magnetostratigraphic data to the GPTS. Nevertheless, the charophyte-rich Escanilla Fm should be densely re-sampled in future studies to unravel all the Bartonian-Priabonian reversals.

5.5.2. Sedimentary implications

The proposed magnetostratigraphic correlation (Figures 18 to 21 and 26) permits an accurate dating of sedimentologic events and an estimate for sediment accumulation rates (Figures 27 and 28) during the Eocene in the Aínsa Basin. We can constrain the bottom of the studied sequence in SBZ6 likely not far from the base of C24r. The top of the Alveolina Limestone would tentatively be at 55.7 M.y. according to the inaccurate magnetostratigraphic calibration at the base of the profile (defined by the top of the SBZ6). The following temporal boundaries were constrained by magnetostratigraphic reversals. The top of the Yeba Fm can be dated at 53.4 M.y. The top of the Ascaso Mb, that separates Lower and Upper Boltaña Fm, can be dated at 52.2 M.y. (Figure 26 and Table 6). The top of the Ara River profile can be considered to reach 50.0 M.y. It must be taken into account that the top of the Boltaña Fm is frequently eroded, which may be the cause for an undetermined portion of the upper Cuisian to be missing (Barnolas et al., 1991).

The Boltaña Fm-Paules Mb boundary is established at 49.5 M.y. (in the Bf1 section). The Coscollar level at the top of the Paules Mb is dated at 43.6 M.y. and the top of La Patra Mb (characterized by a regional anoxic level) at 41.6 M.y. The top of the Sobrarbe Fm was found at 40.9 M.y., constraining the temporal limits for the series in the eastern limb of the Boltaña anticline (see details in figure 27). The base of the Escanilla Fm in this section is a lateral equivalent to the Sobrarbe Fm, therefore it begins earlier than in other sections surveyed by Bentham (1992). In the sections here studied, the Escanilla Fm started at the Late Lutetian. Bentham (1992) determined the top of the Escanilla Fm at 35 M.y.

The Lutetian is characterized by dramatic changes in the average accumulation rate as deduced from this magnetostratigraphic study (Figures 28, 29 and Table 6). This is consistent with the sedimentary features of each formation. The lower part of the Paules Mb corresponds to a retrogradational pattern with low sedimentation rate and a sedimentary instability which is evidenced by the abundance of internal stratigraphic truncations. This retrogradational character turns to a progradational one in the upper part of the Paules Mb (Barnolas et al., 1992) with the consistent increase of their sedimentation rate (Figures 28 and 29).

The transition to La Patra Mb is located in a flooding surface with glauconite and followed by a carbonate breccia. The La Patra Mb, in the Coscollar profile corresponds to an accretionary base of slope carbonate breccias, interlayered with slope marls and scarce distal siliciclastic turbidites from the basin trough. This carbonate breccia slope apron develops at the foot of an erosional truncation in the shallow carbonate Guara Fm limestones (Barnolas et al., 1992). These sedimentary evidences explain their high sedimentary rate.

Chron	Top (m)	Tickness (m)	Top (M.a.)	Duration (M.a.)	Accumulation Rate (cm/kyr)	Medium age	Absolute age
R1	439	372	53,8	1,85	20,1	0,925	54,725
N1	617	178	52,65	1,15	15,5	0,575	53,225
R2	804,5	187,5	51,9	0,75	25	0,375	52,275
N2	875	70,5	50,75	1,15	6,1	0,575	51,325
R3	1104	229	49,4	1,35	17	0,675	50,075
N3	1181	77	48,6	0,8	9,6	0,4	49
R4	1266,5	85,5	47,25	1,35	6,3	0,675	47,925
N4	1305	38,5	45,4	1,85	2,1	0,925	46,325
R5	1596,5	291,5	42,8	2,6	11,2	1,3	44,1
N5	1963,5	367	41,6	1,2	30,6	0,6	42,2
R6	2264,5	301	40,7	0,9	33,4	0,45	41,15
N6	2332,5	68	40,5	0,2	34	0,1	40,6
R7	2457	124,5	39,45	1,05	11,9	0,525	39,975
N7	2555	98	39,05	0,4	24,5	0,2	39,25
R8	2608	53	38,95	0,1	53	0,05	39
N8	3044	406	35,75	3,2	12,7	1,6	37,35
R9	3088	44	35,6	0,15	29,3	0,075	35,675
N9	3122	34	35,4	0,2	17	0,1	35,5
R10	3198,5	76,5	35	0,4	19,1	0,2	35,2

Table 6. Position of the chron boundaries within the sedimentary pile, durations, accumulation rates and absolute ages are showed.

Bartonian sedimentation evolved towards suprafeeding conditions with a basin shallowing and progradating deltaic systems (Puigdefàbregas, 1975; Barnolas et al., 2004). It is evidenced by an increase of the sedimentation rate in the Sobrarbe Fm (Figures 28 and 29; Table 6). The Escanilla Fm in the study area is characterized by strong changes in sedimentation rates. These changes are most likely artifacts produced by the lack of resolution and the uncertainty of the correlation within the Escanilla section (Bentham, 1992). Relatively higher accumulation rates would be expected at the top of the section (Priabonian) in relation to quick and abrupt continentalization in the Southwestern Pyrenees as proposed by Costa et al. (2009) reinterpreting data by Hogan and Burbank (1996).

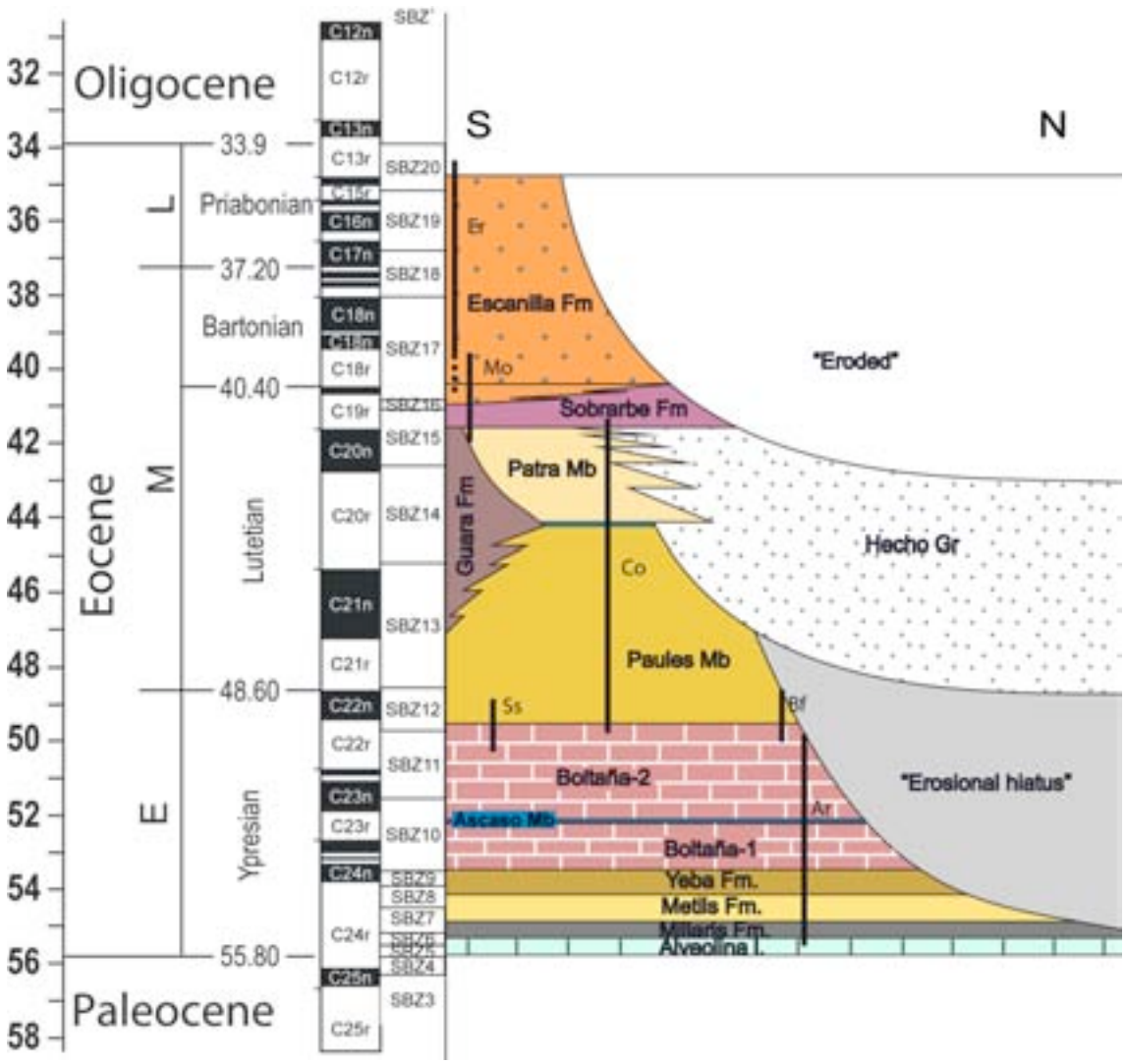

Figure 29. Chronostratigraphic correlation of the units involved in this work. The sampled sections and the reinterpreted Eripol section (Er, Bentham, 1992) are showed in dark gray. The dashed stretch represents the interpretation presented by Bentham (1992).

6. Rotational kinematics of the Boltaña anticline

6.1. Introduction

Excellent exposure conditions and syn-tectonic record related to the growth of oblique structures in the Southern Pyrenees allow for an accurate investigation of the rotational kinematics of the Boltaña anticline. The interest of this set of N-S structures (Southern Pyrenenan Zone) lies in its contrasted orientation with regard to the frontal thrusts of WNW-ESE trend. The Boltaña anticline requires special attention since it is the structural boundary between the Graus-Tremp (E) and Jaca-Pamplona (W) Basins. Moreover, it delimits the Ainsa Basin, which is the westernmost edge of the piggyback- Graus-Tremp Basin, transported in the hangingwall of the Marginal Sierras thrusts.

Paleomagnetism has been revealed as an efficient tool to characterize vertical-axis rotations in thrust belts (McCaig and McClelland, 1992; Allerton, 1998). Applications to Pyrenean problems (Pueyo et al., 2003a and b; Oliva-Urcia and Pueyo, 2007a; Oliva-Urcia et al., 2011b) allowed for shortening correction in cross-sections (Millán et al., 1996; Oliva-Urcia and Pueyo, 2007b) as well as map-view (Pueyo et al., 2004a) and 3D restorations to be established (Ramón et al., 2011a). By means of paleomagentic data the origin of these oblique structures have been determined as secondary, linked to significant clockwise rotations (Dinarès 1992; Parés and Dinarès 1993; Pueyo, 2000; Fernández et al., 2004; Oms et al., 2006).

The exceptional chronostratigraphic frame based on the detailed magnetostratigraphy performed in the Ainsa Basin (chapter 5) and the primary character of magnetization, provided us well-dated paleomagetic directions throughout the pre-, syn- and post-folding rocks of the Boltaña anticline. These rocks belonging to all kind of sedimentary environments (from shallow marine to continental) almost completely represent the Eocene record on the Southern Pyrenees. The same samples used in the magnetostratigraphic study (Chapter 5) were used for determining VARs. This homogeneous distribution of samples along the stratigraphic pile was discretely clustered to provide VAR sites. Additionally, another two areas were revisited to perform a classic sampling focus on VAR characterization (as standard sites). One of them was the Escanilla Fm that had previously been the goal for a magnetostratigraphic study (Bentham, 1992; Bentham and Burbank, 1996). Seven VAR sites were sampled with the aim to determine the decrease of the magnitude of rotation in the Ainsa Basin as suggested by a preliminary analysis (Mochales et al., 2008). The second sampling zone was the San Felizes area, placed in the western limb of the Boltaña anticline where very little previous information (Pueyo, 2000; Fernández-Bellón 2004) and anomalous paleomagnetic directions had been obtained. A special treatment was developed for these thirteen sites affected by several folding stages.

Significant studies related to the oblique structures of the Ainsa Basin have been carried out (Parés and Dinarès, 1993; Pueyo, 2000; Fernández-Bellón 2004; Oms et al., 2006). Conclusions of these studies are that sedimentation and fold growth as well as progressively decreasing rotations were coeval during Lutetian times, as occurred in the Mediano anticline (Fernández-Bellón, 2004). Nevertheless, preliminary processing derived from magnetostratigraphic series obtained during this

work, revealed a non-steady scenario and a younger rotation age (Mochales et al., 2008). These uncertainties motivated us to try and establish an accurate chronological frame and the magnitude of the rotation for the Boltaña anticline, helping to unravel the kinematics of this key area in the southern Pyrenean margin.

6.2. Paleomagnetic methods

6.2.1. Sampling

The analysis of paleomagnetic rotations was based on different data sets: 1) Classic sites developed in this work (7 in the Escanilla Fm and 13 in San Felizes). 2) Reprocessing of our own magnetostratigraphic data which has turned into 37 "sites". 3) Reprocessing of other authors profiles (4 profiles form Bentham, 1992) giving 11 "sites". 4) 7 classic sites from other authors (Dinarès, 1992; Parés and Dinarès, 1993; Pueyo, 2000), see Figure 1 and Table 1. Samples were extracted using a petrol-powered drill cooled by water. All the cores were geo-referenced in situ with a GPSMap 76CSx by Garmin and oriented with a magnetic compass; they were sliced in standard paleomagnetic specimens (cylinders 21 x 25 mmØ).

The re-processed sections were Ara River (Figure 2), Coscollar (Figure 3) and Mondot from Mochales et al. (2011a) and Eripol section (Figure 4) from Bentham (1992). Besides, we have reprocessed the remaining sections by Bentham (1992) in the Escanilla Fm (Almazorre; Ligüerre and Mediano sections) that gave 11 more reliable sites (15 specimens in average). VAR sites derived from our magnetostratigraphic profiles (chapter 5 and Mochales et al. 2011a) were established according to the following criteria: 1) Geographic proximity of individual sampling levels; 2) Levels within the same magnetostratigraphic section; 3) Levels belonging to the same Chron; 4) A minimum of 10 samples per site belonging to the same stratigraphic unit (except for sites Ara8, Ara9, Ssa1, Cas3, Cas8 were high quality samples add up to 5, 5, 6, 6 and 3 samples respectively). 5) Only high quality samples (Q1) from the magnetostratigraphy were used to obtain VAR values (see below). 37 discrete VAR sites were obtained by means of this re-processing. Seven previous VAR sites (90J sites by Dinarès, 1992; Parés and Dinarès, 1993; and LIG1&2 and CAM1 sites by Pueyo, 2000) have also been considered (Figure 1). Finally, 7 new paleomagnetic sites were drilled and added to this large dataset along the Escanilla Fm (ESC sites in this work, figure 4) and 13 more in the western flank of the Boltaña anticline close to the Ara river (San Felizes area, figure 2). The chronological background established by means of magnetostratigraphy (chapter 5 and Mochales et al., 2011a), allows for the accurate age of VAR changes through Eocene times (the entire infill of the Ainsa Basin) to be hypothesised.

An absolute age has been assigned to each site. The stratigraphic location of the "site" has been converted to absolute time considering the magnetostratigraphic (Figure 28, chapter 5). An error has been assigned accordingly.

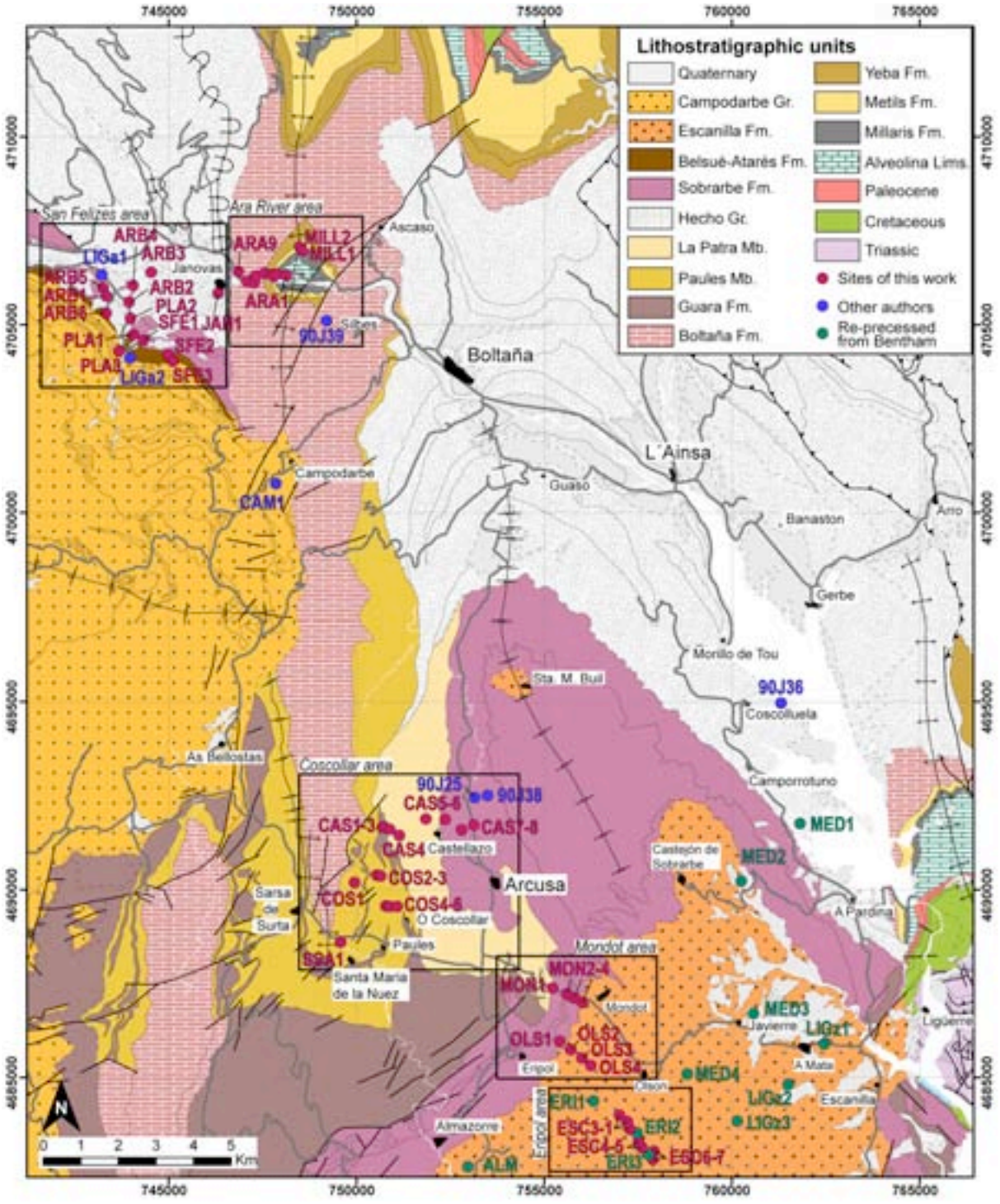

Figure 1. Geological setting of the studied area (modified from Barnolas et al. *in press* a and b). Red points represent the sites sampled for this study (ARA, MILL, SSA, COS, CAS, MON, OLS, ESC), those reprocessed from Bentham (1992) (MED, LIGz, ERI, ALM) in green and individual sites from other authors in blue: 90J25, 36, 38 39 from Dinarès (1992) and Dinarès and Parés (1996); LIG and CAM from Pueyo (2000). UMT coordinates system ED50, zone 30T.

a)

b)

Figure 2. Ara River (eastwards) and San Felizes areas (westwards). a) Geological map (same key as in figure 1) where VAR sites of this work are represented in red and from other authors in blue (for numerical data see table 1). b) Orthophotograph mosaic made from GIS including VAR sites. Original 1:5000 photos from http://sitar.aragon.es/.

a)

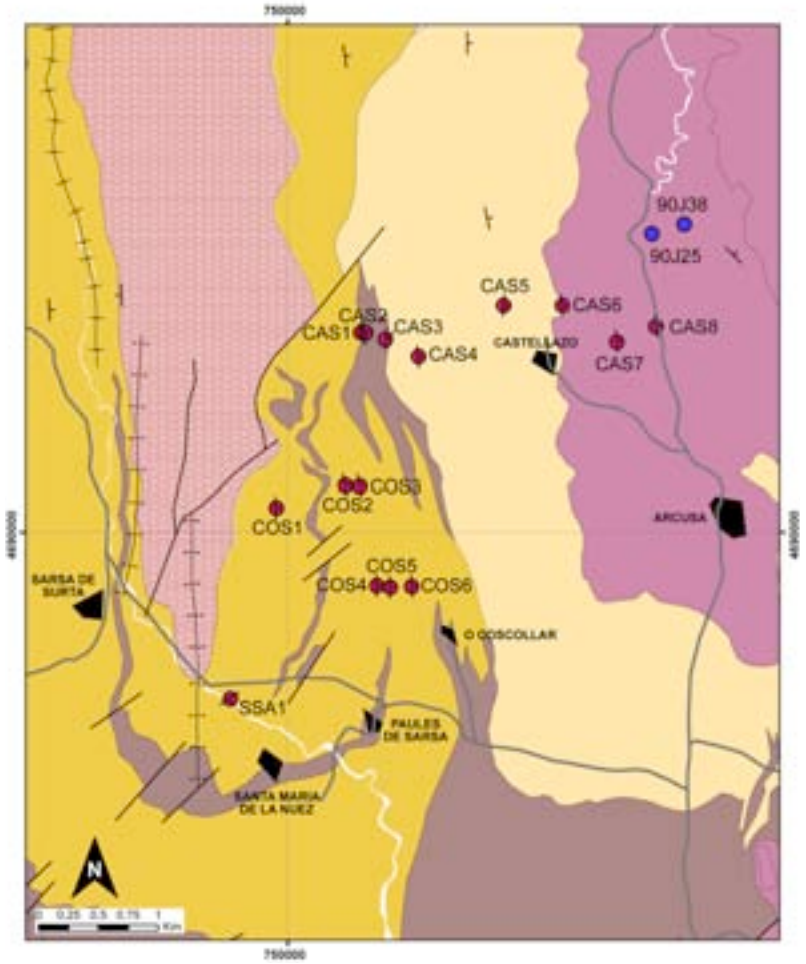

b)

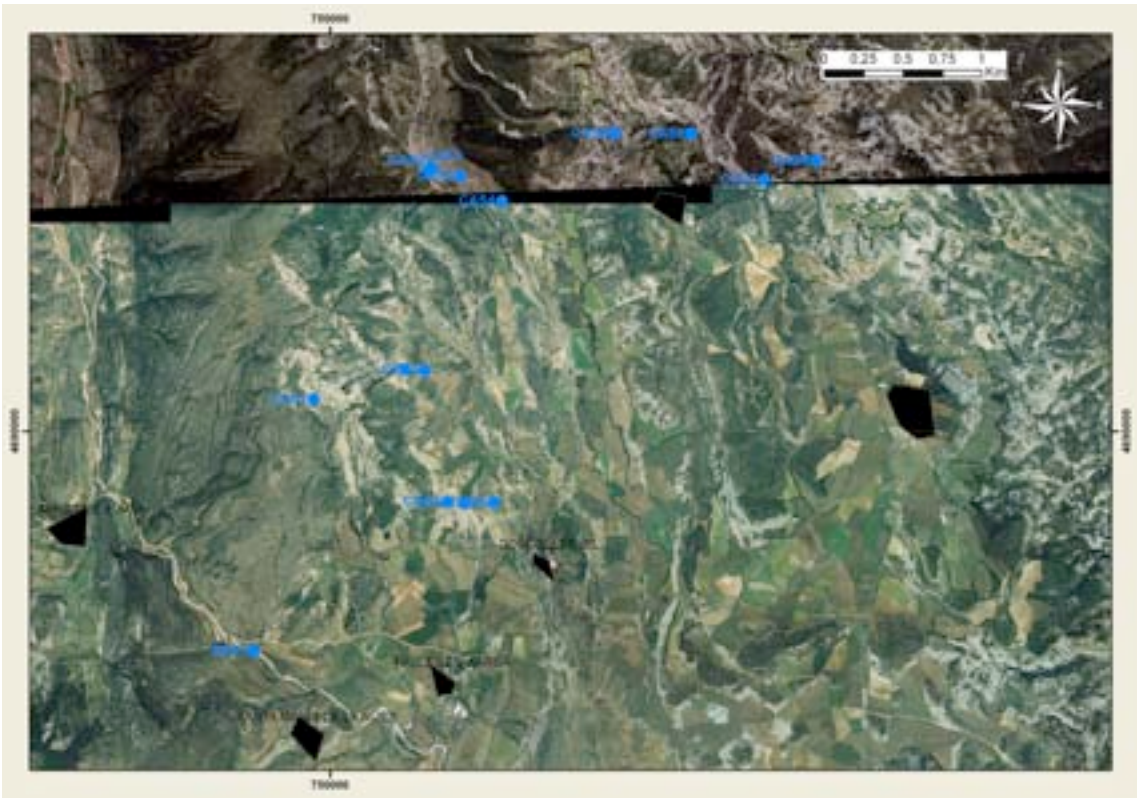

Figure 3. Coscollar area a) Geological map and b) Orthophotograph (caption as in figure 2)

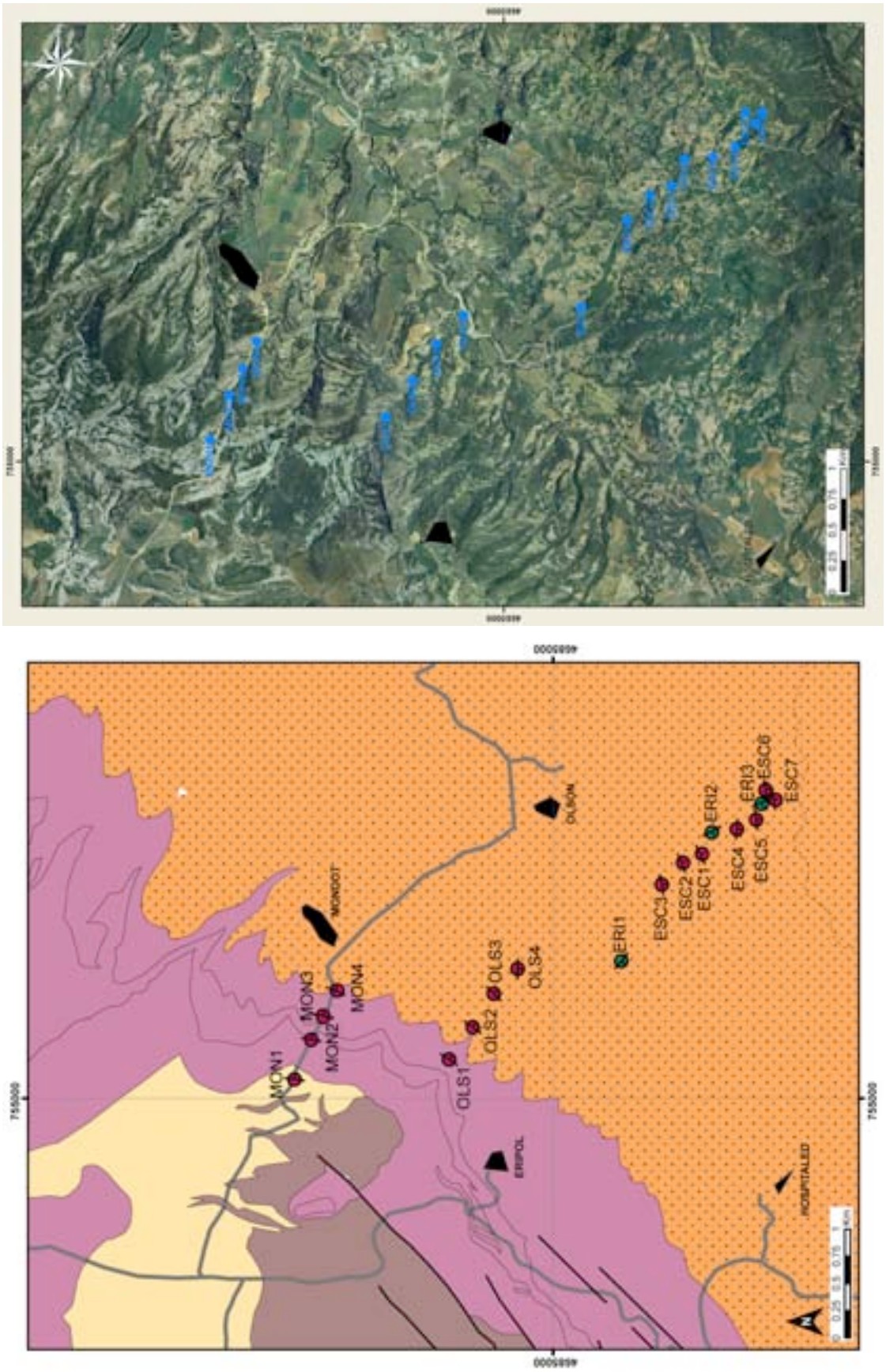

Figure 4.Mondot area northwards and Eripol area southwards. a) Geological map and b) Orthophotograph (caption as in as figure 2)

#	Site	Pol.	Site (m)	Age (Ma)	Age E	Chron	n/N	Z	UTM-X	UTM-Y	Strike	Dip	DD	Dec	Inc	α95	k	Dec'	Inc'	α95'	k'	Source	Unit
1	ARA1	R	54,0	56,411	0,90	C24R	11/11	31T	254791	4706181	183	29	W	225	-35	12,7	17,1	200	-50	11,7	20,0	1	Alveolina lims.
2	MILL1	R	45,0	56,062	0,90	C24R	14/15	31T	255245	4706873	193	6	W	240	-50	8,2	26,4	235	-54	8,4	24,9	1	MillarisFm
3	MILL2	R	48,5	55,727	0,90	C24R	15/15	31T	255192	4706943	190	6	W	236	-37	7,9	28,3	231	-43	8,0	27,9	1	MillarisFm
4	ARA2	R	60,5	55,513	0,90	C24R	15/16	31T	254554	4706256	183	29	W	226	-29	10,4	15,5	209	-53	9,5	16,1	1	Metils Fm
5	ARA3	R	32,5	55,180	0,90	C24R	11/11	31T	254464	4706224	182	50	W	249	-9	10,7	21,1	230	-52	13,6	13,4	1	Yeba Fm
6	ARA4	N+R	88,0	54,764	0,90	C24R	10/12	31T	254394	4706252	189	54	W	243	3	24,4	5,4	39	32	28,0	4,9	1	Yeba Fm
7	ARA5	R	124,0	53,313	0,57	C24N	12/13	31T	254216	4706317	184	63	W	67	-7	13,7	12,1	52	46	14,6	10,7	1	Lw Boltaña Mb
8	ARA7	R+N	104,5	52,571	0,37	C23R	8/11	31T	253975	4706280	184	64	W	245	2	24,7	6,8	227	-52	19,8	10,0	1	Lw Boltaña Mb
9	ARA6	R	97,0	52,565	0,37	C23R	14/14	31T	253910	4706069	188	72	W	252	22	8,3	25,7	246	-43	8,2	26,2	1	Lw Boltaña Mb
10	ARA8	R	85,0	52,074	0,37	C23R	5/8	31T	253750	4706135	186	68	W	249	13	13,7	40,4	226	-50	15,0	33,6	1	Upp Boltaña Mb
11	ARA9	R	85,0	50,241	0,65	C22R	4/6	31T	253519	4706413	187	82	W	229	33	35,9	19,3	226	-35	18,9	65,4	1	Upp Boltaña Mb
12	SSA1	R	24,5	48,384	0,68	C21R	6/7	31T	254974	4688452	56	16	W	210	-55	8,4	77,4	232	-59	10,5	50,1	1	Paules Mb
13	COS1	R+N	75,0	47,436	0,68	C21R	12/14	31T	255470	4690014	358	18	E	197	-67	7,0	43,6	223	-58	7,1	41,9	1	Paules Mb
14	COS2	R+N	42,0	45,226	1,29	C20R	13/15	31T	256062	4690160	350	27	E	184	-63	6,5	45,4	221	-48	7,3	36,1	1	Paules Mb
15	COS3	R	30,0	44,889	1,29	C20R	14/14	31T	256184	4690146	350	25	E	199	-63	5,4	59,7	225	-46	6,2	45,6	1	Paules Mb
16	COS4	R	48,0	44,734	1,29	C20R	11/11	31T	256266	4689306	359	20	E	203	-64	4,3	124,0	224	-50	7,2	45,7	1	Paules Mb
17	COS5	R	42,0	44,308	1,29	C20R	11/11	31T	256376	4689286	359	27	E	199	-67	12,0	17,0	226	-50	12,2	16,6	1	Paules Mb
18	COS6	R	42,0	43,900	1,29	C20R	12/12	31T	256562	4689281	356	26	E	188	-69	7,7	35,7	226	-55	6,5	50,3	1	Paules Mb
19	CAS1	R	45,0	43,346	1,29	C20R	9/10	31T	256294	4691407	350	23	E	218	-73	7,1	59,5	240	-52	7,0	61,3	1	La Patra Mb
20	CAS2	R	35,0	42,982	1,29	C20R	10/10	31T	256321	4691421	352	26	E	210	-60	20,4	7,3	227	-45	21,0	7,0	1	La Patra Mb
21	CAS3	N+R	65,0	42,620	0,59	C20N	6/7	31T	256494	4691358	5	27	E	3	63	22,0	12,3	41	53	19,8	14,8	1	La Patra Mb
22	CAS4	N+R	72,0	42,369	0,59	C20N	12/13	31T	256746	4691181	356	20	E	45	60	18,9	6,8	57	50	16,1	9,0	1	La Patra Mb
23	CAS5	N+1R	42,0	42,115	0,59	C20N	8/10	31T	257491	4691559	4	22	E	340	56	13,8	19,5	15	58	12,7	22,7	1	La Patra Mb
24	CAS6	N	139,0	41,777	0,59	C20N	11/12	31T	257975	4691523	357	24	E	18	59	10,9	20,4	44	46	11,1	19,8	1	La Patra Mb
25	MON1	R+N	47,5	41,619	0,59	C20N	9/11	31T	260535	4686825	8	23	E	195	-52	12,0	21,7	218	-41	12,3	20,7	1	Sobrarbe Fm
26	CAS7	R	105,0	41,377	0,46	C19R	10/12	31T	258412	4691197	354	21	E	207	-56	8,1	40,9	224	-41	8,3	38,4	1	Sobrarbe Fm
27	MON2	R+N	71,0	41,367	0,46	C19R	10/12	31T	260888	4686646	10	22	E	180	-59	7,5	46,8	213	-55	6,4	64,0	1	Sobrarbe Fm
28	MON3	R	39,0	41,193	0,46	C19R	11/11	31T	261090	4686522	10	23	E	193	-51	9,5	26,7	218	-45	9,3	27,5	1	Sobrarbe Fm
29	CAS8	R	11,0	41,152	0,46	C19R	3/4	31T	258754	4691296	352	22	E	205	-55	20,5	55,8	224	-41	20,6	55,4	1	Sobrarbe Fm
30	OLS1	R	122,0	41,084	0,46	C19R	9/10	31T	260618	4685394	34	25	E	215	-36	16,0	12,7	233	-32	14,8	14,6	1	Sobrarbe Fm
31	MON4	N+R	75,5	40,993	0,46	C19R	12/12	31T	261307	4686392	23	17	E	16	49	19,0	7,4	33	49	18,0	8,2	1	Sobrarbe Fm
32	OLS2	R+N	93,5	40,703	0,46	C19R	8/12	31T	260898	4685156	36	21	E	215	-32	13,4	20,5	218	-24	14,7	17,4	1	Escanilla Fm
33	OLS3	R+N	80,5	40,439	0,49	C18R	9/11	31T	261182	4684942	45	16	E	208	-16	24,4	6,1	206	-21	24,4	6,1	1	Escanilla Fm
34	OLS4	R+1N	56,5	39,777	0,49	C18R	10/11	31T	261394	4684706	91	16	E	29	36	13,2	16,0	214	-41	12,8	17,0	1	Escanilla Fm
35	ERI1	N+R	345	38,548	0,47	C18N.1n	13/18	30T	756252	4684372	130	14	S					36	55	15,6	8,7	2	Escanilla Fm
36	ESC3	N	4	37,451	0,10	≈C17N.2n	15/15	31T	262072	4683329	80	10	S	31	27	13,4	9,7	35	34	13,4	9,7	1	Escanilla Fm
37	ESC2	N	10	37,129	0,36	≈C17N.1n	10/14	31T	262256	4683133	68	13	SE	27	45	14,0	14,2	39	52	14,0	14,2	1	Escanilla Fm
38	ESC1	N	17	36,814	0,29	≈C16N.2n	11/15	31T	262320	4682955	65	15	SE	18	50	8,9	30,0	35	60	8,9	30,0	1	Escanilla Fm
39	ERI2	N+1R	279	36,401	0,36	≈C17N.1n	13/14	30T	757446	4683539	151	11	W					27	48	9,0	23,9	2	Escanilla Fm
40	ESC4	N	6	35,902	0,29	≈16N.2n	11/13	31T	262532	4682604	95	10	S	26	17	9,7	25,5	27	26	9,7	25,5	1	Escanilla Fm
41	ESC5	R	5	35,707	0,07	C16N.1r	7/11	31T	262605	4682420	85	16	S	195	21	12,5	28,5	198	-36	12,5	28,5	1	Escanilla Fm

#	Site	Pol.	Site (m)	Age (Ma)	Age E	Chron	n/N	Z	UTM-X	UTM-Y	Strike	Dip	DD	Dec	Inc	α95	k	Dec'	Inc'	α95'	k'	Source	Unit
42	ERI3	N+R	200	35,284	0,18	C15R	13/14	30T	757824	4682909	155	10	W					21	47	13,0	12,1	2	Escanilla Fm
43	ESC6	R	2	35,067	0,31	≈C15	10/10	31T	262776	4682247	85	16	S	180	-31	7,3	49,3	181	-47	7,3	49,3	1	Escanilla Fm
44	ESC7	N+1R	5	35,043	0,13	C15N	13/13	31T	262872	4682316	83	3	S	1	44	4,1	110,6	2	47	4,1	110,6	1	Escanilla Fm
45	ALM1	R+N	275	38,870	0,50	trC18R.1r/ 18N.1n	11/13	30T	753214	4681982	128	90	S					26	38	15,8	10,2	2	Escanilla Fm
46	MED1	N+R	549	41,58	0,59	C20N	14/15	30T	761828	4691753	247	26	N					17	52	14,3	9,4	2	Hecho Gp
47	MED2	N	425	40,55	0,12	C19n	14/14	30T	760233	4690298	241	18	N					27	59	9,0	22,1	2	Sobr./Esc. Fm
48	MED3	N+R	296	36,980	0,21	trC17N.3n /17N.2n	15/15	30T	760540	4686788	230, 6	11,8	NW					32	33	14,3	8,7	2	Escanilla Fm
49	MED4	N+R	359	37,240	0,42	trC17N.1r/ 17N.1n	11/14	30T	758799	4685249	183	6	W					27	46	10,2	23	2	Escanilla Fm
50	LIGz1	R+N	259	38,660	1,20	trC18R/ 18N.1n	11/14	30T	762707	4685831	227	12	N					22	42	17,9	8,2	2	Escanilla Fm
51	LIGz2	N+1R	316	36,480	0,42	trC17N.1r/ 17N.1n	11/14	30T	761430	4684836	230	9	N					24	51	12,1	16,6	2	Escanilla Fm
52	LIGz3	N+R	223	35,010	0,39	trC16N.1n /15N	14/14	30T	760173	4683885	165	11	W					22	47	14,4	9,2	2	Escanilla Fm
53	LIGa1	R+N		40,670	0,56	trC19r/ 19n	10/10	30T	743317	4706473	146	68	W	226	29	22	5	222	-38	22	5	3	Sobrarbe Fm
54	LIGa2	R	5	42,27	0,59	C20N	10/10	30T	743823	4704271	154	54	W	230	18	20	6	225	-34	20	6	3	Belsué-Atarés Fm
55	CAM1	N	5	37,99	0,72	trC18N.2n /18N.1n	6/7	31T	254105	4101043	150	20	W	5	37	21	9	346	45	21	9	3	Campodarbe Gp
56	90J25	N		41,06	0,46	C19R	4/4	31T	258700	4692000	155	7	SW	45	42	38,8	6,6	42	49	38,8	6,6	4	Sobrarbe Fm
57	90J36	N+R		42,6	0,6	C20n	5/5	31T	268000	4694000	143	17	SW	48	38	8,8	76,3	46	55	9,3	69	4	Hecho Gp
58	90J38	R		41,370	0,46	C19R	2/2	31T	259100	4692000	351	40	E	161	-66	23	120,5	224	-48	23	120,4	4	Sobrarbe Fm
59	90J39	R		50,320	0,65	C22R	5/7	31T	255900	4705000	17	15	SW	233	-57	14,1	19,2	247	-47	14,1	19,3	4	Boltaña Fm
60	JAN1	R	34	44,52	1,29	C20r	11/12	30T	746274	4705824	169	85	W	268	45	13,0	14,7	237	-39	13,0	14,7	1	Hecho Gp
61	SFE1	R	18	41,44	0,46	C19R	10/12	30T	744262	4704583	146	57	W	195	-1	12,3	18,3	168	-40	12,3	18,3	1	Sobrarbe Fm
62	SFE2	R	30	41,14	0,46	C19R	10/12	30T	744923	4704196	89	81	S	215	21	15,5	11,8	255	-44	15,5	11,8	1	Belsué-Atarés Fm
63	SFE3	R	26	40,76	0,46	C19R	8/12	30T	745062	4703986	65	78	S	199	24	11,7	32,4	246	-34	11,7	32,4	1	Belsué-Atarés Fm
64	ARB1	R	22	41,29	0,46	C19R	10/12	30T	743279	4705764	129	77	S	224	26	7,1	52,3	225	-51	7,1	52,3	1	Sobrarbe Fm
65	ARB2	N+R	20	41,67	0,59	C20N	8/12	30T	743858	4705605	130	91	S	48	-62	28,1	6,5	43	29	28,1	6,5	1	Sobrarbe Fm
66	ARB3	R	18	42,52	0,59	C20N	9/13	30T	744478	4706401	128	95	S	16	-37	9,9	37,1	9	52	9,9	37,1	1	Hecho Gp
67	ARB4	N+R	20	42,10	0,59	C20N	6/12	30T	743999	4706054	131	89	S	214	58	33,3	6,0	214	-31	33,3	6,0	1	Hecho Gp
68	ARB5	N+R	12	41,58	1,05	trC20N /19R	9/12	30T	743197	4705981	127	93	S	188	48	27,8	4,4	193	-39	27,8	4,4	1	Sobrarbe Fm
69	ARB6	R	10	40,84	0,46	C19R	12/13	30T	743289	4705323	139	76	W	212	17	11,7	16,1	193	-55	11,7	16,1	1	Belsué-Atarés Fm
70	PLA1	N+R	16	40,99	0,46	C19R	5/12	30T	743997	4704750	160	67	W	222	46	28,3	10,3	211	-17	28,3	10,3	1	Sobrarbe Fm
71	PLA2	R	11	41,44	0,46	C19R	10/11	30T	743927	4705189	150	70	W	221	22	10,0	27,0	202	-44	10,0	27,0	1	Sobrarbe Fm
72	PLA3	R	25	39,95	0,49	18R	12/12	30T	743608	4704284	155	59	W	230	-3	7,6	37,0	201	-59	7,6	37,0	1	Campodarbe Gp

Table 1. Paleomagnetic data. New and previous individual sites presented in this work and data reprocessed from Bentham (1992) and Mochales et al., (2011a). Description: # number of site; Site label; polarity; Stratigraphic thickness of sampling site; Age and Age error in M.a.; Chron; n/N: specimens considered and measured; Z: Zone; X and Y: UTM coordinates ED50; Bedding data following the right-hand rule convention; Paleomagnetic data in situ (Dec, Inc, a95 and kappa); Paleomagnetic data restored (Dec', Inc', a95' and kappa'); Source in literature (1. This work; 2. Bentham, 2000; 3. Pueyo, 2000; 4. Parés and Dinarès, 1993); Unit: Gp, Fm, Mb: Group, Formation, Member.

6.2.2. Laboratory procedures

From the 20 new sites, samples were measured by means of 2G DC-SQUID magnetometers located in the paleomagnetism laboratories of Burgos, Rome and Barcelona. The noise level in all of them was below 5 x 10^{-6} A/m. Depending on the rock type, different progressive demagnetization procedures were performed. At least one specimen per core was thermally demagnetized. Several sister samples were demagnetized by alternating field procedures, but thermal treatment revealed more efficiently ChRMs. Thermal demagnetization in marls (San Felizes area) included 12-20 steps, with the smallest increments of 20º, up to 600ºC. In detrital rocks (Eripol area), demagnetizations were performed with 20-25 steps, with key intervals of 5º, reaching 695ºC. Alternating field demagnetization followed arithmetic increments up to 100 mT. For procedures or reprocessed samples see secion 5.2.2.

To gain reliability, only high quality ChRMs derived from magnetostratigraphy were used for VAR studies (Q1, see section 5.2.2.), and 55% (687 specimens) from the total analyzed samples (1253 specimens) were rejected. Fold test was performed by means of the superIAPD software (by T.H. Torsvik, J.C. Briden and M.A. Smethurst, 1996), based on McElhinny (1964) criteria. Antiparallelism was checked by Fisher's statistics (1953). The temporal guideline considered was Gradstein et al. (2004).

Magnetic carriers were deduced from rock magnetism analyses. 2G pulse magnetizer (Rome) and 2G cryogenic magnetometer were used to perform IRM coercitivity spectrum analyses. Between 24 and 30 increasing fields up to 1.8 Tesla were applied. 13 samples (one per site) endured Lowrie's test (1990): 1.2 Tesla was applied to the z-axis, 0.3 T to the x-axis and 0.1 T to the y-axis. Subsequently, thermal stepwise demagnetization was carried out with 35º to 50ºC increments, up to 600ºC. For rock magnetism procedures of reprocessed samples see section 5.2.2.

6.3. Results

6.3.1. NRM components

The ChRMs could be isolated in the 350-580ºC temperature interval in the Lutetian slope marls and deltaic facies (Sobrarbe and Belsué-Atarés Fms) and between 360-580ºC in the fluvial materials of the Escanilla Fm (Bartonian-Priabonian). Thermal demagnetizations allowed recognizing a low-temperature component unblocking below 200ºC and AF analysis a low-field component below 10mT, which were discarded (Figure 5). For temperature intervals of the reprocessed samples see section 5.4.1.1. The magnetic mineralogy obtained form the Coscollar and San Felizes areas magnetite and iron sulphides are the responsible of the magnetization. Nevertheless, sites from Eripol area presented an assorted magnetic mineralogy constituted by magnetite, iron sulphides and hematite, according to the continental origin of the rocks (Figure 6). The magnetic carriers detected in the reprocessed samples are shown in the 5.4.2. section.

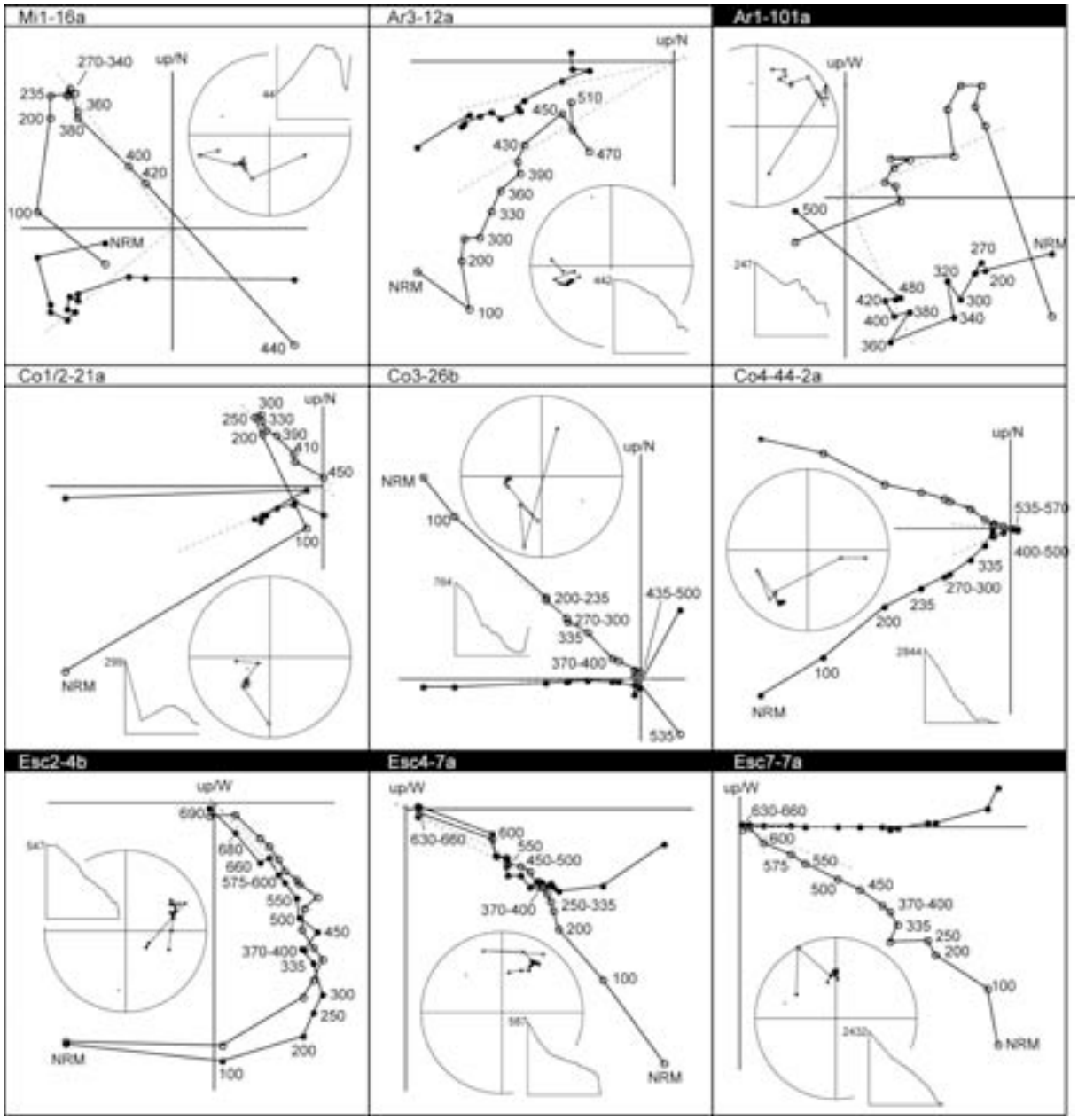

Figure 5. Representative Zijderveld (1967) diagrams of thermal demagnetizations from several sites. Diagrams are *in-situ* coordinate system MI and AR correspond to Ypresian rocks, CO to Lutetian and ESC to Bartonian-Priabonian. Stereoplots with intensity drops are shown. NRM is 10^{-6} A/m magnitude.

In total, 72 site-mean paleomagnetic mean directions were calculated (Table 1). All sites in marly units give well-defined directions, with α_{95}<9.5 (MILL1, MILL2, ARA2) and limestones remain relatively clustered (ARA1). Scattering in paleomagnetic vectors is observed for detrital sites (ARA4, 7 and 9). In the case of carbonate slope marls, clustering is observed in each site, with maximum α_{95} of 12.7 (Figure 7), except for CAS2, 3, 4 where a turbiditic channel was sampled. The upper part of the Sobrarbe Fm and the Escanilla Fm show slightly higher α_{95} angles, especially CAS8 and OLS3. ESC sites a well-defined clustering is detected. Re-processed Bentham's (1992) data offered better results grouped into stratigraphically homogeneous sets, showing acceptable α_{95} angles (Table 1).

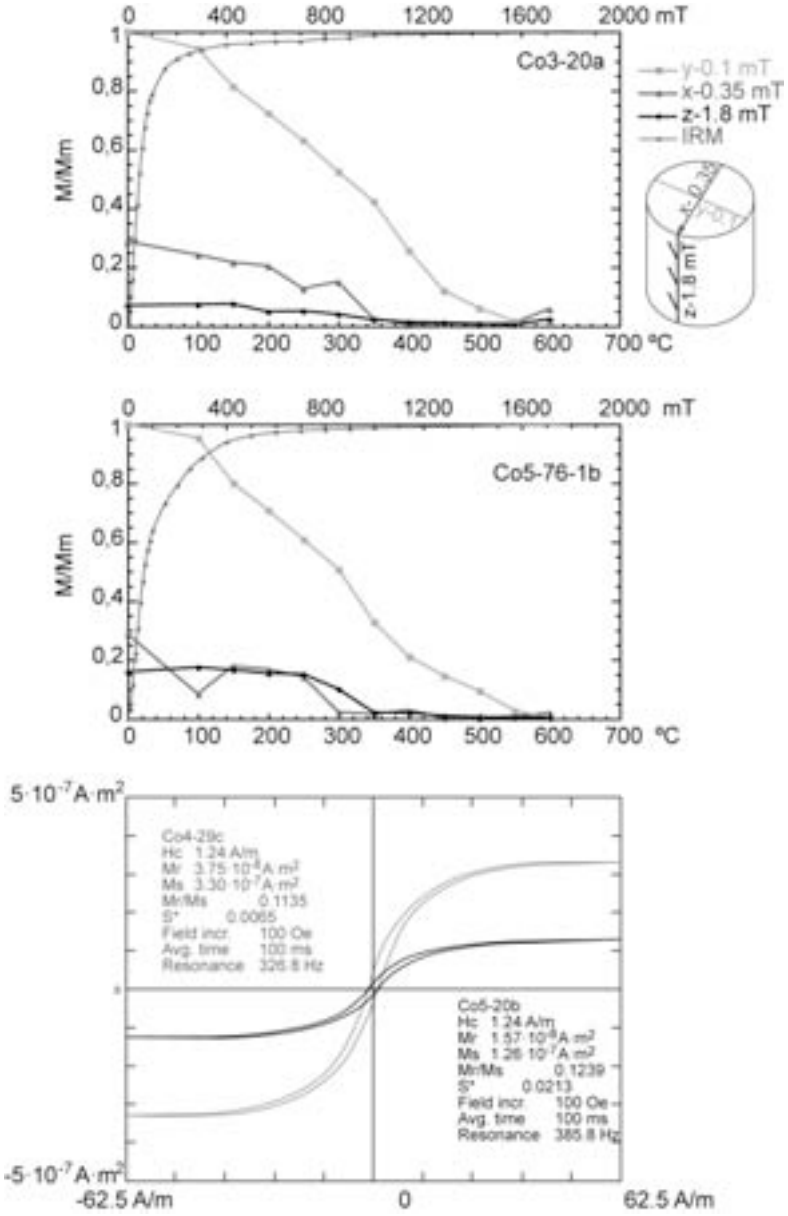

Figure 6. Rockmag analyses. a) and b) Lower abscissas are Lowrie test (1990) temperatures, upper abscissas are the increasing field (mT) applied to IRM. In ordinates, normalized remanent magnetization. c) Hysteresis loops, in abscissas the magnetic field strength and in ordinates the magnetic moment. Hysteresis loops showed low magnetic energy contained indicative of low coercivity minerals as magnetite and iron sulphides.

Therefore, most sites (≈ 70%) yielded reliable Characteristic Remanent Magnetization (ChRM) with α_{95} angles lower than 15º (both before and after bedding correction), except for 10 sites from the re-processed magnetostratigraphy (Bentham, 1992; Mochales et al., 2011a) and five individual sites from other authors (Pueyo, 2000; Dinarès, 1992; Parés and Dinarès 1993). We were able to assign a reliable age to our sites using the local chronological calibration (Chapter 5, Mochales et al. 2011a and Table 1). Finally, we derived our local paleomagnetic reference (Dec: 004.6, Inc: 53.2, α_{95}: 4.6º; k: 9.6) using the Lutetian data from the Southeastern Pyrenean foreland Basin (Taberner et al., 1999) to constraint the local VARs in the studied area (see calculation in chapter 5).

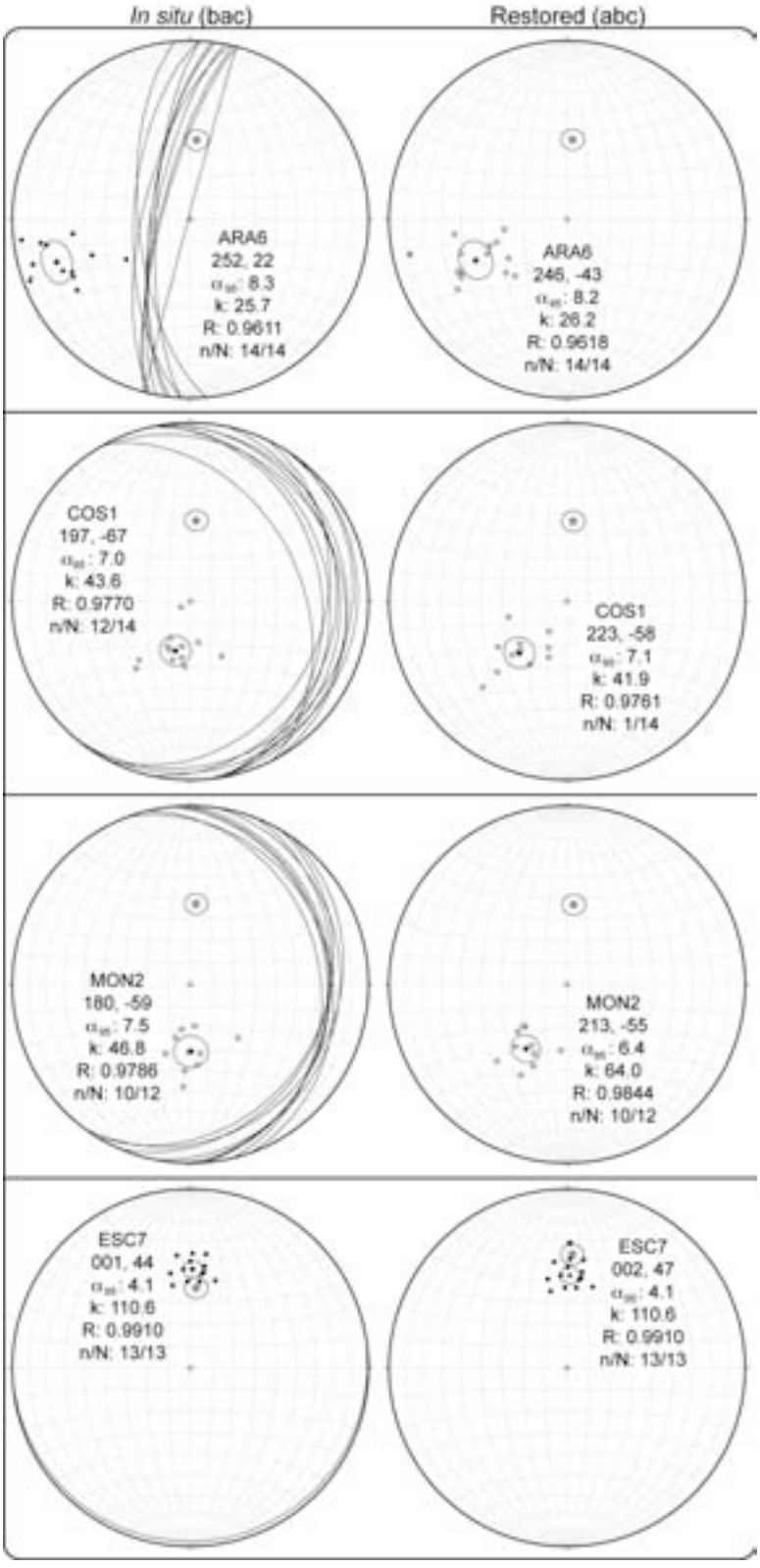

Figure 7. Some examples of site means (equal area) with Dec, Inc, a_{95}, kappa, R and n/N sites details. Left column shows *in situ* vectors (bac) with bedding, whereas right column represents restored vectors (abc). Stars indicate the Eocene reference (Dec, Inc, a_{95}: 005, 53, 4.6) calculated form Taberner et al. (1999).

6.3.2. Paleomagnetic stability

Site means were considered for the fold test. Sites are located on the western (ARA), and eastern (COS and CAS) limbs of the Boltaña anticline and western limb of the Buil syncline (MON. OLS and ESC). Only sites with α_{95} lower than 10º (*in situ*) were selected. The fold test, according to McElhinny (1964) statistics, confirms the pre-folding character of the ChRM component (Figure 8a), in agreement with several evidences in the Southernmost Pyrenean units (Dinarès, 1992; Larrasoaña, 2000; Pueyo, 2000). Due to the lack of internal deformation and the absence of restoration problems (Pueyo, 2010), except for the San Felizes sector, the slightly and non-significant synfolding character of the magnetization is probably due to an unimportant overlapping with younger components, as already pointed out in the Lutetian platform facies (Rodríguez-Pintó et al., 2011b).

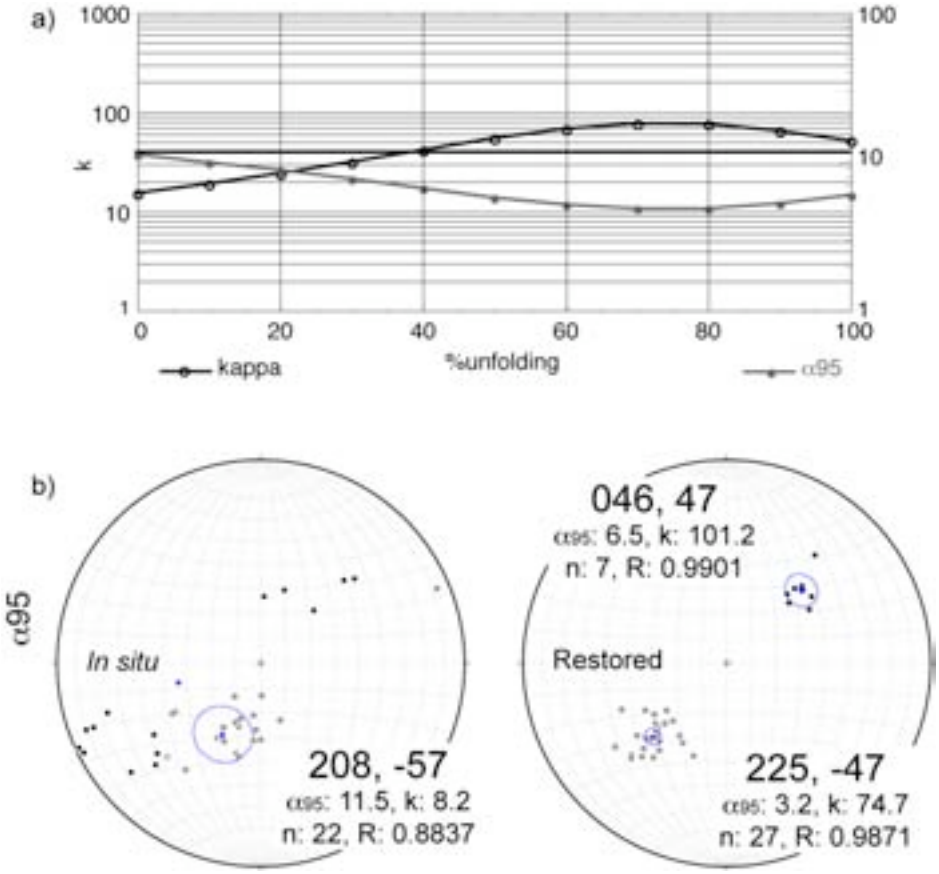

Figure 8. a) Significant fold test at 70% (McElhinny, 1964 run under SuperIAPD) performed with high quality sites (α_{95}<10º). b) *In situ* and *restored* projections also suggest a pre-folding magnetization.

Statistics of both isolated polarities (site means) reveal pseudo-antipodal directions, considering the α_{95} angles (Figure 8b): Normal: n=12, Dec, Inc= 035,47, α_{95}= 7.8, k= 34.5, R= 0.9710 and Reverse: n=29, Dec, Inc= 221,-46, α_{95}= 4.4, k= 38.8, R= 0.9751. All these evidences based on all the sites sampled in this work (ARA, COS, CAS, MON, OLS and ESC) together with the suitable pattern of reversals (Mochales et al., 2011a) indicate the primary character of the magnetization.

6.3.3. Reliability of data

Datasets in paleomagnetism have to respect some reliability criteria (Van der Voo, 1990) and be carefully evaluated to guarantee the absence of the more common sources of error (Pueyo, 2010): 1) non-existence of internal deformation (rigid body assumption), 2) a perfect laboratory isolation of components (absence of overlapping) and 3) correct restoration to the ancient reference system (not necessarily based on the bedding correction). Some overlapping of components has been observed, especially in Ilerdian rocks (Ypresian). Therefore, aiming to avoid sites with noisy signal, a strict filtering was done at the sample and site scales. From the vast dataset only samples with unambiguous interpretation and straight to the coordinates origin ChRMs were selected for VAR interpretation. Sites with anomalous inclinations and high α_{95} angles (>20°) were discarded, remaining the 68% of the original sites in the dataset (Table 1).

6.4. Interpretations

A considerable amount of studies have been carried out with the aim of clarifying the kinematics of oblique structures west of the SPCU. Nonetheless, several aspects are not solved so far. Existing data indicate clockwise rotation values ranging from 25º to 85º (Dinarès, 1992; Parés and Dinarès, 1993; Bentham and Burbank, 1996; Pueyo, 2000; Fernández-Bellón 2004; Oms et al., 2006). These authors point out a decrease of the rotation value eastwards, either due to synsedimentary character of rotation, or due to deposition of progressively younger sediments placed in less oblique positions. The accurate chronological frame of rotation of structures and the exact amount of rotation (Fernández-Bellón, 2004; Mochales et al., 2008) are not solved yet, becoming key questions for the complete 3D understanding of the geometry and kinematics of the South Pyrenean Zone.

6.4.1. Rotation magnitudes

Differences between declination angles and the expected Eocene reference in the Ainsa area (Dec: 004.6, Inc: 53.2, α_{95}: 4.6º; k: 9.6) are vertical axis rotations. Temporal-rotation relationships were established considering only the data acquired or reprocessed in this work (Figure 9). A first attempt to establish a pattern between these two variables was done using our own magnetostratigraphic dataset that almost covers the entire stratigraphic pile of the basin.

Using the best site means (only highly reliable sample and site data) confirm both observations; individual sites still display variable magnitudes of clockwise rotations ranging between +63° and -3° (non significant VAR) being +34° the global average (Figure 10a). This average is strongly influenced by a clear rotation-decreasing pattern during Bartonian times. Now is clearer since we can include our Bartonian data (ESC sites). Thus, we went one step further to reduce noise and to obtain a robust time/rotation dataset and we grouped (Fisher, 1953) the selected sites into nine 2 M.y. age-sets. The final goal was to obtain a trustworthy temporal evolution of the VAR (Figures 10b and 15c). This net picture shows clockwise rotations ranging between +52° and non-significant, with a clear pattern of decreasing rotation values in younger sediments. Nevertheless, a relative CCW

rotation of 14º is present in the first age-set, with a maximum declination close to Ilerdian-Cuisian transition. An apparent and non-significant CCW rotation of 14º appears in the first age-set, with a maximum declination close to Ilerdian-Cuisian transition. This value is caused by two anomalous sites (ARA1 and ARA2).

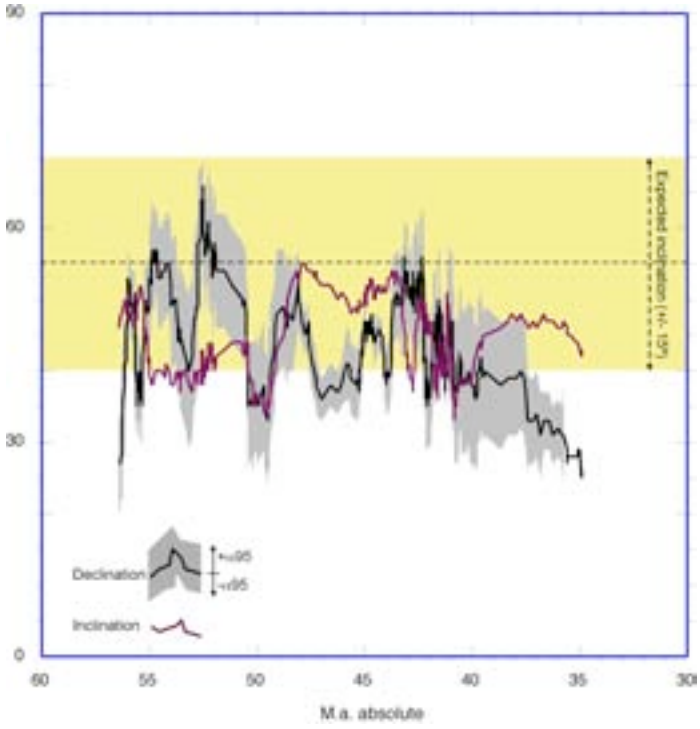

Figure 9. Running fisherian averages of the ChRM vectors (only those reliable, see criteria above) with a 25 specimens window, clearly reflects two facts: 1) the noise along the sequence (probably caused by the lithological effect), 2) a slight decreasing trend with time.

Rotational evolution fits a logarithmic curve (Figure 10). A stable trend from Ilerdian (+52°) to the Late Lutetian (+37°; giving 15º of CW VAR during this period), and an abrupt decay of rotation values from the Late Lutetian to Priabonian times (0°) are observed. Discarding the first set-age due to its irregular signal, the age-sets dispersed throughout 20 M.y. describe a well-fit logarithmic curve (R: 0.96). The adjustment gives a first trend with a gentle slope, changing at approximately 42 M.a. to a second decreasing trend until 37-38 M.a. A final and abrupt fall in the rotational value takes place from this age to the 35 M.a. The first trend would accumulate 15º of declination decay in 14 M.y. with the turning point around at 42 M.y. progressing to a pronounced downfall of 37º degrees in 7 M.y.

A logarithmic curve implies an acceleration of the movement linked to the emplacement of the related thrust sheets. The first stage would imply a gradual, low CW rotation affecting Ypresian and Lutetian rocks of the Ainsa Basin. A second stage, starting at the Late Lutetian, definitively rotated the Boltaña-Balzes sheet. Priabonian sites record paleomagnetic vectors parallel to the reference direction and therefore the end of the rotational motion. In both cases the gradual initial rotation would be related to the movement of the Ainsa Basin and the thrusting of the Boltaña sheet, probably linked to the Larra thrust development (Teixell, 1996). The subsequent, limited rotational movement would be related to the final activity of the hanging wall of the Boltaña-Balzes thrust or maybe passively recording the rotational activity of an underneath thrust sheet (Tozal-Alcanadre, defined by Millán,

1996). Once rotational movement ended, deformation migrated to the west, towards the External Sierras (Millán et al., 2000).

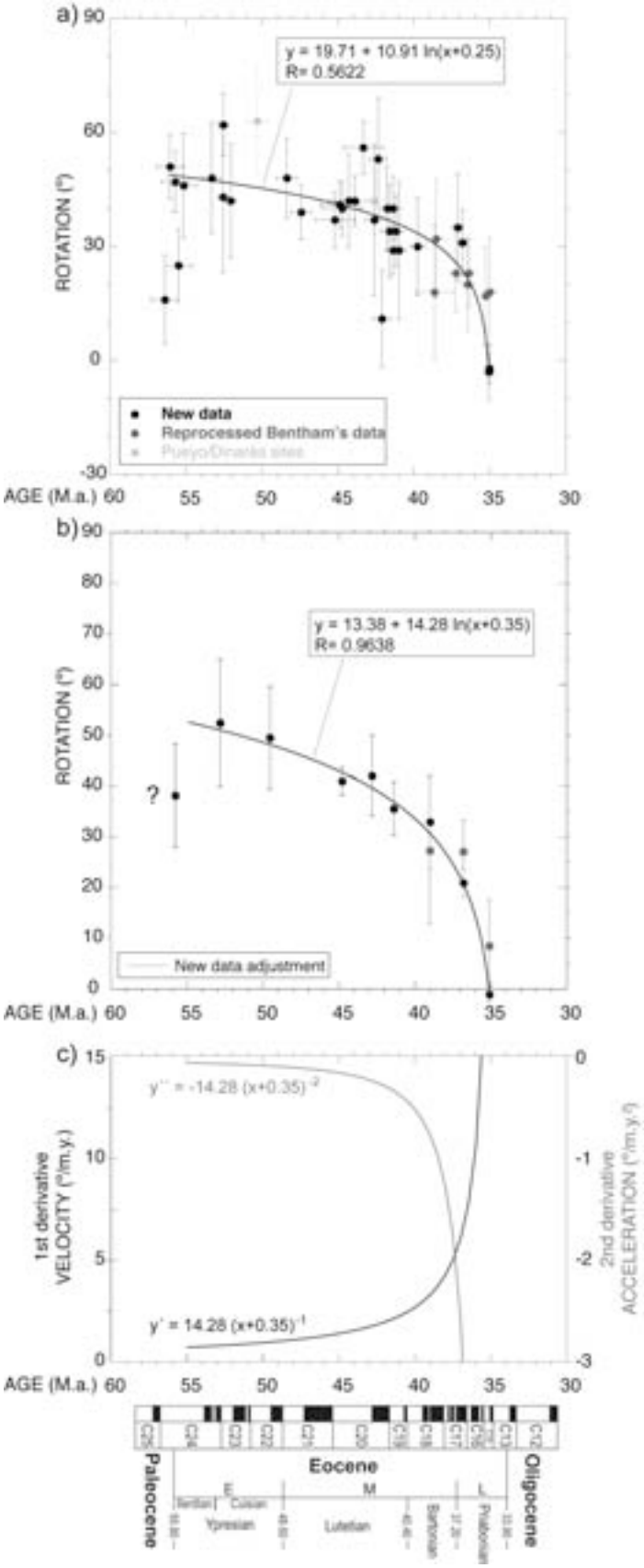

Figure 10. Rotation Vs Age (time scale according to Gradstein et al., 2004) for the results obtained. a) Black points represent the data obtained in this work, dark gray data reprocessed from Bentham's magnetostratigraphic profiles and light gray represent sites studied by other authors (Dinarès 1992; Parés and Dinarès 1993; Pueyo, 2000). In figure 10b and c, only the new data obtained in this work have been gathered into nine set-ages. Logarithmic adjustments for the rotational pattern (b) and the first and second derivatives that represent the velocity and acceleration rates respectively (c), helping to constrain the trend of the rotational deformation.

6.4.2. Rotation dating

The available chronostratigraphy based on paleomagnetic data along the entire Ainsa Basin sequence (Mochales et al. 2011a) allow us to propose a chronological frame for the rotation magnitudes. In the case of polynomial fit and considering the α_{95} angles, a first episode of moderate rotation took place from 56 M.a. to 42 M.a. (Ilerdian-Lutetian). The rotational motion would be accelerated from 42 M.y. to 35 M.y. (Late Lutetian-Middle Priabonian), with a rotation rate that progressively increase form 2.6 to 10º/M.y. (Figure 10b). Therefore the definitive rotation of the Boltaña-Balzes sheet occurred from Bartonian to Middle Priabonian. When the data are adjusted to a logrithmic fit, two different rotational rates are obtained. Considering only new (and filtered) data (Figure 10c), the first linear trend from 56 to 42 M.a. ((Ilerdian- Lutetian) shows a rotational rate of 1.2º/M.y., remaining stable through 14 M.y. during the Early-Middle Eocene. The second trend, from 42 M.a. to 37-38 M.a. shows a decreasing rate of 2.6º/M.y. The third trend occurred from 37-38 M.a. to 35 M.a. records rotational rates of 10º/m.y. in average. Then, the most important declination change would be produced from Late Lutetian to Middle Priabonian (from bottom to top of the Escanilla Fm). It is worth mentioning that all these rates fall within the range of the western Pyrenean sole thrust, where thrust rotation rates (≤10°/Ma) have been obtained (Pueyo et al., 2002; Rodríguez-Pintó et al., 2008).

A number of previous studies indicate clockwise rotations in the Ainsa Basin and the External Sierras (Figure 11 and Table 1: Bentham, 1992; Dinarès, 1992; Parés and Dinarès, 1996; Fernández-Bellón, 2004; Fernández et al., 2004). Fernández-Bellón (2004) proposed a regional 40-50º clockwise rotation in the Ainsa Basin, homogeneously accommodated from Early to Late Lutetian. In this paper, we propose a non-steady scenario with the main rotational movement younger than the one proposed by Pueyo et al. (1999) and Fernández-Bellón (2004). Rotational values remain relatively stable from Ilerdian to Upper Lutetian, with a slight decrease of 15º in 14 M.y. Afterwards, 37º of discontinuous decreasing rotation occurred from Late Lutetian to Middle Priabonian times (7 M.y.), see Table 1 and figures 10 and 11. This rotation explains the current N-S orientation of the Boltaña anticline, oblique to the WNW-ESE Pyrenean trend.

6..4. 3. Paleomagnetic sequential restoration of the western flank of the Boltaña anticline (San Felizes area).

The structural complexity in the western flank of the Boltaña anticline, partially affected by the northern limb of the Guarga synclinorium, has motivated a specific treatment of the thirteen paleomagnetic sites (168 specimens) there located (San Felizes area, Figures 2 and 12, Tables 1 and 2). Two previous sites located in the San Felizes area were also considered (Pueyo, 2000).

Within this tectono-stratigraphic frame, three different non-coaxial episodes of deformation converge in the studied region: i) The Boltaña folding affected the San Felizes area in Lutetian times. The Gavarnie basement thrust emplacement during Lutetian-Bartonian times (Séguret, 1972; Teixell, 1996) is responsible for the cover deformation in the Internal Sierras (Larra, Monte Perdido units) and

in the turbiditic trough. Frontal structures migrated southwards into the foreland forming the External Sierras, as the Boltaña-Balzes thrust sheet (Millán et al., 2000). Its oblique ramp in the northern sector, where the Boltaña anticline is located, connects NW-SE trending structures (i.e. Boltaña) with WNW-ESE Pyrenean structures (Basa anticline). ii) A subsequent Late Lutetian-Priabonian clockwise rotation (≈52°) related to the emplacement of thrusts in piggyback sequence (Tozal-Alcanadre) produced the passive rotation of the Balzes-Boltaña sheet during Bartonian to Middle Priabonian times (see section 6.4.2. and Mochales et al., 2011b). This clockwise rotation affected the entire region changing the former trend of NW-SE structures to their present N-S orientation, but this rotation decreases westwards (Pueyo, 2000; Oliva-Urcia, 2004) as attested by the gradual change in fold axes orientations in the flysch rocks. At the western limb of the Boltaña anticline (San Felizes area), there is a sequence of folds with variable trends from WNW-ESE to N-S (Figure 12 and Tables 1 and 2). This frontal deformation style is due to the Boltaña folding progression plus the re-arrangement caused by the Bartonian VAR. iii) A third stage related with the E-W Guarga basement thrust emplacement propagated from Bartonian-Priabonain (eastern portion, Martínez-Peña and Casas-Sainz, 2003) to Oligocene-Miocene times (western portion, Teixell, 1996) and eventually tilted to the South the San Felizes structures. Therefore, this region is suitable to explore how the restoration method may affect the final interpretation of paleomagnetic data in such complex scenarios. In this section, we will compare the sequential restoration (following a reverse order of deformation events) with the standard bedding correction to illustrate how large the errors can be when polyphase deformation is not taken into account.

This complex history is attested by the variability of the bedding strikes in the sampled sited, which change depending on the position within the fold system (Figure 12, Table 2). The age of the sampled rocks ranges from C20r (Middle Lutetian) to C18r (Early Bartonian) as deduced from detailed magnetostratigraphy of the Aínsa Basin (chapter 5 of this work and Mochales et al., 2011a). As the equivalent rocks from the Eastern flank (chapter 5), the characteristic magnetization (mainly borne by magnetite and iron sulphides) displays two-polarities a positive fold test and an can be considered a primary record of the ancient magnetic field. Surveyed sites were grouped depending upon their structural position to control VAR variations across the study area; eastern sites display bedding attitudes consistent with the N-S trend of the Boltaña anticline (SF1 sector); central (SF2) and western (SF3) sectors are increasingly similar to Gavarnie-related WNW-ESE structures (Figures 13, 14 and Table 3), such as the Basa anticline.

A correct restoration must follow the reverse sequence of deformation events, firstly removing the younger deformation (Guarga tilting) to finally unfold the remaining dip and paleomagnetic vectors till definitive restitution (Gavarnie related deformation). In this way, we will accomplish a real restoration to the paleogeographic reference system and the difference with the paleomagnetic reference will be the real VAR. The Guarga syncline tilted the studied area with an average N128E strike and dipping 65S. These data exclusively reflect the local Guarga deformation and were obtained from Puigdefàbregas (1975) regional mapping in the vicinity of sampling sites. Sequential restoration shows a significant variation of the VAR from E to W; 62º (α_{95}: 12.8°) at SF1 sector and, 21º (α_{95}: 14.5°) and 22º (α_{95}: 12.6°) at SF2 and SF3, respectively. This variation, based on significant differences of VAR, can be related to the diminishing influence of the Boltaña anticline rotation (≈52º) in favour of the WNW-ESE Pyrenean deformation (Figure 14), where rottions are smaller (≈21º, Basa anticline rotation; Pueyo, 2000).

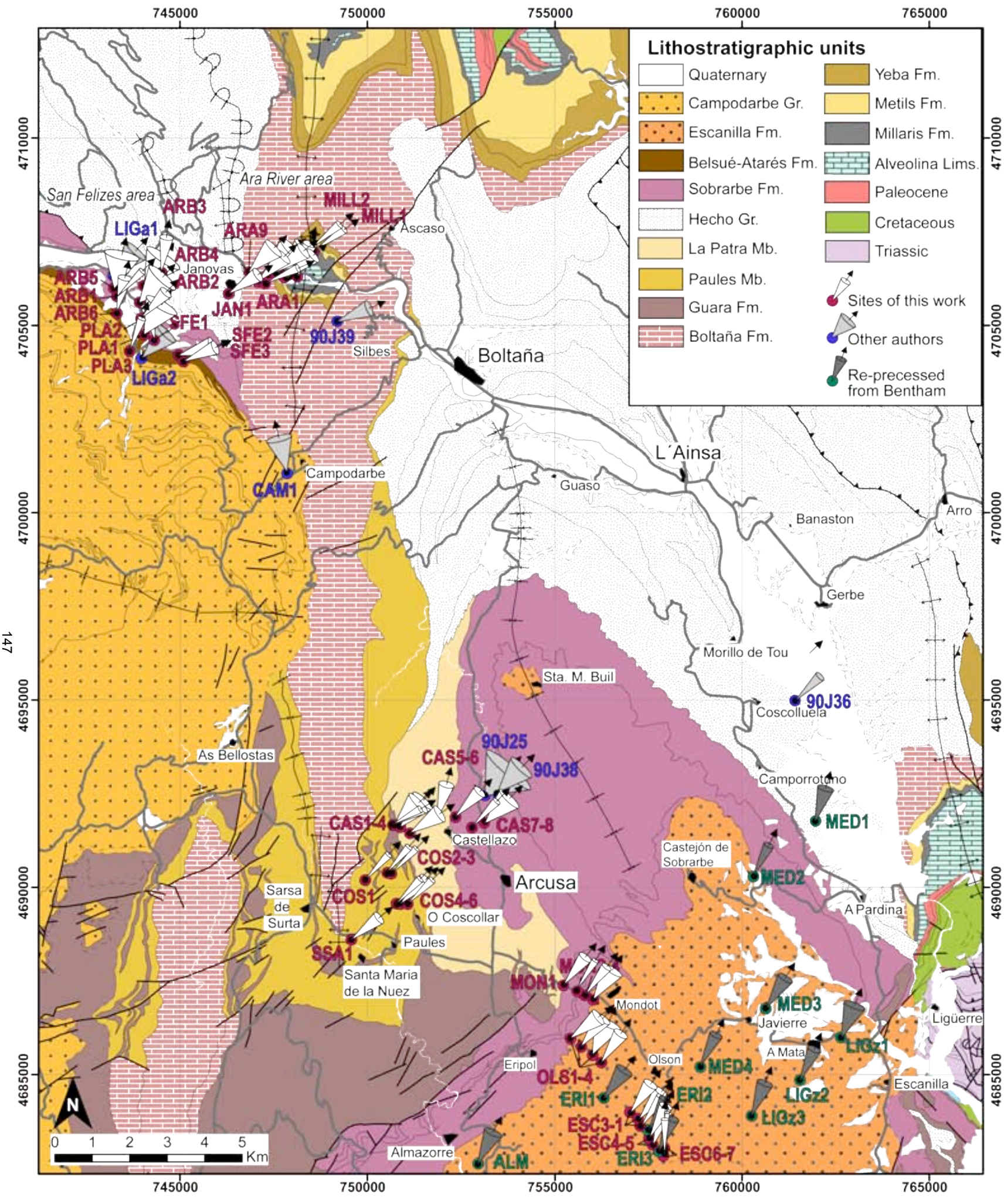

Figure 11. Rotations in map view (axes of the cone represent the magnetic declination, semiapical angle of the cones is the α_{95}). Cartographic base from Barnolas et al. (*in press* a, b)White cones represent the data obtained in this work. Reprocessed Bentham's data are shown in dark grey. Data from Dinarès (1992), Parés and Dinarès (1993) and Pueyo (2000) are represented in light grey. Map modified form Barnolas et al. (in press a and b). UTM projection, ED50, zone 30T. For higher resolution see Appendix 3.

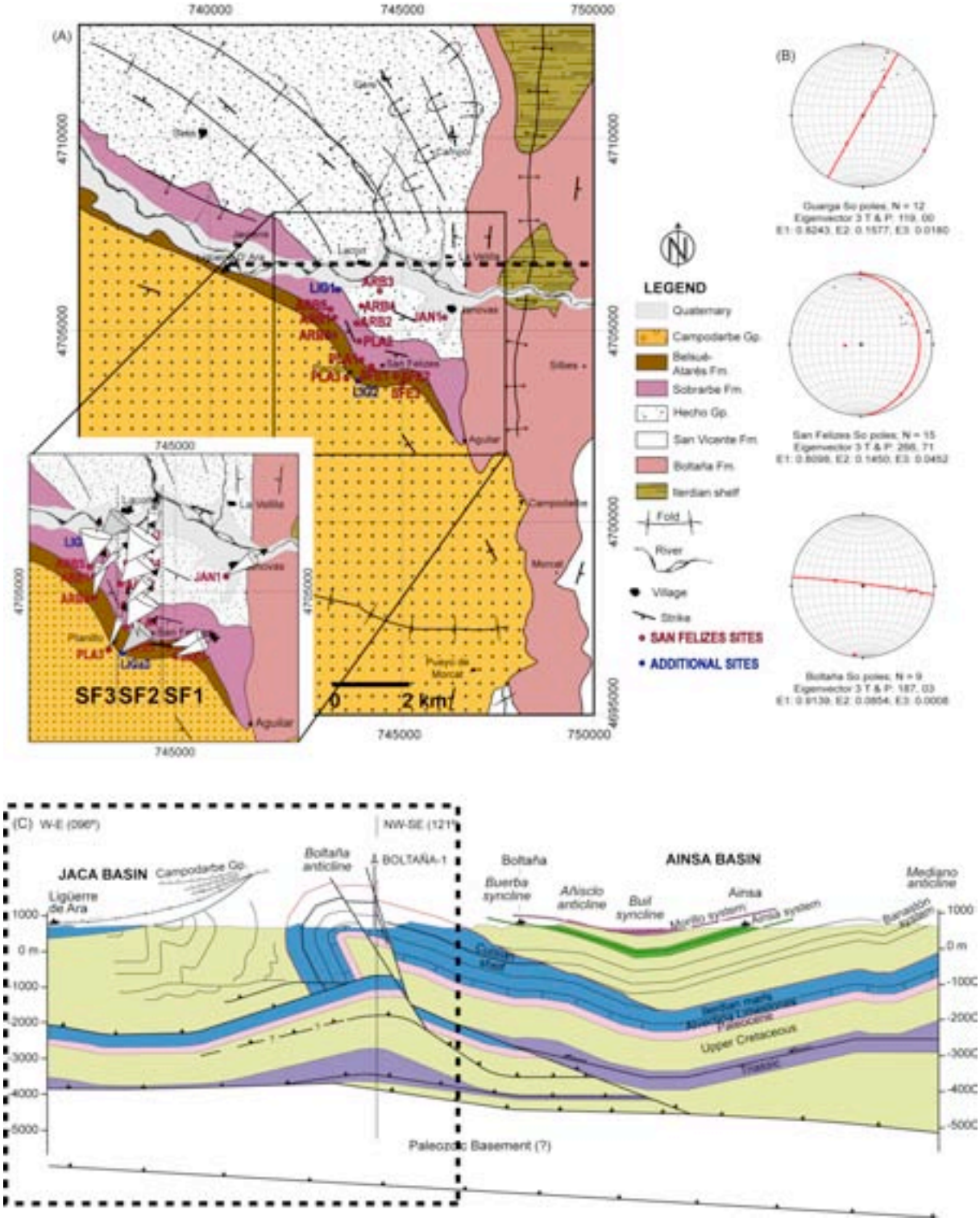

Figure 12. A) Simplified geological map of the San Felizes area, modified from Barnolas et al. (*in press* a). VAR sites are depicted as points. UTM Coordinate system, datum ED50, zone 30T. B) Bingham (1974) fitting statistics of fold axes for the three sectors. Data from Boltaña come from Ara River sites, San Felizes site and Guarga axis from Barnolas et al. (*in press*). C) Cross section of the Boltaña anticline (Fernández et al., 2004).

	Site	Strike	Dip	D D		D (bac)	I (bac)	a95 (bac)	K (bac)	D (abc)	I (abc)	D (aGc)	I (aGc)	Strike (aGc)	Dip (aGc)	DD aGc)	D (aTc)	I (aTc)	Formation
SF1	JAN1	169	85	W		268	45	13,0	14,7	267,2	-39,4	251	-6,5	197,9	44,1	W	237,4	-39,4	Hecho Gp
SF1	SFE3	65	78	S		199	24	11,7	32,4	204,9	-33,9	195,9	-37,7	38	60,6	E	245,7	-33,9	Belsué-Atarés Fm
SF1	SFE2	89	81	S		215	21	15,5	11,8	228,3	-43,6	214,1	-43,9	54,4	40,4	S	255,4	-43,6	Belsué-Atarés Fm
SF2	ARB3	128	95	S	o	16	-37	9,9	37,1	8,8	52,2	18,8	24,6	128	30	S	8,8	52,2	Hecho Gp
SF2	SFE1	146	57	W		195	-1	12,3	18,3	177,1	-40	171,7	-57,3	249,1	17,6	N	167,9	-40	Sobrarbe Fm
SF2	PLA1	160	67	W		222	46	28,3	10,3	230,1	-16,5	220,9	-18,9	220,8	29,2	W	211,4	-16,5	Sobrarbe Fm
SF2	ARB4	131	89	S		214	58	33,3	6,0	216,7	-30,7	215,9	-6,9	135,3	24,2	W	214,4	-30,7	Hecho Gp
SF2	LIG2	154	54	W		230	18	20	6	227,8	-34,4	234,4	-45,4	250,4	24,8	N	215,2	-34,4	Belsué-Atarés Fm
SF2	PLA2	150	70	W		221	22	10,0	27,0	215,2	-44,1	221,8	-42,9	208,6	20,9	W	201,7	-44,1	Sobrarbe Fm
SF2	ARB2	130	91	S	o	48	-62	28,1	6,5	44,3	28,7	42,7	2,6	132,6	26,1	S	42,7	28,7	Sobrarbe Fm
SF3	PLA3	155	59	W		230	-3	7,6	37,0	215,2	-58,6	247,6	-65,1	238,3	24,5	N	201,1	-58,6	Campodarbe Gp
SF3	ARB6	139	76	W		212	17	11,7	16,1	200	-54,7	209,5	-47,6	173,3	15,1	W	192,7	-54,7	Belsué-Atarés Fm
SF3	ARB1	129	77	S		224	26	7,1	52,3	226,1	-50,7	224,9	-38,7	132,7	12	S	225,4	-50,7	Sobrarbe Fm
SF3	LIG1	146	68	W		226	29	22	5	224,9	-38,1	226,6	-35,5	211,4	16,8	W	214,1	-38,1	Sobrarbe Fm
SF3	ARB5	127	93	S	o	188	48	27,8	4,4	192,5	-38,6	198	-12,2	125,9	28	S	193,3	-38,6	Sobrarbe Fm

Table 2 Paleomagnetic data of individual sites arranged from E (SF1) to W (SF3) with Site: site label; n/N: number of specimens considered/measured; Pol: polarity; m: stratigraphic thickness of the site; Age and Age E: Age and Age error in M.y.; Chron; UTM coordinates in ED50, Zone 30; Strike, Dip, DD: bedding (rhr); o: overturned beds; Paleomagnetic data in situ (bac), after simple correction (abc), after Guarga correction (aGc), partial restoration of So (So-aGc), after total correction (aTc); Formation.

Simple bedding correction also indicates a gradual but moderate decrease in rotation means from E to W: 49º (α_{95}: 39.5°) for the eastern SF1, 30º (α_{95}: 15.1°) for SF2, and 28º (α_{95}: 13.3°) for the western SF3 sector (Table 3). Data in the hanging wall of the Boltaña thrust (ARA sites, Table 1) display similar rotation values (42° +/- 6°). Taking into account their confidence angles, they could fit into the expected rotational magnitude. However, stronger internal scattering in all sectors arises when superposed folding is not taken into account (α_{95} > 13º), figure 14. Comparing the results, the sequential restoration seems to give better results. An important increase of the error angles is produced, especially in SF1 sector (almost 40°) and requires special attention. Here, one of the sites (JAN1) records -30° of apparent (spurious) rotation in one of the flanks, whereas the other flank (two sites; SF2&3) records up to +41° of error. In the case of SF2 and SF3 means they present a better-defined clustering and a moderate decreasing of the α_{95} angle (≈1°).

In general, VARs derived from simple bedding correction are larger, in absolute value, than those coming from the sequential restoration (Table 2), and the spurious component (error) is clockwise. The difference between them (error) is larger for increasing magnitudes of VARs, although this is controlled by their structural location (Pueyo, 2000).

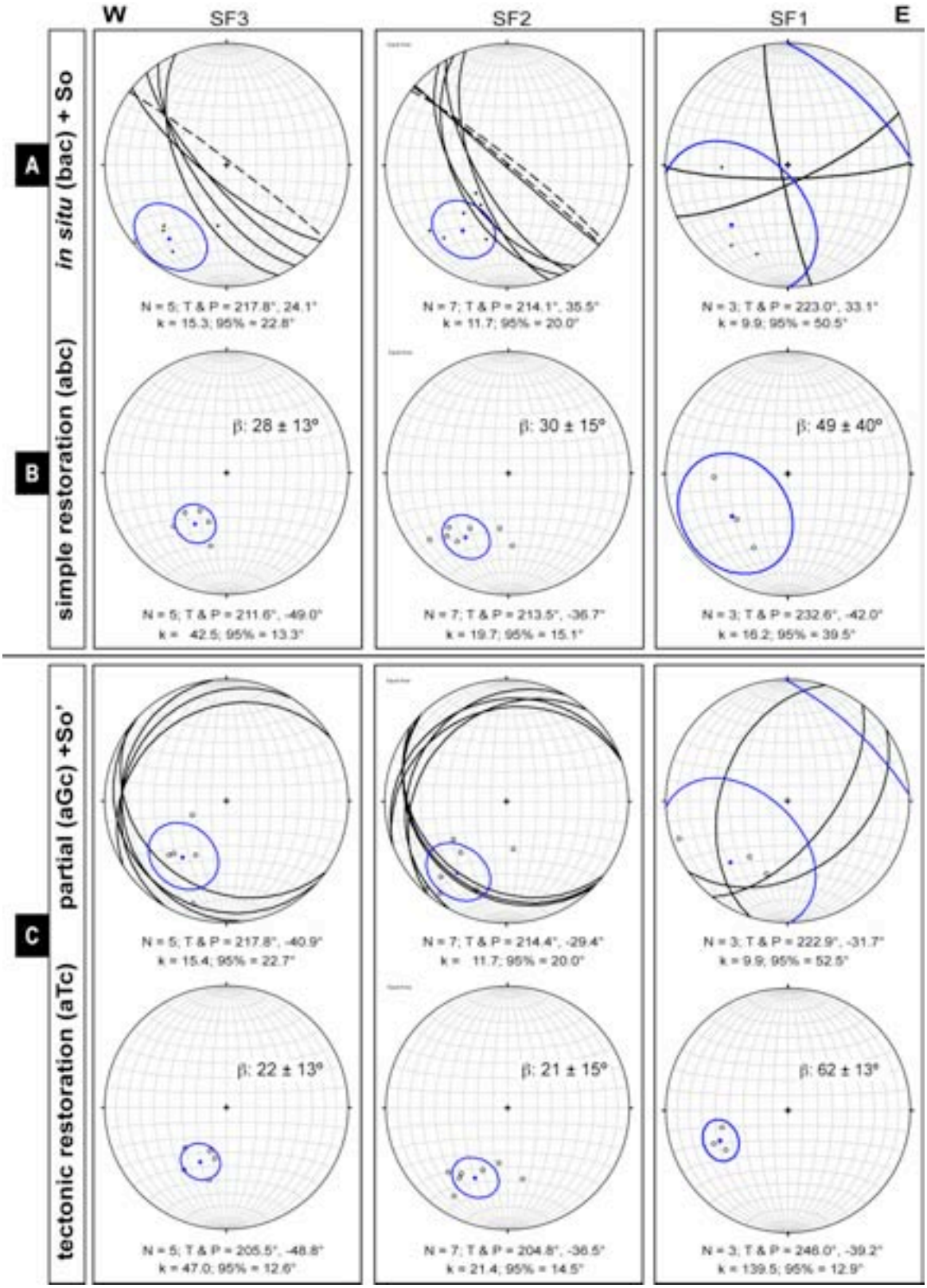

Figure 13. Restoration A) *In situ* (bac) Fisher (1953) means by W-E sectors with bedding field data. Overturned beds are shown with dashed lines. b: Vertical Axis Rotations (VAR). B) Simple restoration (abc) stages are presented. C) Sequential fold axis correction by W-E sectors. First stage after Guarga untilting with partial bedding (aGc+So') and total restoration, removing the remaining deformation to the non-deformed stage (aTc). b: VAR.

	bac				abc				aGc				aTc			
E-W Sector	Dec	Inc	α95	k	Dec	Inc	α95	k	Dec	Inc	α95	k	Dec	Inc	α95	k
SF1 (E)	223	33	52,5	9,9	53	42	39,5	16,2	43	32	52,5	9,9	66	39	12,9	139,5
SF2	214	36	20,0	11,7	34	38	15,1	19,7	34	29	20,0	11,7	25	37	14,5	21,4
SF3 (W)	218	24	22,8	15,3	32	49	13,3	42,5	38	41	22,7	15,4	26	49	12,6	47,0

Table 3. Paleomagnetic data (E-W sectors means). *In situ* (bac); after simple correction (abc); after Guarga correction (aGc); after total correction (aTc).

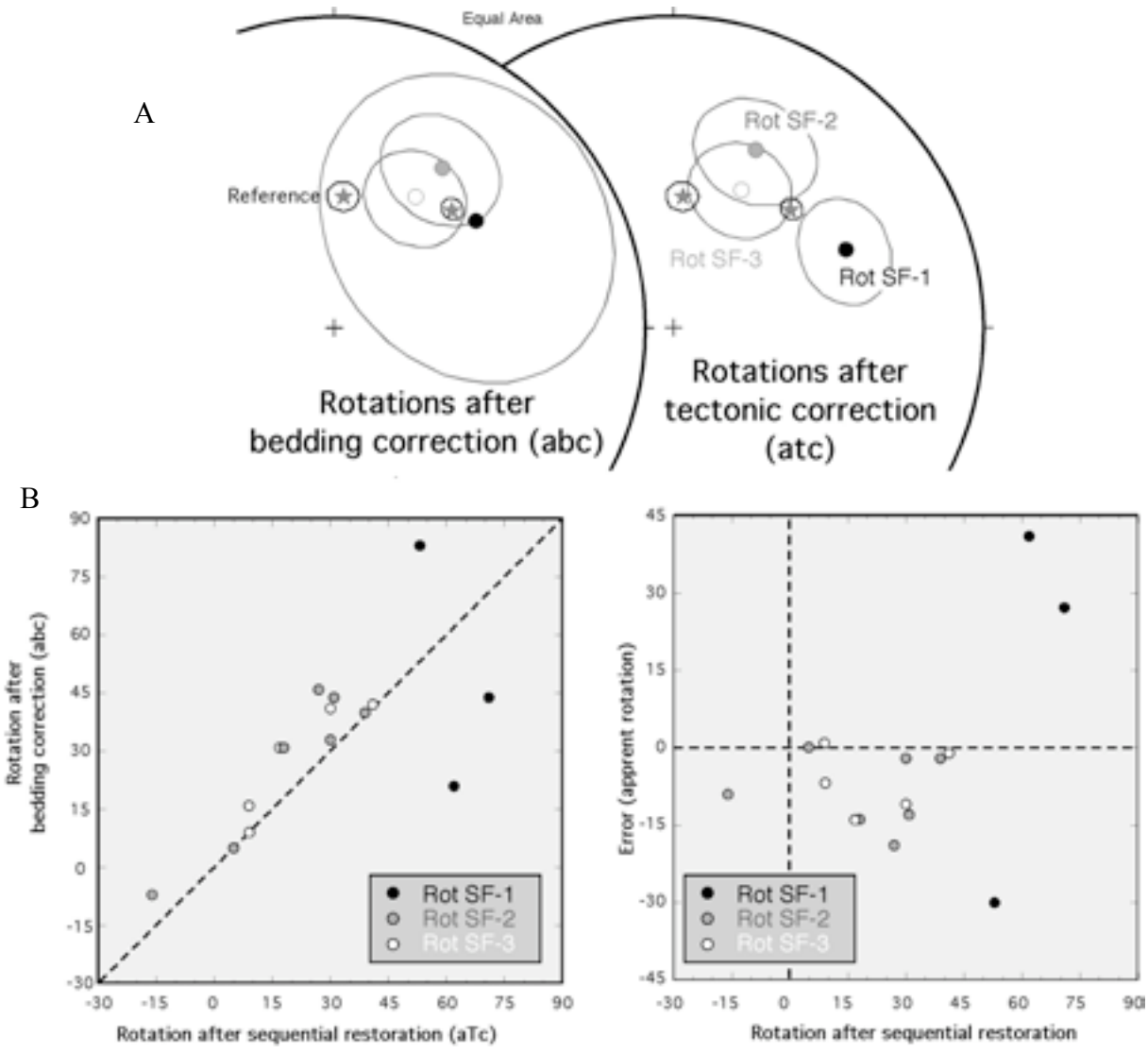

Figure 14. A) Stereographic projection of sector means for both situations. Eocene reference is DEC: 005, INC: 53; a_{95}: 4.6° (calculated from Taberner et al., 1999). Mean rotation of the Boltaña-Aínsa hangingwall (Mochales et al., 2011b) is also projected for comparison. B) Error analysis. Comparison of VARs after bedding correction and sequential restoration in a superposed folding area.

6.4.4. Paleocurrents and fold axis restoration

The results obtained allow for paleogeography of the Aínsa basin during the Eocene to be reconsidered. Taking into account paleomagnetic information, paleocurrents were restored to their original configuration before the rotation of the Boltaña anticline. Compiled data include 70 directions from Van Lunsen (1970), 28 from Mutti (1985), 29 from De Federico (1981), and 43 from the Barnolas et al. (*in press a*), considering bedding correction. Paleocurrents present S-N trends to the East of the Boltaña anticline, clearly defined in the south since they represent proximal areas of the continental margin, changing to a northwards NW trend due its distal position. To the west they show ESE-WNW trends (Figure 15).

After rotation restoration, considering the obtained rotation magnitudes, paleocurrents become ESE-WNW with scattering towards the SE (figure 15b) and better clustering. Therefore an ESE-WNW trough in the Buil syncline can be interpreted for the marine Eocene deposits. The Boltaña anticline would be nucleated in Early Lutetian times (Mochales et al., 2010), but not emerged, permitting connection between its limbs during Early-Middle Lutetian times. During the Lutetian-Bartonian boundary, once the main rotational motion began, rocks located on the Boltaña-Balzes sheet rotated. Paleocurrent directions remained fairly constant (WNW-ESE) as witnessed by the directions indicated by the slightly rotated sediments of Bartonian age.

The Boltaña anticline fold axis can be restored in a similar way. Its present-day N004E trend (Mochales et al., 2010) has to be restored considering that its bulk clockwise rotation accommodates in two pulses (15° Cuisian-Middle Lutetian + 37° Late Lutetian-Priabonian = 52º, considering the Eocene reference). Therefore a N128E orientation would be its original trend during the onset of deformation. In any case, this orientation would be slightly oblique to the main Gavarnie trend (E-W to WNW-ESE) according to previous interpretations based on the obliquity caused by the thickening of the sedimentary pile (Soto et al. 2001 and 2002).

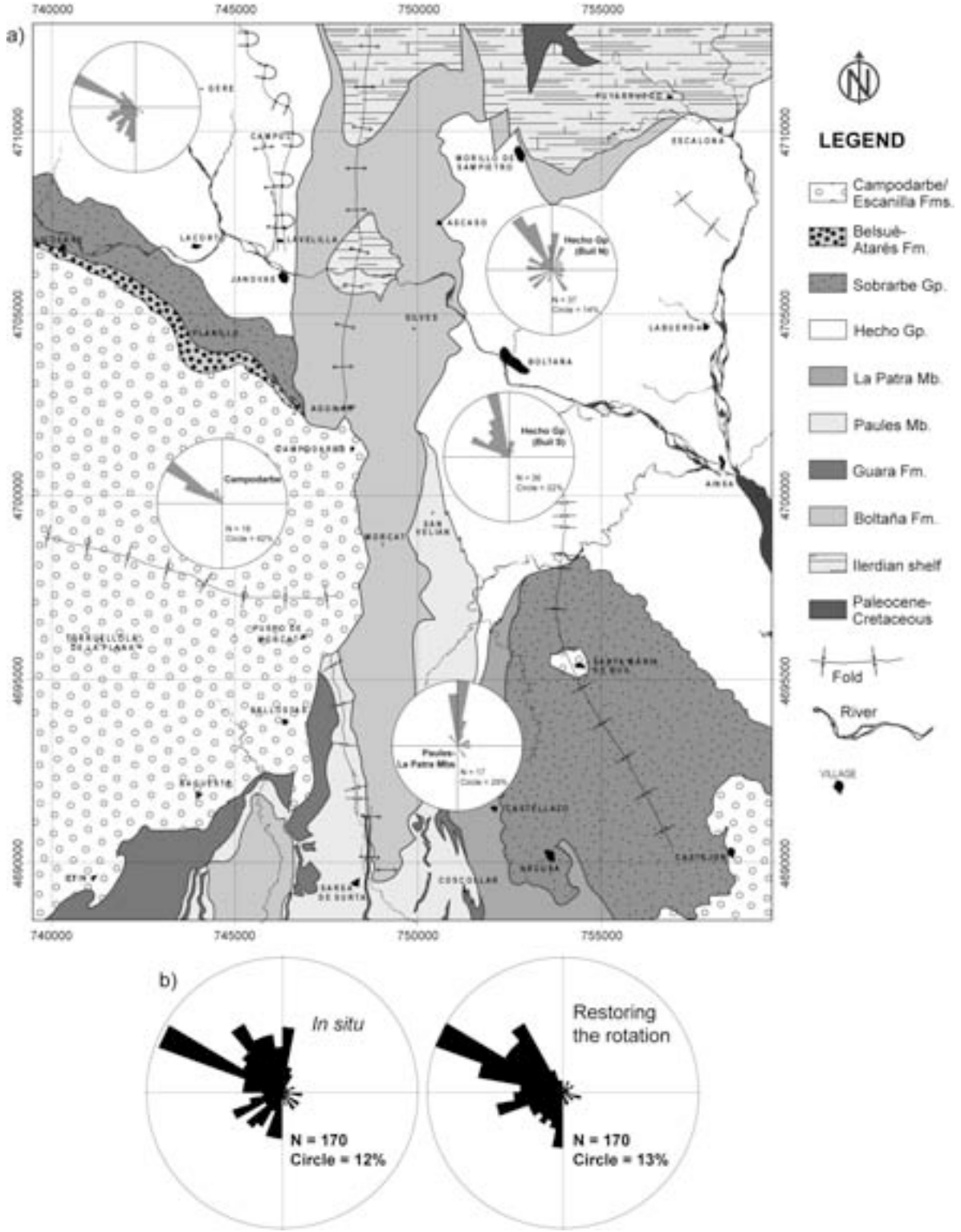

Figure 15. a) Paleoflows represented according to their lithostratigraphic position and geographic location, considering bedding restoration. b) Ensemble of paleoflow directions *in situ* (considering bedding) and restored according to the value of vertical axis rotation in each point. A better grouping of them is observed after rotation restoration.

A similar analysis can be done for the orientation of the fold axes to the West of the Boltaña anticline, paying special attention to the San Felizes area. Trends from the Basa (Larrasoaña et al.,

1996) and Boltaña (Mochales et al., 2010) anticlines and the Guarga syncline (Pueyo, 2000) were also considered in a wider regional frame. They show a variable pattern along a W-E section (present day coordinates), as denoted by the geological maps of the area (Figure 16). It is worth noticing that all significant plunges disappear from the San Felizes interference zone after the removal of the Guarga tilting (Figure 16).

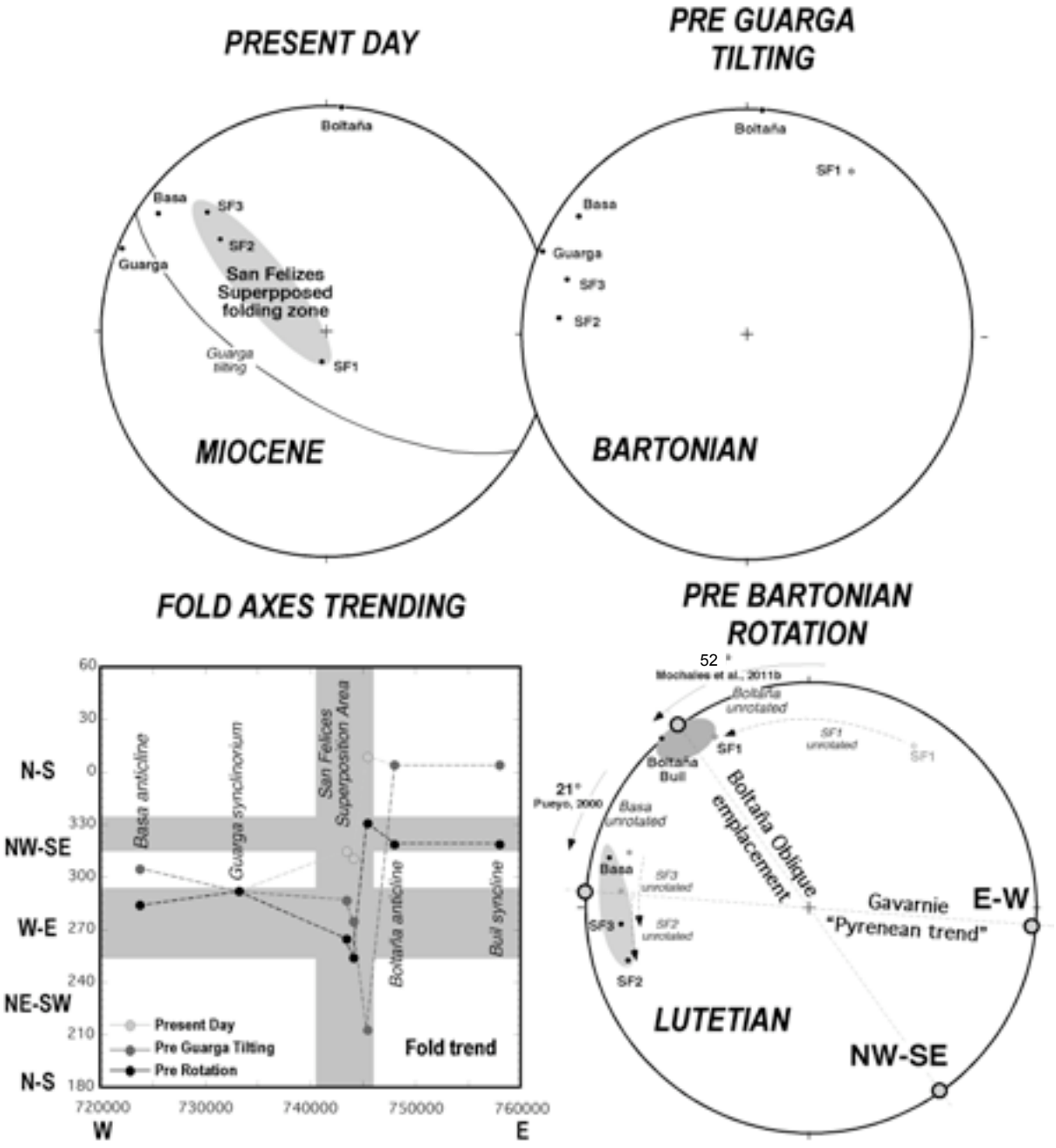

Figure 16. Sequential restorations of fold axes in the region after considering both the Guarga tilting (affects only the studied area) and the VARs. The box represents the geographic W-E plot versus fold axis trend for the three deformational stages. In the equal area stereoplots, the sequential restoration (step by step from Lutetian to Miocene) is shown. All vectors normalized to the lower hemisphere.

These fold axes can be restored for the known VAR, taking into account the 21° CW rotation of the Basa anticline (Pueyo, 2000), the 52° CW rotation of the Boltaña anticline (defined in section

6.4.1. and Mochales et al., 2011b) and the data acquired in SF1 and SF2+SF3. After restoring these VARs we obtain the attitude of fold axis during the Lutetian. SF2 and SF3 fold axes tend to converge with the Basa orientation (the Pyrenean trend related to the Gavarnie thrusting and folding during Lutetian times). Conversely, SF1 approaches the Boltaña and Buil orientations (NW). Both sets are distinct and better clustered after the total removal of deformation (pre rotational stage) and are clearly consistent with the oblique original emplacement of the Boltaña thrust sheet (Figure 14a).

7. Anisotropy of magnetic susceptibility record of the kinematics of the Boltaña anticline

7.1. AMS as kinematics indicator

Magnetic fabric is expressed as a magnetic ellipsoid and is usually related to mineral preferred orientation (finite or infinitesimal depending upon the deformation intensity and the magnetic mineralogy). Optimal conditions are found in dominant-paramagnetic and low susceptibility rocks, where the ASM reflects the preferential orientation of the phyllosilicates. Taking into account that clay minerals (the main component of most pelitic rocks) are paramagnetic, the magnetic fabric can be interpreted in terms of mineral preferred orientation since the magnetic ellipsoid fits the crystallographic fabric in most common phyllosilicates (biotite, muscovite and chlorite; Martín-Hernández and Hirt, 2003 and references therein).

Interpretation of rock fabric must nevertheless take into account the particular deformational conditions of rocks in their structural setting, especially when the shape of the bulk magnetic ellipsoid does not fit the shapes of ellipsoids of individual grains, implying that the magnetic fabric is the result of the interaction of orientations of different grains. Therefore, cautiously interpreted, AMS represents a useful tool to determine some parameters of deformation in weakly deformed sedimentary rocks, and it is particularly sensitive where the deformation intensity is beneath the minimum threshold for most geological strain analysis techniques (Hrouda, 1982; Borradaile, 1988; Borradaile and Henry, 1997; Mattei et al., 1997; Parés and van der Pluijm, 2002; Soto et al., 2003; Oliva et al., 2004).

In tectonically deformed rocks (and magnetic fabric associated to paramagnetic minerals), the main axes of the susceptibility often coincide with main deformational directions, determined by conventional strain markers. The ellipsoid of the magnetic susceptibility is coaxial with the finite strain ellipsoid (Rathore, 1979; Hrouda, 1982; Borradaile, 1991; Dinarès et al., 1992). In areas subjected to compressional deformation, such as thrust-and-fold belts and inverted basins, the magnetic fabric of apparently undeformed or weakly deformed rocks is usually controlled by folding or layer-parallel shortening (LPS) (Kissel et al., 1986; Lowrie and Hirt, 1987; Averbuch et al., 1992; Sagnotti et al., 1998; Parés et al., 1999; Parés and van der Pluijm, 2002; Larrasoaña et al., 2003). The magnetic lineation (mineral elongation) is then parallel to the stretching direction, which is usually parallel to the fold axes or perpendicular to the LPS (Hrouda, 1982; Pueyo et al., 1997; Larrasoaña et al., 1997; Sagnotti et al., 1998; Soto et al., 2003). Moreover, when subsequent deformation is not very intense (i.e. in areas beyond or above the cleavage front), the magnetic fabric acquired in early diagenesis behaves as a passive marker during subsequent deformation (Larrasoaña et al., 2004; Soto et al., 2008; Oliva-Urcia et al., 2009; Pueyo-Anchuela et al., 2001). These snapshots allow the early history of rock deformation to be deciphered.

Among the numerous AMS studies performed in southern Pyrenees, the most relevant to our study is Dinarès and Parés (1992) since it is located in the Aínsa Basin. This study inferred that an

increase of the deformation is observed from S to N, as attested by foliation in northern outcrops. Southern sites revealed sedimentary magnetic fabrics affected by flattening. Northern N-S structures seem to define the coaxial orientation of the lineation of the magnetic fabric, presenting prolate ellipsoids. Once reached the cleavage front, the minimum axes of the magnetic ellipsoid is disposed perpendicular to the clevage plane.

Our aim is therefore to verify the imprint of the deformation in the magnetic fabric far away from the cleavage front. The extensive dataset sampled throughout the Aínsa Basin in this work will allow us determining the fluctuations of the magnetic fabric *Vs* the stratigraphic height (along time). The main objective was to determine if some thrusting episodes of the Boltaña anticline related to compression could be characterised by means of AMS analysis, assuming that the blocking of the magnetic fabric is a relatively early process during the diagenesis of sediments. The importance of using this tool lies in the fact that, despite the long and relatively complex tectonic history and the syntectonic materials involved, there are very few options or techniques in empirically determining the kinematics of folds when located ahead of the cleavage front. Therefore, AMS is here used as an independent and sensitive indicator of mineral preferred orientation related to the kinematics of the deformation processes (i.e. folding).

7.2. AMS methods

7.2.1. Sampling

The methodology used is aimed at the accurate study of the magnetic fabric during the deformation history of the Boltaña anticline by means of profiles located on both limbs of the fold. These profiles include a continuous stratigraphic succession deposited during 13 Myr. The unusually large amount of data originally collected for magnetostratigraphy allows for changes in the trend and shape of the magnetic ellipsoid to be studied along the sedimentary pile. Both limbs were sampled to detect possible asymmetries in the deformation and, therefore, the development of the fold that would help to independently constrain the existing kinematic models for the Boltaña anticline. The rocks at the sampled profiles are not strongly deformed, as they are clearly located beyond the cleavage front (Choukroune and Séguret, 1973; Holl and Anastasio, 1995a) and, therefore, they do not show penetrative structures at outcrop or microscopic scales.

Samples were taken along continuous stratigraphic sections of the pre- and syn-tectonic sequences. From the profiles sampled with magnetostratigraphic aims, the sections named Ara (Ar1), Coscollar (Co1 to 6) and Mondot (Mo1) were analyzed with AMS aims (Figure 1a). Sampled lithologies comprise limestones, marls and sandstones, although preference was given to fine-grained sedimentary rocks in order to optimize the AMS results. 688 cores were drilled along the Lower Ypresian- Upper Lutetian (Lower and Middle Eocene), with a sample every 2.7 m of stratigraphic section on average (Figure 1a). From each core, two to four specimens were analysed, being altogether 1454 specimens for AMS purposes. To reduce noise in the data, specimens were grouped in 60 lithologically homogeneous and stratigraphically continuous AMS sites, each comprising 24 specimens on average (Table 1), these criteria were mostly coincident to those applied in the previous chapter 6 (rotations).

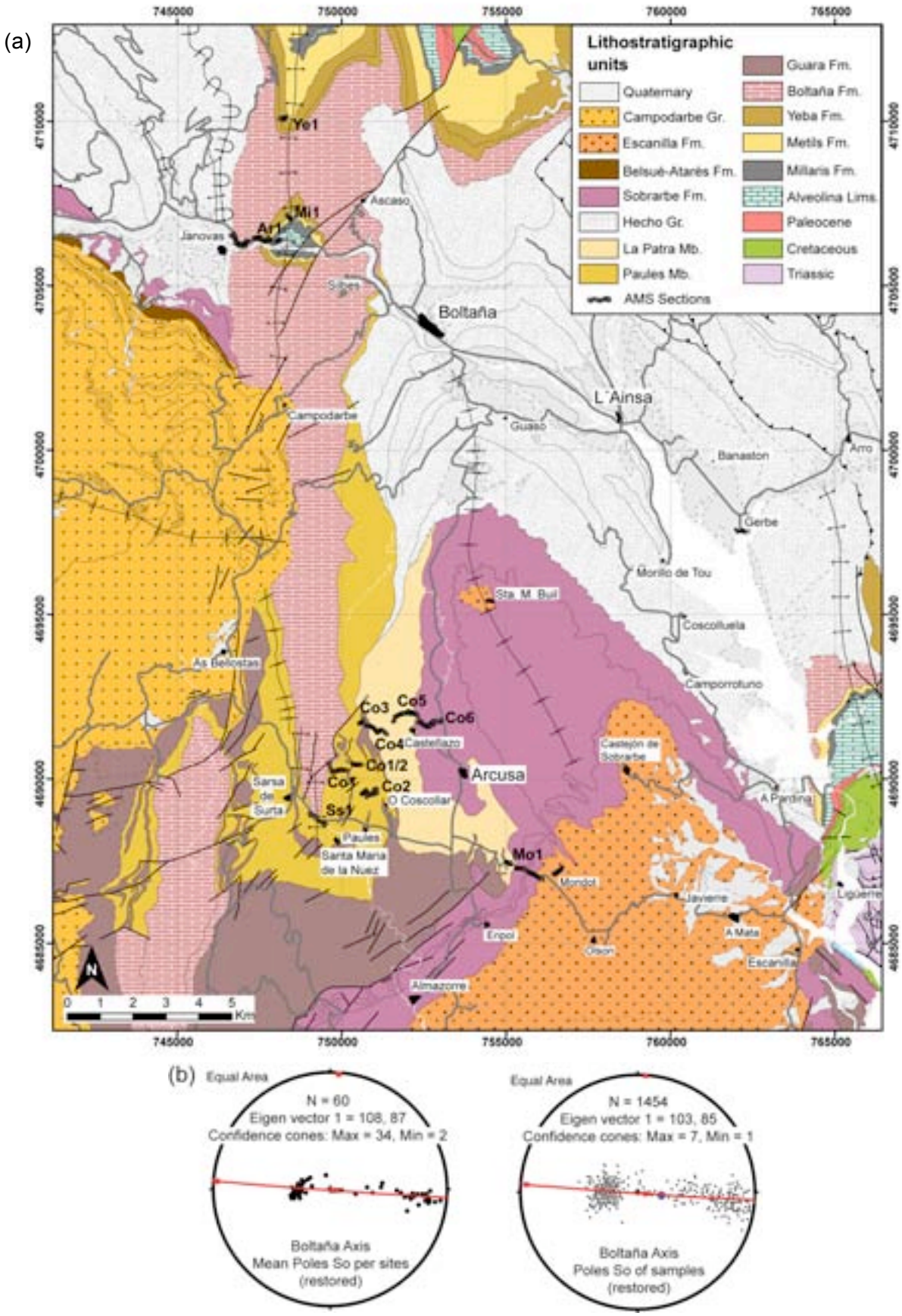

Figure 1. (a) Geological map of the studied area, modified from Barnolas et al. (in press a and b). AMS sections (Ar1, Co1 to 6 and Mo1) are located. UTM ED50, zone 30T. (b) Stereoplots showing bedding poles orientation of the Boltaña anticline; left: site mean bedding poles, right individual bedding poles (sample scale) altogether.

Site	n	Height	TZ	UTM-x	UTM-y	Strike	Dip	DD	Lithology	Formation	Age	Km	KMX-Ds	KMX-Is	KMX-Dr	KMX-Ir	KMN-Ds	KMN-Is	KMN-Dr	KMN-Ir	P'	T
BO01	22	16	31T	254795	4706176	177	26	W	Limestones	Alveoline L.	Early Ilerdian	2,39E-05	208	15	213	11	71	71	301	81	1,037	0,192
BO02	30	63	31T	254764	4706173	185	30	W	Limestones	Alveoline L.	Early Ilerdian	9,02E-06	223	20	230	11	76	65	327	80	1,120	0,138
BO03	23	75	31T	255268	4706843	191	18	W	Marls	Millaris	Middle Ilerdian	5,13E-05	209	2	33	3	300	80	288	62	1,023	0,436
BO04	25	104	31T	255205	4706916	187	6	W	Marls	Millaris	Middle Ilerdian	1,38E-04	205	1	204	2	83	88	284	86	1,035	0,596
BO05	19	135	31T	255187	4706952	187	8	W	Marls	Millaris	Middle Ilerdian	7,34E-05	201	5	201	5	353	88	290	81	1,028	0,195
BO06	7	154	31T	254613	4706261	178	36	W	Marls	Millaris	Middle Ilerdian	9,87E-05	8	3	8	3	110	47	160	74	1,028	0,328
BO07	24	169	31T	254564	4706237	173	37	W	Limestones	Metils	Middle Ilerdian	2,85E-05	217	18	218	14	102	48	158	77	1,030	0,054
BO08	32	202	31T	254544	4706310	178	36	W	Limestones	Metils	Middle Ilerdian	3,80E-05	201	14	203	11	91	53	150	88	1,036	0,376
BO09	32	230	31T	254479	4706223	181	48	W	Marls	Lw. Yeba	Ilerd.-Cuisian	7,13E-05	209	16	208	17	106	37	163	77	1,017	0,225
BO10	28	258	31T	254448	4706228	186	54	W	Marls	Lw. Yeba	Ilerd.-Cuisian	4,80E-05	198	20	196	21	96	31	96	85	1,013	0,052
BO11	27	284	31T	254425	4706238	185	57	W	Marls	Lw. Yeba	Ilerd.-Cuisian	5,64E-05	196	29	194	30	92	33	4	88	1,018	0,190
BO12	22	312	31T	254385	4706250	183	51	W	Marls	Lw. Yeba	Ilerd.-Cuisian	8,90E-05	197	9	196	10	103	30	138	78	1,014	0,064
BO13	31	338	31T	254359	4706271	196	58	W	Limestones	Mid. Yeba	Middle Cuisian	2,89E-05	204	19	207	18	325	43	134	7	1,037	0,058
BO14	23	372	31T	255034	4709838	186	74	W	Marls	Upp. Yeba	Middle Cuisian	9,29E-05	354	35	351	34	96	10	96	84	1,022	0,253
BO15	21	402	31T	254964	4709833	187	71	W	Marls	Upp. Yeba	Middle Cuisian	1,21E-04	8	23	4	23	104	10	135	79	1,020	0,447
BO16	25	426	31T	254247	4706350	187	59	W	Limestones	Lw. Boltaña	Late Cuisian	9,10E-05	199	20	202	18	87	42	310	76	1,019	0,428
BO17	28	450	31T	254254	4706324	183	60	W	Limestones	Lw. Boltaña	Late Cuisian	9,41E-05	201	25	208	18	107	8	127	64	1,008	0,131
BO18	24	474	31T	254190	4706330	185	61	W	Limestones	Lw. Boltaña	Late Cuisian	2,53E-05	77	81	279	38	314	6	148	39	1,008	0,045
BO19	24	499	31T	254132	4706314	183	64	W	Limestones	Lw. Boltaña	Late Cuisian	6,06E-05	196	0	9	12	102	48	258	67	1,012	0,013
BO20	33	525	31T	254109	4706306	185	62	W	Limestones	Lw. Boltaña	Late Cuisian	7,51E-05	17	1	10	11	284	12	109	49	1,007	0,152
BO21	33	555	31T	253902	4706274	183	68	W	Limestones	Lw. Boltaña	Late Cuisian	8,95E-05	5	4	0	3	265	2	74	65	1,011	-0,071
BO22	26	578	31T	253863	4706167	181	75	W	Limestones	Ascaso Mb	Late Cuisian	5,57E-06	343	19	158	11	70	4	27	67	1,085	-0,131
BO23	23	596	31T	253830	4706143	187	75	W	Limestones	Ascaso Mb	Late Cuisian	1,21E-05	6	43	325	9	115	10	173	72	1,048	0,153
BO24	26	619	31T	253777	4706146	185	73	W	Limestones	Upp.Boltaña	Cuis.-Lutetian.	8,83E-05	1	35	330	7	272	4	87	69	1,010	0,277
BO25	28	643	31T	253741	4706128	184	69	W	Limestones	Upp.Boltaña	Cuis.-Lutetian.	4,91E-05	28	45	323	32	114	4	146	64	1,010	0,200
BO26	26	668	31T	253713	4706127	190	66	W	Limestones	Upp.Boltaña	Cuis.-Lutetian.	6,64E-05	5	61	311	19	252	4	52	51	1,006	0,092
BO27	20	694	31T	253645	4706192	183	72	W	Limestones	Upp.Boltaña	Cuis.-Lutetian.	4,33E-05	19	33	334	23	125	37	224	56	1,064	0,247
BO28	21	724	31T	253564	4706215	187	80	W	Limestones	Upp.Boltaña	Cuis.-Lutetian.	3,42E-05	27	61	306	18	211	27	39	16	1,022	0,316
BO29	18	747	31T	253550	4706387	186	85	W	Limestones	Upp.Boltaña	Cuis.-Lutetian.	2,74E-05	13	25	341	8	267	18	75	65	1,016	0,010
BO30	17	773	31T	253489	4706475	188	74	W	Limestones	Upp.Boltaña	Cuis.-Lutetian.	4,59E-05	348	61	305	5	73	1	37	61	1,008	0,050
BO31	28	805	31T	254572	4688782	72	10	S	Lims.-marls	Paules Mb	Early Lutetian	1,16E-05	151	1	331	9	86	82	129	76	1,031	0,060
BO32	32	836	31T	255328	4689980	10	13	E	Marls	Paules Mb	Early Lutetian	1,02E-05	16	6	17	5	260	70	231	81	1,085	0,113
BO33	36	883	31T	255567	4690023	343	22	E	Marls	Paules Mb	Early Lutetian	1,38E-05	43	9	223	10	265	76	54	81	1,040	0,296
BO34	35	925	31T	255714	4690015	356	24	E	Marls	Paules Mb	Early Lutetian	2,31E-05	12	2	192	5	280	71	47	83	1,015	0,120
BO35	32	993	31T	256116	4690151	355	26	E	Marls	Paules Mb	Early Lutetian	1,94E-05	103	11	283	14	273	79	79	75	1,019	0,373
BO36	31	1025	31T	256199	4690143	346	26	E	Marls	Paules Mb	Early Lutetian	1,50E-05	62	7	241	18	313	76	43	68	1,037	0,101
BO37	30	1055	31T	256238	4689282	352	17	E	Marls	Paules Mb	Early Lutetian	2,24E-05	96	56	92	39	288	30	294	45	1,008	0,249

Site	n	Height	TZ	UTM-x	UTM-y	Strike	Dip	DD	Lithology	Formation	Age	Km	KMX-Ds	KMX-Is	KMX-Dr	KMX-Ir	KMN-Ds	KMN-Is	KMN-Dr	KMN-Ir	P'	T
BO38	30	1082	31T	256304	4689336	0	20	E	Marls	Paules Mb	Early Lutetian	4,22E-05	191	14	186	17	275	59	283	79	1,008	0,032
BO39	30	1107	31T	256367	4689270	349	25	E	Marls	Paules Mb	Early Lutetian	1,98E-05	180	25	168	27	305	44	332	57	1,011	0,027
BO40	24	1130	31T	256455	4689226	0	20	E	Marls	Paules Mb	Early Lutetian	2,16E-05	121	43	115	25	305	47	325	61	1,010	0,026
BO41	31	1152	31T	256585	4689295	351	28	E	Marls	Paules Mb	Early Lutetian	1,47E-05	89	34	88	6	343	40	6	38	1,016	0,082
BO42	20	1175	31T	256631	4689378	347	28	E	Marls	Paules Mb	Early Lutetian	2,88E-05	3	11	6	2	214	77	103	70	1,007	0,157
BO43	20	1200	31T	256293	4691402	349	22	E	Marls	La Patra Mb	Middle Lutetian	4,71E-05	11	4	191	4	226	87	84	71	1,019	0,280
BO44	23	1263	31T	256350	4691435	3	27	E	Marls	La Patra Mb	Middle Lutetian	3,17E-05	17	32	30	22	248	75	119	75	1,051	0,170
BO45	21	1319	31T	256531	4691316	1	21	E	Turbidites	La Patra Mb	Middle Lutetian	1,91E-05	263	64	235	84	301	20	307	38	0,976	0,018
BO46	21	1394	31T	256798	4691083	0	21	E	Turbidites	La Patra Mb	Middle Lutetian	5,56E-05	33	7	213	5	285	69	7	85	1,015	0,444
BO47	21	1466	31T	257520	4691588	6	21	E	Marls	La Patra Mb	Middle Lutetian	1,02E-04	7	2	8	2	273	65	258	86	1,033	0,623
BO48	20	1515	31T	257788	4691661	8	20	E	Marls	La Patra Mb	Middle Lutetian	5,94E-05	1	2	2	4	266	71	168	86	1,033	0,479
BO49	20	1584	31T	258025	4691526	357	24	E	Marls	La Patra Mb	Middle Lutetian	8,90E-05	5	1	185	2	251	73	118	81	1,031	0,657
BO50	20	1644	31T	258305	4691159	355	20	E	Marls	Sobrarbe	Late Lutetian	8,55E-05	186	0	185	4	275	67	320	85	1,022	0,356
BO51	19	1710	31T	258521	4691269	357	25	E	Marls	Sobrarbe	Late Lutetian	9,54E-05	22	10	204	1	279	66	14	85	1,024	0,457
BO52	5	1768	31T	258763	4691298	354	22	E	Marls	Sobrarbe	Late Lutetian	7,27E-05	36	5	215	10	223	71	143	76	1,021	0,429
BO53	9	1596	31T	260468	4686856	8	22	E	Marls	La Patra Mb	Middle Lutetian	5,48E-05	137	20	134	3	285	68	11	87	1,043	0,747
BO54	23	1647	31T	260552	4686819	5	23	E	Marls	Sobrarbe	Late Lutetian	7,31E-05	146	18	143	3	279	65	316	87	1,032	0,743
BO55	23	1704	31T	260867	4686648	10	20	E	Marls	Sobrarbe	Late Lutetian	8,37E-05	107	28	106	8	271	61	253	80	1,029	0,577
BO56	24	1733	31T	261037	4686559	10	23	E	Marls	Sobrarbe	Late Lutetian	7,44E-05	143	16	321	1	276	64	249	87	1,018	0,539
BO57	21	1757	31T	261155	4686485	18	21	E	Sandstone	Sobrarbe	Late Lutetian	3,97E-05	129	11	309	9	281	71	155	87	1,010	0,210
BO58	22	1777	31T	261223	4686443	17	19	E	Sandstone	Sobrarbe	Late Lutetian	6,72E-05	132	19	131	2	295	74	72	86	1,025	0,535
BO59	22	1802	31T	261317	4686387	24	17	E	Sandstone	Sobrarbe	Late Lutetian	9,89E-05	146	20	144	5	292	68	285	85	1,020	0,699
BO60	22	1824	31T	261402	4686315	30	16	E	Sandstone	Sobrarbe	Late Lutetian	1,73E-04	164	13	163	1	309	75	57	87	1,032	0,434
60	1453	1824	**TOTAL**																			
sites	**sp.**	**m**																				

Table 1. Complete information about AMS parameters and field features. The values represent the mean of all samples involved in each site. Site: name of the site; n: number of samples gathered in each site; Height: stratigraphic position along the section (in metres); TZ: time zone; UTM-x and UTM-y; Strike: using the right hand rule; Dip; DD: dip direction; Lithology: type of rock where the samples were taken; Formation; Age; Km: Mean susceptibility; K_{MX}-Ds: K_{MAX} Declination *in situ* (bac); K_{MX}-Is: K_{MAX} Inclination *in situ*; K_{MX} -Dr: K_{MAX} Declination restored (abc); K_{MX} -Ir: K_{MAX} Declination restored. K_{MN}-Ds: K_{MIN} Declination *in situ*; K_{MN}-Is: K_{MIN} Inclination *in situ*; K_{MN}-Dr: K_{MIN} Declination restored; K_{MN}-Ir: K_{MIN} Declination restored; P': corrected degree of anisotropy; T: shape parametres

7.2.2. Laboratory procedures

One of the most convenient techniques used to determine the preferred orientation in mudrocks is the AMS, as it is often an effective tool to deduce the fabric of rocks that do not show evidences of deformation at the mesoscopic scale (Tarling and Hrouda, 1993; Borradaile and Henry, 1997; Bouchez, 1997; Parés et al., 1999; Latta and Anastasio, 2007). The orientation of the magnetic ellipsoid it is expressed by the directions of its three main axes ($K_{MAX}>K_{INT}>K_{MIN}$). The measuring and statistical procedures are based on Jelinek's (1977, 1981) method. The magnetic fabric is characterized by the magnetic lineation (K_{MAX}) and the magnetic foliation (perpendicular to K_{MIN}).

Tensorial parameters (Jelinek, 1981) were used to characterize the shape and degree of anisotropy of the ellipsoids: (a) the corrected anisotropy degree, P', indicating the total eccentricity of the magnetic ellipsoid and, (b) T, the shape parameter, ranging from $0>T>-1$ (prolate ellipsoids) and $0<T<+1$ (oblate ellipsoids). In this work, AMS analyses were done at room temperature and at low temperature with a low-susceptibility bridge, KLY-3S Kappabridge (AGICO), at 875 Hz AC and a field intensity of 300 Am^{-1} (AGICO) at the University of Zaragoza (Geotransfer Research Group).

The fact that all rocks are magnetically anisotropic (Bouchez, 1997) allows magnetic preferred orientation to be analysed in a qualitative way, more universally than by using techniques based on other strain indicators. AMS due to phyllosilicates (paramagnetic) is directly related to their crystallographic lattices (Martín-Hernández and Hirt, 2003) and it is a direct way to quickly measure the rock anisotropy. Therefore, to ensure that AMS reflects the orientation and magnitude of the mineral fabric, a relationship between AMS and paramagnetic minerals must be established. In order to assess the relative contribution of paramagnetic minerals to the mean susceptibility, low temperature measurements of AMS can be used (Richter and van der Pluijm, 1994; Parés and van der Pluijm, 2002; Oliva et al., 2009). Whereas diamagnetic susceptibility is independent of the temperature and can be considered constant as a rock-matrix parameter (Rochette, 1987; Schmidt et al., 2006, 2007), paramagnetic susceptibility (mainly borne by phyllosilicates) increases during cooling, according to the Curie–Weiss law. Consequently, paramagnetic dominance can be recognized from its temperature-dependence. To check this relationship, low temperature AMS (LT–AMS) measurements were taken in a KLY-3S from 21 samples with different lithology and age, and with varied bulk susceptibility at room temperature. Samples were immersed in liquid nitrogen (77K for 45 min) before the magnetic susceptibility was measured in air. Between the three different changes of position for the rotator (every spinning position takes less than 30 s), the samples were immersed again in liquid nitrogen for 10 min. At liquid nitrogen temperatures the magnitude of K_{MAX} increases by a factor larger than the K_{MIN}. This increases bulk magnetic susceptibility by a factor of 3 to 5 times the susceptibility at room temperature (Parés and van der Pluijm, 2002), which mainly reflects the subfabric associated to paramagnetic minerals.

In the same way and to establish precisely the paramagnetic and ferromagnetic contributions (Rochette, 1987; Hrouda and Jelinek, 1990; Pueyo et al., 2005b), several low field and high field (LF/HF) measurements were taken. Eleven samples, representatives of the different lithological types, were selected for analysis. Measurements were carried out with the MPMS-XL SQUID magnetometer

(Quantum Design Ltd.) of the Physical Measurements Facility at ICMA (Universidad de Zaragoza - CSIC). The steps followed are: Centring in Direct Current (DC); Susceptibility measurement in LF, Alternating Current (AC), 4 Oe, 920 Hz and 0,04 T (similar conditions to KLY-3S); HF susceptibility measurements and DC at 1T, 1,5T and 2T. Since the high field susceptibility can be considered only paramagnetic (providing a complete saturation of any ferromagnetic mineral), any deviation of the LF susceptibility with respect to the HF susceptibility will be the ferromagnetic contribution. The aim is to compare susceptibilities obtained at LF and HF; if both measurements (K_{LF} and K_{HF}) are similar, a dominant paramagnetic contribution will be proven. Otherwise, if the measurement at HF differs significantly from measurement at LF, an important ferromagnetic contribution can be inferred.

Finally, the directional statistical treatment of site means (K_{MAX} and K_{MIN}) has been done following Bingham (1974) distribution and Pueyo et al. (2004b) reliability criteria. The maximum axis (eigenvector) of the orientation matrix (Scheidegger, 1965) for each value (K_{MAX} and K_{MIN}) is supported by the elliptical confidence cone (95%).

7.3. Results

7.3.1. Magnetic mineralogy and scalar parameters

AMS is based on the determination of preferred orientation of paramagnetic minerals by means of magnetic properties. The influence of different proportions of ferromagnetic minerals makes the interpretation of magnetic fabrics difficult, when concerning the orientation and shape of the magnetic ellipsoid and the bulk susceptibility. Paramagnetic minerals dominate the magnetic susceptibility, in Rochette (1987) and Housen and van der Pluijm (1991) for example, although small quantities of ferromagnetic minerals can significantly contribute to the AMS. Therefore it is necessary to quantify the ferro/paramagnetics ratio. With that aim LT–AMS (77 K) and LF/HF analysis, based on the specific behaviour of the magnetic susceptibility in different fields and temperatures (Rochette 1987 and Richter and van der Pluijm, 1994) were carried out.

The bulk susceptibilities of the rocks analysed range from 20 to $100 \cdot 10^{-6}$ S.I. (Figure 2a, Table 1) within a purely paramagnetic rock matrix (Rochette, 1987). In most of the samples the magnetic susceptibility at low temperature increased by a factor of 2 with respect to room temperature (Figure 2c). Only five samples did not enhance their susceptibility at LT. Considering all the data, the average KLT/KRT ratio is 2.4. Low angular deviations (lower than 258) between measurements at low and room temperatures are observed in most cases (Figure 2d). As the Curie-Weiss Law is valid only for paramagnetic materials these results indicate that in 70% of the analysed samples the AMS contribution is due to paramagnetic minerals. Samples with high angular deviation between LT and RT measurements correspond to limestones from the Metils and Upper Boltaña Fms. and marls from the Paules Mb. In these cases it would be necessary to consider that other components (dia- or ferro-magnetic) contribute to susceptibility.

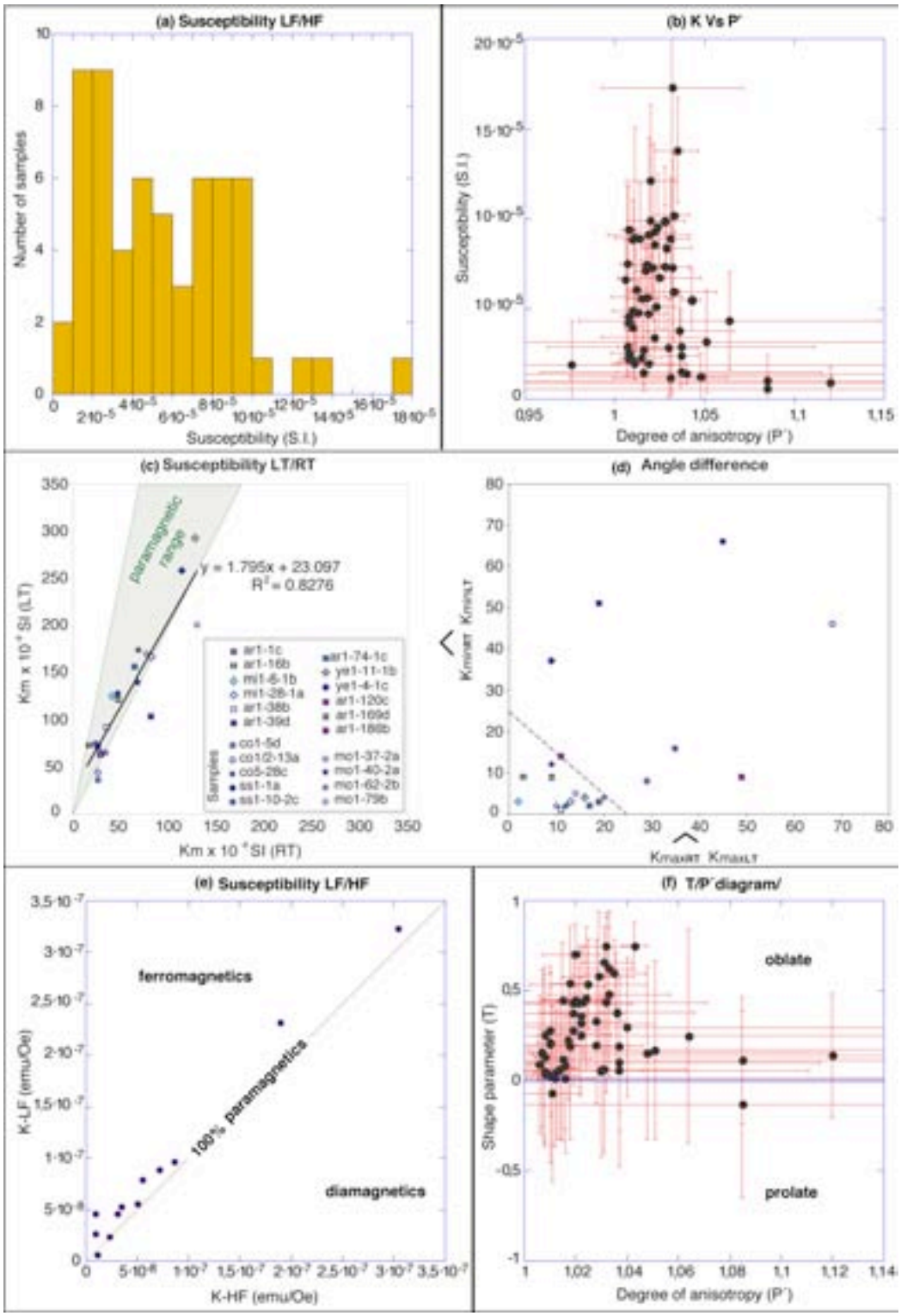

Figure 2. Scalar parameters of the room temperature magnetic fabric and low-temperature and high field experiments. (a) Histogram of bulk susceptibility *versus* number of sites. (b) Susceptibility (S.I.) versus corrected degree of anisotropy (P'). (c) Susceptibility of all rock types analysed at room and low temperatures, with relationships indicating their paramagnetic contribution. (d) Angles between K_{MAX} and K_{MIN} measured at low and room temperatures. In diagrams (c) and (d), each sample is represented by a different symbol. (e) Low and high field susceptibilities, indicating the paramagnetic-bearing samples on the straight diagonal line. (f) T/P' diagram showing the shape and the corrected anisotropy degree of magnetic ellipsoids, which are mainly oblate and weakly anisotropic.

The LF/HF ratio from the studied samples (Figure 2e) display values close to 1 (pure paramagnetic); for example, samples Ar1-1c (limestones, Ager Fm.) and Ye1-22c (marlstones, Yeba Fm.) are exactly placed on the pure paramagnetic domain line. The mean LF/HF slope value is 0.83, therefore a main paramagnetic contribution (83%) of the LF susceptibility (and the AMS) can be inferred and a insignificant effect of the ferromagnetic and diamagnetic minerals can be expected, except for a few exceptions: Ar1- 26c (limestones, Metils Fm.) shows LF/HF<1 due to a slight diamagnetic contribution to KLF.

The corrected anisotropy degree (P') falls within the expected anisotropy for phyllosilicates (1 and 1.1, Martín-Hernández and Hirt, 2003) at most sites (Figure 2b and f), except for two cases, one of them showing values lower than 1 (BO45), related to diamagnetic behaviour and the other one higher than 1.1 (BO02), related to a very low bulk value. Regarding the shape parameter (T), analysed sites are within the oblate domain, with values between 0 and 0.8, most of them below 0.5. Few sites are located above the triaxial-ellipsoid line, indicating an overall pattern (Figure 2f) of oblate ellipsoids. The described results suggest that the paramagnetic contribution is dominant, although some directional and parametric noise (below 20-30% of the bulk susceptibilty) can arise from the analysis of some rock types, especially limestones. Thus, the AMS in the studied rocks can be interpreted to indicate the mineral preferred orientation within the rock matrix.

7.3.2. Directional and tensorial data

Directional data (orientation of K_{MAX} and K_{MIN}) are represented before bedding correction (*in situ*) and restored (restoring bedding to the horizontal), and considering both, all the samples (raw) and samples grouped in sites (60 in total, Figure 3). As expectable, the diagrams where samples are arranged in sites display less noise and show better-defined directional maxima (Figures 3c,d,g,h). Both in raw sample diagram and site-averaged diagrams, better clustering of K_{MAX} axes is observed after bedding correction (Figures 3b,d), showing a tendency to be contained within the bedding plane (horizontal after restoring). 58% of the measured samples have their K_{MIN} axes nearly perpendicular to bedding, considering as such K_{MIN} plunge angles higher than 60º after tectonic correction (Figure 3f). If Bingham (1974) mean directions for sites are considered, 83% of sites show K_{MIN} sub-perpendicular or perpendicular to bedding (Figure 3h). In the density diagrams of K_{MAX} axes, three main maxima can be distinguished: the most common trend is N006E (varying between N351E and N017E, included within the bedding plane), parallel to the Boltaña anticline.

The second K_{MAX} maximum shows a NNE–SSW trend (N22E to N55E), with a slight and non-significant plunge after bedding correction (201,11). The third maximum has an ESE–WNW trend (N125E, from N140E to N161E, contained in the bedding plane). Despite its variability, K_{MAX} is systematically contained within the bedding plane and reasonably well-grouped, pointing to an incipient blocking of the fabric as has been extensively proven in the South Pyrenean Basin (Pueyo et al., 1997; Larrasoaña et al., 2004; Troy et al., 2008; Oliva-Urcia et al., 2009; Pueyo-Anchuela et al., 2010).

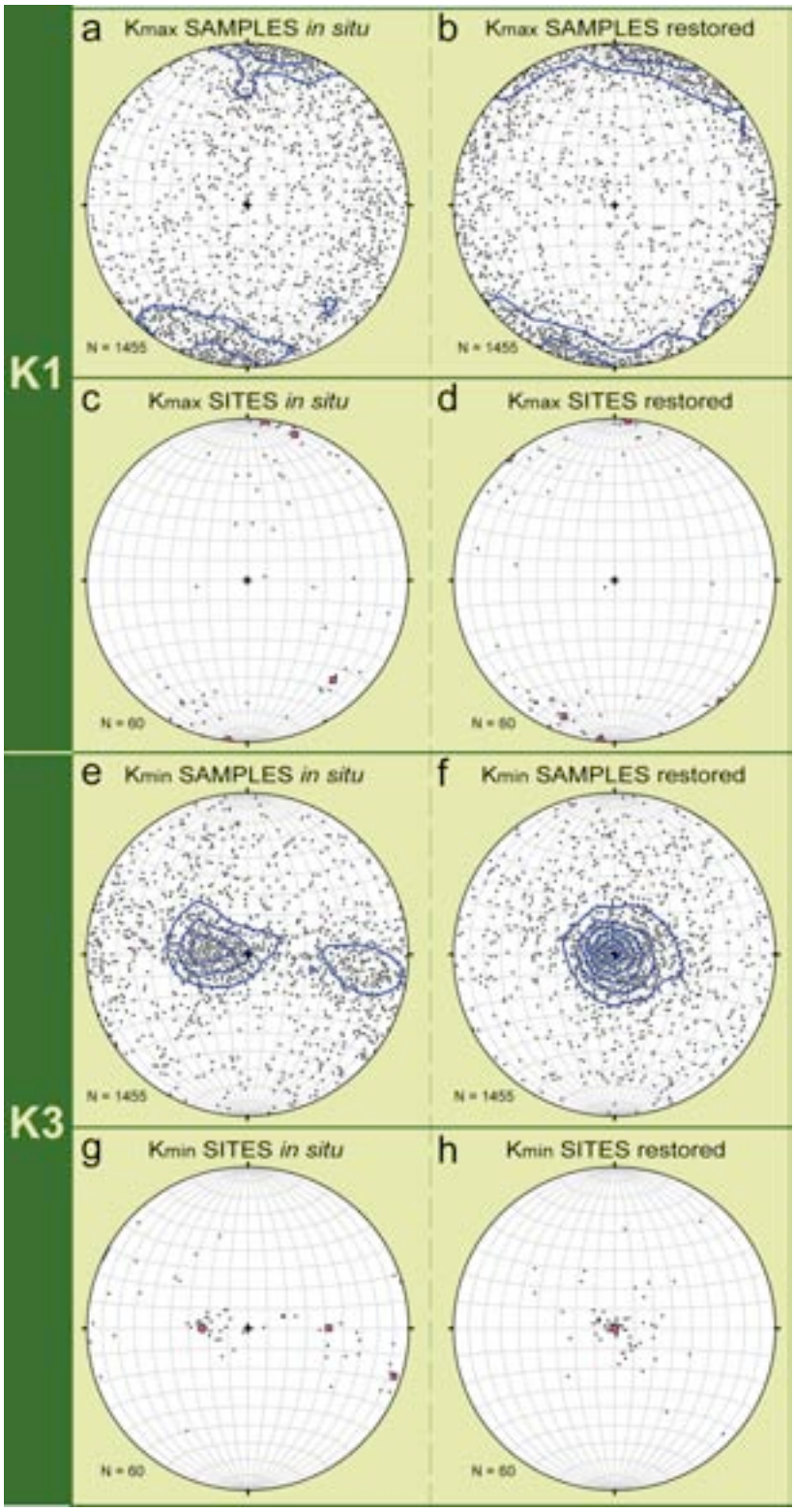

Figure 3. Stereoplots showing directional data of the complete collection of samples (equal area, lower hemisphere, Contour Interval: 2%). Circles: absolute maxima. Squares: relative maxima. (a) K_{MAX} Density stereoplot of all samples *in situ*. (b) K_{MAX} Density stereoplot of all samples after bedding restoration. (c) K_{MAX} Density stereoplot per site *in situ*. (d) K_{MAX} Density, bedding-restored stereoplot per sites. (e) K_{MIN} Density stereoplot of the all samples *in situ*. (f) K_{MIN} Density diagram of all samples, bedding-restored. (g) K_{MIN} Density stereoplot per sites *in situ*. (h) K_{MIN} Density stereoplot per sites, bedding-restored.

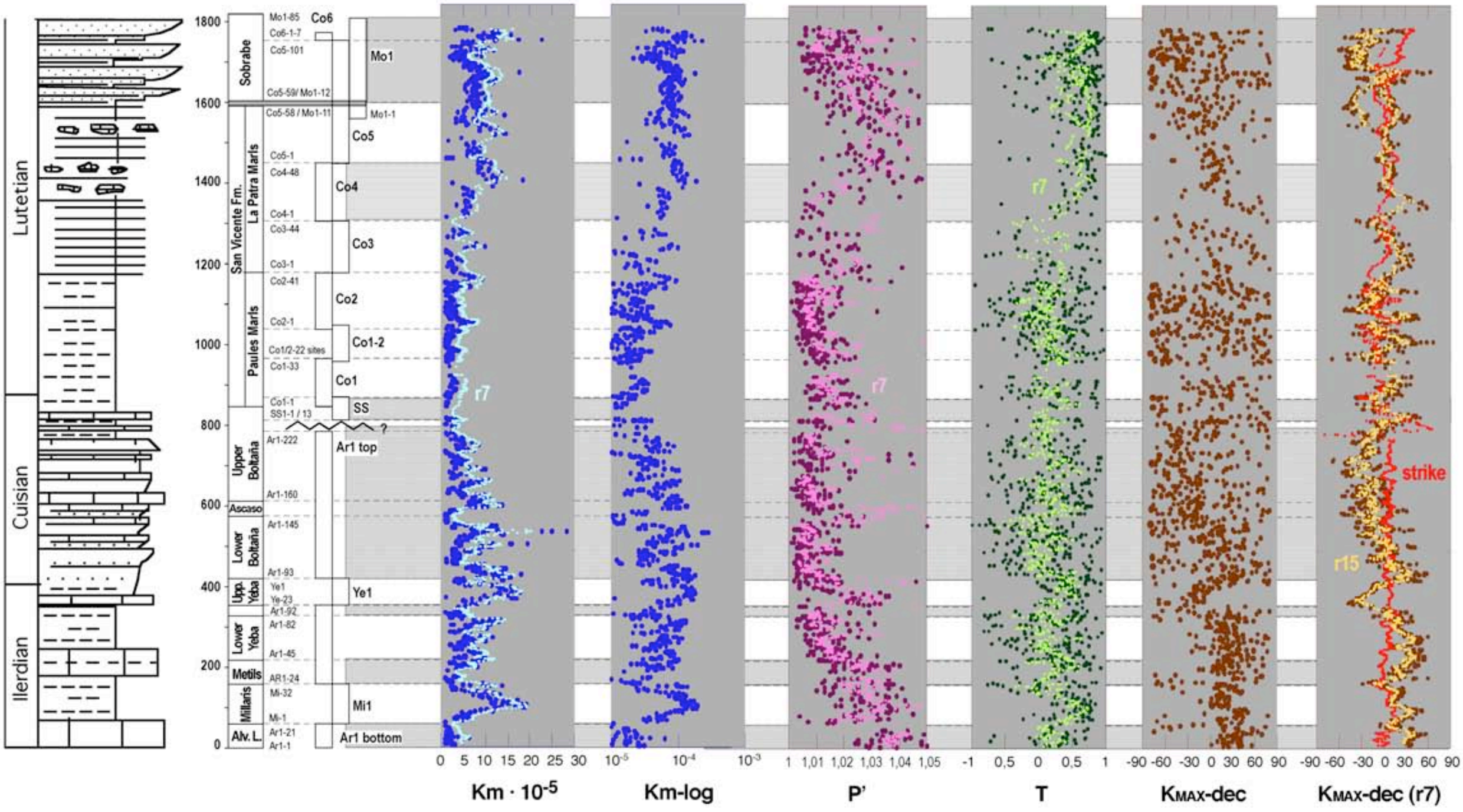

Figure 4. (a) Diagrams showing the variation of the different parameters along the stratigraphic section. In the background, the different lithologies are shown. The white background corresponds to marls and the bricked-pattern background to limestones; the dashed background corresponds to turbidites; towards the top of the pile the dotted pattern indicates siliciclastic material. On the left part of the figure the stratigraphic log with the main units present on the study area, age, height, profiles sampled and their stratigraphic overlapping are shown. The parameters shown are: Bulk susceptibility (Km) represented in linear (Km10_5) with the running averages of seven specimens in bright points and logarithmic scale (km-log). Corrected degree of anisotropy (P'), shape parameter (T). The dark circles represent the raw data whereas the bright points represent the running averages of seven specimens, aiming to smooth the curve. Raw data of the declination of K_{MAX} is shown in K_{MAX}-dec and their running averages are presented in K_{MAX}-dec (r7). The dark circles represent the running average of seven samples and the bright ones of 15. The red line is the strike of beds (raw data)

The K_{MAX} axis orientation is variable compared to stable bedding (see Table 1 and Figures 3–6). The angle between K_{MAX} and the bedding strike shows three maxima along the stratigraphic succession (Table 1 and Figure 4). The N-S and NNE-SSW maxima are observed towards the base of the series (sites 1–21), where the Alveoline Limestones, Millaris, Metils, Yeba and Lower Boltaña Fms. are involved. Somehow, four cycles of K_{MAX}/bedding strike angle appear along the pile. In the upper part of the Boltaña Fm. the K_{MAX} orientation shows a NW–SE trend (sites 22–31). The lowermost part of the Paules Mb. seems to recover the N-S trend (sites 32–34). The middle and upper parts of this Member are prone to E-W scattered trends (sites 35–41). Ascending through the series, the top of the Paules Mb. (site 42), La Patra Mb. (sites 43–49) and the Lower part of the Sobrarbe Fm. (sites 50–52) show N–S trends. The uppermost part of the Sobrarbe Fm. records (sites 53–59 from), ESE– WNW maxima.

Some consistent patterns can be deduced from variations of the bulk magnetic susceptibility (Km) through the stratigraphic sequence (Figure 4). The Km (bulk) is probably controlled by lithology and therefore by the sedimentary environment (see Table 1 and Figure 4). Several bulk susceptibility increases have been observed along the pile; they serve to check the lithological control on the bulk susceptibility: Relatively high values of Km are found in detrital deposits within the Alveoline limestones, the Upper Yeba unit and towards the top of the studied series (Sobrarbe Fm.). Variations within the La Patra Mb. can be related to a flooding maximum and a glauconite level and to the arrival of a turbiditic system. The strong change of Km recorded at the top of the Mb. is related to debris-flow deposits.

Since a dominant paramagnetic behaviour has been demonstrated, this lithological control only affects the bulk value but not the tensor orientation, and then, the mineral preferred orientation has to be controlled by external factors (Figure 7).

The shape parameter (T) does not seem to follow a variation pattern linked to lithological changes. Most samples show positive values, indicating dominantly oblate magnetic ellipsoids, common in weakly deformed rocks. Only two sites, located at the top of the Lower Boltaña Mb. and the Ascaso Mb., show a prolate shape and very low tensor anisotropy (P'). The oblate trend becomes stronger at the top of the studied sequence, with values close to 1. In the case of P', the values obtained seem to mimic the sedimentary cycles recorded through the studied sequence (Figure 6).

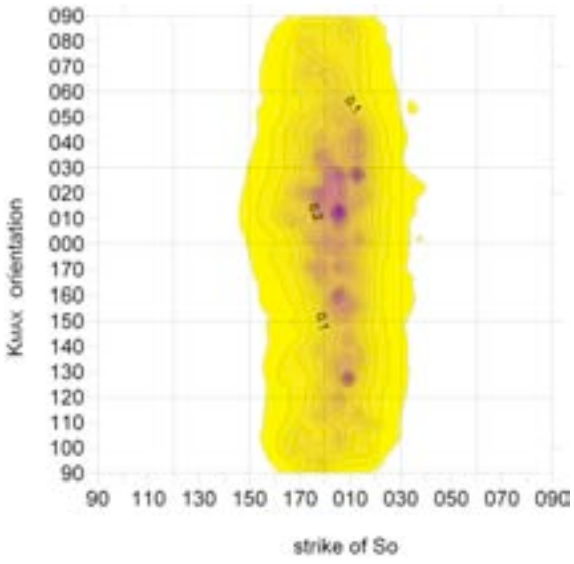

Figure 5. K_{MAX} orientation versus So strike for the whole of the data, showing the scattering of K_{MAX} orientation, and a clear maximum.

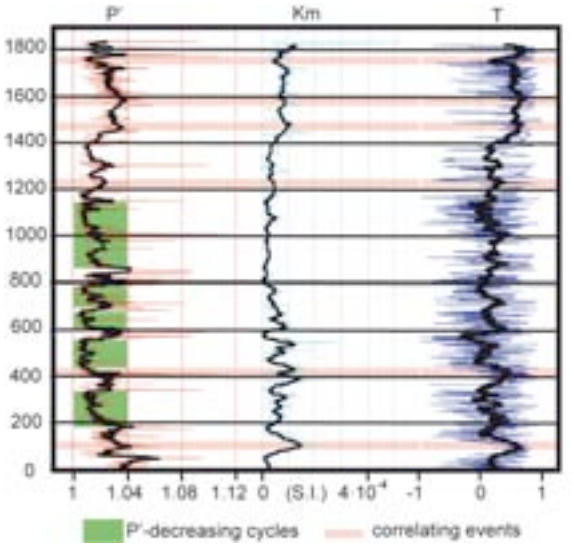

Figure 6. Clean data of P', Km and T parameters along the stratigraphic log. The hairline indicates the raw data and the solid line the running averages. Upward-decreasing cycles are indicated by shadowed squares and correlating events by horizontal lines.

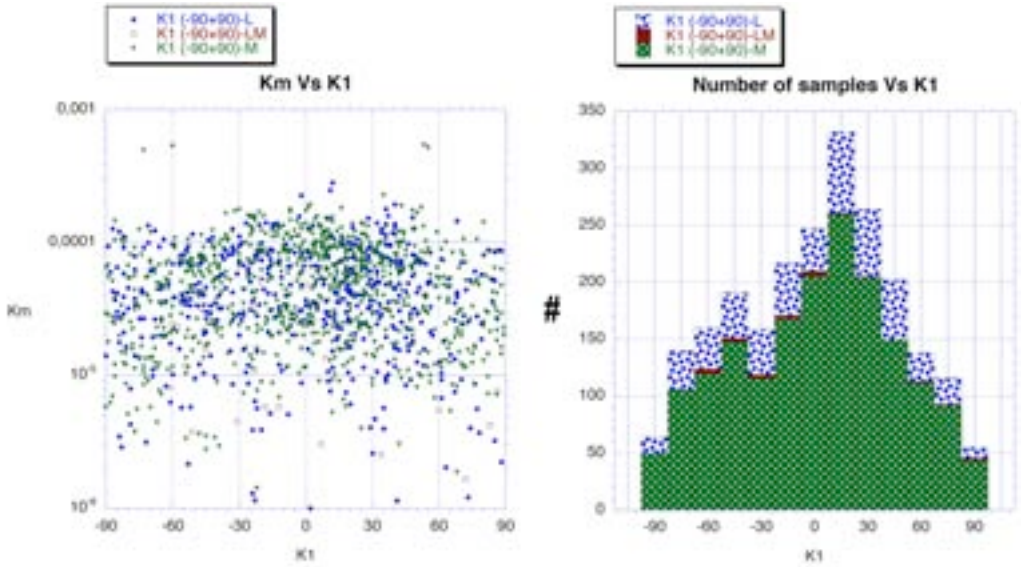

Figure 7. Left: Bulk versus K_{MAX} azimuth (restored). Right: K_{MAX} histogram by lithologies. L: limestones; M: marls; LM: marly limestones (diamagnetic samples were removed to allow log scale).

7.3.3. Significance of directional data

The sampling method used allows for a specific treatment of data that permits the reliability of the variations along the stratigraphic log to be evaluated. Apart from the grouping, some basic filtering of data at the sample scale was done according to the criteria exposed in Pueyo et al. (2004b) using the F12, F23, F13 angles by Jelinek (1981). It is worth mentioning that only the marly part of the sequence (Paules and La Patra Fms) was used for this statistical procedure. Clearly oblate fabrics were not considered to calculate magnetic lineations, and strongly scattered averages (associated to pseudo-isotropic samples) were avoided by means of eigenvalues. Filtering was done with two intensities, strong and soft, according to the severity in the application of the following criteria:

- Strong filtering, consists in three levels:

1) The parameter F13 (≈E31°) was considered to eliminate the samples describing an isotropic magnetic ellipsoid. Samples with F13<10 were removed, thus selecting anisotropic samples.

2) With the aim of ruling out the samples with oblate magnetic ellipsoids (K1≈ K2), those ellipsoids with F12 (≈E21°) < 8 were eliminated. Only samples with contrasted K1 and K2 axes were retained.

3) To ensure the perpendicularity of K3 respect to bedding, with K1 contained in the bedding plane, the samples with inclination lower than 60º (after bedding correction) have been removed. Then, only samples with K3 sub-perpendicular or perpendicular to bedding have been considered.

- In a similar way, the soft filtering consists in three sub-filtering with the same aim, but less strict application of conditions, only removing:

1) Samples with F13<4

2) Samples with F12<5

3) Samples with K3 inclination < 50º

Results obtained after different types of filtering are shown in figures 8 and 9, thus allowing for direct evaluation of the noise/signal reduction along the studied profile.

In general, there are not significant differences in the trend of the magnetic lineation along the profile between the non-filtered and the filtered data sets, what supports the consistency of the results obtained. The orientations of K1 and K3 are relatively homogeneous along the sampled profile. K3 is usually perpendicular to bedding (figure 10); K1 values show a clear maximum in N-S direction, with scattering towards NNE and NNW orientations. Two other secondary maxima of K1 orientation appear in NE-SW and NW-SE directions, and can be clearly distinguished in the filtered data sets.

Considering the changes in orientation along the stratigraphic log, a slight change is observed between the lower part of the profile, where a N-S to NNE-SSW is dominant, and the upper part of the profile, with its maximum shifted toward the NNW-SSE direction (figure 10). However, these changes are not significant if the confidence errors are considered.

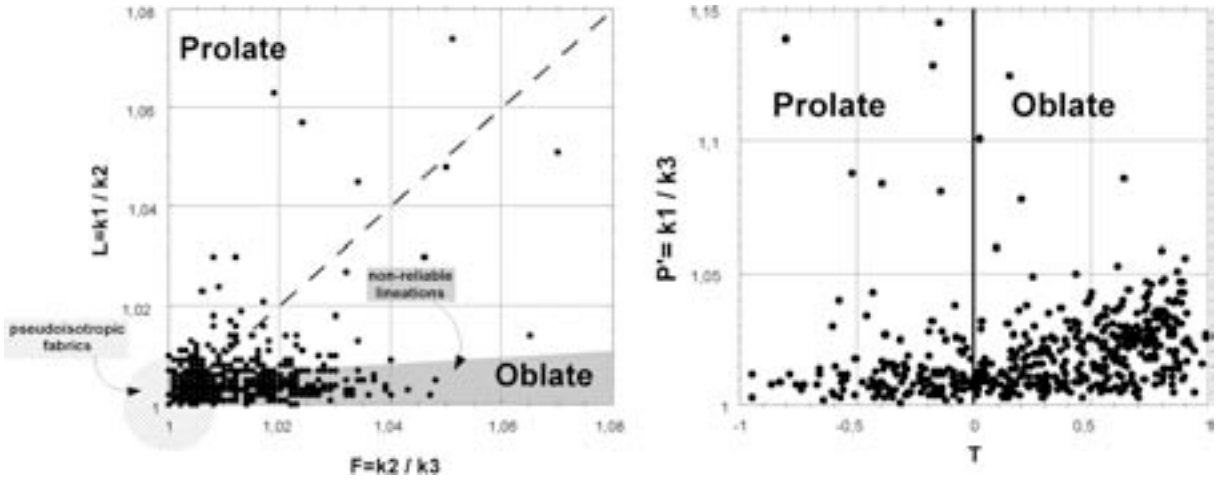

Figure 8. AMS Shape parameters expressed by means of Flinn diagram (Flinn, 1962). Magnetic fabrics show a low degree of anisotropy and are mostly oblate. Jelinek (1981) diagram also shows this tendency.

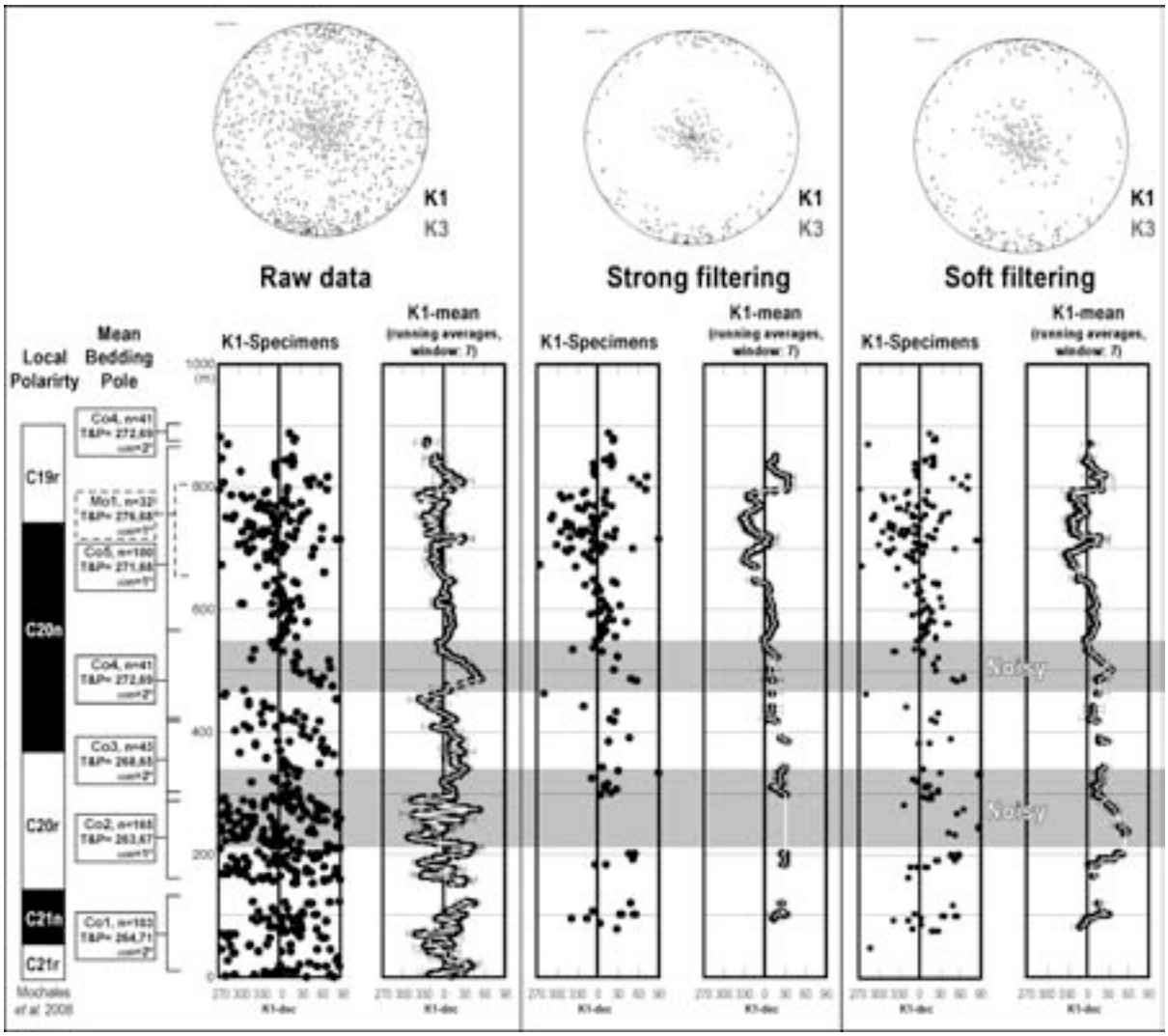

Figure 9. Stereoplots obtained from magnetic ellipsoids of the studied section, after and before filtering; K1 and K3 values are shown in black and grey, respectively. These values are situated in a stratigraphic log vs. declination of the K1 diagram. Raw data and running averages (with their standard error bar) are displayed together; grey areas present a noise signal. Subsections and the magnetostratigraphic log are shown.

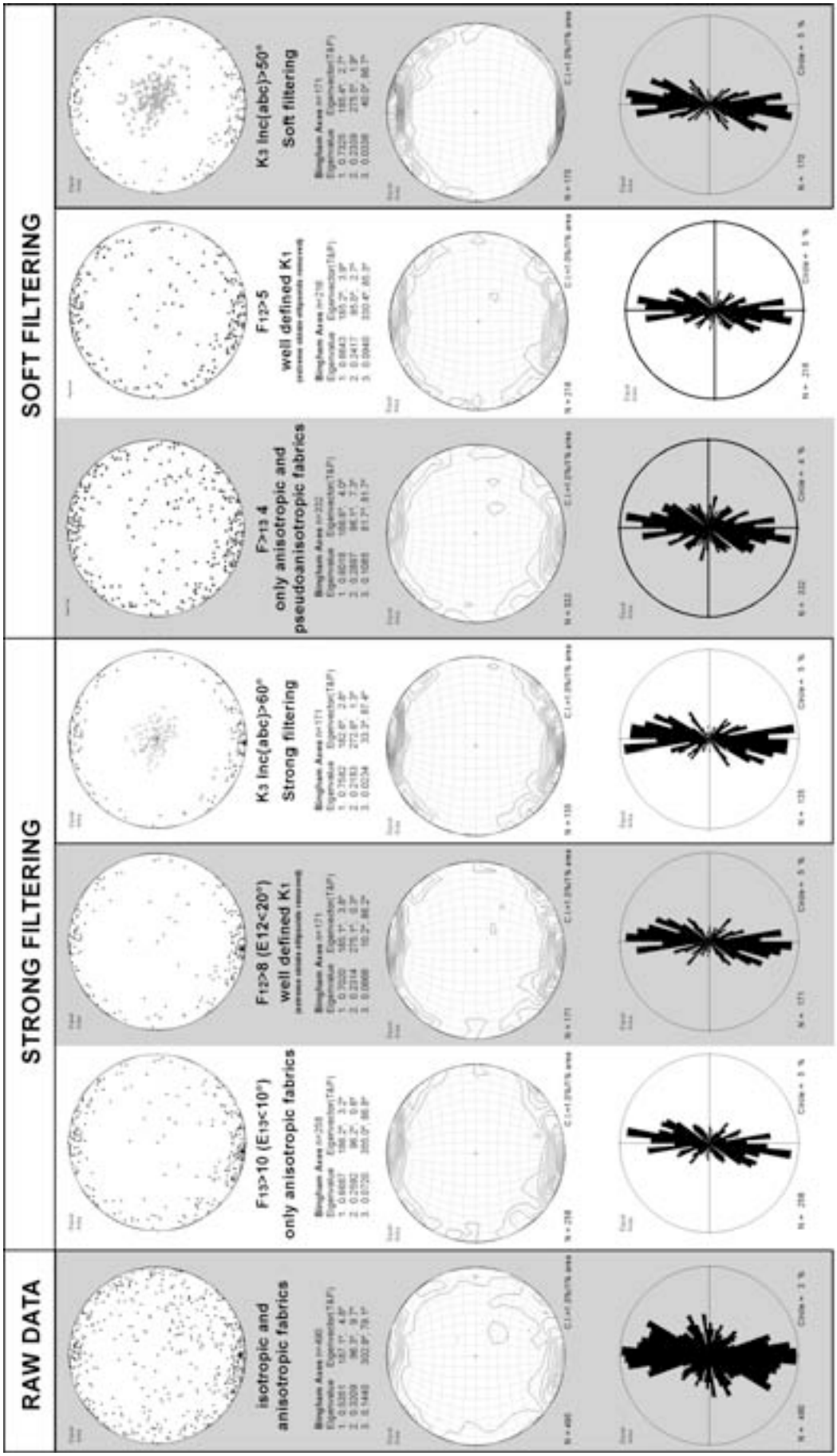

Figure 10. In colums: K1 declination from raw data and filtered data (strong and soft filtering). In rows: equal-area projection (including eigenvalues), density stereoplots and rose diagrams of K1 obtained through the section after step-by-step filtering

7.4. Interpretation

7.4.1. Interpretation of directional data

The directional data obtained in this work can be interpreted in the light of three main considerations:

(1) AMS is locked in a relatively early stage of lithification and diagenesis (Sintubin, 1994; Mattei et al., 1995; Sagnotti et al., 1998, 1999; Parés et al., 1999; Coutand et al., 2001; Larrasoaña et al., 2004; Day-Stirrat et al., 2008), and therefore reflects tectonic deformation at the time on sedimentation or slightly post-dates it (insignificant delay in terms of geological time; Larrasoaña et al., 2004), as demonstrated in many works dealing with AMS interpretation of extensional (Soto et al., 2007, 2008) and compressional (Larrasoaña et al., 2004; Soto et al., 2003) magnetic fabrics. This early lock-in mechanism has been extensively proven in the Southwestern Pyrenean Basin (Larrasoaña et al., 2004; Troy et al., 2008; Oliva-Urcia et al., 2009; Pueyo-Anchuela et al., 2011). In any case, later deformation was not intense enough to modify this early fabric.

(2) The long axis of the magnetic ellipsoid, K_{MAX}, represents the preferred mineral elongation and would be approximately perpendicular to the shortening direction at the moment of magnetic fabric blocking, according to far-field deformation in foreland basins i.e. layer parallel shortening (LPS) or near-field deformation within the orogenic front (folding or thrusting). Since paramagnetic minerals are phyllosilicates and almost perfectly oblate at the crystal-scale (Martín-Hernández and Hirt, 2003), the measured anisotropy probably relates to the intersection lineation of crystals, that is, the zone-axis (Bouchez, 1997). After incipient fabric blocking, AMS behaves as a passive marker during folding (horizontal axis of rotation) or during vertical axis rotation. Later stages have not internally modified the initial orientation of the magnetic fabric, because no foliation or other type of continuous structure is developed within the rock volume. It is worth mentioning that our samples are located south of the Pyrenean cleavage front. The magnetic fabrics obtained may be ascribed to an early tectonic deformation (type 2 of Parés et al., 1999), where magnetic foliation poles (K_{MIN}) are perpendicular to the bedding planes, and magnetic lineations (K_{MAX}) axes are grouped and reflect some early deformation lineation. The initial planar, sedimentary fabric is slightly modified and shows a weak linear orientation normal to the shortening.

(3) During and after fabric acquisition, blocking and folding (i.e. formation of the Boltaña anticline and its corresponding synclines), the whole area rotated clockwise. The lateral extent of this rotation to the East and West is not well known yet, but it undoubtedly involved the Boltaña and Mediano anticlines and the Buil Syncline (Pueyo, 2000; Fernández-bellón, 2004; Fernández et al., 2004; Oms et al., 2006; Mochales et al., 2008; López et al., 2008). This rotation was probably favoured by the existence of the Upper Triassic detachment level, and since no penetrative deformation is associated with this stage in the Boltaña anticline, it brought about a change in the orientation of fabrics that probably behaved as passive markers, together with folds.

Magnetic elongation trends (declinations) are variable, with well-defined maxima parallel to the orientation of the main structure (i.e. the Boltaña fold axis, Figures 1b, 4 and 5). Assuming that magnetic fabric was locked in at a relatively early stage of diagenesis, the different trends can be correlated with syntectonic events. These main trends can be interpreted in relation to Tertiary

compression events, associated with the emplacement of basement and cover thrust sheets of the Axial Zone. Three main trends can be distinguished through the stratigraphic pile: (1) In the lower 800 m, lineation changes from a roughly NNE-SSW to a NW-SE trend; (2) The central part shows constant K_{MAX} directions, with a N–S trend; (3) From 1700m upwards lineation acquires a NW-SE trend. The consistent change in trend from the lower to the upper part of the sequence can be attributed to changing deformation stages, associated with the diachronous emplacement of thrust sheets along oblique, lateral and frontal ramps. While sediments were being deposited in the foreland, LPS was generated by compressional, far-field structures. Growing onset of the Boltaña anticline brought about near-field deformation conditions thus giving rise to a widespread N–S (in present-day co-ordinates) magnetic lineation (Figure 11).

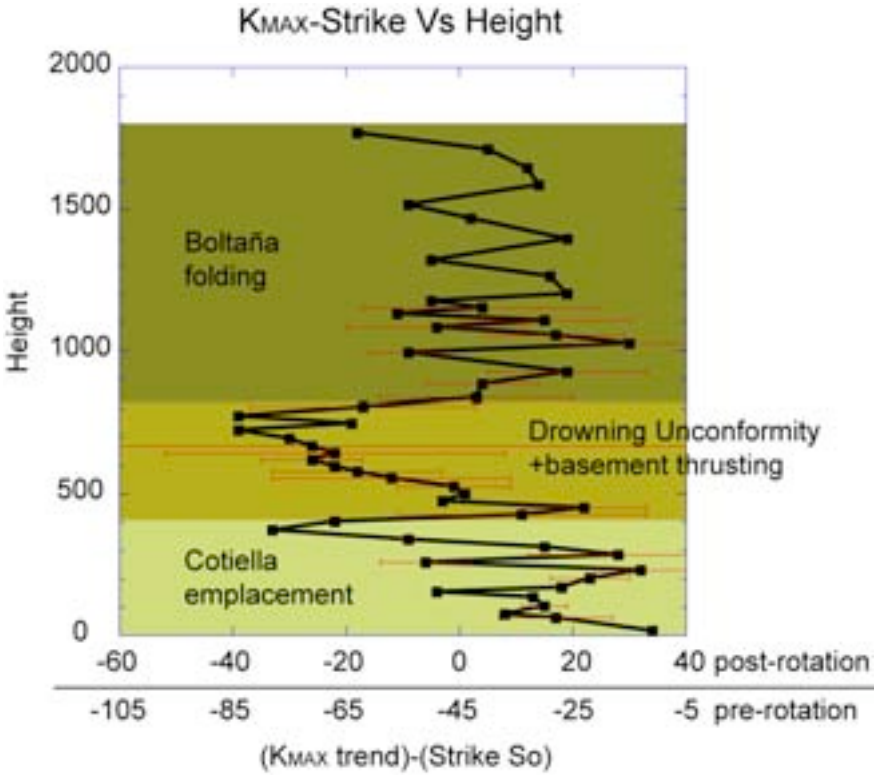

Figure 11. Diagram showing site by site angle between bedding strike and the magnetic lineation versus stratigraphic position; these angles have been plotted between -90 (West direction) and 90º (East one) of declination. Three stages have been recognized related to several regional tectonic events (see text for explanation).

Otherwise, the different directions obtained could be interpreted in terms of the variability of the directions recorded as a result of strain history variations. However, existing data point to a relatively constant history of shortening in the South Pyrenean Zone near the Boltaña anticline (Martínez-Peña and Casas-Sainz, 2003; Muñoz, 1992; Anastasio and Holl, 2001), making it plausible to explain magnetic lineation changes in relation to thrust sheet emplacement and rotation of relatively large areas.

The pre-folding, pre-rotation materials cropping out in the foreland basin (present location of the Boltaña anticline) record a variable fabric, which can be linked to the movement of the oblique ramp of the Cotiella Thrust during Ypresian times (Figure 11). A subsequent WNW–ESE lineation can be interpreted to be associated with basement thrust sheet emplacement. AMS seems to be sensitive enough to these far-field deformation events. During this stage, interference between the effects of the Cotiella Nappe and a basement thrust (Axial Zone) emplacements would take place. During Lutetian times a pervasive magnetic lineation developed. At this moment the Boltaña anticline nucleation would start, arranging the magnetic lineation according to a NW–SE trend (in Eocene coordinates). Therefore, during this stage, the magnetic fabric became more sensitive to the, probably more intense, near-field conditions. Afterwards, the end of the thrust sheet deformation and the emplacement of an underneath thrust would contribute to passively CW rotate the Boltaña anticline and all the magnetic lineations about 52º (chapter 5). To discriminate the near- and far-field effects in the pattern, K_{MAX} declinations can be used, because lineations generated by far-field structures show more variable trends (Cotiella and basement thrusting, Figure 11), whereas the near-field influence is more uniform (Boltaña anticline in Figure 11).

7.4.2. Interpretation of scalar parameters

According to the analyses described in previous sections, AMS in the studied rocks is mainly controlled by paramagnetic minerals, and therefore the magnetic tensors can be interpreted in terms of mineral (phyllosilicates) preferred orientation.

The total corrected degree of anisotropy of the tensor (P' parameter) shows mean values of 1.026, and most sites show values below 1.05 (Figure 2f). Many K_{MAX} and K_{MIN} directions are strongly scattered, also consistent with low anisotropy values and therefore low deformation of the involved rocks at the time of the fabric blocking. The shape parameter (considering both site-averaged values and individual data, Figures 2f and 4) indicates a predominantly oblate shape, with a mean value of 0.249. The lower part of the studied sequence (Boltaña Fm.) shows lower T values (more triaxial ellipsoids), whereas the upper part of the series, postdating the Boltaña anticline (Sobrarbe Delta Fm.), is markedly oblate.

Since P', Km and T are three parameters based on different magnetic variables, we suggest analysing the vertical trend of sedimentary sequences based on these parameters. Changes in trend can be considered more reliable when they involve the three parameters. However, since P' seems to be more sensitive, several upward-decreasing cycles can be defined through the studied sequence (Figure 6). Other prominent high values of P' can be correlated with high values of Km and T (indicated in Figure 6). These correlated events seem to be linked to sedimentary cycles, driven in turn by climatic and/or tectonic factors. The values of the three parameters increase during stages corresponding to either sea-level maxima or detrital deposition within the carbonate platforms (Figures 4 and 6). These changes can be linked to major tectonic events influencing the sedimentation rate and accommodation space (thrust emplacement in the Axial Zone, Barnolas and Teixell, 1994).

Latta and Anastasio (2007) interpreted anisotropy variations as the result of different

competence of the units and their differential response during cleavage formation. In the section examined in this study these changes cannot be attributed to deformation, because of the structural position of sampling profiles, tens of kilometres away from the cleavage front and with no visible penetrative structures. In our opinion, the pattern of variation of the magnetic parameters can be interpreted as related to the sedimentary evolution. Although more detailed work is needed in this regard, the results obtained point to acquisition of the magnetic fabric in discrete intervals of about 100–300m (cycles of P' represented in Figures 4 and 6), equivalent to approximate periods of 2 Myr. A long time of dewatering would take place for marls and sandstones during the time of compaction for defining the magnetic fabric. Nevertheless, in the case of limestones, a shorter dewatering and cementation time would result in a not so well-defined magnetic fabric.

8. Discussion and integration of results within the South Pyrenean tectonosedimentary evolution.

8.1. Summary of acquired data.

Three new magnetostratigraphic sections (914 demagnetized samples in total) have been studied in this work (Ara River, Coscollar and Mondot). The anchoring to the GPTS (Gradstein et al., 2004) based on biostratigraphic data, allows attaining some chronostratigraphic implications (Figure 1) for the Aínsa Basin; The Ara River section covers Ypresian (Ilerdian-Cuisian) rocks, ranging from chron C24r to C22r. The short Bal Ferrera section allows for identification on the C22r/22n reversal. The Coscollar section spans from C22n to C19r (mostly Lutetian). The Mondot section overlaps the previous one and encompasses the Lutetian/Bartonian boundary (C20n-C18r). The reinterpretation of the Eripol section by Bentham (1992) establishes a new age for its bottom at C18r and ends at C15n as previously interpreted (Bartonian-Priabonian). These new datasets accurately constrain the age of the studied stratigraphic units: The Alveoline limestones, Millaris, Metils and Yeba Fms are Ilerdian in age (Ypresian). The Yeba Fm recorded the Ilerdian/Cuisian boundary whereas the Boltaña Fm covered the Cuisian stage. The Paules Mb registers the Ypresian/Lutetian transition and extends to Middle Lutetian. The La Patra Mb is included into the Middle Lutetian. The Sobrarbe Fm spans from Middle to Late Lutetian. The Escanilla Fm starts in Late Lutetian and reaches the Middle Priabonian.

The accumulation rates evolved according to the sedimentary environment, that ranges from shelf environments (Ypresian) to fluctuating retro- and progradational pattern during Early and Middle Lutetian. During Middle Lutetian an accretion related to shelf development occurred. From Middle Lutetian the deltaic progradation increased the accumulation rate to suprafeeding conditions with the continental sediments incoming (Bartonian-Priabonian).

This large paleomagnetic dataset offers the possibility to control the vertical-axis rotation along the stratigraphic pile. Derived VAR sites from magnetostratigraphic sections (chapter 5), new discrete sites (chapter 6), reprocessing from previous magnetostratigraphic data (Bentham, 1992) and published sites located in the study area (Parés and Dinarès, 1993; Pueyo, 2000) allow us for determining the rotational kinematics of the Boltaña anticline and Aínsa Basin during the Eocene. The restored data provide a mean declination of 036, that means 31º of clockwise rotation recorded by the Eocene rocks (Figure 2), taking into account the expected Eocene reference (Dec, Inc: 005, 53; α_{95}: 4.6, see chapter 4). The best clustering observed after restoration together with the antiparallel character of normal and reverse polarities suggests the primary origin of the magnetization (as attested in several fold and reversal tests explained in chapters 5 and 6).

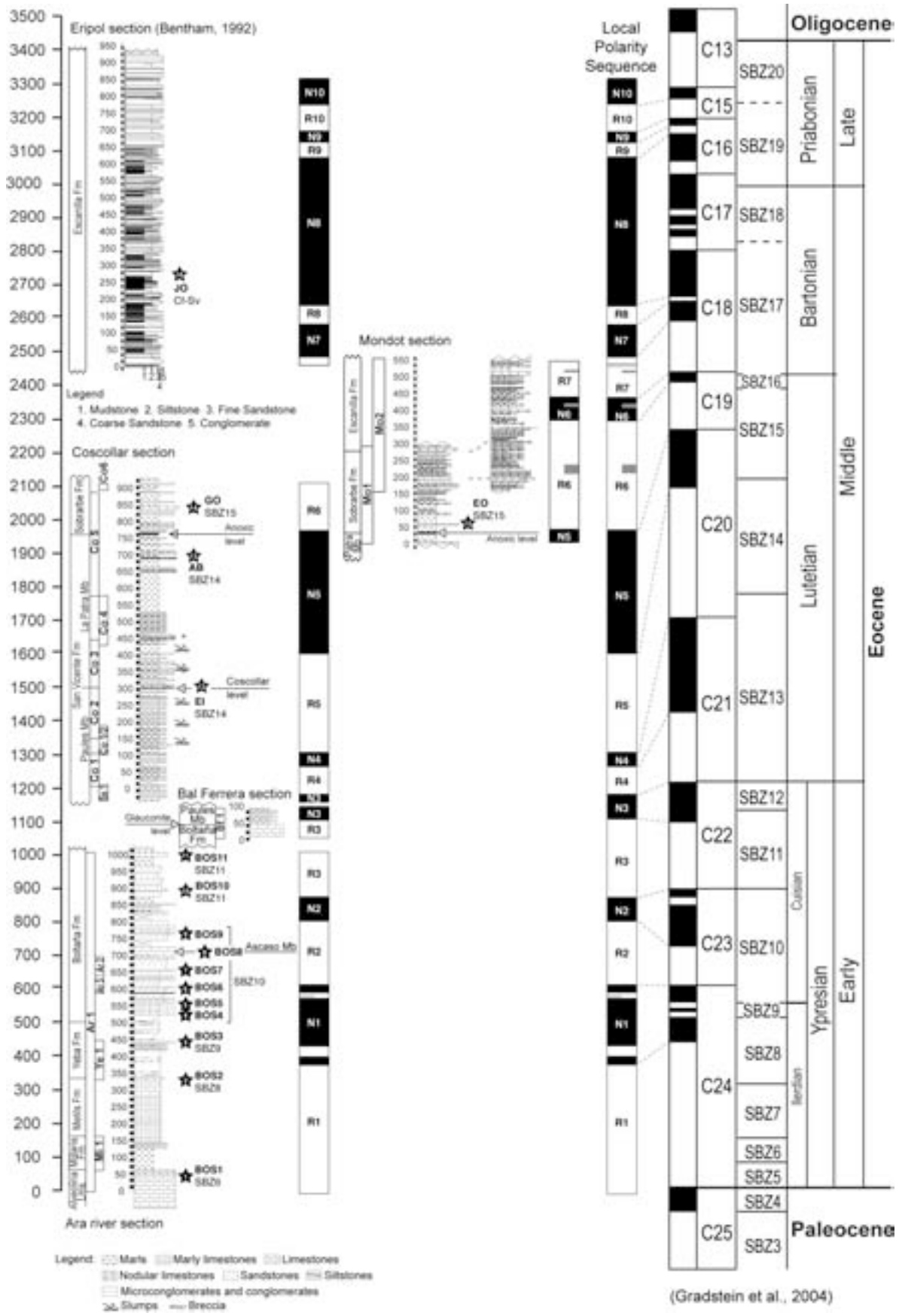

Figure 1. Composite section along the Aínsa Basin. The Local Polarity Sequence built from the Ara, Coscollar, Mondot and Eripol sections is related to the GPTS (Gradstein et al., 2004).

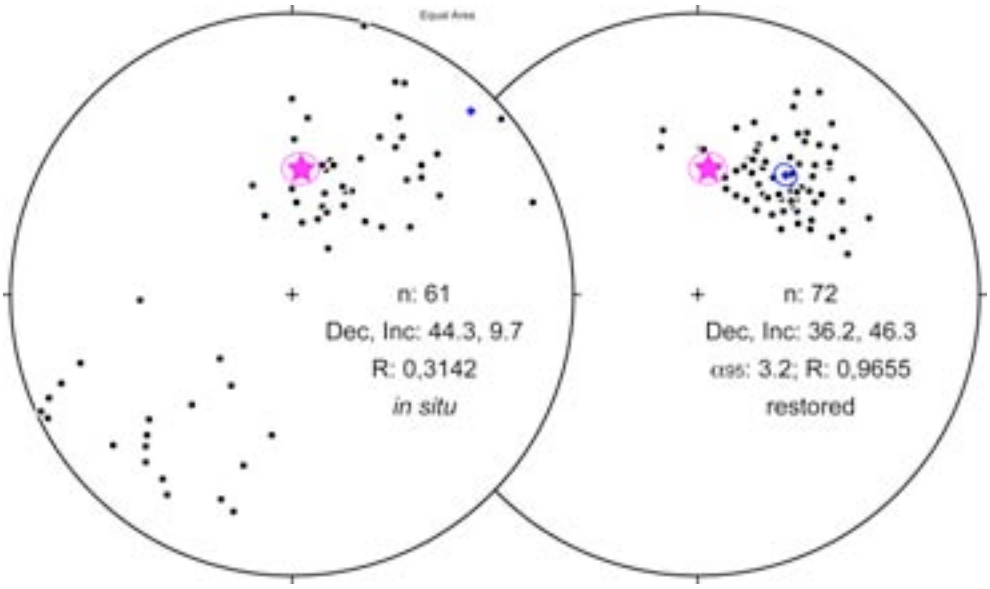

Figure 2. Lower hemisphere equal area stereoplots of the sites studied in this work (reverse polarities were projected in the lower hemisphere). 34 sites come from derived magnetostratigraphic data obtained in this work, 20 new sites were obtained in the San Felizes area (where a complex sequential restoration was performed) and Escanilla Fm and 7 sites from other authors (Pueyo, 2000; Parés and Dinarès, 1993). 11 sites come from the reprocessing of previous magnetostratigraphic sections (Bentham, 1992) not shown on the *in situ* steroplot. Scattering of *in situ* data prevent to determine a confidence angle. On the other hand, restored data provide meaningful VAR (the average is strongly influenced by a clear rotation-decreasing pattern from Bartonian times). Star represents the Eocene reference calculated from Taberner et al. (1999)

This banana-like clustering is not only caused by natural scattering as can be deduced when plotting the rotation versus the geological time. A non-significant (considering the confidence angles) progressive increasing of the rotation is observed from Ilerdian to Middle Lutetian. Approximately at the Late Lutetian the rotational value starts to decrease (Figure 3). Aiming to reduce the noise in this dataset, we grouped the sites into nine age-sets (2 Ma duration each), leading to logarithmic fit (Figure 3b). By means of the first and second derivatives the turning point has can be constrained. The turning point detected during the Late Lutetian points to the onset of the main rotational event. This rotation occurred from 42 to 37-38 M.a. (Late Lutetian-Bartonian)with a rotational rate of 2.6 º/m.y. The rate increased to 10 º/m.y. form 37-38 M.a. to 35 M.a. (Bartonian-Priabonian boundary to Middle Priabonian)

Finally, the dominant paramagnetic signal found in most marine rocks of the Aínsa Basin (as rockmag analyses testify, chapter 7), together with the location of the study area within the orogenic building allows the interpretation of AMS data as a record of mineral preferred orientation. Since the magnetic fabric seems to be locked-in at a relatively early stage of diagenesis (being a passive recorder of later deformation events), the different trends can be correlated with syntectonic events. Three main trends can be distinguished through the stratigraphic pile (pre-rotation, Figure 4):

(1) N-S to NNE-SSW lineation of the magnetic ellipsoid has been observed where the Alveoline Limestones, Millaris, Metils, Yeba and lower Boltaña Fm were involved. Since this part of the pile can be undoubtedly considered as pre-tectonic (pre-Boltaña anticline folding), this more variable

signal would be related to the record of a far-field deformation event such as the oblique ramping of the Cotiella thrust during Ypresian times.

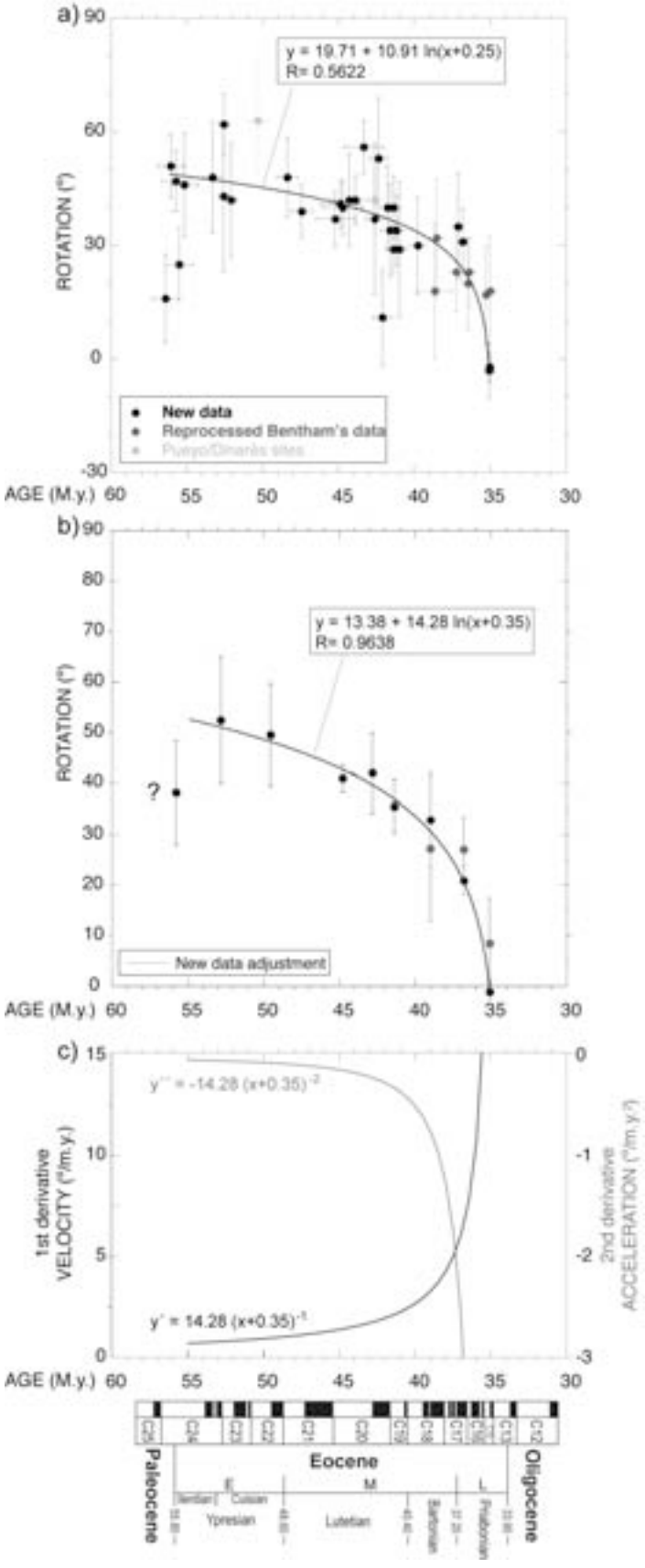

Figure 3. Rotation *vs* age (timescale according to Gradstein, 2004). a) Raw data (new and previous data by Parés and Dinarés, 1993; Pueyo, 2000). b) Logarithmic adjustment for new data obtained in this work. The rotational activity starts from 42 M.a. and increases at 37-38 M.a. c) First and second derivatives indicate the velocity and acceleration rates.

(2) The upper Boltaña Fm, records a NW-SE preferred mineral trend. Again, the AMS seems to be sensitive enough to far-field deformation events and it could be associated with active basement thrust sheet emplacement during Cuisian times. During this stage, interference between the effects of the Cotiella Nappe and the Axial Zone emplacements would take place explaining the high variability of the mineral preferred orientation in the pre-folding materials.

(3) From the Paules Mb (San Vicente Fm) to the Sobrarbe Fm, a pervasive magnetic lineation seems to recover a much more constant N-S trending. At this moment the Boltaña anticline nucleation would start, arranging the magnetic lineation according to an, almost invariable, NW–SE trend (in Eocene coordinates, Figure 4). Therefore, during this stage, the magnetic fabric became more sensitive to the near-field conditions.

Magnetic lineation pattern can be used to discriminate the near- and far field effects, because records generated by far-field structures show more variable trends (Cotiella and basement thrusting), whereas the near-field influence is more uniform (Boltaña anticline, Figure 4).

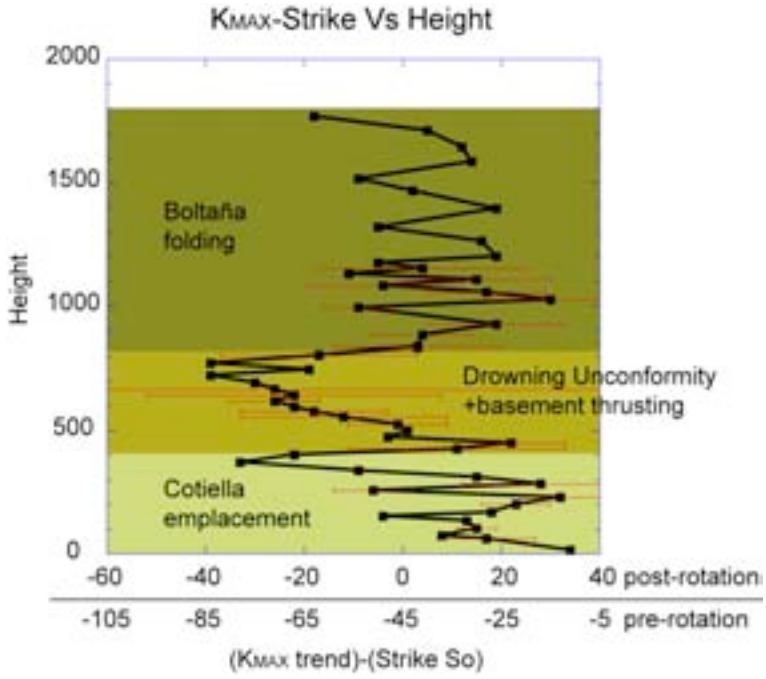

Figure 4. Diagram showing the angle between bed strike and the magnetic lineation versus stratigraphic position; these angles have been plotted between -90 and 90º of declination. Pre-rotation and post-rotation lineations are shown for the three recognized stages.

8.2. Kinematic model

Valuable tools have therefore been obtained to shed light on the deformational history of the Boltaña anticline and the Aínsa Basin during Eocene times; paleomagnetic implications, both chronostratigraphic and rotational, as well as the record of weak internal deformation (mineral preferred orientation) attested by the AMS data allow proposing a new kinematic model for the area. Considering main inflection points in the variable trends we have split the anticline history in four different moments.

1st stage- Ilerdian (56 Ma to 53 Ma): pre-folding, pre-rotation

The pre-tectonic sequence cropping out in the foreland basin (present-day location of the Boltaña anticline) was sampled in the Ara River section. According to the interpretation proposed in this work, the early stages of deformation are characterized by the imprint of N–S lineations in the magnetic ellipsoid. As previously stated, this might be related to a far-field effect of the emplacement of the westernmost oblique ramp of the Cotiella Thrust (Figure 5a). This event was probably Ypresian in age (Puigdefàbregas, 1975; Farrell et al., 1987; Martínez-Peña and Casas-Sainz, 2003) and was accompanied by cleavage development near the thrust front (Choukroune and Séguret, 1973), which would be far north from our position.

Regarding the paleomagnetic vectors a relative counter-clockwise rotation (-14º, α95: 10.2) have been recorded from Ilerdian with maximum declination close to the Ilerdian/Cuisian boundary. However this CCW rotation seems to be non-significant and could be produced by the noise caused by the lower sites (ARA1-ARA2) were higher variability was observed.

As a whole, the movement of the Cotiella-Bòixols nappe was diachronous, beginning in the east and progressively migrating westwards (Martínez-Peña and Casas-Sainz, 2003). In the east, the E–W thrusting began during the Campanian–Maastrichtian (Garrido-Mejías and Ríos-Aragüés, 1972; Simó, 1985; Berástegui et al., 1990; Bond and McClay. 1995; García-Senz, 2002). In the west, the emplacement of the Cotiella-Bóixols nappe was contemporary to the Early Eocene marine deposition (Garrido-Mejías and Ríos-Aragüés, 1972; Nijman and Nio, 1975; Martínez-Peña, 1991; Farrell et al., 1987; Mutti et al., 1988). We interpret that the N-S lineation detected by AMS analyses in the Ilerdian sequence corresponds to the western deformational episode of the Cotiella-Bòixols thrust system. These fabrics would be associated to a N-S first stage of folding related to oblique ramps progressively distorted by a second LPS event linked to WNW-ESE thrusting-folding (Soto et al., 2003). Non-outcropping oblique ramps with NNW-SSE to N-S trend, consistent with the magnetic lineations were deduced from seismic analysis (Ardèvol et al., 2000).

In summary, during Ilerdian times the study area belonged to the Pyrenean foreland basin, and was macroscopically undeformed. Some preferred-orientation record on the AMS seems to be the effect of a far-field process (Cotiella-Bòixols emplacement). Rotations can be discarded during this period.

2nd stage-Cuisian (53 Ma to 49 Ma): pre-folding, pre-rotation

From the sedimentation of the Ascaso Mb until the end of deposition of Boltaña Fm., mineral preferred orientation record by the magnetic fabric are oriented NW–SE (Eocene reference). This process would be contemporary with a regional-scale drowning unconformity (Barnolas and Teixell, 1994), as a probable consequence of Pyrenean compression. A tectonic reactivation linked to the emplacement of new structural units would give rise to deepening and constriction of the basin (Barnolas et al., 1991). The tilting and foreland-wards displacement of the depocentre would generate a generalized drowning unconformity. The deviation from the WNW–ESE Pyrenean direction could be the consequence of the influence of the oblique Cotiella and basement thrust sheets to the north (Figure 4). During Ypresian times, we interpret that fabrics are more sensitive and display more variability due to changing far-field effects on this part of the foreland.

Regarding paleomagnetic declinations, a scattering is observed in Cuisian deposits, rather prone to maintain the broad 45º of rotation. As aforementioned, we consider a slow rotation rate during Ypresian-Lutetian times, maybe non-significant if the error bars are considered but consistent along more than 10 Ma. The pre-folding and pre-rotational character (at least, the main rotational event) endures during the Cuisian stage.

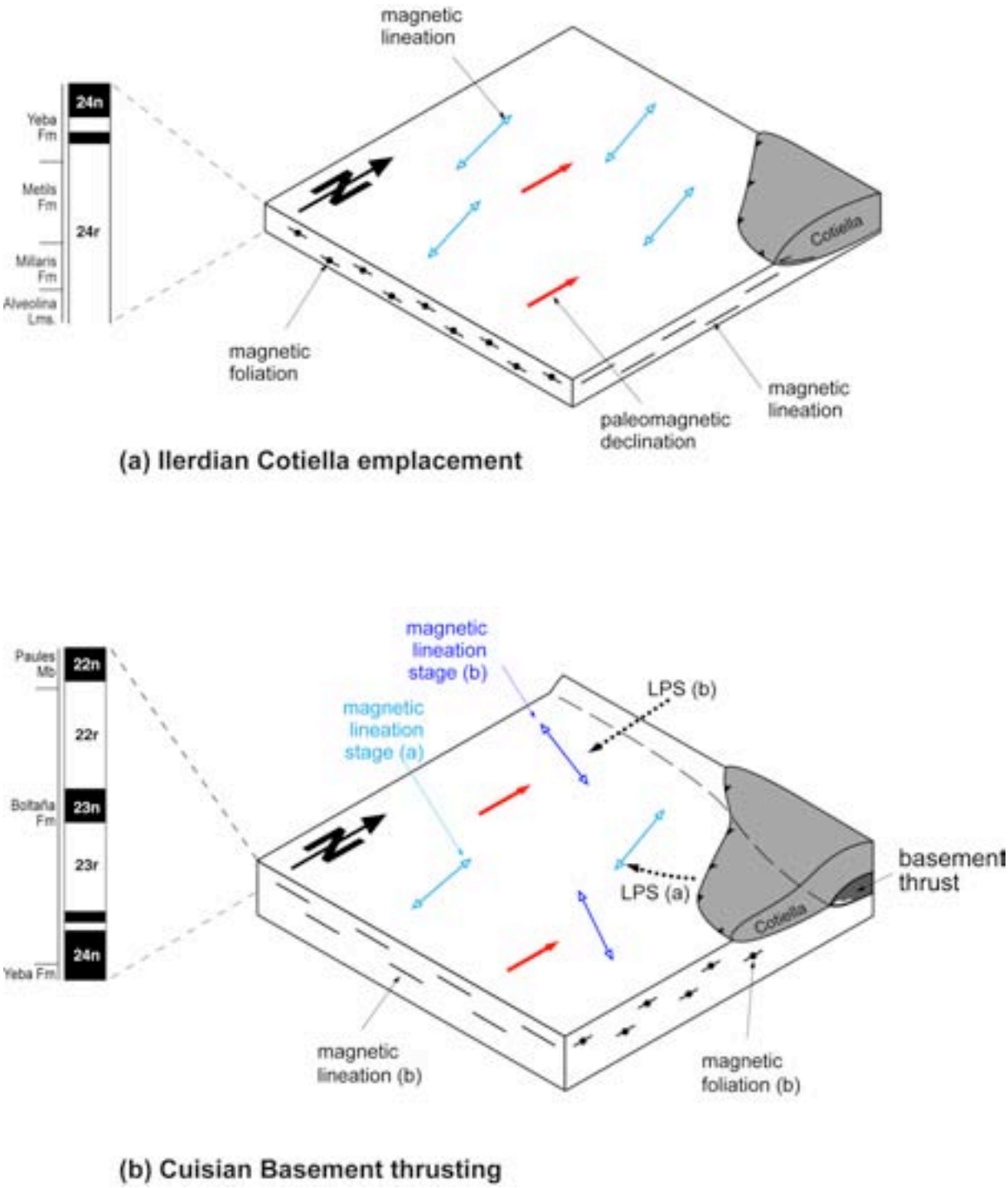

Figure 5. Simplified sketch of the western boundary of the SPCU, showing the proposed evolutionary model to describe the role of the magnetic declination (red arrows) and AMS (blue arrows) during the formation of Boltaña anticline. The figure shows that the record of the effect of the LPS previous to the formation of the Boltaña anticline is very variable and influenced by tectonic far-field effects. (a) The Ilerdian stage is related to the Cotiella emplacement. (b) During the Cuisian, basement thrusting in the Axial Zone leaves its imprint on the AMS markers. On the other hand, the paleomagnetic vectors undergo a small rotation with respect to their former northerly trend, related to the slow rotation rate during the Ypresian-Lutetian interval. The pattern of magnetozones detected in each stage is included as well as the units sedimented during each stage.

In the southwards propagating piggyback setting where the southern Pyrenees are involved, the Cotiella-Boixols unit was transported passively on the Montsec thrust sheet. This thrust was active from Ilerdian through Cuisian times (Garrido-Majías and Ríos-Aragüés, 1972; Nijman and Nio, 1975; Farrell et al., 1987; Muñoz, 1992; Teixell and Muñoz, 2000) generating minor normal fault movements during flexural subsidence associated with thrust sheet loading. Considering the trend of the recorded mineral preferred orientation (NW-SE) and the location of the sections studied in this work (WNW from the Montsec thrust), this magnetic lineation does not seem to be linked to the oblique ramps of the Montsec thrust. Nevertheless, the initial stages of this thrust are coeval with the Cotiella-Bòixols thrusting, indicating that at least during Cuisian times both systems were synchronous, what could slightly re-orient the magnetic lineation during this stage.

In summary, during Cuisian (Ypresian) times the study area still belonged to the Pyrenean foreland basin, and was macroscopically undeformed. The origin of a more patent mineral preferred-orientation record on the AMS is hard to decipher and could be the combined or isolated effect of different far-field processes: northern basement thrusting (Bielsa), eastern cover thrusting (Monsec), north-eastern thrusting (Cotiella movement).

3rd stage Early-Middle Lutetian: (49 Ma to 42 Ma): syn-folding, pre-rotation.

During Lutetian times a pervasive magnetic lineation parallel to the fold axis developed coinciding with the onset of the Boltaña anticline folding that would arrange the mineral preferred orientation according to a NW–SE trend (in Eocene pre-rotational coordinates). Therefore, during this stage, the magnetic fabric became more sensitive to the near-field conditions (folding). Since there is no agreement about the onset of folding in the Boltaña anticline, we cannot accurately evaluate the relative timing of the AMS record and the Boltaña folding, or if this record is much earlier than the folding. Several studies suggest that its growth started in Early Lutetian (Arbués et al., 1998; see mapping in Poblet et al., 1998, and thickness variations in depth in Soto and Casas, 2001). Nevertheless, other authors suggest a later start of deformation, during the Middle Lutetian (Millán, 1996; Montes, 1992; Teixell, 1996) or at least not before this period (Barnolas et al., 1991). Mapping from Puigdefàbregas (1975) indicates that the deformation might have started as late as the Late Lutetian. If folding started in Early Lutetian, AMS reveals not only as a geometrical indicator but also as a tentative temporal marker (Pueyo-Anchuela et al., 2007, 2008). The syntectonic deposits found in the western limb of the anticline suggest that folding started, at least, in Mid-Lutetian, therefore AMS would record between 3 and 4 Ma in advance the folding. This could be interpreted in terms of a buried nucleation that would constrain the magnetic lineation about 4-3 M.y. before the Boltaña-Balzes thrust showed any cartographic evidence of movement. A progressive unconformity found within the Guara Fm at the western limb of the Balzes anticline, dated as Mid-Lutetian, denotes the synsedimentary character of this fold (Millán et al., 2000; Barnolas and Gil, 2001; Rodríguez-Pintó et al., 2011b). Therefore, the Boltaña and Balzes folds have been interpreted as the result of the Boltaña-Balzes thrust sheet, synchronously deformed in Middle Lutetian, as inferred from previous seismic interpretations (Millán, 1996, 2006).

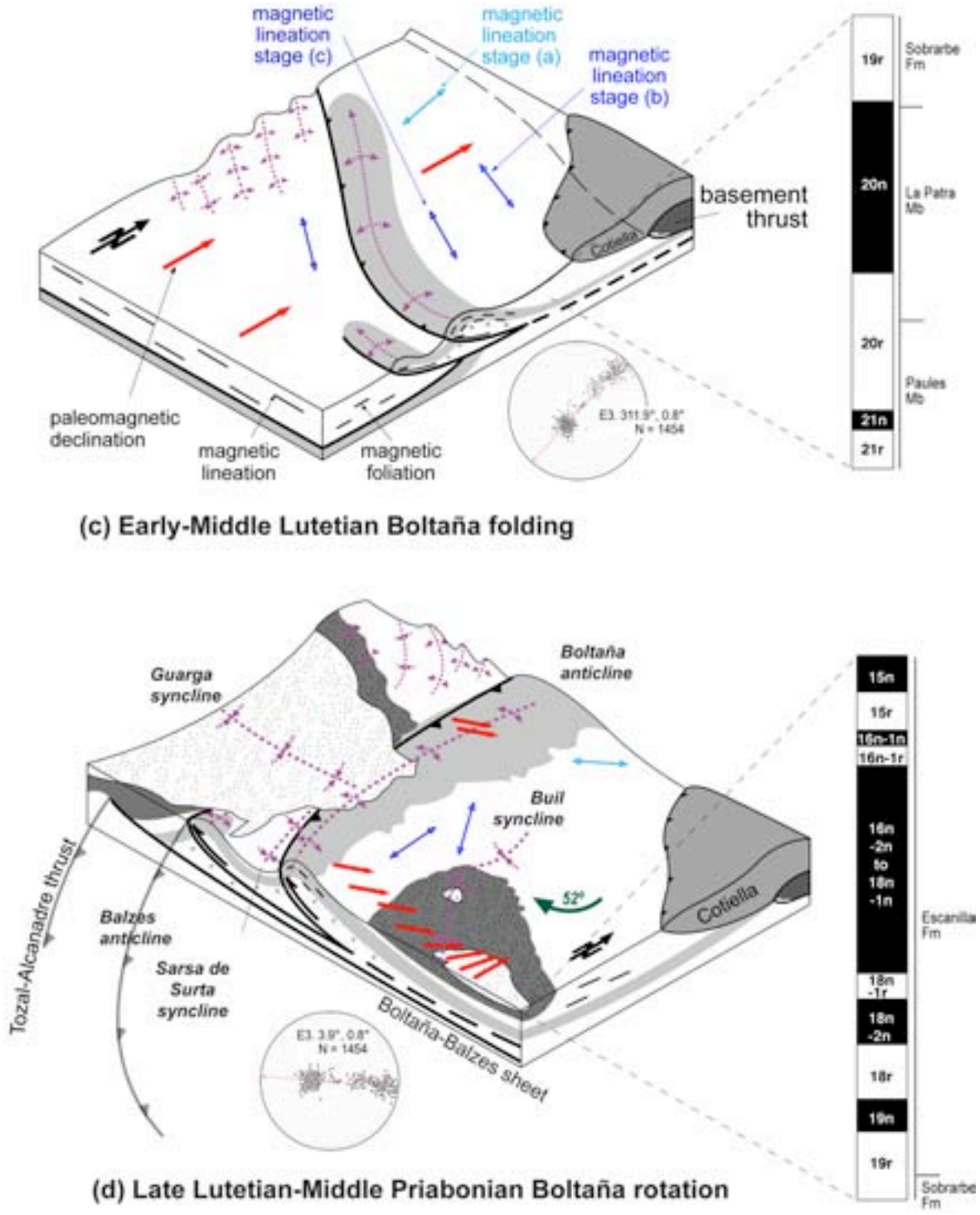

Figure 6. Simplified sketch of the western boundary of the SPCU. c) The Early-Mid Lutetian stage shows the Boltaña and Balzes anticlines with Pyrenean trend. Paleomagnetic vectors are parallel and N-directed during early diagenesis episodes. Equal area and E3 Bingham's distribution (1974) of bedding poles are shown (restored to their pre-rotational orientation). In Lutetian times the near-field events are responsible for the lineation orientations. d) In the Late Lutetian-Mid Priabonian stage rotational motion was due to the movement of the Alcanadre-Tozal thrust sheet, responsible for the passive rotation of the Boltaña-Balzes thrust sheet. Paleomagnetic vectors approach the magnetic north as rotation diminishes in younger sediments, dying out in Middle Priabonian. Equal area and minimum eigenvector of bedding poles are shown (field data). The rotation (37º) is responsible for deflecting the previous lineations that act as passive markers. Age and formations involved in each stage are represented.

Therefore the N-S alignment (in present-day coordinates) of the mineral preferred orientation coarsely marks the onset of folding of the Boltaña anticline during Lutetian Early times. At the beginning of the Lutetian, scattered directions are probably due to the contemporary emplacement of the basement Bielsa thrust and the Boltaña anticline uplift. Now, the mineral preferred orientation is considerably less-scattered and emphasizes a constant N–S trend along Lutetian times, corresponding to the growing of the Boltaña anticline. In this stage, near-field deformation would control the record of the mineral preferred orientation. In comparison with the far-field effects of LPS on the magnetic fabrics (i.e. Ebro Basin, Pueyo-Anchuela et al., 2010), the relative scattering observed during Lutetian is due to the influence of near-field processes (folding). It is worth mentioning, that the SS01 profile located within the limestones (Boltaña Fm.) and the marls (Paules Mb) is of key importance to reject a possible lithological effect on the lineation orientation, because the magnetic lineation axes coincide in both rock types.

Considering the paleomagnetic data for this period, they form part of the non-significant rotational pattern previously mentioned in the Cuisian stage. This would imply a low velocity of rotation as well as a little amount of accommodated rotation during this time. As in previous temporal reconstructions, the overlapping of confidence angles prevents to unambiguously state this decreasing VAR pattern. The sedimentary succession can still be considered as syn-folding and pre-rotational since constant values of 45º– 50º clockwise rotation are found along this time interval (Mochales et al., 2008). Therefore the syn-folding and pre-rotational stage corresponds to the Early and Middle Lutetian. During this period, the western limb would control the architecture of the San Felizes folds. We interpret that initially they presented a variable trend ranging from NW-SE to WNW-ESE (Eocene coordinates) and were originated as a compromise of the interference between the Boltaña thrusting (NW) and the effect of the Larra and Gavarnie thrusting (WNW-ESE) within the Hecho turbidites (flysch). As consequence of the subsequent rotation they underwent a differential shortening to present the current fan-shape disposition.

As earlier suggested by Cámara and Klimowitz (1985), attending to the regional frame, the Boltaña oblique ramp anticline could be laterally related to the Larra-Monte Perdido thrust system (Internal Sierras), through the Añisclo anticline (Soler and Puigdefàbregas, 1970; Teixell, 1996). This, large-scale sigmoid geometry will share deformational ages during mid-late Lutetian to Bartonian times (Montes 1992; Teixell, 1996; Tavani et al., 2006).

4th stage, Late Lutetian-Middle Priabonian: (42 Ma to 35 Ma): syn- and end of folding, syn-rotation

An abrupt decay of rotation magnitudes is observed between the Late Lutetian (37°) and the Middle Priabonian (0°). Logarithmic fitting (Figure 3b and c) displays an inflection point at approximately 42 M.a., opening a second trend with an abrupt fall in the rotational value. The rotational motion would be started from 42 M.a. to 37-38 M.a. (Late Lutetian to the Bartonian-Priabonian boundary), with a rotation rate of 2.6º/M.a. and accelerated during Priabonian times (10º/M.a.). Therefore the main rotational event recorded by the Boltaña anticline occurred between Late Lutetian and Middle Priabonian (Escanilla Fm). As consequence of a contrasting gradient of shortening with the western units (Gavarnie related, i.e.Basa anticline among others), the western limb

of the Boltaña anticline (San Felizes area) would be bended forming a fan of folds in the Lutetian sequence.

A logarithmic curve implies an acceleration of the movement linked to the emplacement of the related thrust sheets. The first stage would imply a gradual, low-rate CW rotation affecting Ypresian and Lutetian rocks of the Aínsa Basin. A second stage, starting at the Late Lutetian, definitively rotated the Boltaña-Balzes sheet. Priabonian sites record paleomagnetic vectors parallel to the reference direction and therefore the end of the rotational motion.

The subsequent and main rotational movement would be related to the final activity of the Boltaña-Balzes thrust sheet and/or maybe would be the effect of the rotational activity of an underneath and younger thrust sheet (Tozal-Alcanadre, defined by Millán, 1996). Although the Tozal-Alcanadre thrust sheet does not crop out in the study area, there exist evidences supporting the Tozal-Alcanadre movement during Bartonian times, as the outcrops of the Nasarre anticline and Sierra de Guara as well as the interpretation of seismic lines (Millán, 1996) indicate. No data allow at this moment to locate the pinpoint of the rotation of the Tozal-Alcandre thrust sheet, whose northern portion is buried underneath the Campodarbe Gp in the Guarga synclinorium. Nevertheless, the fan-like set of folds in the San Felizes area, where N-S narrow and overturned folds change rapidly to WNW-ESE and wide folds, suggest that the pin-point the Tozal-Alcanadre sheet could be located under this area. Once rotational movement ended, deformation migrated to the west, towards the External Sierras (Millán et al., 2000; Pueyo, 2000).

The rotational motion is the consequence of the southwestwards advancement of the South Pyrenean sole thrust. The Montsec thrust, developed during Ilerdian and mainly Cuisian times (Garrido-Mejías and Ríos-Aragüés, 1972; Nijman and Nio, 1975; Farrell et al., 1987; Muñoz, 1992; Teixell and Muñoz, 2000), is very unlikely related to the rotation of the Boltaña anticline. On the other hand, the Marginal Sierras thrust sheet initiated in Early Eocene, having a second deformational stage from Late-Middle Eocene to Early Oligocene (Pocoví, 1978; Vergés and Muñoz, 1990; Muñoz, 1992). In the Marginal Sierras sheet there are numerous oblique ramps, back-thrusts and hangingwall thrust sequences (Martínez-Peña and Pocoví, 1988; Muñoz, 1988; Vergés and Muñoz, 1990; Martínez-Peña *et al.*, 1992; Teixell and Muñoz, 2002) as a consequence of several emerging episodes along the thrust front (Martínez-Peña, 1991). This structural complexity with respect to the Montsec or Bòixols thrusts is associated with a thick detachment level (Keuper) and thin hanging-wall cover sequences, making difficult the tracking of the front. Due to the long-lasting thrusting time span of the Marginal Sierras and its structural style, we interpret that the Boltaña thrust sheet could be associated to an oblique zone of this system. A younger imbricate thrust sheet (Tozal-Alcanadre) is located in the footwall of this oblique zone (Millán, 1996).

Regarding previous interpretations of the rotation of the Aínsa Basin, Fernández-Bellón (2004) proposed a regional 40-50º clockwise rotation in the Aínsa Basin, homogeneously accommodated from Early to Late Lutetian. This decreasing continuous pattern was also proposed for the Boltaña anticline according to clockwise rotations from 50-70º in Early Lutetian to 30º in Late Lutetian times (Fernández-Bellón, 2004). Against this hypothesis, we propose a non-steady scenario with the main rotational movement younger than the one proposed by Pueyo et al. (1999), Pueyo

(2000) and Fernández-Bellón (2004). Rotational values remain relatively stable from Ilerdian to Upper Lutetian, with a slight decrease of 15º in 13 M.a. Afterwards, 37º of CW rotation occurred between the Late Lutetian and the Middle Priabonian (≈ 7 M.y.). This rotation explains the current N-S orientation of the Boltaña anticline, oblique to the WNW-ESE Pyrenean trend. The end of the Boltaña anticline folding would mark the end of this stage.

The final stages of the Boltaña folding would be bounded at the Late Bartonian times (Puigdefàbregas, 1975; Montes, 1992; Barnolas and Gil-Peña, 2001), synchronously to the end of the Larra thrusting (Teixell, 1996). Despite the end of the folding, the rotational pattern of the Boltaña and Balzes anticlines endured to Middle Priabonian. Younger deformation patterns can be found westwards in the External Sierras front (Millán, 1996; Millán et al., 2000) where thrust propagation and thrust rotation ages seem to follow a parallel model (Pueyo, 2000).

In the southern part of the Jaca Basin a subsequent system of folds are dominant defining the ESE-trend on the Guarga synclinorium (Puigdefàbregas, 1975). The Jaca unit would have been displaced southwards related to the Gavarnie and Guarga thrust frontal emplacement, defining the structure of the Guarga syncline and the South Pyrenean frontal thrust. The Guarga blind thrust with Pyrenean trend, might have partitioned the foreland basin, displacing the depocentre towards the Ebro Basin in Late Oligocene to Early Miocene times (Teixell, 1996). On the other hand, Martínez-Peña and Casas-Sainz (2003) suggested an earlier emplacement for the eastern portion of Guarga thrust as Bartonian-Priabonian. The hypothesis here presented is that previous marine (Hecho Gp., Sobrarbe and Belsué-Atarés Fms.) and continental (Campodarbe Gp.) rocks would be reoriented according this deformational stage. Therefore the set of folds comprising the San Felizes area would experience a southwards tilting consistent with the northern limb of the Guarga syncline.

8.3. Basin-scale implications

8.3.1. Accumulation rates

The results obtained in this work allow for a comparison with accumulation rates based on magnetostratigraphic studies in closer areas of the South-Pyrenean basin. Hogan and Burbank (1996) and Oms et al. (2003) on one side (Jaca Basin) and Bentham and Burbank (1996) and Beamud et al. (2003) on the other (Graus-Tremp Basin) provide magnetostratigraphic profiles west and east, respectively, of our work area (Figure 7). Albeit constrained within narrower time windows, these profiles allow defining variations in accumulation rate along a longitudinal E-W profile within the South-Pyrenean basin. The overall pattern shows a westward migration of subsidence areas during the Early-Middle Eocene (Esera-Mediano-Boltaña, figure 7), a process that culminated with the onset of strong subsidence in the Jaca basin. This was already postulated within the Jaca turbiditic basin (Labaume et al., 1985). Accumulation velocity increased from the Middle Eocene (C20) onwards both for the Aínsa and Jaca basins, although accumulation rate was higher in the turbiditic Jaca basin during the recorded basinal history.

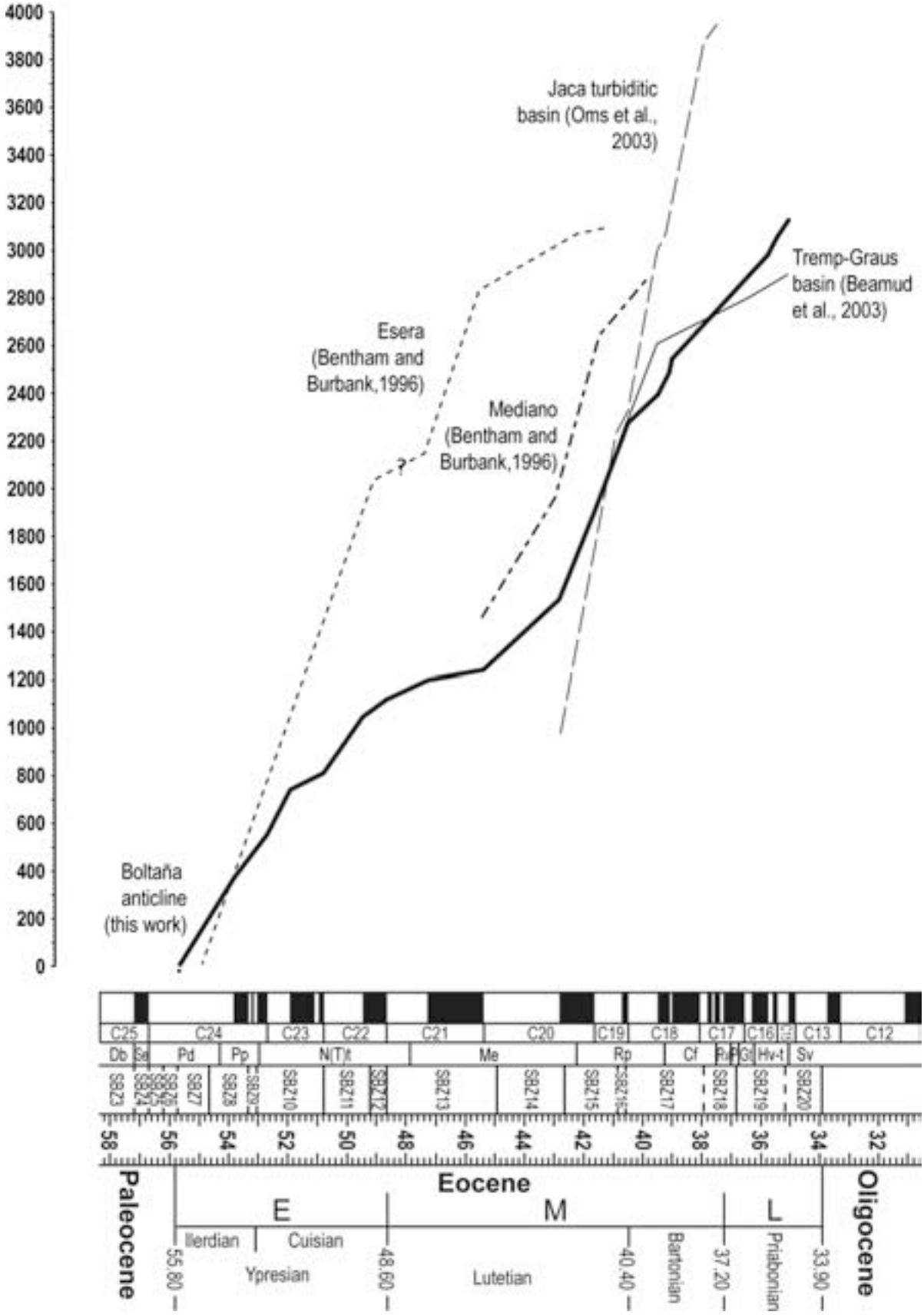

Figure 7. Accumulation rates (m/M.a.) deduced from magnetostratigraphic studies in the Aínsa Basin (study area in bold line) and adjacent areas (Jaca and Graus-Tremp basins).

During C18 accumulation rate slowed dramatically in the Graus-Tremp basin, where continental deposition took place (Beamud et al., 2003), and likely not so strongly in the Aínsa basin, probably defining the ultimate migration of subsidence from the Eastern to the Central and Western Pyrenees, accordingly with progressively younger tectonic structures to the West (Puigdefábregas, 1975; Martínez-Peña, 1991; Millán et al., 2000).

8.3.2. Sedimentary implications

During the Late Lutetian the Jaca basin underwent shallowing with turbidite-prodelta transition in its northern sector. In its southern part a deepening occurs, flooding the Guara limestone shelf, indicating a southwards displacement of the basin induced by the Gavarnie thrust sheet emplacement. The Boltaña anticline, conforming the same structural unit, underwent uplift, thus ending the stage of marine sedimentation.

Complete cessation of the rotational movement in the Boltaña Sector occurred in the Middle Priabonian. During this time, the sedimentary scenario consisted of a fluvial network with meandering rivers flowing from SE to WNW (Escanilla Fm. and Campodarbe Gp.). This deduction helps to clarify the lateral correlation between the Escanilla Fm and the Campodarbe Gp, whose nearest outcrops are located south-eastwards and westwards to the Boltaña anticline respectively. Since the rotation endured still the Middle Priabonian and the Campodarbe Gp has not been affected by this rotation (Pueyo, 2000; Mochales et al., 2011), this entails that the Campodarbe Gp would be coeval with the upper Mb of the Escanilla Fm, as previous authors stated (Bentham, 1992). This result would challenge the hypothesis of coeval development for both units (Puigdefàbregas, 1975; De Federico, 1981). Although they belong to the same fluvial system dominating during the final deformational stages of the Aínsa Basin, it would flow down before in the southeastern portion, according to the SE provenance of the fluvial system.

8.3.3. Thrust kinematics at regional scale

Growth of the Boltaña anticline with Pyrenean trend (N128E) began in the Middle Lutetian. The growth has been associated with the Larra thrust system (Teixell, 1996), which would connect through the Monte Perdido thrust system and the Añisclo anticline (Figure 8). The age of the Larra thrust system seems coeval with the folding of the Boltaña anticline (Teixell, 1992). According the deformational pattern established by Garrido-Mejías (1973), the N-S folds of the Aínsa Basin would have evolved during a tectonic stage following the emplacement of the Montsec unit and prior to the emplacement of the Gavarnie Nappe (Figure 8). Therefore the Middle Lutetian reveals as the moment for the Boltaña folding, consistently with the AMS analyses obtained in this work. The origin of the folding would be the result of formation of oblique structures located between the Mediano and Balzes anticline. Likewise, the configuration and geometry of the Boltaña and Añisclo anticlines suggests that both structures experienced a common deformation, although deformation could start earlier in Añisclo (Fernández-Bellón, 2004; Tavani et al., 2006).

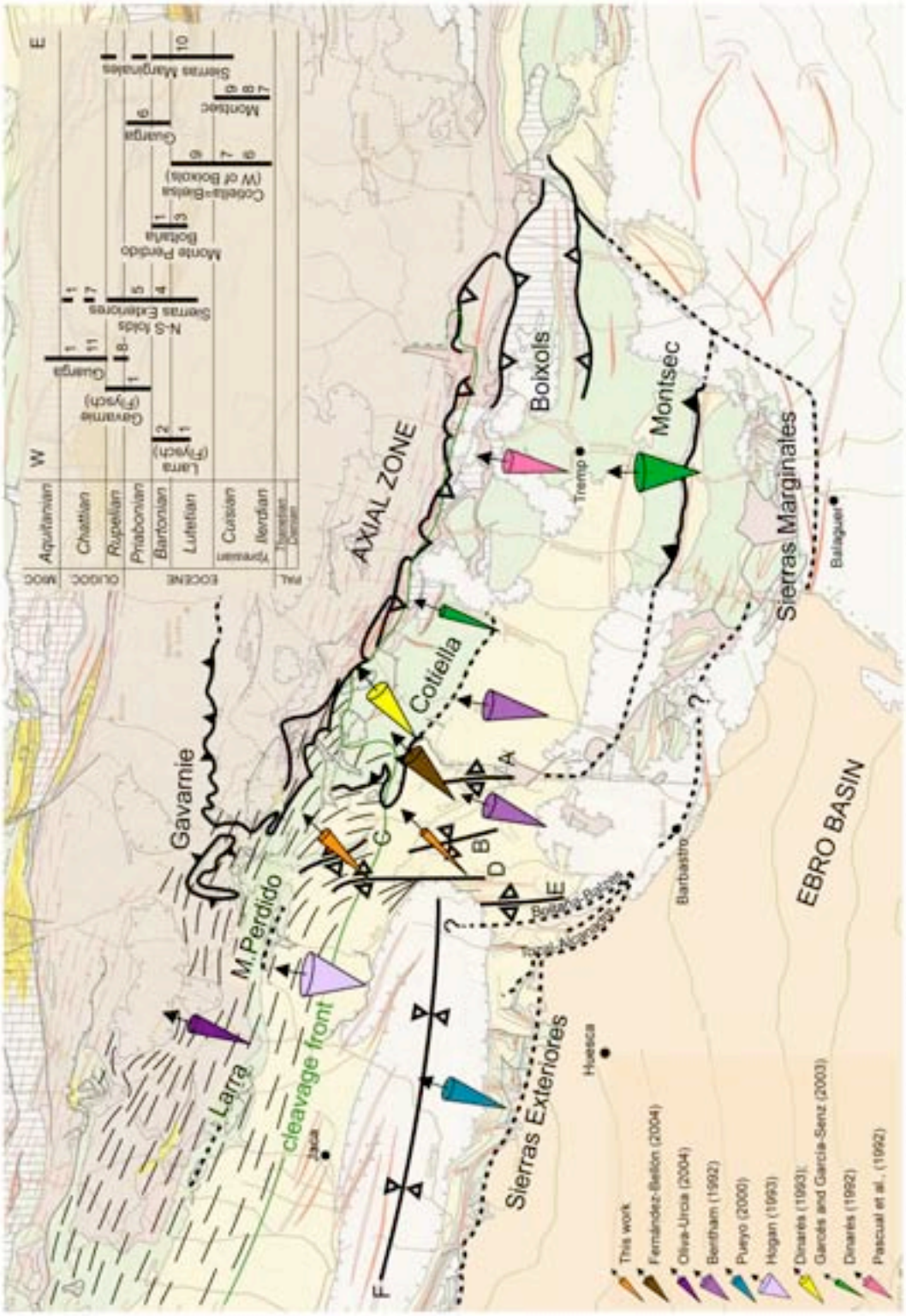

Figure 8. Geologic map base from Choukroune and Séguret (1973) modified by López et al. (2008) including well data from Lanaja (1987). The main structures involved in this work are suggested. A. Mediano anticline; B. Bull syncline; C. Abiscio anticline; D. Boltaña anticline; E. Balzes anticline; F. Guarga syncline. Paleomagnetic rotations (collected from different authors) are displayed as cones. Their axes represent the Vertical Axis Rotation in that point and the semi-apical angle of the cone represents the precision angle (α95). Age of the thrusting development has been compiled from the literature: 1. Teixell, 1996; 1998; 2. Labaume et al., 1985; 3. Soler and Puigdefábregas, 1970; 4. Puigdefábregas, 1975; Millán et al., 1992; 5. Millán, 1996; 6. Martínez-Peña, 1991; Martínez-Peña and Casas-Sainz, 2003; 7. Garrido-Mejías and Ríos, 1972; 8. Muñoz, 1992; 9. Farrell et al., 1987; 10. Poyová, 1978; 11. Oliva-Urcia, 2004 .

Cámara and Klimowitz (1985), Mutti et al., (1988) and Martínez-Peña (1991) interpret these anticlines as the result of folding over oblique ramps with small development in comparison to the regional-scale thrust-sheets in a more frontal position. On the other hand, alternative hypotheses relate these anticlines to an oblique ramp of the Gavarnie thrust (Holl and Anastasio, 1995a and b; Anastasio and Holl, 2001) that do not coincide in time, since other authors propose later ages for the Gavarnie thrusting (Priabonian-Rupelian, Teixell, 1996; Bartonian-Rupelian, Oliva-Urcia, 2004). The lack of large volumes of Triassic evaporites seems to hamper the halokinesis associated to both anticlines as proposed in other structures like the Mediano anticline (Anastasio, 1992; Holl and Anastasio, 1993).

Although the Añisclo and Boltaña anticlines have common features and represent relay faults of the Lutetian deformation, we do not have data to attribute an age of folding for the Añisclo anticline. Field data evidences that the Lutetian San Vicente turbidites lie mostly unconformably over this sequence and are partially coeval with the growth of the Añisclo anticline (e.g. Fernández et al., 2004). The dating of the Boltaña anticline constrained in this work by the AMS record and the syntectonic features associated to Balzes anticline (Barnolas al Gil-Peña, 2001; Rodríguez-Pintó et al., 20011d) point to the synchronous growing up of both structures (Figure 8) in agreement with the geometrical relationships between them established by seismic profiles (Millán, 1996). We cannot precise the age of growth of the set of folds located in the San Felizes area; however we can tentatively bound its age as prior to the beginning of the Boltaña rotation (around the Late Lutetian) and therefore coeval to the Boltaña-Balzes thrusting. The end of the Boltaña anticline uplift occurred prior to the deposition of the lower segment of the Campodarbe Gp (Puigdefábregas, 1975; Montes, 1992; Barnolas and Gil-Peña, 2001; Teixell, 1996), which is not folded by the anticline in the vicinity of the Campodarbe village, almost located at the hinge of the fold. The age of the basal Campodarbe sequence in this position is Late Bartonian as attested by the lateral correlation of the Monrepós magnetostratigraphic section (Hogan, 1993; Hogan and Burbank, 1996).

8.3.4. Dating the end of the Boltaña folding.

The analysis performed in this work (paleomagnetism and AMS) could not determine the end of the folding activity. However, an attempt aimed to determine the growth rate of the Boltaña folding, has been performed. Taking advantage of the continuous control of the bedding throughout the complete sequence here presented, some features can be extracted from the dip versus age correlation (Figure 9). The sequence belonging to the Ara River section (W limb) describes the expected polynomial curve (Busk's construction [1929]) compatible with folding of pretectonic units (excepting for the record located around 56 M.a. which were sampled at the core of the fold, Ye1 section). However, the eastern limb has syntectonic features that cannot properly characterized from dip of beds only. The dip recorded at strata dated at 48 M.a. has lower values since it was located in the southern periclinal termination (Ss1 section). At the end of the profile there is an interference of structures (N-S of the Boltaña anticline with the NE-SW orientation in the profiles of Mondot and Eripol) that preclude a detailed analysis of dips by separating dip decrease due to (i) increasing distance to the anticline hinge (according to flexural-slip models) and (ii) upwards decreasing dip because of the syntectonic character of the sedimentary sequence. Somehow, we still can obtain some interesting

information facing to the stable value of the dip of beds corresponding to the Lutetian-Bartonian period; the beds deposited from 40 to 39 M.a. display a relevant decrease of dip (10º) (Figure 10). This could indicate the end of the growth of the Boltaña anticline, as previous authors suggested (Puigdefàbregas, 1975; Montes, 1992; Teixell 1996; Barnolas and Gil-Peña, 2001).

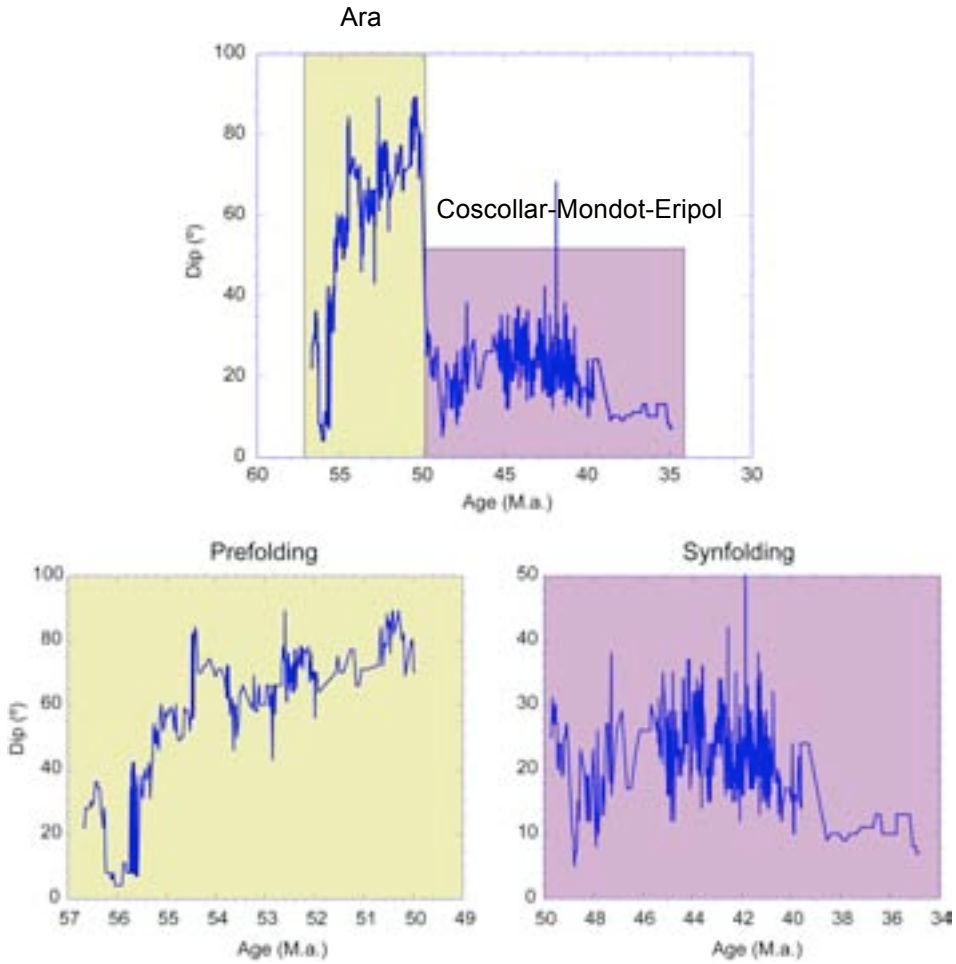

Figure 9. Dip (º) Vs Age (M.a.) throughout the stratigraphic sequence (pre- and syn-tectonic) studied in this work.

8.3.5. Rotational kinematics in the South-Central Pyrenees

Contemporary rocks sampled in the Mediano anticline, located immediately eastwards of the Boltaña anticline (Bentham's 1992 re-processed data) also indicate the final stages of rotation. Nevertheless, the sites located in the western limb of the Mediano anticline record lower declination angles than their equivalent located on the eastern limb of the Boltaña anticline (Figure 10).

Consequently, the Mediano anticline rotated earlier than the Boltaña anticline, probably during Lutetian times (Poblet et al., 1998) as has been described with paleomagnetic data by Fernández-Bellón (2004). However, it must be taken into account that eastwards the rotation detected by magnetostratigraphic data (Bentham 1992, Figure 8) is close to nil, and therefore a longitudinal

gradient must also be established between the Boltaña area (probably located over the oblique ramp) and the non-rotated areas of the SPCU.

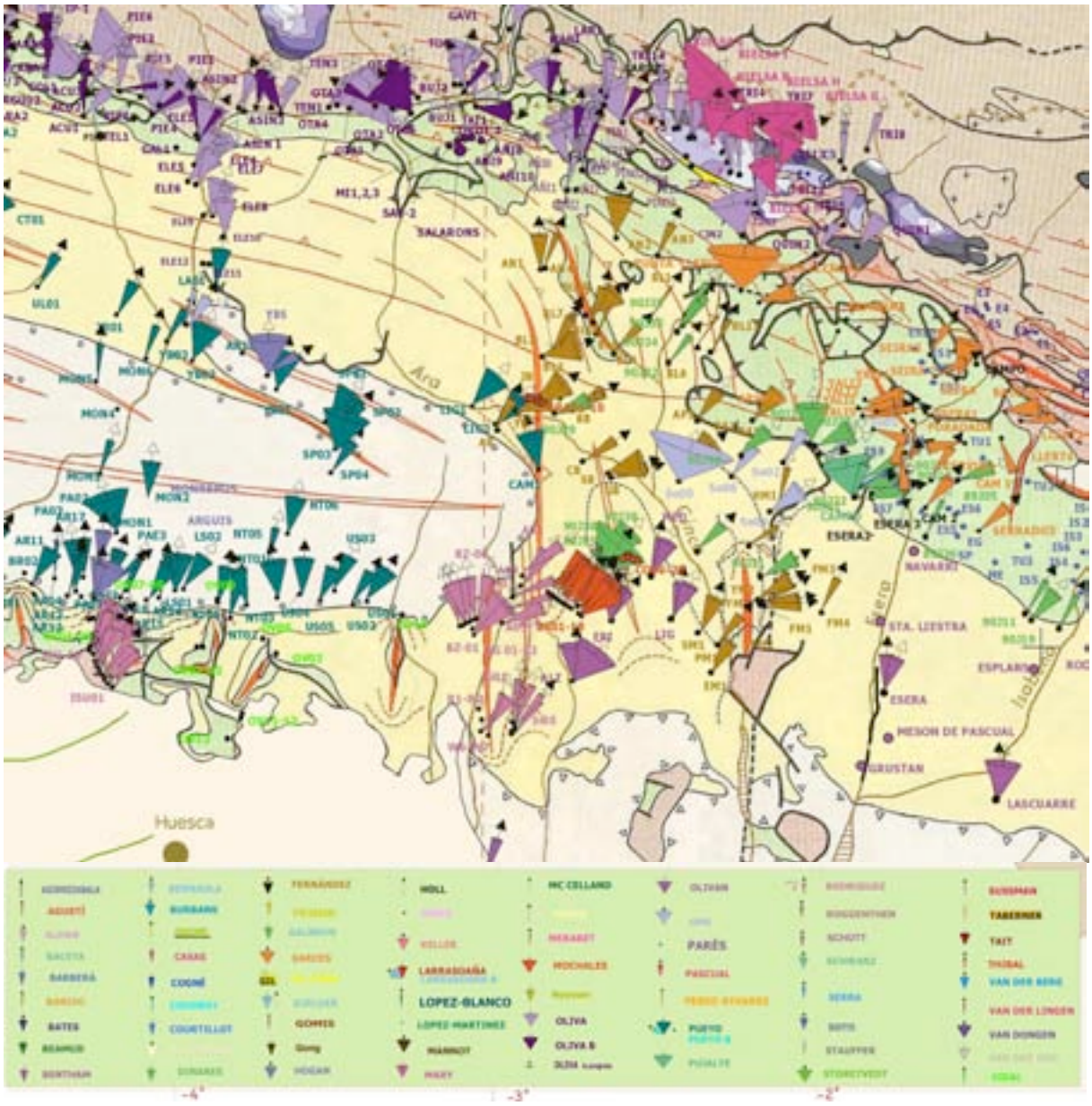

Figure 10. Raw paleomagnetic data (López et al., 2008) in the surroundings of the Aínsa Basin

Since there are not structures able to accommodate differential shortening between the Boltaña and Balzes anticlines, located south-westwards, a joint rotational movement must be invoked, probably related to the rotational motion of an underlying and younger thrust sheet (Tozal-Alcanadre; Millán, 1996). The rotation of the Tozal-Alcanadre thrust would be related to the activity of the Marginal-External Sierras thrust sheets, but with the existing data we are unable to indicate what sheet it relates to, due to the complex geometry of the Marginal-External Sierras front (Figure 8). A well-defined progressive unconformity within marine limestones denotes the onset of the Balzes anticline folding (and likely its rotation) during the Lutetian-Bartonian transition (Barnolas and Gil, 2001;

Rodríguez et al., 2011b). The Pico del Águila anticline, located westwards, underwent a quick CW rotation (7 to 10°/M.y) during the Bartonian (Pueyo et al., 2002; Rodríguez et al., 2008). Therefore the kinematic hypothesis of the progressive westwards migration of the rotational deformation in the External Sierras (Pueyo et al., 1999; Pueyo, 2000) can be redefined with the results here obtained. Since Boltaña and Balzes anticlines could have been rotated synchronously, partly coinciding with rotation of the Pico del Águila anticline, a non-steady and more complex rotational deformation pattern can be proposed for the External Sierras basal thrust. The deformation would be effectively propagated westwards during the frontal basal thrust emplacement (Marginal Sierras). Nevertheless this process is not continuous, and showed a very slow rate during the Ypresian-Lutetian and a significant higher velocity during the Bartonian to Middle Priabonian episode (Millán et al., 2000). The nucleation of the N-S structures seems to bear some relationship to displacement gradients, push of previous oblique ramps in the hinterland or to the underlying evaporitic strata. The previous extensional structures and the Keuper, which acted as a detachment level, could have favoured the development of oblique structures. Nevertheless, we cannot precise if the cause is directly linked to the evaporite thickness or to a basement thrust, transmitted in the basement-cover interface, which expression in the foreland is the N-S structures.

A global view on the paleomagnetic vectors of the southwestern Pyrenees (Figure 8) shows that both the External Sierras (Hogan, 1993; Pueyo, 2000) and the Internal Sierras (Oliva-Urcia, 2004) display significant rotations much lower (20-30°) than those found at the Boltaña anticline. Non-significant rotations can be observed at the frontal thrust sheets of the Marginal Ranges (Dinarès, 1992; Dinarès et al., 1992) and Montsec units (Pascual et al., 1992; Bentham, 1992; Beamud et al., 2004) as well as the eastern sector of the Cotiella-Bòixols thrust (Dinarès, 1992). Nonetheless, the Aínsa Basin, precisely in the area comprised between the Mediano and the Balzes anticlines has undergone a generalized CW rotation that ranges between 40 and 60º (Dinarès, 1992; Fernández-Bellón, 2004; this work), progressively dying out from Late Lutetian to Middle Priabonian. Considering the time span of the structures involved at a larger scale, the rotation would be bounded between the main movements on the Larra-Monte Perdido (Teixell, 1996; Oliva-Urcia, 2004) and Marginal Sierras (Dinarès, 1992; Meiggs et al., 1996) thrust systems. Therefore, during the formation of the Pyrenees, as consequence of the convergence between the European and Iberian plates, deformation was propagated according to NNE-SSW shortening from Late Cretaceous to Ypresian times. From Middle Lutetian, as the rotations recorded by Mediano anticline attest, to Middle Priabonian (as determined in this work) the western sector of the Aínsa Basin experimented a clockwise rotation originated by the forelandwards advancement of the basal thrust front at that time. The precursor Larra thrust, the inherited previous extensional structures and the distribution of the Keuper in the footwall probably conditioned the sinusoidal geometry of this area, as suggested by Cámara and Klimowitz (1985).

8.3.6. Map-view restoration

Assuming a length of 25 km for the Boltaña anticline with a mean of 52º of CW rotation, 21.9 km of additional differential shortening must be accommodated in its southern sector according to the

map-view modelling of differences of shortening and rotations (Pueyo et al., 2004a), figure 11. Although structures with NE-SW orientation, some of them showing a curved trace in map view, could accommodate and absorb part of this gradient, they do not suffice for the relatively important strike-slip displacement at the tip of the anticline. Therefore, this accommodation must invoke the activity of orogen-parallel thrusts both at the foreland and the hinterland of the Boltaña anticline.

The SPCU advanced southwards displacing the Aínsa Basin and the Boltaña-Balzes sheet would accommodate this differential shortening as rotational deformation at the western end of the thrust sheets (Figure 8). Therefore, rotation is the expression of the 3D architecture of this part of the orogen and it is associated with the lateral termination of thrust sheets towards the west. This secondary role of rotation explains the increase in velocity of rotation at later stages of the process, just before its sudden ending in the Priabonian. This end of rotational deformation is however compatible with the continuation of the southward displacement of thrust sheets both in the SPCU and the External Sierras, because new or reactivated thrust sheets in the hinterland may account for the kinematic compatibility of oblique structures.

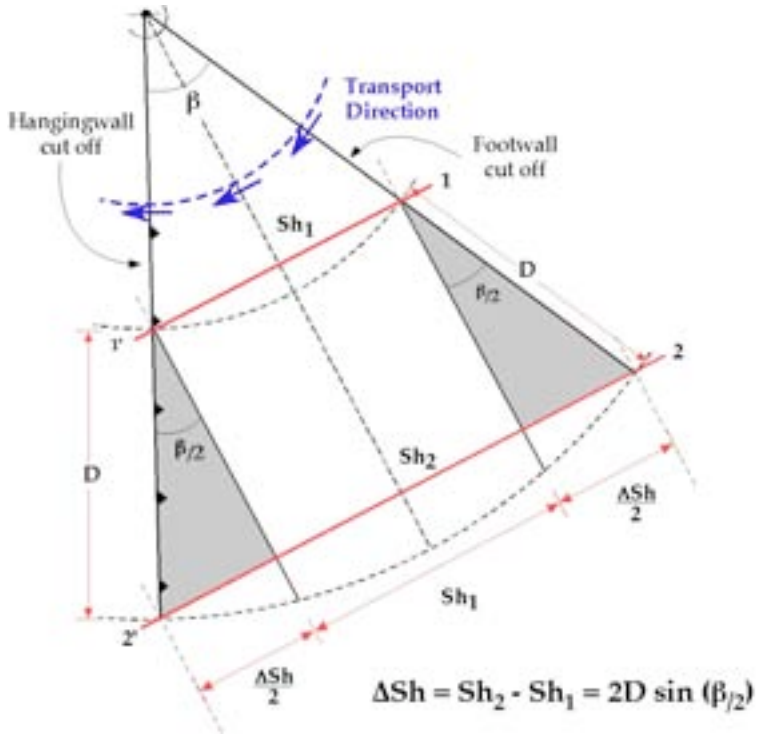

Figure 11. Idealized sketch map-view reconstruction to show the differential shortening related to 52° clockwise rotation. Note that the footwall ramp must display a N125E orientation to produce a present N-S hanging wall trend, although natural complexity may be considerably higher.

8.3.7. Relations between accumulation and rotational velocity rates

Finally, we have checked a possible relation between the accumulation and the rotational rates. The idea behind is to test if the rotational movements of the thrust sheets have an imprint in the

basin evolution (accommodation spaces, accumulation rates, etc.). First we have "smoothed" the sedimentary signal comparing the accumulation rate and its depositional pattern (Figure 12).

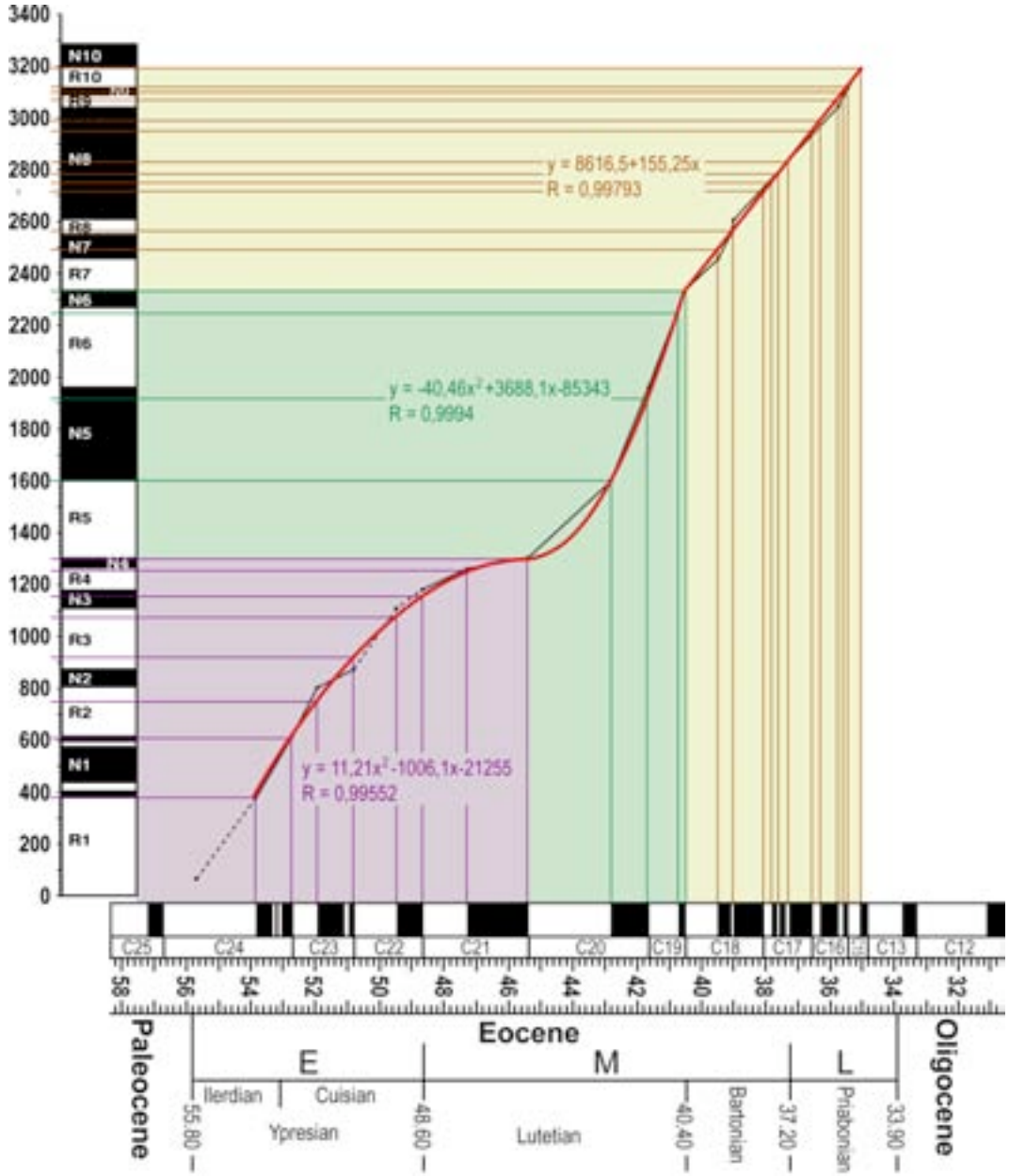

Figure 12. Direct accumulation rates (black line). Modelled accumulation rate (red line) in three depositional patterns through Eocene times.

Three major cycles can be described. The lower interval (purple) is correlated to the deposition of carbonates on the Ypresian shelf and the retrogradational stage of the Early Lutetian (chapter 5). The second (green) one is associated with the progradational evolution in the Lutetian carbonate slope facies and the deltaic progradation at the end of the Lutetian. The last interval (yellow) is mainly linked to the fluvial sedimentation in Bartonian-Priabonian times. The modelled rates have been numerically constrained and compared with the aim to establish the possible correlation between the accumulation and the rotation throughout the time (Table 1). Magnetic chron boundaries have been used as the increment boundaries to obtain both the accumulation and the rotation rates. The rotation

rates have been derived from the logarithmic model. It is worth noticing the uncertainty related to the upper part of the section (Eripol profile by Bentham, 1992). As we already stated, here the sampling density is much lower and the correlation of the upper part may significantly change if all magnetic chrons were undoubtedly recognised.

Asolute age (M.a.)	Time span (M.y.)	Rotation-log(ª)	Rot/M.y. (log)	Thickness (m)	Thick/M.y.
53,225	1,2	0,9	0,750	230	191,667
52,275	0,8	0,6	0,750	135	168,750
51,325	1,2	1	0,833	180	150,000
50,075	1,4	1,1	0,786	150	107,143
49	0,8	1	1,250	75	93,750
47,925	1,4	1,5	1,071	100	71,429
46,325	1,9	2,4	1,263	55	28,947
44,1	2,7	3,9	1,444	325	120,370
42,2	1,2	2,4	2,000	265	220,833
41,15	1	2	2,000	335	335,000
40,6	0,2	0,4	2,000	105	525,000
39,975	1	2,5	2,500	155	155,000
39,2	0,4	2	5,000	75	187,500
38,55	1	3,3	3,300	150	150,000
37,95	0,25	1,2	4,800	35	140,000
37,7	0,2	0,8	4,000	35	175,000
37,45	0,3	1,5	5,000	45	150,000
36,95	0,8	4,8	6,000	125	156,250
36,45	0,3	2,5	8,333	40	133,333
36,1	0,6	5,3	8,833	80	133,333
35,7	0,15	2,3	15,333	30	200,000
35,55	0,12	2	16,667	20	166,667
35,25	0,37	6,5	17,568	70	189,189

Table 1. Rotational (Rot/M.y.) and Accumulation (Thick/M.y.) rates for the modelled curves (rotational logatithmic and accumulation rate, figure 12). Description: Absolute age of each chron; Time span considered to calculate the slope in each interval; Rotation-log (º) rotation for the interval considered; Thickness of the interval.

As can be seen, there is a slight ascent and coarse correlation between the accumulation and the rotational rates (Figure 13). A better definition of the Bartonian chronology, as well as the comparison with other closer basins where both accumulation and rotation rates could be obtained will shed light on this hypothesis, although the present results cannot unambiguously indicate a relation between the sediment filling and the thrust sheets rotational activity and likely point to the independence of both variables, a logical result if we consider that rotation is a secondary process linked to the western edge of southward-directed movement of Pyrenean thrust sheets. As a secondary process is here meant that rotation is not linked to orogenic motions.

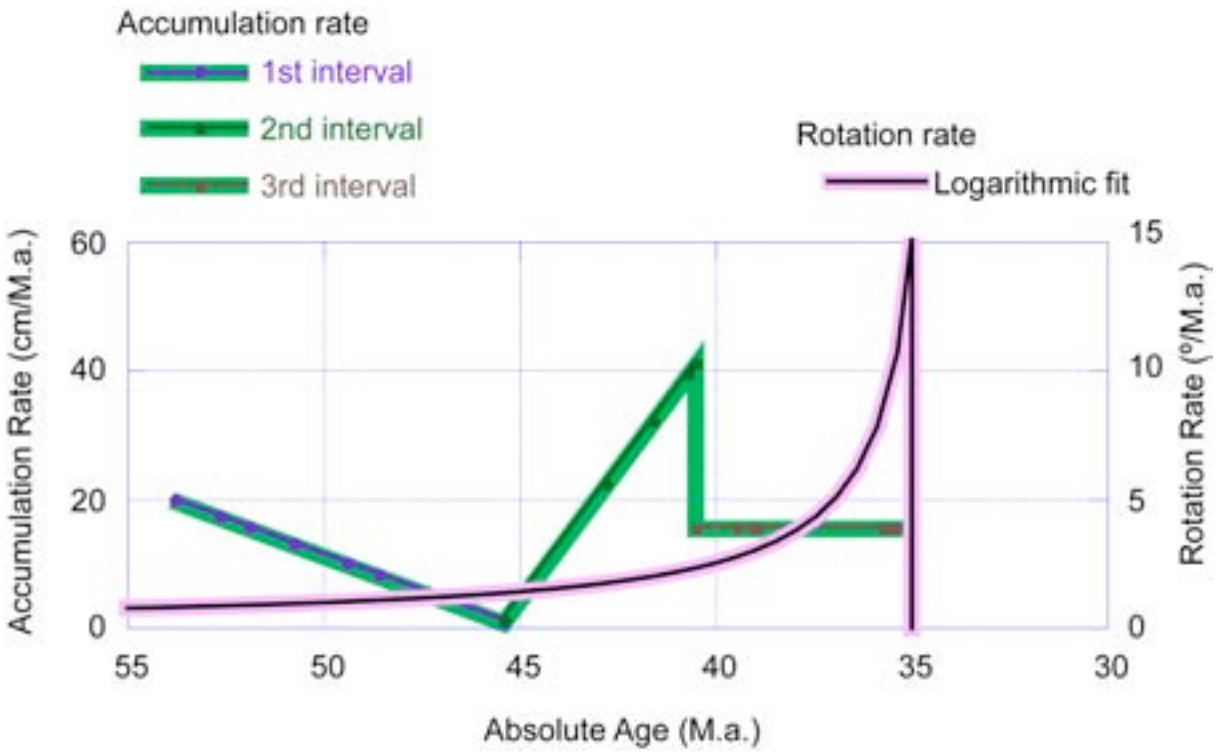

Figure 13. Correlation between the accumulation rate (red) and the rotation rate (blue), polynomial fit (bright blue) and linear fit (dark blue) throughout the time.

Conclusiones

El estudio magnetoestratigráfico continuo de 3.3 km (914 desmagnetizaciones) a partir de los perfiles Ara (1008 m), Coscollar (965 m) y Mondot (417 m), y reprocesado del perfil Eripol (840 m; Bentham, 1992) y su correlación con la escala de polaridad global (GPTS, Gradstein et al., 2004) por medio de datos biostratigráficos inéditos (foraminíferos bentónicos y carófitas) ha permitido establecer un nuevo marco cronoestratigráfico para la cuenca de Aínsa y los sedimentos pre-, sin- y post-tectónicos con el anticlinal del Boltaña. El estudio de 72 estaciones de rotación (34 derivadas del estudio magnetoestratigráfico, 20 nuevas estaciones ubicadas en zonas clave del anticlinal de Boltaña [248 desmagnetizaciones adicionales], 11 procedentes del reprocesado de perfiles de Bentham [1992] y 7 realizadas por otros autores) situadas en variadas posiciones estructurales del anticlinal de Boltaña, nos ha dado las claves para acotar la magnitud y la edad de rotación del anticlinal de Boltaña. Asimismo, a partir del estudio del las fábricas magnética (AMS) se han desentrañado aspectos cinemáticos adicionales sobre la historia deformacional del anticlinal. Considerando el conjunto de datos obtenidos así como los estudios existentes que atañen a la zona de estudio, se pueden establecer las siguientes conclusiones:

1) La magnetización de las rocas estudiadas reside fundamentalmente en la magnetita y en diferentes proporciones de sulfuros magnéticos (también hematites en las facies continentales) y representa un registro estable del paleocampo magnético Eoceno avalado por las pruebas de inversión y del pliegue. Esta conclusión está respaldada por los análisis paleomagnéticos (desmagnetizaciones térmicas y por campos alternos) y de magnetismo de rocas (curvas de saturación de IRM e desmagnetización TH de IRM de tres componentes, histéresis, etc…) que se han llevado a cabo en los laboratorios de paleomagnetismo de las Universidades de Burgos, Barcelona, Tübingen (Alemania), Lehigh (PA, USA) y Roma (Italia), así como en los laboratorios de ASM del Grupo de investigación Geotransfer y el del Servicio de Medidas Físicas de la Universidad de Zaragoza. Dicha magnetización primaria ha permitido construir una secuencia magnética local de 20 zonas (todas ellas basadas en multitud de datos de buena calidad), la correlación con la Escala de Tiempo Geológico (Gradstein et al., 2004) se ha basado en la información proveniente de 15 localidades de foraminíferos bentónicos y una de oogonios de algas caráceas.

2) Implicaciones cronológicas en la estratigrafía local: La unidad calizas de Alveolinas (SBZ6) es Ilerdiense inferior. La Fm Metils (SBZ8) es Luteciense Medio 2. Estas unidades y la parte inferior de la Fm Yeba pertenecen al cron C24r. El resto de la Fm Yeba (SBZ9) es Ilerdiense superior y corresponde a la zona C24n. La parte inferior de la Fm Boltaña (SBZ10) es Cuisiense inferior y también pertenece al cron C24n. El Cuisiense inferior (SBZ10) se extendería desde la parte inferior de la Fm Boltaña hasta la base de la parte superior de la Fm Boltaña, registrando la transición C24n/23r. La parte superior de la Fm Boltaña es Cuisiense Medio (SBZ11) y pertenece al cron C22r. El contacto Fm Boltaña-Mb Paules estaría incluido en el C22n. El límite Ypresiense/Luteciense se correlaciona con la transición C22n/21r. El Mb Paules abarca desde el Luteciense inferior al Luteciense medio 1 (SBZ14), alcanzando el cron C20r. El Mb La Patra Mb es Luteciense medio 1 (SBZ14) y abarca las

zonas C20r/20n. La Fm Sobrarbe es Luteciense Medio 2 (SBZ15) y casi coincide con el inicio de la zona C19r. El miembro inferior de la Fm Escanilla Fm se extiende desde finales Luteciense hasta el Priaboniense Medio (Cf-Sv) y registra la inversión de polaridad de C19r a C15n.

3) Análisis de la evolución de la cuenca Surpirenaica (basado en la calibración cronológica de la serie estudiada). Se reconocen tres grandes ciclos relacionados con el desarrollo de la plataforma carbonatada Eocena (Barnolas et al., 2011). Estos episodios estarían relacionados con el registro Ilerdiense (caliza de alveolinas, Fms Millares y Metils), Cuisiense (Fm Boltaña) y Luteciense medio (inundación correspondiente al nivel Coscollar, límite entre los Mbs Paules y La Patra) respectivamente. Las tasas de acumulación oscilan de 3 cm/ka a 33 cm/ka durante el Ypresiense, con ligero descenso hacia la parte superior del piso. Al comienzo del Luteciense la tasa de acumulación disminuye bruscamente, lo que podría relacionarse con la retrogradación observada a la base del Mb Paules. Esta tendencia cambia con las condiciones progradantes de la parte superior del Mb Paules, que alcanza unos 10 cm/ka, coincidiendo con el desarrollo de la plataforma carbonatada. Desde el Luteciense superior la cuenca sufrió una incremento en la tasa de sedimentación relacionado con la progradación del delta del Sobrarbe (alcanzando tasas de acumulación de 52.5 cm/ka). El intervalo Bartoniense-Priaboniense se caracteriza por grandes fluctuaciones en la tasa de acumulación propias de los medios continentales, con tasas promedio de 24 cm/ka, si bien la calibración de esta parte de la serie tiene mayor incertidumbre debido a la baja densidad de muestreo del perfil de Eripol (Bentham, 1992).

4) Comparando las tasas de acumulación con valores disponibles (Bentham 1992; Beamud et al., 2003; Oms et al., 2003) en las cuencas adyacentes (Jaca, Graus-Tremp), se observa que la cuenca Surpirenaica sufre una migración de la subsidencia hacia el oeste. Esta cuantificación de la migración de los depocentros estaría relacionada con la transferencia diacrónica de la deformación en el frente surpirenaico, progresivamente más joven hacia el Oeste (Labaume et al., 1985; Millán et al., 2000), y probablemente relacionados con la geometría y cinemática de los cabalgamientos de zócalo de la Zona Axial.

5) La fábrica magnética (ASM) refleja la orientación mineral preferente de los minerales de la arcilla en las rocas estudiadas según se deduce del alto porcentaje de susceptibilidad paramagnética obtenido en los análisis de magnetismo de rocas (histéresis, susceptibilidad de alto/bajo campo y de baja temperatura) realizados en el Servicio de Medidas Física del ICMA (UZ-CSIC). Además dicha orientación preferente refleja el campo de deformación local en el momento del depósito que es bloqueado rápidamente y se comporta como un indicador pasivo de la deformación posterior.

6) El análisis de la orientación preferente sinsedimentaria registrada por la ASM permite detectar, en la serie previa al plegamiento (pre-tectónica), los efectos de procesos tectónicos alejados (*far-field*). Durante el Ilerdiense, la influencia de rampas oblicuas del cabalgamiento de Cotiella, situado al NE, quedaría registrada en la lineación magnética en las rocas estudiadas. Asimismo, los efectos de cabalgamientos de zócalo, situados al Norte, habrían dejado su impronta en las rocas correspondientes al periodo Luteciense. Los efectos del plegamiento de Boltaña (*near-field*) son evidentes en la fábrica magnética desde el Luteciense inferior, sin embrago las evidencias cartográficas parecen indicar que el plegamiento no tuvo lugar hasta el Luteciense medio.

7) Las rotaciones de eje vertical registradas en estaciones individuales (o discretizaciones de la serie magnetoestratigrafica) en el anticlinal de Boltaña-sinclinal del Buil oscilan entre 1º (+/-7.3) y 67º (+/-14.1) con valores promedio de 36º (+/-3.2). La abundancia de datos (1189 muestras desmagnetizadas en total) y su calibración temporal (basada en la magnetoestratigrafía desarrollada) nos han permitido obtener promedios muy robustos para periodos de 2 Ma entre el Ilerdiense y el Priaboniense que oscilan entre 2º (+/- 1.5) y 55º (+/- 12.5). Los rangos de variación observados a nivel de estación en posiciones estructurales similares dejan patente la necesidad de obtener numerosos datos paleomagnéticos en este tipo de estudios para alcanzar conclusiones fiables.

8) La evolución temporal de los valores robustos de rotación para periodos de 2 Ma permite establecer un comportamiento logarítmico (neperiano) diferenciado en dos etapas: A) Desde el Ilerdiense al Luteciense Medio se detecta una ligera actividad rotacional no significativa cuya tasa es 1,2º/M.a y que podría acomodar hasta 15° de rotación horaria. B) Sin embargo a partir del Luteciense superior (42 M.y.) se observa una aceleración significativa de la actividad rotacional (2.6°/Ma de media) que se prolonga hasta el límite Bartoniense-Priaboniense. A partir de ese momento la tasa de rotación aumenta bruscamente para finalizar en el Priaboniense medio. Este evento principal de rotación acomoda hasta 37° de rotación horaria, comenzaría en la parte superior de la Fm Sobrarbe y finalizaría hacia el techo de la Fm Escanilla.

9) La edad de plegamiento del anticlinal de Boltaña ha sido acotada entre el Luteciense medio y Bartoniense, actividad relacionada con el desarrollo del cabalgamiento de Larra (Teixell, 1996). La rotación registrada por el anticlinal de Boltaña es por lo tanto tardía respecto a la etapa principal de plegamiento de dicho anticlinal y estaría posiblemente asociada al movimiento de una lámina inferior y más joven (lámina Tozal -Alcanadre). El cabalgamiento de Tozal-Alcanadre es un cabalgamiento imbricado en secuencia de bloque inferior, con mayor desplazamiento en la zona sur en relación al N, y de vergencia SW, bien caracterizado en las Sierras Exteriores (Millán, 1996) y cuya geometría en posiciones más septentrionales es incierta al estar fosilizado por la formación Campodarbe.

10) La rotación horaria eocena neta de 52° daría lugar a la configuración N-S actual del anticlinal de Boltaña, dando explicación a la distribución de paleocorrientes en la cuenca de Aínsa. El análisis de sus orientaciones indica una proveniencia de dirección SE para las paleocorrientes más antiguas (Luteciense-Bartoniense), rotadas hasta adquirir de N-S configuración actual y una orientación NW-SE para las paleocorrinetes más modernas (Bartoniense-Priaboniense). La restitución de las paleocorrientes originadas previamente a la rotación da lugar a una confluencia en estas orientaciones, de acuerdo con la geometría del surco turbidítico Eoceno de dirección SE-NW.

11) Considerando los valores de rotación obtenidos en las áreas adyacentes se puede determinar que el conjunto de la cuenca Surpirenaica occidental sufrió un gradiente moderado de acortamiento durante su deformación, hecho que produjo una rotación horaria moderada (entre 20 y 30°, localmente mayor) en la mayoría de las unidades estructurales estudiadas hasta el momento (Sierras Interiores y Exteriores; Oliva, 2004). Este gradiente se agudiza en la zona comprendida entre los anticlinales de Mediano y Balzes, que llega a acomodar rotaciones medias de hasta 50-60º, y desaparece totalmente en las estructuras frontales de la Unidad Surpirenaica Central. Las estructuras extensionales previas y

el sustrato Triásico condicionarían la geometría de la SPCU, cuyo desplazamiento diferencial (de origen no resuelto) habría causado la mayor rotación en la zona de estudio.

12) Este estudio deja abiertas ciertas cuestiones tales como la datación del final del plegamiento de Boltaña, que podría ser abordado por medio del análisis detallado de la geometría de la zona de San Felizes-Campodarbe y el análisis geométrico del flanco este por medio de AMS. Otras de las cuestiones abiertas sería refinar la datación de la Fm Escanilla por medio de un denso muestreo magnetoestratigráfico y biostratigráfico. La correlación directa de la rotación del anticlinal de Boltaña con la lámina de Tozal-Alcanadre llevando a cabo estaciones de rotación sobre esta lámina en las zonas aflorantes meridionales y la evaluación de la prolongación de dicha lámina hacia el norte por medio del estudio de perfiles sísmicos.

References

Alastrué, E., Almela, A. and Ríos, J.M., 1957. Explicación al Mapa Geológico de la Provincia de Huesca, E. 1:200.000. Inst. Geol. Min. España. 253 pp. Madrid.

Allen, P.A. and Allen, J.R., 2005. Basin Analysis: Principles and Applications, 2nd Ed., Blackwell Publishing, 549 pp.

Allerton, S., 1998. Geometry and kinematics of vertical-axis rotations in fold and thrust belts. Tectonophysics. 299, 1-3, 15-30.

Allmendinger, R., 2006. Stereonet Program for Mackintosh. V.6.3.3. Freeware. (http:// www.*geo*.cornell.edu/geology/faculty/RWA/)

Almela, A., Gálvez-Cañero, A. and Ríos, J.M., 1958. Memoria y Hoja Geológica número 211 (Boltaña) del Mapa Geológico de España 1:50.000: Instituto Geológico y Minero de España, 42 p.

Anastasio, D.J., 1992. Structural evolution of the External Sierra, Spanish Pyrenees, *In:* The Structural Geology of Fold and Thrust Beltsm (S. Mitra and G. W. Fisher Eds.), p. 239–251, Johns Hopkins Univ. Press, Baltimore, Md.

Anastasio D.J. and Holl, J.E. 2001. Traverse fold evolution in the External Sierra, southern Pyrenees. Journal of Structural Geology. 23, (2-3), 379-392.

Arbués, P., Muñoz, J.A., Poblet, J., Puigdefàbregas, C. and McClay, K., 1998. Significance of submarine truncation surfaces in the sedimentary infill of the Ainsa basin (Eocene of southcentral Pyrenees, Spain). Abstracts of the 15th International Sedimentological Congress, Alacant, Spain, p. 145–146.

Ardèvol, L., Klimowitz, J., Malagón, J. and Nagtegaal, P.J.C., 2000. Depositional sequence response to foreland deformation in the Upper Cretaceous of the Southern Pyrenees, Spain, Am. Assoc. Petrol. Geol. Bull. 84, 566–587.

Arriagada,C., Roperch, P., Mpodozis, C. and Cobbold, P.R., 2008. Paleogene building of the Bolivian Orocline: Tectonic restoration of the central Andes in 2-D map view. Tectonics, Vol. 27. doi 10.1029/2008TC002269

Averbuch O., Frizon de Lamotte D. and Kissel C., 1992. Magnetic fabric as a structural indicator of the deformation path within a fold–thrust structure: a test case from the Corbieres (NE Pyreness, France). J. Struct. Geol. 14: 461–474.

Barnolas, A., Samsó, J.M., Teixell, A., Tosquella, J. and Zamorano, M., 1991. Evolución sedimentaria entre la cuenca de Graus-Tremp y la cuenca de Jaca-Pamplona. I Congreso del Grupo Español del Terciario. Libro-Guía de la excursión nº 1, EUMO Gràfic, Vic, 123 p.

Barnolas, A., Teixell, A., Samsó, J.M. and Zamorano, M., 1992. Estructura y evolución sedimentaria del sector central de la cuenca surpirenaica. III Congreso Geológico de España, VIII Congreso Latinoamericano de Geología, Salamanca, Excursiones, p. 74-114.

Barnolas A. and Teixell, A., 1994. Platform sedimentation and collapse in a carbonate-dominated margin of a foreland basin (Jaca basin, Eocene, southern Pyrenees). Geology, vol. 22, no 12, p. 1107-1110.

Barnolas, A. and Gil-Peña, I., 2001. Ejemplos de relleno sedimentario multiepisódico en una cuenca de antepaís fragmentada: La Cuenca Surpirenaica. Boletín Geológico y Minero, 112 (3): 17-38.

Barnolas, A. and Pujalte, V. (Eds.), 2004. La Cordillera Pirenaica. *In*: Geología de España (J.A. Vera, Ed.), SGE-IGME, Madrid, 233-343. *In*: Geología de España (J.A. Vera, Ed.), SGE-IGME, Madrid, 233-341.

Barnolas, A., Payrós, A., Samsó, J.M., Serra-Kiel, J. and Tosquella, J., 2004. La Cuenca surpirenaica desde el Ilerdiense medio al Priaboniense. *In*: Geología de España (J.A. Vera, Ed.), SGE-IGME, Madrid, 313-320.

Barnolas, A., Samsó, J.M., Mochales, T., Rodríguez-Pintó, A., Gil-Peña, I., Serra-Kiel, J.M. and Pueyo, E.L., 2011. The Boltaña-Balzes transect of the South Pyrenean Foreland Carbonate margin (Jaca-Pamplona Basin). IAS Meeting, Zaragoza. Abstract (accepted).

Barnolas, A., Montes, M., Malagón, J., Gil-Peña, I. and Rico, M., (*in press* a), Memoria y Hoja Geológica número 211 (Boltaña) del Mapa Geológico de España, 1:50.000 (2 Serie Magna). Instituto Geológico y Minero de España.

Barnolas, A., Samsó J.M., Malagón, J., Gil-Peña, I., Montes and M., Rico, M., (*in press* b), Memoria y Hoja Geológica número 249 (Alquezar) del Mapa Geológico de España, 1:50.000 (2 Serie Magna). Instituto Geológico y Minero de España.

Beamud, E., Garcés, M., Muñoz and J.A., Cabrera, L., 2001. Datación de la secuencia de deformación en la Zona Surpirenaica Central. Magnetoestratigrafía de la Fm. Collegats. *In:* Simposio de Paleomagnetismo Ibérico (Magiber I), Burgos. Sept. 26-29, 2001.

Beamud, E., Garcés, M., Cabrera, L., Muñoz, J.A. and Almar, Y., 2003. A new Middle to late Eocene continental chronostratigraphy from NE Spain. Earth and Planetary Letters, v. 216, p. 501-514.

Beamud, E., Garcés, M., Muñoz, J.A., Cabrera, Ll. and Almar, Y., 2004. Distribución de las rotaciones paleomagnéticas en la cuenca de Graus-Tremp durante el Terciario. Geotemas 6 (4), 283-286.

Beaumont, C., Muñoz, J.A., Hamilton, J. and Fullsack, P., 2000. Factors controlling the Alpine evolution of the central Pyrenees inferred from a comparison of observations and geodynamical models. J. Geophys. Res., 105, B4, 8121-8145.

Bentham P.A., 1992. The tectono-stratigraphic development of the western oblique ramp of the south-central Pyrenean thrust system, Northern Spain. Ph.D Thesis. University of Southern California. 253pp.

Bentham, P. and Burbank, D.W., 1996. Chronology of Eocene foreland basin evolution along the western oblique margin of the South-Central Pyrenees. *In*: Tertiary Basin of Spain (P.F. Friend, C.J. Dabrio, Eds.). Cambridge University Press, Cambridge, UK, 144–152.

Berástegui, X., García-Senz, J.M. and Losantos, M., 1990. Tecto-sedimentary evolution of the Organyà extensional basin (central south Pyrenean unit, Spain) during the Lower Cretaceous. Bull. Soc. Géol. France VI (2), 251-264.

Berástegui, X., Losantos, M., Muñoz, J.A. and Puigdefàbregas, C., 1993. Tall Geològic del Pirineu central 1:200.000. Servei Geològic de Catalunya, Institut Cartogràfic de Catalunya, Barcelona.

Berggren, W.A., Kent, D.V.,Flynn, J.J. and Van Couvering, J.A, 1985. Cenozoic geochronology. Geological Society of America Bulletin, v. 96, p. 1407-1418.

Bingham C. 1974. An antipodally symmetric distribution on the sphere. Annales of Statistics 2, 1201-1225.

Bond, R.M.G. and McClay, K.R., 1995. Inversion of a Lower Cretaceous extensional basin, south central Pyrenees, Spain. *In.* Basin inversion (J.G Buchanan, P.G. Buchnan, Eds.), Geological Society Special Publication, 88, 415-431.

Borradaile, G.J. 1988. Magnetic susceptibility, petrofabrics and strain. Tectonophysics 156, 1–20.

Borradaile GJ.and Henry B., 1997. Tectonic applications of magnetic susceptibility and its anisotropy, Earth-Sci. Rev., 42, 49–93.

Bouchez, J.L. 1997. Granite is never isotropic: an introduction to AMS studies of granitic rocks. *In*: Granite: from segregation of melt to emplacement fabrics (J.L. Bouchez, D.H.W. Hutton, W.E. Stephens Eds.). Kluwer Academic Publishers: Dordrecht, 95–112.

Burbank, K.D.W. , Hogan, P. , King, M. and Jolley, Z.J., 1987. Preliminary results of magnetostratigraphic studies in the South Pyrenean foreland basin. Workshop of paleomagnetism in the Iberian Peninsula. Servei Geològic de Catalunya. Abstracts, 1-3.

Burbank, D.W., Vergés, J., Muñoz, J.A. and Bentham, P., 1992. Coeval hindward- and forwardimbricating thrusting in the South-Central Pyrenees, Spain; timing and rates of shortening and deposition. Geol. Soc. Amer. Bull., 104, 1, 3-17.

Busk, H.G., 1929. Earth flexures. Cambridge University Press, London, 186 pp.

Butler, R.F., 1992. Paleomagnetism, Magnetic Domains to Geologic Terranes, Boston, Blackwell, 319 p.

Calassou, S., Larroque, C. and Malavieille, J., 1993. Tranasfer zones of deformation in thrust wedges: an experimental study. Tectonophysics, 221, 325-344.

Calvo, M., Osete, M.L. and Vegas, R., 1992. Rotaciones de bloques observadas a partir de resultados paleomagnéticos en la región del Cabo de Gata, Almería. *In*: Física de la Tierra. Vol. 4: Paleomagnetismo y Tectónica en las Cordilleras Béticas. (M.L. Osete, M. Calvo., Eds.) Editorial de la Universidad Complutense, Madrid. Pgs. 215-229.

Cámara, P. and Klimowitz, J., 1985. Interpretación geodinámica de la vertiente centro-occidental surpirenaica

(Cuencas de Jaca-Tremp). Estudios geológicos, 41, 391–404.

Cande, S.C. and Kent, D.V., 1992. A new geomagnetic polarity time scale for the Late Cretaceous and Cenozoic. J. geophys. Res., 97, 13917-13951.

Cande, S.C. and Kent, D.V., 1995. Revised calibration of the geomagnetic polarity timescale for the Late Cretaceous and Cenozoic, J. Geophys. Res., 100, 6093 – 6096.

Canudo, J.I., 1990. Los foraminíferos planctónicos del Paleoceno-Eoceno del Prepirineo oscense en el sector de Arguis. PhD Thesis. Universidad de Zaragoza, p. 435.

Casas, A., Kearey, P., Rivero, L. and Adam, C.R., 1997. Gravity anomaly map of the Pyrenean region and a comparison of the deep geological structure of the western and eastern Pyrenees., Earth Planet. Sci. Lett., 150, 65-78.

Casas-Sainz, A.M., 1993. Oblique tectonic inversion and basement thrusting in the Cameros Massif (Northern Spain). Geodinamica Acta, 6, 3, 202-216.

Channell, J.E.T., 2007. Paleomagnetism, Deep-Sea Sediments. *In:* Encyclopedia of geomagnetism (D. Gubbins, E. Herrero-Bervera, Eds.) Dordrecht, Netherlands, Springer, p. 781-788.

Channell, J.E.T., Olodow, J.S., Catalano, R. and D'Argenio, B., 1990. Paleomagnetically determined rotations in the western Sicilian fold and thrust belt, Tectonics, 9, 641-660.

Choukroune, P., 1976. Structure et évolution tectonique de la zone nord-pyrénéene (analyse de la déformation dans une portion de chaîne à schistosité subverticale). Mémoires Soc. Géol. Fr., 127, 116 pp.

Choukroune P. and Séguret, M. 1973. Carte structurale des Pyrénées, 1/500.000, Université de Montpellier – ELF Aquitaine.

Choukroune, P. and ECORS team, 1989. The ECORS Pyrenean deep seismic profile reflection data and the overall structure of an orogenic belt. Tectonics, 8(1): 23-39.

Coney, P.J., Muñoz, J.A., McClay, K.R. and Evenchick, C.A., 1996. Syntectonic burial and post-tectonic exhumation of the southern Pyrenees foreland fold-and-thrust belt. J. Geol. Soc. London, 153, 9-16.

Corrado, S., Di Bucci, D., Naso, G. and Faccenna, C., 1998. Influence of palaeogeography on thrust system geometries: an analogue modelling approach for the Abruzzi-Molise (Italy) case history. Tectonophysics, 296, 437-453.

Costa, E., Garcés, M, López-Blanco, M., Beamud, E., Gómez-Paccard, M. and Larrasoaña, J.C., 2009. Closing and continentalization of the South Pyrenees foreland basin (NE Spain): magnetochronological constraints. Basin Research, v. 22 (6), p. 904-917.

Cotton, J.T. and Koyi, H.A., 2000. Modeling of thrust fronts above ductile and frictional detachments: Application to structures in the Salt Range and Potwar Plateau, Pakistan. Geol. Soc. Amer. Bull., 112, 3, 351-363.

Coutand, I., Cobbold, PR., De Urreiztieta, M., Gautier, P. and Chauvin, A., 2001. Style and history of Andean deformation, Puna plateau, northwestern Argentina. Tectonics, 20,210-234.

Daignières, M., Gallart, J., Banda, E. and Hirn, A., 1982. Implications of the seismic structure for the orogenic evolution of the Pyrenean range. Earth Planet. Sci. Letters, 57: 88-100.

Daignières, M., Séguret, M., Specht, M. and ECORS team, 1994. The Arzacq-Western Pyrenees ECORS Deep Seismic Profile. *In*: Hydrocarbon and Petroleum Geology of France (A. Mascle, Ed.). Eur. Ass. Petr. Geosci. Spec. Publ. 4, Springer-Verlag, 199-208.

Day-Stirrat R.J., Loucks R.G., MIlliken, K.L., Hillier S. and Van der Pluijm B.A. 2008. Phyllosilicate orientation demonstrates early timing of compactional stabilization in calcite-cemented concretions in the Barnett Shale (Late Mississippian), Fort Worth Basin, Texas (U.S.A.). Sedimentary Geology, 208, 27-35

De Federico, A., 1981. La sedimentación de talud en el sector occidental de la cuenca paleógena de Aínsa. PhD Thesis. Universidad Autónoma de Barcelona, Publicaciones de Geología, v. 12, 271 p.

De Miguel, L. 1974. Geomagnetismo. Instituto Geográfico y Catastral, 160 pp.

Delfaud, J., 1969. Essais sur la géologie dynamique du domaine Aquitano-Pyrénéen Durant le jurassique et le Crétacé Inférieur. PhD Thesis, Bordeaux, 6 vols.

Dinarès J. 1992. Paleomagnetisme a les Unitats Sudpirinenques Superiors. Implicacions estructurals. PhD Thesis. Universidad de Barcelona. 462 pp.

Dinarès, J., Parés, M., 1992. Determinación de fábricas mediante a la anisotropía de la susceptibidad magnética (ASM) en rocas con diferente grado de deformación. Ejemplo de materiales eocenos de la cuenca de Aínsa (Pirineo Central), Geogaceta, 12, 22-25.

Dinarès-Turell J., McClelland, E. and Santanach, P., 1992. Contrasting rotations within thrust sheets and kinematics of thrust tectonics as derived from palaeomagnetic data: an example from Southern Pyrenees. *In*: Thrust tectonics (K.R. McClay Ed.), Chapman and Hall, London, 265-275.

Dreyer, T., Corregidor, J., Arbués, P. and Puigdefàbregas, C., 1999. Architecture of the tectonically influenced Sobrarbe deltaic complex in the Ainsa Basin, northern Spain: Sedimentary Geology, v. 127, p. 127-169.

ECORS Pyrenees Team, 1988. The ECORS deep reflexion seismic survey across the Pyrenees. Nature, 331: 508-511.

Elliott, D., 1976. The energy balance and deformation mechanisms of thrust sheets. Philosophical Transactions of the Royal Society of London, 283, 289-312.

Everitt, C.W.P. and Clegg, J.A., 1962. A field test of paleomagentic stability. Geophys. J. R. Astron. Soc., 6, 312-319.

Farrell SG., Williams GD., and Atkinson CD., 1987. Constraints on the age of movement of the Montsech and Cotiella thrusts, south central Pyrenees, Spain. Journ. Geol. Soc. of London, 144: 907-914.

Fauré, P., 1984. Le Lias de la partie centro-orientale des Pyrénées espagnoles (Prov. De Huesca, Lérida et Barcelona). Bull. Soc. Hist. Nat. Toulouse, 121, 23-37.

Fernández-Bellón, O., 2004. Reconstruction of geological structures in 3D. An example from the Southern Pyrenees. Ph.D Thesis. Universitat de Barcelona. 321 p.

Fernández, O., Beamud, B., Muñoz, J. A. , Dinarès, J. and Poblet, J., 2003. Distribución de las rotaciones paleomagnéticas en los anticlinales de Boltaña y Añisclo (Pirineos Centrales). Resúmenes del MAGIBER II- Coimbra.

Fernández, O., Muñoz, J.A., Arbués, P., Falivene, O. and Marzo, M., 2004. Three-dimensional reconstruction of geological surfaces: an example of growth strata and turbidite systems from the Aínsa Basin (Pyrenees, Spain). American Association of Petroleum Geologists Bulletin, v. 88 (8), p. 1049–1068.

Fisher, R. A., 1953, Dispersion on a sphere: Proceeding of thee Royal Society of London, Serie. A, 217, p. 295-305.

Fitzgerald, P.G., Muñoz, J.A., Coney, P.J. and Baldwin. S.L, 1999. Asymmetric exhumation across the Pyrenean orogen: implication for the tectonic evolution of a collisional orogen., Earth and Plan. Sci. Lett., 173, 157-170.

Flinn, D., 1962. On folding during three-dimensional progressive deformation. Quarterly Journal of the Geological Society of London, 118, 385–433.

Fonnesu, F. 1984. Estratigrafía y análisis de facies de la secuencia de Fígols, entre el río Noguera-Pallaresa e Isclés (prov. de Lérida y Huesca). PhD Thesis. Universidad Autónoma de Barcelona, 317 p.

García-Castellanos, D., Vergés, J., Gaspar-Escribano, J. and Cloetingh, S. 2003. Interplay between tectonics, climate, and fluvial transport during the Cenozoic evolution of the Ebro Basin (NE Iberia). Journal of Geophysical Research, 108 (B7), 2347.

García-Lobón, J.L., Pueyo, E.L., Klimowitz, J.P. et al. (in alphabetical order: Alcolea. M., Arbués, P., Arche, A., Aurell, M., Baceta, J.I., Bastante, R., Bausá, J., Bello, D.A., Cortés, A.L., Escalante, S., Gratacós, O., Hermida, E., Juez, F.J., Larrasoaña, J.C., Mencos, J., Morante, M., Muñoz, J.A., Murelaga, X., Pardos, M., Roca, E., Ruíz, G., 2010. Selección y caracterización de áreas y estructuras favorables para el almacenamiento geológico de CO_2 en España, v. II-1 Cadena Pirenaica y Cuenca del Ebro – Geología (Atlas, 200 p.): Instituto Geológico y Minero de España.

García-Senz, J., 2002. Cuenca extensivas del Cretácico Inferior en los Pirineos Centrales, formación y subsecuente inversión. PhD Thesis. Universidad de Barcelona, 310 pp.

Garfunkel, Z., 1988. Regional deformetion by block traslation and rotation, *In:* Paleomagnetic rotations and continental deformation (C. Kissel, C. Laj, Eds.), Nato ASI Ser. 254, 181-208.

Garrido-Megías A., 1968. Sobre la estratigrafía de los conglomerados de Campanué (Santa Liestra) y formaciones superiores del Eoceno (extremo occidental de la cuenca Graus-Tremp, Pirineo Central,

provincia de Huesca). Acta Geol. Hispánica, v. 3 (2), p. 39 43.

Garrido-Megías, A., 1973. Estudio geológico y relación entre tectónica y sedimentación del secundario y terciario de la vertiente meridional pirenaica en su zona central. Ph.D Thesis. Universidad de Granada. 395 p.

Garrido-Megías, A., 1992a. Sobre la colocación del manto de Pedraforca y sus consecuencias: una nueva actividad tectónica independiente, "el manto del Montsec". Bol. Geol. Min. LXXXIII-III, 242-248.

Garrido-Megías, A., 1992b. Precisiones sobre la "mise en place" del manto de Gavarnie en el borde norte del valle del Ebro (Región de Barbastro, Provincia de Huesca). Acta Geol. Hisp. VII (2), 50-52.

Garrido-Megías, A. and Ríos-Aragüés, L.M., 1972. Síntesis geológica del Secundario y Terciario entre los ríos Cinca y Segre. Bol. Geol. y Min. 83: 147.

Gibbons W., Moreno, M.T., 2002. Introduction and overview. *In*: The Geology of Spain. (W. Gibbons, M.T. Moreno, Eds.). Geological Society of London, 649 p.

Gil-Imaz, A., 2001. La estructura de la Sierra de Cameros: deformación dúctil y su significado a escala cortical. PhD Thesis. Ed. Gobierno de la Rioja, Instituto de Estudios Riojanos, Logroño, 304 pp.

Gillcrist, R., Coward, M.P. and Mugnier, J.L., 1987. Structural inversion and its control: examples from the Alpine foreland and the French Alps. Geodinamica Acta, 1, 5-34.

Gil-Peña, I. and Barnolas, A., 2004. Introducción al ciclo varisco en los Pirineos. *In*: Geología de España (J.A. Vera, Ed.), SGE-IGME, Madrid, 241 p.

Girdler, R.W., 1961. Some preliminary measurements of anisotropy of magnetic susceptibility of rocks. Geophysical Journal of London. 5, (3) 197-206.

Gleizes, G. and Bouchez, J.L., 1989. Le granite de Mont-Louis (Zone axiale des Pyrénées): anisotropie magnétique, structures et microstructures. Comptes Rendus Geoscience, 309 (II): 1075-1082.

Golberg. J.M., Maluski, H. and Leyreloup, A.F., 1986. Petrological and age relationship between emplacement of magmatic breccia, alkaline magmatism, and static metamorphism in the North Pyrenean Zone. Tectonophysics, 129, 275-290.

Gradstein, F.M., Ogg, J.G. and Smith, A.G., 2004. A geologic Time Scale. Cambridge, Cambridge University Press, 589 p.

Graham., J.W., 1949. The stability and significance of magnetism in sedimentary rocks. J. Geophys. Res., 54, 131-167.

Grubbs, K.L. and Van der Voo, R., 1976. Structural deformation of the Idazo-Wyoming overthrust belt (USA) as determined by Trassic paleomagnetism, Tectonophysics, 33, 321-336.

Hardenbol, J., Thierry, J., Martin, B.F., Jacquin, T., Graciansky., P.C. and Vail, P.R., 1998. Mesozoic and Cenozoic Sequence Chronostratigraphic Framework of European Basins. SEPM (Society of Sedimentary Geology) Special Publication 60. Chart 3.

Harland, W.B., Armstrong, R.L., Cox, A.V., Craig, L.E., Smith, A.G. and Smith, D.G., 1990. A geologic time scale 1989. Cambridge, Cambridge University Press, 263 p.

Hogan, P.J., 1993. Geochronologic, tectonic and stratigraphic evolution of the Southwest Pyrenean foreland basin, Northern Spain. PhD. Thesis. University of Southern California, 219 p.

Hogan, P.J. and Burbank, D.W., 1996. Evolution of the Jaca piggy-back basin and emergence of the External Sierras, southern Pyrenees. *In:* Tertiary basins of Spain (P.F. Friend, C.J. Dabrio, Eds.) Cambridge, Cambridge University Press, p. 153-160.

Holl, J.E. and Anastasio, D.J., 1993. Paleomagnetically derived folding rates, southern Pyrenees, Spain. Geology, 21; 3, 271-274.

Holl J.E. and Anastasio D.J., 1995a. Cleavage development within a foreland fold and thrust belt, southern Pyrenees, Spain. Journal of Structural Geology. 17; 3, 357-369.

Holl, J.E. and Anastasio, D.J., 1995b. Kinematics around a large-scale oblique ramp, southern Pyrenees, Spain. Tectonics. 14; 6, 1368-1379.

Hopman, T.M., Keukenmeester, K.A., Deenen, M.H.L., Van Roermund, H.L.M. and Krijgsman, W., 2008. A Paleomagnetic study of the snake-like fold in Aliaga, Spain. Abstract NAC9; Veldhoven, The Netherland

Hossack, J.R., Deramond, J. and Graham, R.H., 1984. The geological structure and development of the Pyrenees. Colloque sur Chevauchement et deformation, Toulouse, 46-47.

Hottinger, L., 1960. Recherches sur les Alvéolines du Paléocène et de l'Éocène. Mémoires suisses de Paléontologie, v. 75, p. 243 p., v. 76, 18 plates.

Housen B. and Van del Pluijm B.A., 1991. Slaty cleavage development and magnetic anisotropy fabrics. Journal of Geophysical Research 96, 9937– 9946.

Housen, B.A., Van der Pluijm, B.A. and Van der Voo, R., 1993. Magnetite dissolution and neocrystallization during cleavage formation; paleomagnetic study of the Martinsburg Formation, Lehigh Gap, Pennsylvania. Journal of Geophysical Research, B, Solid Earth and Planets. 98 (8), 13,799-13,813.

Hrouda, F., 1982. Magnetic anisotropy of rocks and its application in Geology and Geophysics. Geophysical Surveys 5, 37–82.

Hrouda F. and Jelinek V., 1990. Resolution of ferrimagnetic and paramagnetic anisotropies in rocks, using combined low-field and high-field measurement, Geophys. J. Int., 103, 75–84

Jackson, M., 1990. Diagenetic sources of stable remanence in remagnetized cratonic carbonates; a rock magnetic study. Journal of Geophysical Research, B, Solid Earth, v. 95, p. 2753-2761.

Jelinek, V., 1977. The statistical Theory of Measuring Anisotropy of Magnetic Susceptibility of Rocks and its Application. Geofyzika, Brno, 88 pp.

Jelinek, V., 1981. Characterization of the magnetic fabric of rocks. Tectonophysics 79, 63–70.

Katz, B., Elmore, R.D., Cogoini, M. and Ferry, S., 1998. Widespread chemical remagnetization: orogenic fluid or burial diagenesis of clays? Geology.26 (7), 603–606.

Kent, D.V. 1982. Paleomagnetic evidence for post-Devonian displacement of the Avalon Platform (Newfoundland). J. Geophys. Res. 87: 8709-16.

Kirschvink, J.L., 1980. The least-squares line and plane and the analysis of paleomagnetic data: Geophysical Journal. Royal Astronomical Society, v. 62, p. 699-718.

Kissel C., Barrier E., Laj C. and Lee T.Q., 1986. Magnetic fabric in 'undeformed' marine clays from compressional zones. Tectonics 5, 769– 781.

Kissel, C., Averbuch, O., Frizon de Lamotte, D., Monod, O. and Allerton, S., 1993. First paleomagnetic evidence for a post-Eocene clockwise rotation of the Western Taurides thrust belt east of the Isparta reentrant (Southwestern Turkey). Earth planet. Sci. Lett., 117, 1–14

Klootwijk, C.T., Nazirullah, R. and DeJong, K.A., 1986. Paleomagnetic constraints on formation of the Mianwali Re-entrant, Trans-Indus and Western Salt Range, Pakistan, Herat Plan. Sc. Lett., 80, p. 394-414.

Kodama, K.P., Anastasio, D.J., Newton, M.L., Pares, J.M. and Hinnov L.A., 2010. High-resolution rock magnetic cyclostratigraphy in an Eocene flysch, Spanish Pyrenees, Geochem. Geophys. Geosyst., 11, Q0AA07, doi:10.1029/2010GC003069.

Kruiver, P.P., Dekkers, M.J. and Heslop, D., 2001. Quantification of magnetic coercivity components by the analysis of acquisition curves of isothermal remanent magnetisation. Earth Planet. Sci. Lett., 189, 269-276.

Kulik, D.M. and Schmidt, C.J., 1988. Region of overlap and styles of interaction of Cordilleran thrust belt and Rocky Mountain foreland. Geol. Soc. Amer. Mem., 171, 75-98.

Labaume, P., Séguret, M. and Seyve, C., 1985. Evolution of a turbiditic foreland basin an analogy with an accretionary prism: Example of the Eocene South-Pyrenean basin: Tectonics, v. 4 (7), p. 661-685.

Lanaja, J.M., 1987. Contribución de la exploración petrolífera al conocimiento de la Geología de España. (Inst.Geol.Mine.España Ed.). 465 pp., 17 mapas.

Larrasoaña, J.C., 2000. Estudio magnetotectónico de la zona de transición entre el Pirineo central y occidental; implicaciones estructurales y geodinámicas. PhD Thesis. Universidad de Zaragoza, 287 pp.

Larrasoaña, J.C., Pueyo, E.L., Del Valle, J., Millán, H, Parés, J.M., Pocoví, A. and Dinarès, J., 1996. Datos magnetotectónicos del Eoceno de la Cuenca de Jaca-Pamplona: resultados iniciales. Geogaceta, 20 (vol.4), 1058-1061.

Larrasoaña, J.C., Pueyo-Morer, E.L., Millán, H., Parés, J.M. and del Valle, J., 1997. Deformation mechanism deduced from AMS data in the Jaca-Pamplona basin (Southern Pyrenees). Physics and Chemistry of the Earth, vol 22 nº 1-2, 147-152.

Larrasoaña, J.C., Parés, J.M. and Pueyo, E.L., 2003a. Stable Eocene magnetization carried by magnetite and iron sulphides in marine marls (Pamoplona-Arguis Formation, southern Pyrenees, northern Spain), Stud. Geophys. Geod., 47, 237–254, doi:10.1023/A:1023770106613.

Larrasoaña, J.C., Parés, J.M., Millán, H., del Valle, J. and Pueyo, E.L., 2003b. Paleomagnetic, structural and stratigraphic constraints on the traverse fault kinematics during basin inversion. The Pamplona Fault (Pyrenees, north Spain): Tectonics, v. 22 (6), doi: 10.1029/2002TC001446.

Larrasoaña, J.C., Pueyo-Morer, E.L. and Parés, J.M., 2004. An integrated AMS, structural, palaeo- and rock-magnetic study of the Eocene marine marls from the Jaca-Pamplona basin (Pyrenees, N Spain); new insights into the timing of magnetic fabric acquisition in weakly deformed mudrocks. *In:* Magnetic fabrics: Methods and applications (F. Martín-Hernádez, A. Hirt, Eds.). Geological Society of London Special Publication 238, 127-143.

Larrasoaña, J.C., Gonzalvo, C., Molina, E., Monechi, S., Ortiz, S., Tori, F. and Tosquella, J., 2008. Integrated magnetobiochronology of the Early/Middle Eocene transition at Agost (Spain): Implications for defining the Ypresian/Lutetian boundary stratotype. Lethaia, v. 41, p. 395-415.

Latta, D.K. and Anastasio, D.J. 2007. Multiple scales of mechanical stratification and décollement fold kinematics, Sierra Madre Oriental foreland, northeast Mexico. Journal of Structural Geology 29 1241-1255.

Little, T.A. and Roberts, A.P., 1997. Distribution and mechanism of Neogene to present-day vertical axis rotations, Pacific-Australian plate boundary zone, South Island, New Zealand. J. Geophys. Res., 102 (B9), 20447-20468.

Liu, H., McClay, K.R. and Powell, D., 1992. Physical models of thrust wedges. *In:* Thrust Tectonics (K.R. McClay Ed.), Chapman & Hall, London, 71-81.

López M.A., Oliván C., Oliva B., Pueyo E.L. and the GeoKin3DPyr working. 2008. Pyrenean Paleomagnetic databases. Geotemas, 10, 1219-1222.

Lowrie W., Hirt A.M., 1987. Anisotropy of magnetic susceptibility in the Scaglia Rossa pelagic limestone, Earth Planet. Sci. Lett. 82 349–356.

Lowrie, W., 1990. Identification of ferromagnetic minerals in rock coercivity and unblocking temperature properties. Geophysical Research Letters, v. 17, p. 159-162.

Lucas, C., 1985. Le Grès Rouge du versant nord des Pyrénées. Essai sur la géodynamique de dépôts continentaux du Permian et du Trias. PhD Thesis, University Paul Sabatier, Toulouse, 267 pp.

Luzón-Aguado A., 1999. Evolución estratigráfica de los afloramientos septentrionales de la formación Sariñena (provincia de Huesca, España). Síntesis paleogeográfica. Geogaceta, 26: 59-62.

Marshak, S., Wilkerson, M.S., Hsui and A.T., 1992. Generation of curved fold-thrust belts: Insight from simple physical and analytical models. *In*: Thrust Tectonics (K.R. McClay Ed.), Chapman & Hall, London, 83-93.

Martínez Peña, M.B., 1991. La estructura del límite occidental de la unidad surpirenaica central. Ph.D Thesis. Universidad de Zaragoza, 380 p.

Martínez Peña, M.B. and Pocoví, A., 1988. El amortiguamiento frontal de la estructura de la cobertera surpirenaica y su relación con el anticlinal de Barbastro-Balaguer. Acta Geológica Hispánica, 23 (2), 81-94..

Martínez-Peña, M.B. and Casas-Sainz, A., 2003. Cretaceous-Tertiary tectonic inversion at the Cotiella Nappe (Southern Pyrenees, Spain). Int. J. Earth Sci. (Geol. Rundschau), v. 92, p. 99-113.

Martínez-Torres, L.M., Ramón-Lluch, R. and Eguiluz, R., 1994. Tectonic wedges: Geometry and kinematic interpretation. Journal of Structural Geology, v. 16, p. 1491-1494.

Martín-Hernández, F., Hirt A.M., 2003. The anisotropy of magnetic susceptibility in biotite, muscovite and chlorite single crystals. Thectonophysics, 367, 13-28.

Mattauer, M., 1968. Les traits structuraux esentiels de la chaine Pyrénéenne. Rev. Geogr. Phys. et Géol. Dyn., X, 3-12.

Mattei, M., Funiciello, R. and Kissel, C., 1995. Paleomagnetic and structural evidence for Neogene block rotations in the Central Apennines, Italy. Journal of Geophysical Research, 100, 17863-17883.

Mattei, M., Sagnotti, L., Faccenna, C. and Funiciello, R., 1997. Magnetic fabric of weakly deformed clay-rich sediments in the Italian peninsula: Relationship with compressional and extensional tectonics. Tectonophysics, 271, 107–122.

Mattei, M., Petrocelli, V., Lacava, D. and Schiattarella, M., 2004. Geodynamic implications of Pleistocene ultrarapid vertical-axis rotations in the Southern Apennines, Italy Geology 32 (9), pp. 789-792

McCabe, C. and Elmore, R.D., 1989. The occurrence and origin of late Paleozoic remagnetization in the sedimentary rocks of North America: Revews in Geophysics. 27, 471-494.

McCaig, A.M. and McClelland, E., 1992. Palaeomagnetic techniques applied to thrust belts. *In:* Thrust Tectonics, (K.R. McClay Ed.), pp. 209-216, Chapman y Hall Eds., London. 447 pp.

McClay, K., 1992. Glossary. *In*: Thrust Tectonics (K.R. McClay Ed.), Chapman & Hall, London, 419-433.

McClelland, E.A. and McCaig, A.M., 1988. Paleomagnetic estimates of 3-d rotations in basement thrust sheets, axial zone, southern Pyrenees. *In*: Symposium on the Geology of the Pyrenees and Betics (dedicated to Prof. J.M. Fontbote, Munoz, J. A., Sanz de Galdeano, C., Santanach, P. Eds.). Universitat de Barcelona, Pages 73.

McElhinny, M.W., 1964. Statistical significance of the fold tests in Paleomagnetism. Geophysical Journal. Royal Astronomical Society, v. 8, p. 338-340.

McElhinny, M.W., McFadden, P.L., 2000. Paleomagnetism, continents and oceans. International Geophysics series. Academic Press. 73. 386pp.

McFadden, P.L. 1980. Determination of the angle in a Fisher distribution which will be exceeded with a given probability. Geophys. J.R. Astron. Soc. 60: 391-396.

Meigs, A.J., 1997. Sequential development of selected Pyrenean thrust faults. Journal of Structural Geology, 19 (3-4), 481-502.

Menard, G, Rochette, P., 1992. Utilisation de reaimantations postmetamorphiques pour une étude de l'évolution tectonique et thermique tardive dans les Alpes occidentales (France). Bulletin de la Societé Géologique de France, Huitième Série.163, 4, 381-392.

Mey, P.H.W., Nagtegaal, P.J.C., Roberti, K.J., Hartevelt, J.J.A., 1968. Lithostratigraphic subdivision of post-hercynian deposits in the south-central Pyrenees, Spain. Leidse Geologische Mededelingen, 41, 221-228.

Millán, H., 1996. Estructura de las Sierras Exteriores Aragonesas. PhD Thesis. Universidad de Zaragoza, 213 p.

Millán Garrido, H., 2006. Estructura y cinemática del frente de cabalgamiento surpirenaico en las Sierras Exteriores aragonesas. Colección de Estudios Altoaragoneses, 53. Instituto de Estudios Altoaragoneses ISBN 84-8127-165-9. Huesca, 398 pp.

Millán, H., Pueyo E.L. and Pocoví, A., 1996. Estimación del acortamiento en áreas afectadas por rotaciones y su contrastación con datos paleomagnéticos. Geogaceta 20 vol. 4, p. 755-758.

Millán, H., Pueyo, E.L., Aurell, M., Luzón, A., Oliva, B., Martínez-Peña, M.B. and Pocoví, A., 2000. Actividad tectónica registrada en los depósitos terciarios del frente meriodinal del Pirineo Central: Revista de la Sociedad Geológica de España, v. 13 (2), p. 279-300.

Miller, R.L., 1973. Where and why the Pine Mountain and other major fault planes, Virginia, Kentucky, and Tenessee. Amer. J. Sci., 273-A, 353-371.

Mochales, T., Pueyo, E.L., Casas, A.M. and Barnolas, A., 2008. Cinemática rotacional del anticlinal del Boltaña (Pirineo Central) durante el Luteciense. Geotemas, 10, 1179-1182

Mochales, T., Pueyo, E.L., Casas, A.M., Barnolas, A. and Oliva-Urcia, B., 2010. Anisotropic magnetic susceptibility record of the kinematics of the Boltaña Anticline (Southern Pyrenees): Geological Journal, v. 45, p. 562-581, doi: 10.1002/gj.1207

Mochales, T., Barnolas A., Pueyo E.L., Serra-Kiel J., Casas A.M., Samsó J.M., Ramajo J. and Sanjuán J., 2011a. Chronostratigraphy of the Boltaña anticline and the Ainsa Basin (Southern Pyrenees). Geological Society of America Bulletin (*accepted*)

Mochales, T., Pueyo, E.L., Casas, A.M. and Barnolas, A., 2011b. Non-steady rotational kinematics of oblique structures; a case study in the Boltaña anticline (Southern Pyrenees). Journal of Structural Geology (*accepted*)

T. Mochales, T.; Pueyo E.L., Casas A.M. and Barnolas, 2011c. Restoring paleomagnetic data in complex superposed folding settings: the Boltaña anticline (Southern Pyrenees). Geologica Acta (*in review*)

Molina, E., Canudo, J.I., Guernet, C., McDougall, K., Ortiz, N., Pascual, J.O., Parés, J.M., Samsó, J.M., Serra-Kiel, J. and Tosquella, J., 1992. The stratotipic Ilerdian revisited: integrated stratigraphy across the

Paleocene-Eocene boundary. Revue de Micropaléontologie, v. 35 (2), p. 143- 156.

Montes, M.J., 1992. Sistemas deposicionales del Eoceno medio-Oligoceno del sinclinorio del rio Guarga (cuenca de Jaca, Pirineo central). III Congreso Geol. España. Simposios, 2: 150-160.

Morin, F.J., 1950. Magnetic susceptibility of α-Fe2O3 and α-Fe2O3 with added titanium, *Phys. Rev*., 78, 819-820.

Muñoz, J.A., 1992. Evolution of a continental collision belt: ECORSPyrenees crustal balanced cross-section. *In*: Thrust Tectonics (K.R. McClay Ed.), Chapman and Hall: London; 235–246.

Muñoz, J.A., Martínez, A., Vergés, J., 1986. Thrust sequences in the Spanish eastern Pyrenees. Jour. Struct. Geol., 8, 399-405.

Muñoz, J.A., Coney, P.J., McClay, K.R., Evenchick, C.A., González, A., Arenas, C. and Pardo, G., 1997. Discussion on syntectonic burial and post-tectonic exhumation of the southern Pyrenees foreland fold-thrust belt. Jour. Geol. Soc. London, 154, 361-365.

Muñoz, J.A., Arbués, P. and Serra-Kiel, J., 1998. The Ainsa Basin and the Sobrarbe oblique thrust system: sedimentological and tectonic processes controlling slope and platform sequences deposited synchronously with a submarine emergent thrust system. *In:* Field Trip Guide Book (A.M. Hevia, A.R. Soria, Eds), 15th IAS Congress: Alicante (Spain); 213–223.

Mutti, E., Luterbacher, H., Ferrer, J. and Rosell, J., 1972. Schema stratigrafico e lineamenti di facies di Paleogene marino nella zona centrale subpirenaica tra Tremp (Catalogna) e Pamplona (Navarra): Memorie Società Geologica Italiana. v. 11, p. 391-416.

Mutti, E., Remacha, E., Sgavetti, M., Rosell, J., Valloni, R. and Zamorano, M., 1985. Stratigraphy and Facies Characteristics of the Eocene Hecho Group Turbidite Systems, South-Central Pyrenees. Excursion Guidebook of I.A.S. 6th. European Regional Meeting. Excursion No. 12, p. 519-576.

Mutti, E., Séguret, M. and Sgavetti, M., 1988. Sedimentation and deformation in the Tertiary sequences of the Southern Pyrenees. American Association of Petroleum Geologists Mediteranean Basins Conference, Nice. Field Trip Guidebook 7, 169 p.

Nagata, T. 1961. Rock Magnetism, 2nd edition, Maruzen, Tokyo, pp. 350.

Nijman, W. and Nio, S.D., 1975. The Eocene Montañana delta. *In:* Sedimentary evolution of the Paleogene South Pyrenean Basin (J. Rosell, C. Puigdefabregas, Eds.), IAS 9th International Congress Nice B, 56 p.

Norris, D.K. and Black, R.F., 1961. Application of palaeomagnetism to thrust mechanics. Nature (London). 192; 4806, Pages 933-935.

Oliva-Urcia, B., 2004. Geometría y cinemática rotacional en las Sierras Interiores y Zona Axial (sector de Bielsa) a partir del análisis estructural y paleomagnético. PhD Thesis, Univ. de Zaragoza, 292 p.

Oliva-Urcia, B., Pueyo, E.L. and Casas, A.M., 2006. Fábricas en el Triásico de la lámina de Bielsa (Pirineo Axial): ¿Indicadoras de distinto grado de deformación? MAGIBER I: Paleomagnetismo en la Península Ibérica (M. Calvo, M. Garcés, C. Gomes, J.C. Larrasoaña, E. Pueyo, J.J. Villalaín. Eds.), Universidad de Burgos, 103-114.

Oliva-Urcia, B. and Pueyo, E.L., 2007a. Rotational basement kinematics deduced from remagnetized cover rocks (Internal Sierras, Southwestern Pyrenees). Tectonics, 26 -TC4014.

Oliva-Urcia, B. and Pueyo, E.L., 2007b. Gradient of shortening and vertical-axis rotations in the Southern Pyrenees (Spain), insights from a synthesis of paleomagnetic data. Revista de la Sociedad Geológica de España, 20 (1-2): 105-118.

Oliva-Urcia, B., Larrasoaña, J.C., Pueyo, E.L., Gil-Imaz, A., Mata, P., Parés, J.M. and Schleicher, A.M., 2009. Complex magnetic subfabrics in a well-developed cleavage domain, Internal Sierras (Pyrenees, Spain). Journal of Structural Geology. 31(2), 163-176, doi:10.1016/j.jsg.2008.11.002.

Oliva-Urcia, B., Casas, A.M., Soto, R., Villalaín, J.J. and Kodama, K., 2011a. A transtensional basin model for the Organyà basin (southern Pyrenees) based on magnetic fabric and brittle structures. Geophysical Journal International, Vol. 184 (1), 111–130, doi: 10.1111/j.1365-246X.2010.04865.x

Oliva-Urcia, B., Casas, A.M., Pueyo, E.L. and Pocovi, A., 2011b. Structural and paleomagnetic evidence for non-rotational kinematics in the western termination of the External Sierras (southwestern central Pyrenees). Geologica Acta (in press)

Olivet, J.L., 1996. La cinématique de la plaque Ibérique. Bull. Cent. Rech. Explor. Prod. Elf Aquitaine, 20, 131-195.

Oms, O., Dinarès-Turel, J. and Remacha, E., 2003, Magnetic stratigraphy from deep clastic turbidites: an example from the Eocene Hecho group (southern Pyrenees): Studia Geophysica Geodetica, v. 47, p. 275-288.

Oms O., Babault J., Dinarès-Turell J., Rouby D., Remacha E, Eichenseer H., Urreiztieta M. and Nalpas T. 2006. Validación de modelos geológicos y magnetotectónica. Ejemplo en la Cuenca Surpirenaica Central, MAGIBER I: Paleomagnetismo en la Península Ibérica. Editores: M. Calvo, M. Garcés, C. Gomes, J.C. Larrasoaña, E. Pueyo y J.J. Villalaín. Edit. Universidad de Burgos, 41-44.

Opdyke, N.D., and Channell, J.E.T., 1996. Magnetic stratigraphy. London and San Diego Academia Press, p. 364.

Osete, M.L., Freeman, R. and Vegas, R., 1989. Paleomagnetic evidence for block rotations and distributed deformation of the Iberian-African plate boundary. *In*: Paleomagnetic Rotations and Continental Deformation. (C. Kissel, C. Laj, Eds.). Nato Asi Series: Mathematical and Physical Sciences, 254, Kluwer Academic Publishers. Dordrecht, 381-391.

Osete, M.L., Villalaín, J.J., Palencia, A., Osete, C., Sandoval, J. and García-Dueñas, V., 2004. New Palaeomagnetic data from the Betic Cordillera. Constrains on the timing and the geographical distribution of tectonic rotations in southern Spain. Pure and Applied Geophysics, v. 161, 701-722.

Ouliac, M., 1976. Removal of secondary magnetization from natural remanent magnetization of sedimentary rocks: alternating field or thermal demagnetization technique? Earth and Planetary Science Letters, Vol. 29, p.65

Parés, J.M. and Dinarès, J., 1993. Magnetic fabric in two sedimentary rock types from the Southern Pyrenees. J. Geomag. Geoelectr. 45, 193–205.

Parés, J.M. and Dinarès, J., 1994. Iberian Triassic palaeomagnetism revisited: intraplate block rotations versus polar wandering. Geophys. Res. Lett. 21, 2155– 2158.

Parés, J.M., Van der Pluijm, B.A. and Dinarès-Turell, J., 1999. Evolution of magnetic fabrics during incipient deformation of mudrocks (Pyrenees, Northern Spain). Tectonophysics, 307,1-14.

Parés, J.M. and Van der Pluijm, B.A., 2002. Evaluating magnetic lineations (AMS) in deformed rocks. Tectonophysics. 350; 4, Pages 283-298.

Pascual, J.O., 1992. Magnetoestratigrafía del estratotipo y paraestratotipo del Ilerdiense, seciones de Tremp y Campo (Cuenca de Tremp-Graus). Tesis doctoral Universitat Autònoma de Barcelona.

Pascual, J.O. and Parés, J.M. 1990. Estudio preliminar de los materiales comprendidos en el tránsito Eoceno-Oligoceno en el borde SE de la cuenca del Ebro., Rev. Soc. Geol. España, 3 (3-4); 323-333.

Pascual, J.O., Samsó, J.M., Tosquella, J., Pares, J.M. and Serra-Kiel, J., 1991. Magnetoestratigrafia y bioestratigrafia del estratotipo del Ilerdiense (Tremp, Lleida). *In:* I congreso del Grupo Espanol del Terciario (F. Colombo, E. Ramos-Guerrero, S. Riera, Eds.). Congreso del Grupo Español del Terciario. Pages 244-247.

Pascual, J.O., Parés, J.M, Langereis, C.G. and Zijderveld, J.D.A., 1992. Magnetostratigraphy and rock magnetism of the Ilerdian stratotype at Tremp, Spain: Physics of the Earth and Planetary Interiors, v. 74, p. 139-157.

Payrós, A., 1997. El Eoceno de la Cuenca de Pamplona: Estratigrafía, facies y evolución paleogeográfica. PhD Thesis, Univ. País Vasco, 403 pp.

Payrós, A., Pujalte, V. and Orue-Etxebarria, X., 1999. The South Pyrenean Eocene carbonate megabreccias revisited: new interpretation based on evidence from the Pamplona basin. Sedimentary Geology, 125, 165-194.

Peybernès, B., 1976. Le Jurassique et le Crétacé Inférieur des Pyrénées Franco-Espagnoles entre la Garonne et la Méditerranée. PhD Thesis, C.R.D.P., Toulouse, 459 pp.

Plaziat, J.C., 1981. Late Cretaceous to Late Eocene paleogeographic evolution of southwest Europe. Paleogeography, Paloeclimatology, Paleoecology, 36, 263-320.

Poblet, J. and Hardy, S., 1995. Reverse modelling of detachment folds; application to the Pico de Aguila anticline in the South Central Pyrenees (Spain). Journal of Structural Geology, v. 17, p. 1707-1724.

Poblet, J., Muñoz J.A., Travé A. and Serra-Kiel J., 1998. Quantifying the kinematics of detachment folds using three-dimensional geometry: Application to the Mediano Anticline (Pyrenees, Spain). Geological Society of America Bulletin 110: 111-125.

Pocoví, A., 1978a. Estudio geológico de las Sierras Marginales Catalanas (Prepirineo de Lérida). PhD Thesis. Univ. Barcelona, 218 pp.

Pocoví, A., 1978b. Estudio geológico de las Sierras Marginales Catalanas (Prepirineo de Lerida). Acta Geológica Hispanica, 13, 73-79.

Pocoví, A., 1979. Deformaciones de la cobertera despegada influidas por acidentes de zócalo en las Sierras Marginales Catalanas (Pirineo Meridional). Acta Geológica Hispanica, 14: 143-148.

Pous, J., Lledó, J.J., Queralt, P. and Muñoz, J.A., 1995. Constraints on the deep structure of the Pyrenees from new magnetotelluric data. Rev. Soc. Geol. España, 8 (4); 395-400.

Pueyo-Anchuela, Ó., Gil, A., Pocoví, A., Mochales, T., Ansón, D., Del Río, P. and Pueyo, E.L., 2007. Acortamiento paralelo a las capas y dirección de transporte tectónico deducido a partir de la fábrica magnética (ASM) en rocas post-hercínicas del Pirineo Central, valle del río Aragón-Subordán, Pirineo, Geogaceta, Vol. 42, 15-18 p.

Pueyo-Anchuela, O., Gil-Imaz, A., Ipas-Lloréns, J.F., Pocoví-Juan, A. and Millán-Garrido, H., 2007. Pre-lithification deformations inferred by anisotropy of magnetic susceptibility studies. An example from the Larres marls Formation (Eocene, Southern Pyrenees. Geophysical Research Abstracts, vol. 9. 08773.

Pueyo-Anchuela, O., Gil-Imaz, A., Pocoví-Juan, A. and Pueyo, E.L., 2008. AMS as a fast and sensitive method to test and detect vertical axis rotation in fold and thrust systems. Southern Pyrenees, Aragón, Spain. Geophysical Research Abstracts, 10, EGU2008-A-07853.

Pueyo-Anchuela, O., Gil-Imaz, A. and Pocoví, A., 2010. Significance of AMS in multilayer systems in fold and thrust belts. A case study from the Eocene turbidites in the Southern Pyrenees (Spain). Geological Journal, 45, 544-561. DOI: 10.1002/gj.1194

Pueyo-Anchuela, O., Pueyo, E.L., Pocoví, A. and Gil-Imaz, A. 2011 (in review). Vertical axis rotations in thrust and folds belts: calibration of AMS and paleomagnetic analyses in the Western External Sierras (Southern Pyrenees, Spain). Journal of Structural Geology.

Pueyo, E.L., 2000. Rotaciones paleomagnéticas en sistemas de pliegues y cabalgamientos. Tipos, causas, significado y aplicaciones (ejemplos del Pirineo Aragonés). PhD Thesis, Universidad de Zaragoza. 296 pp.

Pueyo, E.L., 2008. El paleomagnetismo: fundamento, métodos y aplicaciones al estudio de la Cadena Pirenaica. *In:* II Seminario del Geoparque del Sobrarbe Investigacion Geológica y Recursos Didácticos (Boltaña). Edited by Geoparque del Sobrarbe- (Jaume Poc), 9 pp.

Pueyo, E.L., 2010. Evaluating the paleomagnetic reliability in fold and thrust belt studies: Trabajos de Geologia, 30 (1) 145-154

Pueyo, E.L., Millán, H., Parés, J.M. and Pocoví, A., 1997. Determination of the folding mechanism by AMS data. Study of the relation between shortening and magnetic anisotropy (P´): A case study in the Pico del Aguila Anticline (Southern Pyrenees). Physics and Chemistry of the Earth, vol 22 nº 1-2, 195-201.

Pueyo-Morer, E.L., Millán, H., Pocoví, A. and Parés, J.M., 1999. Cinemática rotacional del cabalgamiento basal surpirenaico en las Sierras Exteriores Aragonesas: Datos magnetotectónicos. Acta Geológica Hispánica, 32(3-4), 119-138.

Pueyo, E.L., Millán, H. and Pocoví, A., 2002. Rotation velocity of a thrust: a paleomagnetic study in the External Sierras (Southern Pyrenees). Sedimentary Geology, v. 146, p. 191-208, doi: 10.1016/S0037-0738(01)00172-5.

Pueyo, E.L., Parés, J.M., Millán, H. and Pocoví, A., 2003a. Conical folds and apparent rotations in paleomagnetism (A case studied in the Southern Pyrenees), *In*: Paleomagnetism applied to tectonics; a tribute to Rob Van der Voo (C. Mac Niocaill, T.H. Torsvick, B.A. Van der Pluijm, Eds.), Tectonophyisics, 362(1-4), pp. 345-366, doi: 10.1016/S0040-1951(02)00645-5.

Pueyo, E.L., Pocoví, A., Parés, J.M., Millán, H. and Larrasoaña, J.C., 2003b. Thrust ramp geometry and spurious rotation of paleomagnetic vectors. Studia Geophysica Geodetica, 47: 331-357.

Pueyo, E.L., Pocoví, A., Millán, H. and Sussman, A.J., 2004a. Map-view models for correcting and calculating shortening estimates in rotated thrust fronts using paleomagnetic data, *In:* Orogenic Curvature: Integrating Paleomagnetic and Structural Analyses (A.J. Sussman, A.B. Weil Eds.), Geological Society of America

Special Paper 383, p. 57-71.

Pueyo, E.L., Román-Berdiel, T., Bouchez, J.L., Casas, A.M. and Larrasoaña, J.C., 2004b. Statistical significance of magnetic fabric data in studies of paramagnetic granites. *In*. Magnetic fabric: methods and applications (F. Martın-Hernández, C M. Lüneburg, C. Aubourg, M. Jackson Eds.). Geological Society of London, Special Publications, vol 238, pp 395–420

Pueyo, E.L., Bouchez, J.L., Román, M.T. and Gleizes, G., 2005a. Are paramagnetic granites free of ferromagnetism? 10th Scientific Assembly IAGA (Toulouse), Abstracts 01323.

Pueyo, E.L., Sussman, A.J., Oliva, B., Larrasoaña, J.C., Beamud B., Soto R., Garcés M., Gil-Peña, I., Almar, Y., Fernández, O. and Vidal, O., 2005b. The Pyrenean paleomagnetic database: towards better 3D restoration methods. 10th Scientific Assembly IAGA (Toulouse), Abstracts 01319.

Pueyo, E.L., López, M.A., Oliva, B., Sussman, A.J., Larrasoaña, J.C., Dinarés, J., Beamud, B., Soto, R., Garcés, M., Gil-Peña, I., Rodríguez, A., Almar, Y., Fernández, O., Villalaín, J.J., Calvo, M., Bógalo, M.F., Costa, E., Mochales, T., Vidal, O., Pueyo-Anchuela, O., Gil-Imaz, A., Román, M.T, Navas, J. and the GeoKinDPyr group, 2006. A preliminary compilation of the Pyrenean paleomagnetic database. Proceedings MAGIBER IV, 73-76.

Puigdefàbregas, C.,1975. La sedimentación molásica en la cuenca de Jaca. Pirineos 104, 1–188.

Puigdefàbregas, C. and Souquet, P., 1986. Tecto-sedimentary cycles and depositional sequences of the Mesozoic and Tertiary of the Pyrenees. Tectonophysics, 129, 173- 203.

Puigdefàbregas, C., Nijman, W. and Muñoz, J.A., 1991. Alluvial deposits of the successive foreland basin stages and their relation to the Pyrenean thrust sequences. Excursion Guidebook, 4th International Conference on Fluvial Sedimentology. Barcelona, 176 p.

Pujalte, V., Dinares-Turell, J., Bernaola, G., Baceta J.I. and Payros, A., 2003. A reappraisal of the position of Chron C25n in the Campo section (Huesca province, south-central Pyrenees): Geogaceta, v. 34, p. 155-158.

Quirantes J., 1978. Estudio sedimentológico y estratigráfico del terciario continental de los Monegros. Institución Fernando el Católico (CSIC). Tesis doctorales, 27, 207pp.

Ramón, M.J. and Pueyo, E.L., 2008. Cálculo de direcciones y planos virtuales paleomagnéticas: ejemplos y comparación con otros métodos. Geotemas, v. 10, p. 1203-1206.

Ramón, M.J., Pueyo, E.L. and Oliva, B., Larrasoaña, J.C., 2011a (*in review*). Virtual directions and circles in paleomagnetism: An objective estimation method of the ChRM. Geochem. Geophys. Geosyst (G^3)

Ramón, M.J., Pueyo, E.L., Pocoví, A., Briz, J.L., Ciria, J.C. and Ros, L.H., 2011b. 3D restoration of complex geological structures by using paleomagnetic vectors. Proceedings of the 31th gOcad meeting (Nancy). 10 pp

Razin, P., 1989. Evolution tecto-sédimentaire alpine des Pyrénées basques à l'Ouest de la transfromante de Pamplona (Province de Labourd). PhD Thesis, Univ. Bordeaux III, 464 pp.

Remacha, E., Fernández, L.P., Maestro, E., Oms, O., Estrada, R. and Teixell, A., 1998. The Upper Hecho Group turbidites and their vertical evolution to deltas (Eocene, South-central Pyrenees). 15th international Association of Sedimentologists , International Congress of Sedimentology. Field trip book guide, excursion A.1, Alicante (Spain).

Remacha, E., Oms, O., Gual, G., Bolano, F., Climent, F., Fernandez, L.P., Crumeyrollle, P., Pettingill, H., Vicente, J.C. and Suarez, J., 2003. Sand-rich turbidite systems of the Hecho Group from slope to basin plain; facies, stacking patterns, controlling factors and diagnostic features. AAPG Internacional Conference and Exhibition, Barcelona, Spain, Geological Field Trip 12.

Riba, O., Reguant, S. and Villena, J., 1983. Ensayo de síntesis estratigráfica y evolutiva de la cuenca terciaria del Ebro. Libro Jubilar J.M. Ríos: Geología de España, IGME.

Richter, C. and Van der Pluijm, B.A., 1994. Separation of paramagnetic and ferrimagnetic susceptibilities using low-temperature magnetic susceptibilities and comparison with high field methods. Physics of the Earth and Planetary Interiors 82, 113–123.

Ríos-Aragués, L.M., Lanaja, J.M. and Ríos-Mitchell, J.M., 1982. Memoria y Hoja Geológica número 319 (Bielsa) del Mapa Geológico de España 1/50.000 (2 Serie Magna). Instituto Geológico y Minero de España, 48 p.

Riveline, J., 1986. Les Charophytes du Paléogène et du Miocène Inférieur d'Éurope Occidentale: Cahiers de Paléontologie, 227 p, 38 plates.

Riveline, J., Berger, J.P., Feist, M., Martín-Closas., C, Schudack, M. and Soulié-Märsche, I., 1996. European Mesozoic-Cenozoic charophyte biozonation: Bulletin de la Société Géologique de France, v. 167 (3), p. 437-468.

Robador, A., 1991. Early Paleogene Stratigraphy. *In*: Introduction to the early Paleogene of the South Pyrenean Basin. IGCP 286 "Early Paleogene Benthos" First Meeting, Jaca (Spain), ITGE, Madrid, 41-87.

Rochette, P., 1987. Magnetic susceptibility of the rock matrix related to magnetic fabric studies. Journal of StructuralGeology 9, 1015–1020.

Rochette, P., Fillion, G., Mattei, J.L. and Dekkers, M.J., 1990. Magnetic transition at 30-34 Kelvin in pyrrhotite: insight into a widespread occurrence of this mineral in rocks. Earth and Planetary Science Letters, 98, 319-328.

Rodríguez-Pintó, A., Pueyo, E.L., Barnolas, A., Pocoví, A., Samsó, J.M. and Gil-Peña, I., 2006. Magnetoestratigrafía Cuisiense-Luteciense preliminar de la Cuenca Surpirenaica Occidental: Magiber IV (Vigo), Congreso de Paleomagnetismo Ibérico, Comunicaciones, p. 81–84.

Rodríguez-Pintó, A., Pueyo, E. L., Pocoví, A. and Barnolas, A., 2008. Cronología de la actividad rotacional en el sector central del frente de cabalgamiento de Sierras Exteriores (Pirineo Occidental). Geotemas, 10, 1207-1210.

Rodríguez-Pintó, A., Pueyo, E.L., Pocoví , A. and Barnolas, A., 2010. Paleomagnetic analysis in the Balzez anticline (Southern Pyrenees); Vertical-axis rotations and kinematic implications. Trabajos de Geologia, 30 (1), 169 – 175.

Rodríguez-Pintó, A., Ramón, M.J., Oliva, B., Pueyo, E.L., Pocoví, A., 2011a. Errors in paleomagnetism: Structural control on overlapped vectors, mathematical models. Physics of the Earth and Planetary Interiors, doi:10.1016/j.pepi.2011.02.003.

Rodríguez-Pintó, A., Pueyo, E.L., Pocoví, A., Ramón, M.J. and Oliva-Urcia, B., 2011b. Structural control on overlapped paleomagnetic vectors: A case study in the Balzes anticline (Southern Pyrenees). Physics of the Earth and Planetary Interiors (in review)

Rodríguez-Pintó, A., Pueyo, E.L., Serra-Kiel, J., Samsó, J.M., Barnolas, A. and Pocoví, A., 2011c. Lutetian magnetostratigraphic calibration of larger foraminifers zonation (SBZ) at the Southern Pyrenees. Palaeo 3.

Rodríguez-Pintó, A., Pueyo, E.L., Serra-Kiel, J., Samsó, J.M., Barnolas, A. and Pocoví, A., 2011d. Chronology of the Southwestern Pyrenean Eocene Basin; Magnetostratigraphy from the Balzes anticline. Geologica Acta (*in prep*).

Rosenbaum, G., Lister, G.S. and Duboz, C., 2002. Relative motions of Africa, Iberia and Europe during alpine orogeny. Tectonophysics, 359, 117-129.

Roure, F., Choukroune, P., Berastegui, X., Muñoz, J.A., Villien, A., Matheron, P., Bareyt, M., Seguret, M., Cámara, P. and Deramond, J., 1989. ECORS deep seismic data and balanced cross-sections: geometric constraints on the evolution of the Pyrenees. Tectonics, 8, 41 -50.

Sagnotti L., Speranza F., Winkler A., Mattei M. and Funiciello R., 1998. Magnetic fabric of clay sediments from the external northern Apennines (Italy). Physics of the Earth and Planetary Interiors. 105, 73-93.

Sagnotti, L., Winkler, A., Montone, P., Di Bella, L., Florindo, F., Mariucci, M.T., Marra, F., Alfonsi, L. and Frepoli, A., 1999. Magnetic Anisotropy of Plio-Pleistocene Sediments From the Adriatic Margin of the Northern Apennines (Italy): Implications for the Time-Space Evolution of the Stress-Field. Tectonophysics, 311:139-153

Samsó, J.M., Serra-Kiel, J., Tosquella, J. and Travé, A., 1994. Cronoestratigrafía de las plataformas lutecienses de la zona central de la Cuenca Surpirenaica. II Congr. del Grupo Español del Terciario. Comunicaciones: 205-208. Jaca (Huesca).

San Miguel, G., Hernández, R., Pueyo, E.L. and the Geokin3DPyr, 2010. Pyrenean Paleomagnetic Database; Concept, state-of-the-art, and web interface design. Proceedings MAGIBER VI, (Puigcerda, Gerona) pp 51-54.

Saura, E., 2004. Anàlisi estructural de la zona de les Nogueres Pirineus Centrals. PhD, Thesis, Universitat Autónoma de Barcelona, 355 pp.

Saura, E. and Teixell, A., 2006. Inversion of small basins: effects on structural variations at the leading edge of the Axial Zone antiformal stack (Southern Pyrenees, Spain). Journal of Structural Geology, Volume 28, Issue 11, Pages 1891-2120.

Schaub, H., 1981. Nummulites et Assilines de la Téthys paléogène. Taxinomie, phylogenèse et biostratigraphie: Mémoires suisses de Paléontologie, v. 104, p. 1-236, 18 plates; v. 105 (Atlas I), plates 1-48; v. 106 (Atlas II), plates 49-97.

Scheidegger, A,M., 1965. On the statistics of the orientation of bedding planes, grain axes, and similar sedimentological data. US Geological Survey Professional Papers, 525C, 164–167.

Schmidt, V., Guenther, D. and Hirt, A.M., 2006. Fundamental room-temperature magnetic properties of calcite. Tectonophysics, 418, 63-73

Schmidt, V., Hirt, A.M., Hametner, K. and Gunther, D., 2007. Magnetic anisotropy of carbonate minerals at room temperature and 77 K. American Mineralogist, 92, 10, 1673-1684.

Schwarz, E.J., 1962. Geology and paleomagnetism of the valley of the Río Aragón Subordan north and east of Oza. PhD Thesis. University of Utrecht. Estudios Geológicos, 18, 193-240.

Séguret, M., 1972. Étude tectonique des nappes et séries décollées de la partie centrale du versant sud des Pyrénées - Caractère synsedimentaire, rôle de la compresion et de la gravité. Publications USTELA, Montpellier, Série géologie structurale, 2, 155 p.

Sélles, J., 1988. Las correcciones estructural y tectónica en el tratamiento de los datos magnéticos. Geofísica Internacional, 27-3, 379-393 pp.

Serra-Kiel, J., Canudo, J.I., Dinarés, J., Molina, E., Ortiz, N., Pascual, J.O., Samsó, J.M. and Tosquella, J., 1994. Cronoestratigrafía de los sedimentos marinos del Terciario inferior de la Cuenca de Graus-Tremp (Zona Central Surpirenaica). Revista de la Sociedad Geológica de España, v. 7 (3-4), p. 273-297.

Serra-Kiel, J., Hottinger, L., Caus, E., Drobne, K., Ferràndez, C., Jauhri, A.K., Less, G., Pavlovec, R., Pignatti, J., Samsó, J.M., Schaub, H., Sirel, E., Strougo and A., Tambareau, Y., Tosquella, J., Zakrevskaya, E., 1998. Larger foraminiferal biostratigraphy of the Tethyan Paleocene and Eocene. Bulletin de la Société Géologique de France, v. 169 (2), p. 281-299.

Sibuet, J.C., Srivastava, S.P. and Spakman, W., 2004. Pyrenean orogeny and plate kinematics. Journal of Geophysical Research, VOL. 109, B08104, doi:10.1029/2003JB002514.

Simó, A., 1985. Secuencias deposicionales del Cretácico superior de la Unidad del Montsec (Pirineo Central). PhD Thesis. Universidad de Barcelona, 326 pp.

Sintubin, M., 1994. Clay fabrics in relation to the burial history of shales. *Sedimentology,* 41, 1161-1169.

Soto, R., 2003. Estructuras oblicuas: Modelización analogical y ejemplos de la zona surpirenica. PhD, thesis, Univ. Zaragoza, 342 pp.

Soto, R. and Casas, A.M., 2001. Geometría y cinemática de las estructuras norte-sur de la cuenca de Ainsa. Revista de la Sociedad Geológica de España v. 14, p. 3–4.

Soto, R., Casas, A.M., Storti, F. and Faccenna, C., 2002. Role of lateral thickness variations on the development of oblique structures at the western end of the South Pyrenean Central Unit. Tectonophysics 350, 215–235.

Soto, R., Mattei, M. and Casas, A.M., 2003. Relationship between AMS and folding in an area of superimposed folding (Cotiella-Boixols nappe, Southern Pyrenees). Geodinamica Acta 16, 171–185.

Soto, R., Casas-Sainz, A.M., Villalaín, J.J. and Oliva-Urcia, B., 2007. Mesozoic extension in the Basque-Cantrabian basin (N Spain): Contributions from AMS and brittle mesoestructres. Tectonophysics 445: 373-394.

Soto, R., Casas-Sainz, A.M., Villalaín, J.J., Gil-Imaz, A., Fernández-González, G., Del Rio, P. Calvo, M. and Mochales, T., 2008. Characterizing the Mesozoic extension direction in the northern Iberian plate margin. Journal of the Geological Society 2008; v. 165; p. 1007-1018. doi:10.1144/0016-76492007-163.

Souquet, P. and Déramond, J., 1989. Séquence de chevauchements et séquenles de dépôt dans un bassin d'avant-fosse. Exemple du sillon crétacé du versant sud Pyrénées (Espagne). C. R. Acad. Sci. Paris 309 (Série II) 137–144.

Souriau, A. and Granet, M., 1995. A tomographic study of the lithosphere beneath the Pyrenees from local and teleseismic data. Jour. Geophys. Res. 100 (B9); 18117-18134.

Speranza, F., Sagnotti, L. and Mattei, M., 1997. Tectonics of the Umbria–Marche–Romagna Arc (central–northern Apennines, Italy): new paleomagnetic constrains. J. Geophys. Res. 102, 3153–3166.

Speranza, F., Villa, I.M., Sagnotti, L., Florindo, F., Cosentino, D., Cipollari, P. and Mattei, M. 2002. Age of the Corsica-Sardinia rotation and Liguro-Provencal Basin spreading: New paleomagnetic and Ar/Ar evidence. Tectonophysics 347: 231-251. doi:10.1016/S0040-1951(02)00031-8.

Stamatakos, J., Hirt, A.M. and Lowrie, W., 1996. The age and timing in the central Appalachians from paleomagnetic results. Geological Society of America Bulletin. 108 (7), 815-829.

Stewart, S.A., 1995. Paleomagnetic analysis of plunging fold structures: Errors and a simple fold test. Earth Planetary Science Letters, 130: 57-67

Stewart, S.A. and Jackson, K.C., 1995. Palaeomagnetic analysis of fold closure growth and volumetrics. Geological Society Special Publications, vol.98, pp.283-295.

Sussman, A.J., Chase, C.G., Pueyo, E.L., Mitra, G. and Weil, A.J., 2011 (*in review*). The impact of vertical-axis rotations on shortening estimates. Tectonics

Taberner, C., Dinarés-Turell, J., Jiménez, J. and Docherty, C., 1999. Basin infill architecture and evolution from magnetostratigraphic cross-basin correlations in the southeastern Pyrenean foreland basin. Geological Society of America Bulletin, 11(8), p. 1155-1174.

Tauxe, L., 2002. Paleomagnetic Principles and Practice. Modern Approaches in Geophysics Series Vol. 18, 299 pp. Dordrecht, Boston, London.Kluwer Academic Publishers.

Tauxe, L., Kylstra, N. and Constable, C., 1991. Bootstrap satatistics for paleomagnetic data. J. Geophys. Res*.,* 96: 11723-11740.

Tarling, D.H. and Hrouda F., 1993. The Magnetic Anisotropy of Rocks. Chapman and Hall, London. 217 pp.

Tavani, S., Storti, F., Fernández, O., Muñoz, J.A. and Salvini, F., 2006. 3-D deformation pattern analysis and evolution of the Añisclo anticline, southern Pyrenees. Journal of Structural Geology 28 (2006) 695–712.

Teixell, A., 1996. The Ansó transect of the southern Pyrenees: basement and cover thrust geometries. J. Geol. Soc. London, 153, 301-310.

Teixell, A., 1998. Crustal structure and orogenic material budget in the west central Pyrenees. Tectonics, 17 (3), 395-406.

Teixell, A., 2004. La estructura cortical de la Cordillera Pirenaica. *In*: Geología de España (J.A. Vera, Ed.), SGE-IGME, Madrid, 320-331.

Teixell, A. and Barnolas, A., 1995. Significado de la discordancia de Mediano en relación con las estructuras adyacentes (Pirineo central). Geogaceta, v. 17, p. 186-189.

Teixell, A. and Muñoz, J.A., 2000. Evolución tectono-sedimentaria del Pirineo meridional durante el Terciario: una síntesis basada en la transversal del río Noguera Ribagorçana. Rev. Soc. Geol. España, 13, 2, 251-264.

Tejero, R. and Fernández-Gianotti, J. (editors), 2004. CD-Rom anexo al libro de Geología de España. *In:* Geología de España (J.A. Vera, Ed.), SGE-IGME, Madrid.

Torné, M., De Cabissole, B., Bayer, R., Casas, A., Daignières, M. and Rivero, A., 1989. Gravity constrains on the deep structure of the Pyrenean belt along the ECORS profile. Tectonophysics, 165: 105-116.

Torsvik, T.H., Smethurst, M.A., Van der Voo, R., Trench, A., Abrahamsen, N. and Halvorsen, B., 1992. Baltica. A synopsis of Vendian-Permian palaeomagnetic data and their palaeotectonic implications: Earth-Science Reviews, v. 33, p. 133-152.

Torsvik, T., 1986. Interactive analysis of palaeomagnetic data: IAPD user-guide, Universitetet i Bergen, 74 p.

Torsvik, T.H., Müller, R.D., Van der Voo, R., Steinberger, B. and Gaina, C., 2008. Global Plate Motion Frames: Toward a unified model. Reviews Geophysics, 46, RG3004, doi:10.1029/2007RG000227.

Troy, J.K., Kodama, K.P. and Anastasio, D.J., 2008. Synsedimentary Tectonic Strain and Fold Kinematics Recorded by Anisotropy of Magnetic Susceptibility in Pyrenean Flysch. Joint Meeting of The Geological Society of America Abstracts with Programs, Vol. 40, No. 6, p. 110

Vacher, P., Souriau, A., 2001. A three-dimensional model of the Pyrenean deep structure based on gravity modeling, seismic images and petrological constraints. Geophysical Journal International, vol.145, no.2, pp.460-470.

Van der Lingen, G.J., 1960. Geology of the Spanish Pyrenees, north of Canfranc, Huesca province. (PhD Thesis, University of Utrecht). Estudios Geológicos. Inst. Invest. Geol. "Lucas Mallada", Madrid, 16, 205-242

Van der Velde, E.J., 1967. Geology of the Ordesa overthrust mass, Spanish Pyrénées, province of Huesca. Est. Geológicos, vol. 23, n. 3-4, 163-203.

Van der Voo, R., 1990. The reliability of paleomagnetic data, Tectonophysics, 184, 1-9.

Van der Voo, R., 1993. Paleomagnetism of the Atlantic, Tethys, and Iapetus oceans Cambridge University Press, 411pp.

Van Lunsen, H., 1970. Geology of the Ara-Cinca region, Spanish Pyrenees. Province of Huesca. Thesis, Utrech State University, 1970. Geol. Ultraiectina, 16, 1 -119.

Vergés, J., 2003. Evolución de los sistemas de rampas oblicuas de los Pirineos meridionales: fallas del Segre y Pamplona. Boletín Geológico y Minero, 114 (1): 87-101

Vergés, J. and Muñoz, J.A., 1990. Thrust sequences in the Southern Central Pyrenees. Bull. Soc. Géol. Fr., 8, 6(2), 265-271.

Verwey, E.J., 1939. Electronic conduction of magnetite (Fe3O4) and its transition point at low temperature, *Nature*, 144, 327-328.

Villalaín, J.J., Osete, M.L., Vegas, R. and García-Dueñas, V., 1992. Evidencia de una reimanación en las Béticas Occidentales. Implicaciones tectónicas. *In*: Paleomagnetismo y Tectónica en las Cordilleras Béticas. Física de la Tierra, 4, 165-184, Ed. Universidad Complutense de Madrid.

Waldhör, M. and Appel, E., 2009. Layer parallelisation: An unrecognised mechanism for paleomagnetic rotations in fold belts. Tectonophysics 474, 516-525.

Waldhör, M. and Appel, E., 2006. Intersections of remanence small circles: new tools to improve data processing and interpretation in palaeomagnetism. Geophys. J. Int. 166, 33–45 doi: 10.1111/j.1365-246X.2006.02898.x

Weil, A.B., 2006. Kinematics of orocline tightening in the core of an arc: Paleomagnetic analysis of the Ponga Unit, Cantabrian Arc, northern Spain. Tectonics, 25, TC3012, doi:10.1029/2005TC001861.

Williams, G.D., 1985. Thrust tectonics in the south central Pyrenees. Jour. Struct. Geol., 7: 11-17.

Woodward, N.B., Walker, K.R. and Lutz, C.T., 1988. Relationships between early Paleozoic facies patterns and structural trends in the Saltville thrust family, Tennessee Valley and Ridge, southern Appalachians. Geol. Soc. Amer. Bull, 100, 1758-1769.

Ziegler, P.A., 1989. Geodynamic model for Alpine intra-plate compressional deformation in the Western and central Europe. *In*: Inversion Tectonics (M.A Cooper, G.D Williams, Eds.), Geol. Soc. London, Spec. Publ., 44, 63-85.

Ziegler, P.A., Cloetingh, S., Guiraud, R. and Stampfli, G.M., 2001. PeriTethyan Platforms: Dynamics of Rifting and Basin Inversion. *In:* Peri-Tethyan Rift/Wrench Basins and Passive Margins (Ziegler, P.A., Cavazza, W., Robertson, A.F.H. Eds.). Peri-Tethys Mem. 6, Mém. Mus. Natn. Hist. Nat. (Paris) (186): 9–49.

Ziegler, P.A and Dèzes, P., 2006. Crustal configuration of Western and Central Europe. *In:* European Lithosphere Dynamics (D.G. Gee and R.A. Stephenson Eds.). Geol. Soc., London, Memoirs 32: 43–56.

Zijderveld, J.D.A., 1967. A.C. demagnetization of rocks: analysis of results, *In:* Methods in Palaeomgnetism (D.H. Collinson, S.K. Runcorn., K.M. Creer, Eds.), Esevier, New York, p. 254 – 286.

Zotkevich, I.A., 1972. Reduction of the natural remanent magnetization of a plunging fold to the ancient coordinate system in paleomagnetic studies. Earth Physics, 2: 95-99.

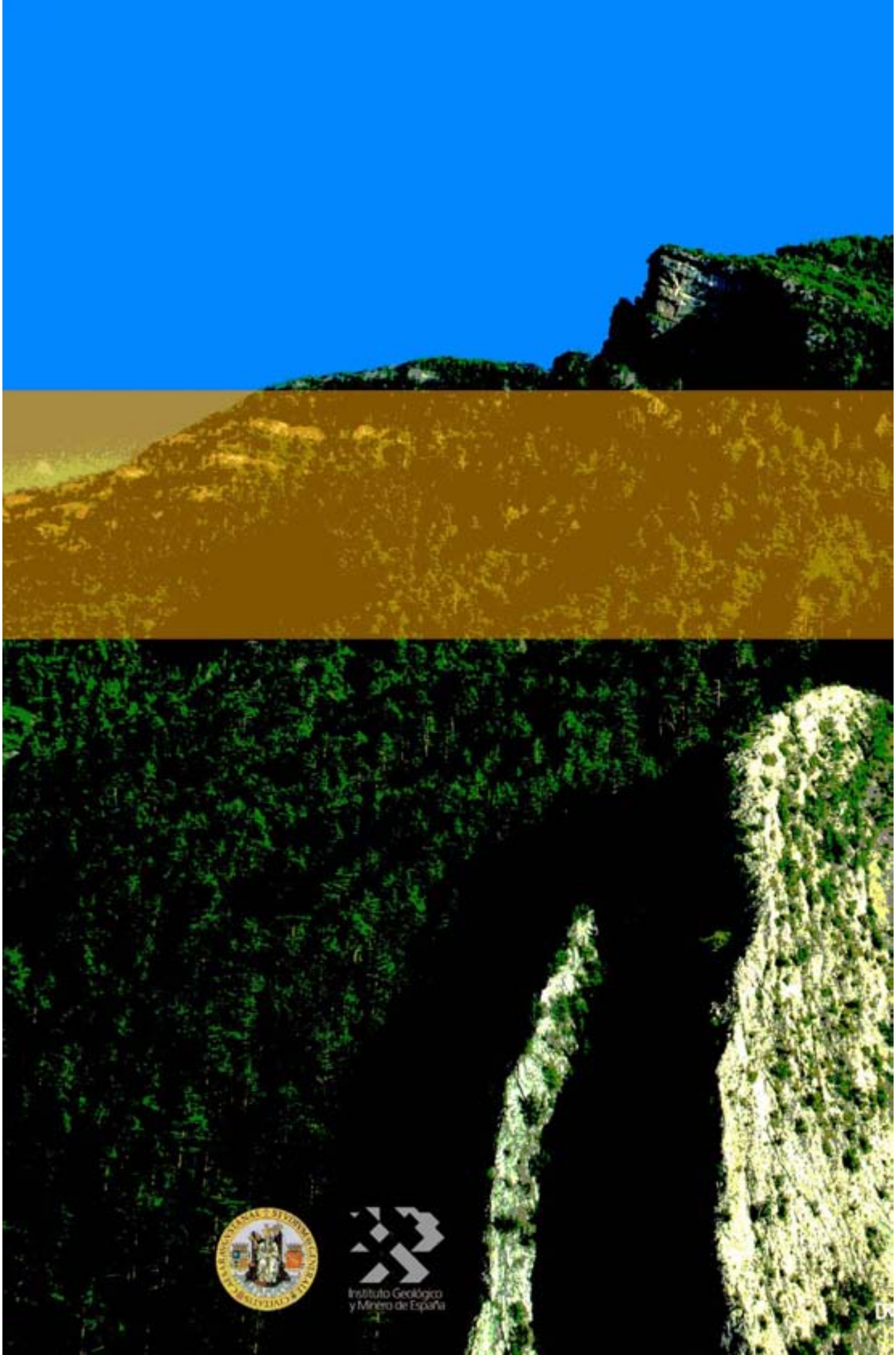

Instituto Geológico
y Minero de España